

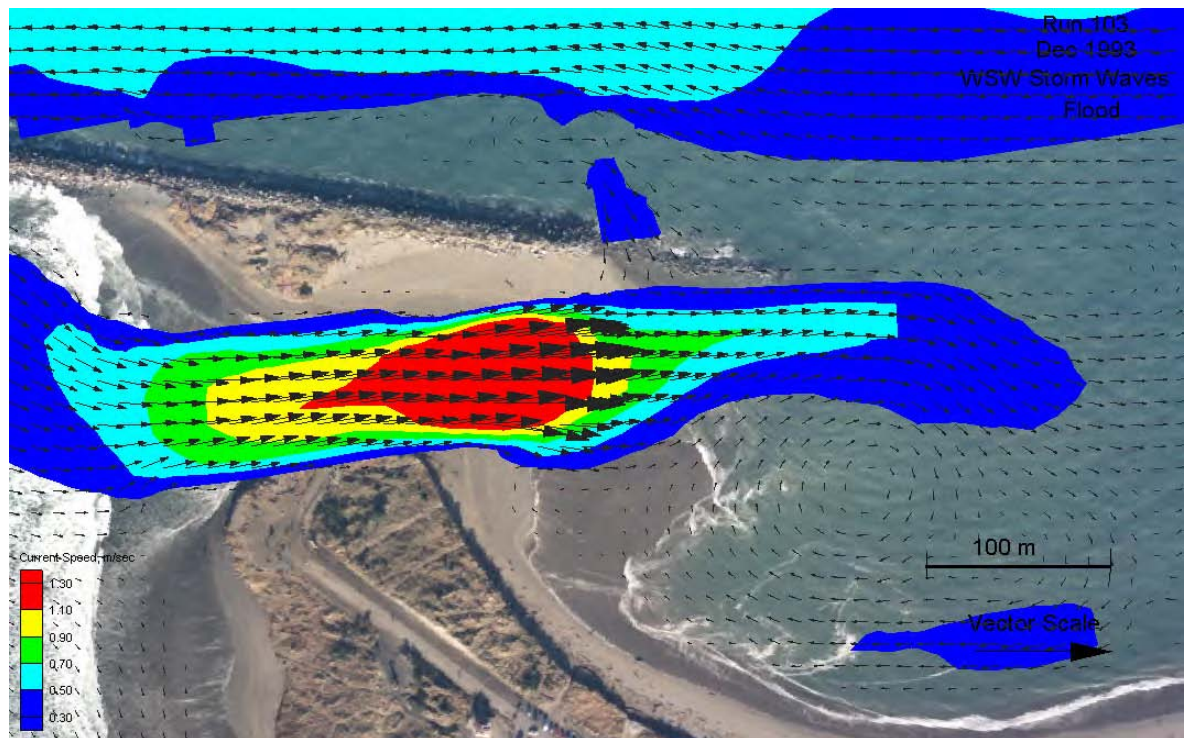


US Army Corps
of Engineers®
Engineer Research and
Development Center

Breach History and Susceptibility Study, South Jetty and Navigation Project, Grays Harbor, Washington

Ty V. Wamsley, Mary A. Cialone, Kenneth J. Connell,
and Nicholas C. Kraus

September 2006



Breach History and Susceptibility Study, South Jetty and Navigation Project, Grays Harbor, Washington

Ty V. Wamsley, Mary A. Cialone, Kenneth J. Connell, and Nicholas C. Kraus

*Coastal and Hydraulics Laboratory
U.S. Army Engineer Research and Development Center
3909 Halls Ferry Road
Vicksburg, MS 39180-6199*

Final report

Approved for public release; distribution is unlimited.

Abstract: The purpose of this study was to analyze the December 1993 breach at Grays Harbor, WA, and assess the threat to the Federal Navigation Project had the breach not been filled the following fall. The study was conducted by quantifying evolution of breach morphology; numerically simulating the ocean wave and water level conditions producing the current through such a breach, including investigation of wide-area implications for the current in Grays Harbor; and numerical modeling breach evolution. Available data on the breach evolution were analyzed with a Geographic Information System. The width of the breach and erosion of the adjacent shoreline are quantified from aerial photographs. Shoreline position and bottom configurations in the vicinity of the now-closed breach are the basis of numerical modeling of wave- and tide-driven currents. Estimates are made of the wave and current climate at South Beach, Pt. Chehalis, and in Half Moon Bay under the assumption of a breach at the jetty. Hydrodynamics for various alternatives of further erosion of the breach are modeled to evaluate flow patterns in a developed breach condition. Sediment transport and evolution of the breach are modeled to assess the potential for continued breach growth and long-term assessment of breach stability. Study products are intended to assist the U.S. Army Engineer District, Seattle, in developing a long-term management plan for protecting Federal navigation project features.

DISCLAIMER: The contents of this report are not to be used for advertising, publication, or promotional purposes. Citation of trade names does not constitute an official endorsement or approval of the use of such commercial products. All product names and trademarks cited are the property of their respective owners. The findings of this report are not to be construed as an official Department of the Army position unless so designated by other authorized documents.

DESTROY THIS REPORT WHEN NO LONGER NEEDED. DO NOT RETURN IT TO THE ORIGINATOR.

Contents

Preface	xiv
Converting non-SI Units of Measurement to SI Units.....	xv
1—Introduction.....	1
Purpose of Study	1
Grays Harbor, Washington.....	2
1993 Breach and Recent Beach Potential.....	3
Overview of Breaching Process	6
Regional Processes.....	8
Independent Technical Review	9
2—Analysis of December 1993 Breach.....	10
Morphology Prior to Federal Navigation Project.....	10
Shoreline Recession and Dune Lowering.....	15
Waves.....	19
Water Level.....	20
Breach Evolution.....	23
Breach width.....	25
Breach depth.....	26
South Beach Shoreline Recession	28
Summary	30
3—Numerical Modeling of Breach Hydrodynamics	31
Numerical Models	32
M2D.....	32
STWAVE.....	32
ADCIRC	33
Model Validation.....	34
Numerical Simulations	39
Analysis of Numerical Simulations.....	46
Pre-breach simulations	46
1993 breach simulations.....	51
December 1993 to August 1994 changes	67
Large-breach simulations	72

Alternative large breach simulations.....	80
Tide-only simulations.....	82
West-southwest storm simulations.....	82
West-northwest storm simulations.....	86
Discussion.....	86
Simulation of historic breach.....	87
Simulation of conceptual large breach.....	87
Example regional implications.....	89
4—Morphologic Numerical Model of 1993 Breach.....	91
Breaching Adjacent to Jetties.....	91
Breaching downdrift of jetties.....	92
Breaching updrift of jetties.....	94
Breaching Model.....	95
Hydrodynamic model.....	96
Sediment transport model.....	99
Morphologic model.....	101
Tests of Breaching Model.....	104
Semicircle barrier island.....	104
Dutch laboratory study.....	106
USACE laboratory study.....	109
1980 breach at Moriches Inlet, New York.....	113
Application to Grays Harbor.....	118
Available data.....	116
Results.....	123
Summary of Breach Simulations.....	127
5—Concluding Discussion.....	128
Synopsis of Study.....	128
Hydrodynamic Simulation of Historic Breach.....	129
Hydrodynamic Simulation of Conceptual Large Breach.....	131
Example Regional Implications from Hydrodynamic Calculations.....	133
Breach Morphology Modeling.....	134
Summary.....	134
References.....	136
Appendix A: Supplemental Photographic Documentation.....	A1
Appendix B: Figures of M2D-STWAVE Model Simulation Results.....	B1
Appendix C: Independent Technical Review and Response.....	C1
Report Documentation Page	

List of Figures

Figure 1.	Grays Harbor Navigation Project	4
Figure 2.	Breached area at Grays Harbor south jetty, 6 March 1994.....	5
Figure 3.	Breach at Moriches Inlet on 21 September 1980, 9 months after formation	8
Figure 4.	Bathymetric morphology for Grays Harbor entrance, 1962	11
Figure 5.	Bathymetric morphology for Grays Harbor entrance, 1881	11
Figure 6.	Bathymetric morphology for Grays Harbor entrance, 1883	12
Figure 7.	Bathymetric morphology for Grays Harbor entrance, 1891	12
Figure 8.	Bathymetric morphology for Grays Harbor entrance, 1894	13
Figure 9.	Bathymetric morphology for Grays Harbor entrance, 1898	13
Figure 10.	Bathymetric morphology for Grays Harbor entrance, 1900.....	14
Figure 11.	Location of marginal flood channel relative to 1993 breach.....	15
Figure 12.	Measured shoreline position at Half Moon Bay 1946-1993.....	17
Figure 13a.	South Beach and Half Moon Bay, May 1993, tide elevation -0.5 m mllw.....	18
Figure 13b.	Interpreted vegetation lines, July 1991 to May 1993	18
Figure 14.	Time series of significant wave height, spectral peak period, and mean direction from which waves are incident at peak period, 8 December 1993 to 15 December 1993	20
Figure 15.	Comparison of measured and estimated October 1999 water levels at Grays Harbor on both ocean and bay sides	22
Figure 16.	Estimated water level at Grays Harbor, 8-16 December 1993	23
Figure 17.	Initial breach formation, looking seaward, 10 December 1993	24
Figure 18.	Breach, 17 December 1993; tide elevation +2.0 m mllw	25
Figure 19.	Comparison of breach channel cross section.....	26
Figure 20.	Difference plot of March 1994 and August 1994 breach bathymetry data sets	27
Figure 21.	Recession of vegetation line at South Beach under breach condition	29
Figure 22.	Field data collection station locations, 1999.....	34
Figure 23.	M2D water level results compared to ADCIRC calculations and measurements.....	35
Figure 24.	M2D current speed results compared to ADCIRC calculations and measurements at sta 4	35

Figure 25.	M2D current speed results compared to ADCIRC calculations and measurements at sta 2	36
Figure 26.	M2D current speed results compared to ADCIRC calculations and measurements at sta 5	36
Figure 27.	Calculated wave height with and without bottom friction at sta 2 compared to measurements	37
Figure 28.	Calculated wave height with and without bottom friction at sta 4 compared to measurements	38
Figure 29.	Calculated wave height with and without bottom friction at sta 5 compared to measurements	38
Figure 30.	Existing condition bathymetry.....	40
Figure 31.	December 1993 bathymetry.....	40
Figure 32.	March 1994 bathymetry.....	41
Figure 33.	August 1994 bathymetry	41
Figure 34.	Large breach bathymetry	42
Figure 35.	Nested M2D grids.....	43
Figure 36.	Nested STWAVE grids.....	43
Figure 37.	Nested M2D and STWAVE grids	44
Figure 38.	Flood flow for pre-breach, tide-only simulation (Run 113)	47
Figure 39.	Ebb flow for pre-breach, tide-only simulation (Run 113)	47
Figure 40.	Flood flow for pre-breach, typical wave simulation (Run 114).....	48
Figure 41.	Ebb flow for pre-breach, typical wave simulation (Run 114)	48
Figure 42.	Flood flow for pre-breach, west-southwest storm wave simulation (Run 115).....	49
Figure 43.	Ebb flow for pre-breach, west-southwest storm wave simulation (Run 115).....	49
Figure 44.	Flood flow for pre-breach, west-northwest storm wave simulation (Run 116).....	50
Figure 45.	Ebb flow for pre-breach, west-northwest storm wave simulation (Run 116).....	50
Figure 46.	Observation Point 1 overlaid on December 1993 aerial photograph of breach.....	52
Figure 47.	Time series of current speed at Point 1 for December 1993 breach.....	52
Figure 48.	Flood flow for December 1993 breach, tide-only simulation (Run 101).....	54
Figure 49.	Ebb flow for December 1993 breach, tide-only simulation (Run 101).....	54

Figure 50.	Flood flow for December 1993 breach, typical wave simulation (Run 102).....	55
Figure 51.	Ebb flow for December 1993 breach, typical wave simulation (Run 102).....	55
Figure 52.	Flood flow at hour 44.5 for December 1993 breach, west-southwest storm wave simulation (Run 103).....	56
Figure 53.	Flood flow at hour 45.5 for December 1993 breach, west-southwest storm wave simulation (Run 103).....	56
Figure 54.	Ebb flow for December 1993 breach, west-southwest storm wave simulation (Run 103).....	57
Figure 55.	Flood flow for December 1993 breach, west-northwest storm wave simulation (Run 104).....	57
Figure 56.	Ebb flow for December 1993 breach, west-northwest storm wave simulation (Run 104).....	58
Figure 57.	Observation points overlaid on March 1994 aerial photograph of breach.....	58
Figure 58.	Time-series of current speed at Point 3 for March 1994 breach.....	59
Figure 59.	Flood flow for March 1994 breach, tide-only simulation (Run 105).....	60
Figure 60.	Ebb flow for March 1994 breach, tide-only simulation (Run 105).....	60
Figure 61.	Flood flow for March 1994 breach, typical wave simulation (Run 106).....	61
Figure 62.	Ebb flow for March 1994 breach, typical wave simulation (Run 106).....	61
Figure 63.	Flood flow for March 1994 breach, west-southwest storm wave simulation (Run 107).....	62
Figure 64.	Ebb flow for March 1994 breach, west-southwest storm wave simulation (Run 107).....	62
Figure 65.	Flood flow for March 1994 breach, west-northwest storm wave simulation (Run 108).....	63
Figure 66.	Ebb flow for March 1994 breach, west-northwest storm wave simulation (Run 108).....	63
Figure 67.	Observation points overlaid on August 1994 aerial photograph of breach.....	64
Figure 68.	Time series of current speed at Point 3 for August 1994 breach.....	65
Figure 69.	Time series of current speed at Point 2 for August 1994 breach.....	65

Figure 70.	Time series of current speed at Point 1 for August 1994 breach.....	66
Figure 71.	Time series of current speed at Point 5 for August 1994 breach.....	66
Figure 72.	Flood flow for August 1994 breach, tide-only simulation (Run 109).....	68
Figure 73.	Ebb flow for August 1994 breach, tide-only simulation (Run 109).....	68
Figure 74.	Flood flow for August 1994 breach, typical wave simulation (Run 110).....	69
Figure 75.	Ebb flow for August 1994 breach, typical wave simulation (Run 110).....	69
Figure 76.	Flood flow for August 1994 breach, west-southwest storm wave simulation (Run 110).....	70
Figure 77.	Ebb flow for August 1994 breach, west-southwest storm wave simulation (Run 110).....	70
Figure 78.	Flood flow for August 1994 breach, west-northwest storm wave simulation (Run 111).....	71
Figure 79.	Ebb flow for August 1994 breach, west-northwest storm wave simulation (Run 111).....	71
Figure 80.	General flow patterns for December 1993, March 1994, and August 1994, and locations of calculation points discussed.....	72
Figure 81.	Original large-breach concept; distances and depths in feet (Source: Seattle District).....	73
Figure 82.	Observation points for large-breach simulations.....	73
Figure 83.	Time series of current speed at Point A for large breach.....	74
Figure 84.	Time series of current speed at Point B for large breach.....	74
Figure 85.	Time series of current speed at Point C for large breach.....	75
Figure 86.	Time series of current speed at Point D for large breach.....	75
Figure 87.	Flood flow for large breach, tide-only simulation (Run 117).....	76
Figure 88.	Ebb flow for large breach, tide-only simulation (Run 117).....	77
Figure 89.	Flood flow for large breach, typical wave simulation (Run 118).....	77
Figure 90.	Ebb flow for large breach, typical wave simulation (Run 118).....	78
Figure 91.	Flood flow for large breach, west-southwest storm wave simulation (Run 119).....	78
Figure 92.	Ebb flow for large breach, west-southwest storm wave simulation (Run 119).....	79

Figure 93.	Flood flow for large breach, west-northwest storm wave simulation (Run 120).....	79
Figure 94.	Ebb flow for large breach, west-northwest storm wave simulation (Run 120).....	80
Figure 95.	Large breach without jetty protective land mass	81
Figure 96.	Large breach without jetty protective land mass and depth reduced to 4.55 m below mtl	81
Figure 97.	Change in flood flow characteristics at hour 39 with large breach.....	83
Figure 98.	Shinnecock Inlet, NY, showing severely eroded downdrift beach adjacent to downdrift jetty.....	93
Figure 99.	Mattituck Inlet, NY, with a spit encroaching from the east through a breach in the barrier island	93
Figure 100.	Degraded north jetty at Coos Bay, OR, and inception of flanking channel expected to lead to a breach	94
Figure 101.	Definition sketch for rectangular barrier island.....	102
Figure 102.	Definition sketch for layered barrier island cross section.....	104
Figure 103.	Definition sketch for vertical layers and horizontal sections.....	104
Figure 104.	Definition sketch for semicircular-segment barrier island cross section	105
Figure 105.	Validation of layer breach model algorithms by comparison to semicircular-segment analytical solution.....	105
Figure 106.	Intial cross-sectional profiles for Cases T2, T4, and T7.....	106
Figure 107.	Measured water-surface elevation from bottom for Cases T2, T4, and T7.....	107
Figure 108.	Measured and calculated width of dike breach, laboratory experiment.....	108
Figure 109.	Calculated velocity in breach, laboratory experiment	108
Figure 110.	USACE breaching laboratory experiment schematic	109
Figure 111.	Measured morphologic evolution at transect D during BR1 laboratory experiment.....	110
Figure 112.	Measured and modeled channel velocity and elevation relative to water-surface elevation for BR1	111
Figure 113.	Breach width and depth, BR1	112
Figure 114.	Breach width and depth, BR2.....	112
Figure 115.	Calculated breach channel velocity in BR1 and BR2.....	113
Figure 116.	Location map for Moriches Inlet, Long Island, NY	114
Figure 117.	Moriches Inlet breach development.....	115

Figure 118. Velocity in Moriches Inlet breach and inlet during breach growth	116
Figure 119. Calculated breach width and observations, 1980, Moriches Inlet	117
Figure 120. Calculated breach depth and observations, 1980, Moriches Inlet	118
Figure 121. Location of lateral sections, Grays Harbor	119
Figure 122. Estimated cross-sectional profiles for Sections 1 and 2, Grays Harbor	120
Figure 123. Wave setup calculated added to input water level	121
Figure 124. Comparison of calculated wave setup with results from IMS-M2D Grays Harbor	122
Figure 125. Linear regression of wave setup comparison shown in Figure 2	122
Figure 126. Calculated breach width and observations, 1993-1995, Grays Harbor	124
Figure 127. Calculated breach depth and observations , 1993-1995, Grays Harbor	125
Figure 128. Calculated current velocity in breach, 1993-1995, Grays Harbor	125
Figure 129. Sediment transport rates at bottom and side of breach, and alongshore, 1993-1995, Grays Harbor.....	126
Figure 130. Ratio of calculated cross-sectional breach area 1993-1995 and inlet entrance area, Grays Harbor.....	126
Figure 131. Sediment budget for the Half Moon Bay and south jetty area developed from net morphology change between 1996 and 2002	131
Figure A1. Breach, January 1994.....	A2
Figure A2. Breach, 2 February 1994, tidal elevation +2.0 ft mllw	A2
Figure A3. Breach, 6 March 1994, tidal elevation +1.3 ft mllw	A3
Figure A4. Breach, 10 August 1994, tidal elevation +2.3 ft mllw	A3
Figure B1. Observation points for large-breach alternatives	B1
Figure B2. Time series of current speed at Point A for large-breach alternatives, tide only	B2
Figure B3. Time series of current speed at Point B for large-breach alternatives, tide only	B2
Figure B4. Time series of current speed at Point C for large-breach alternatives, tide only	B3
Figure B5. Time series of current speed at Point D for large-breach alternatives, tide only	B3

Figure B6.	Time series of current speed at Point E for large-breach alternatives, tide only.....	B4
Figure B7.	Time series of current speed at Point A for large-breach alternatives, tide only.....	B4
Figure B8.	Time series of current speed at Point G for large-breach alternatives, tide only.....	B5
Figure B9.	Time series of current speed at Point H for large-breach alternatives, tide only.....	B5
Figure B10.	Time series of current speed at Point I for large-breach alternatives, tide only.....	B6
Figure B11.	Time series of current speed at Point J for large-breach alternatives, tide only.....	B6
Figure B12.	Time series of current speed at Point K for large-breach alternatives, tide only.....	B7
Figure B13.	Time series of current speed at Point A for large-breach alternatives, west-southwest storm simulations.....	B7
Figure B14.	Time series of current speed at Point B for large-breach alternatives, west-southwest storm simulations.....	B8
Figure B15.	Time series of current speed at Point C for large-breach alternatives, west-southwest storm simulations.....	B8
Figure B16.	Time series of current speed at Point D for large-breach alternatives, west-southwest storm simulations.....	B9
Figure B17.	Time series of current speed at Point E for large-breach alternatives, west-southwest storm simulations.....	B9
Figure B18.	Time series of current speed at Point F for large-breach alternatives, west-southwest storm simulations.....	B10
Figure B19.	Time series of current speed at Point G for large-breach alternatives, west-southwest storm simulations.....	B10
Figure B20.	Time series of current speed at Point H for large-breach alternatives, west-southwest storm simulations.....	B11
Figure B21.	Time series of current speed at Point I for large-breach alternatives, west-southwest storm simulations.....	B11
Figure B22.	Time series of current speed at Point J for large-breach alternatives, west-southwest storm simulations.....	B12
Figure B23.	Time series of current speed at Point K for large-breach alternatives, west-southwest storm simulations.....	B12
Figure B24.	Time series of current speed at Point A for large-breach alternatives, west-northwest storm simulations.....	B13
Figure B25.	Time series of current speed at Point B for large-breach alternatives, west-northwest storm simulations.....	B13

Figure B26. Time series of current speed at Point C for large-breach alternatives, west-northwest storm simulations	B14
Figure B27. Time series of current speed at Point D for large-breach alternatives, west-northwest storm simulations	B14
Figure B28. Time series of current speed at Point E for large-breach alternatives, west-northwest storm simulations	B15
Figure B29. Time series of current speed at Point F for large-breach alternatives, west-northwest storm simulations	B15
Figure B30. Time series of current speed at Point G for large-breach alternatives, west-northwest storm simulations	B16
Figure B31. Time series of current speed at Point H for large-breach alternatives, west-northwest storm simulations	B16
Figure B32. Time series of current speed at Point I for large-breach alternatives, west-northwest storm simulations	B17
Figure B33. Time series of current speed at Point J for large-breach alternatives, west-northwest storm simulations	B17
Figure B34. Time series of current speed at Point K for large-breach alternatives, west-northwest storm simulations	B18
Figure B35. Flood flow for existing (pre-breach), tide only (Run 113)	B18
Figure B36. Ebb flow for existing (pre-breach), tide only (Run 113)	B19
Figure B37. Flood flow for existing (pre-breach), west-southwest storm wave simulation (Run 115)	B19
Figure B38. Ebb flow for existing (pre-breach), west-southwest storm wave simulation (Run 115)	B20
Figure B39. Flood flow for existing (pre-breach), west-northwest storm wave simulation (Run 116)	B20
Figure B40. Ebb flow for existing (pre-breach), west-northwest storm wave simulation (Run 116)	B21
Figure B41. Flood flow for large breach, tide only simulation (Run 117)	B21
Figure B42. Ebb flow for large breach, tide only simulation (Run 117)	B22
Figure B43. Flood flow for large breach, west-southwest storm wave simulation (Run 119)	B22
Figure B44. Ebb flow for large breach, west-southwest storm wave simulation (Run 119)	B23
Figure B45. Flood flow for large breach, west-northwest storm wave simulation (Run 120)	B23
Figure B46. Ebb flow for large breach, west-northwest storm wave simulation (Run 120)	B24
Figure B47. Flood flow for large breach without jetty protective landmass, tide only (Run 121)	B24

Figure B48. Ebb flow for large breach without jetty protective landmass, tide only (Run 121).....	B25
Figure B49. Flood flow for large breach without jetty protective landmass, west-southwest storm wave simulation (Run 122)	B25
Figure B50. Ebb flow for large breach without jetty protective landmass, west-southwest storm wave simulation (Run 122)	B26
Figure B51. Flood flow for large breach without jetty protective landmass, west-northwest storm wave simulation (Run 123)	B26
Figure B52. Ebb flow for large breach without jetty protective landmass, west-northwest storm wave simulation (Run 123)	B27
Figure B53. Flood flow for large breach without jetty protective landmass, depth = 4.55 m, mtl, tide only (Run 124)	B27
Figure B54. Ebb flow for large breach without jetty protective landmass, depth = 4.55, mtl, tide only (Run 124)	B28
Figure B55. Flood flow for large breach without jetty protective landmass, depth = 4.55, mtl, west-southwest storm wave simulation (Run 125).....	B28
Figure B56. Ebb flow for large breach without jetty protective landmass, depth = 4.55 m, mtl, west-southwest storm wave simulation (Run 125).....	B29
Figure B57. Flood flow for large breach without jetty protective landmass, depth = 4.55 m, mtl, west-northwest storm wave simulation (Run 126).....	B29
Figure B58. Ebb flow for large breach without jetty protective landmass, depth = 4.55 m, mtl, west-northwest storm wave simulation (Run 126).....	B30

List of Tables

Table 1. Extreme Significant Wave Height.....	19
Table 2. Tidal Datum Relationships Relative to mllw.....	20
Table 3. Water Level Correlation Factors	21
Table 4. Estimated Breach Width.....	25
Table 5. South Beach Shoreline Recession	29
Table 6. RMS Difference, STWAVE With and Without Bottom Friction.....	37
Table 7. Hydrodynamic-Wave Model Simulations	45
Table 8. Dimensions of 1980 Breach at Moriches Inlet, NY, and Aerial Photograph Analysis in this Study	115

Preface

This report describes the evolution of the December 1993 breach at Grays Harbor, WA, and evaluates the risk to the navigation project and upland facilities to assist in developing a long-term management plan for prevention of breaching at south jetty, Grays Harbor. Work was conducted for the U.S. Army Engineer District, Seattle, by the U.S. Army Engineer Research and Development Center (ERDC), Coastal Hydraulics Laboratory (CHL), Vicksburg, MS. The Coastal Inlets Research Program sponsored by Headquarters, U.S. Army Corps of Engineers, partially supported development work for the breach model applied in this study. Hiram T. Arden, Navigation Section, Operations Division, was the Seattle District point of contact and Program Manager for the study, with technical assistance and review of this report by Seattle District staff members in the Civil Soils Section.

This report was prepared by Ty V. Wamsley, Coastal Processes Branch (CPB), CHL, Mary A. Cialone, CPB, Kenneth J. Connell, Coastal Engineering and Geomorphology Branch (CEGB), CHL, and Dr. Nicholas C. Kraus, Senior Scientists Group, CHL. Dr. Kraus served as CHL point of contact and provided technical direction for the study. J. Holley Messing, CEGB, formatted this report. Work was performed under the general administrative supervision of Thomas W. Richardson, Director, CHL, and Dr. William D. Martin, Deputy Director, CHL.

Dr. James R. Houston was Director of ERDC, and COL Richard B. Jenkens, was Commander and Executive Director.

Conversion Factors: Non-SI to SI Units of Measurement

Non-SI units of measurement appearing in this report can be converted to SI units as follows:

Multiply	By	To Obtain
acres	0.4047	hectare
cubic yards	0.7645549	cubic meters
feet	0.3048	meters
Miles (U.S. Statute)	1.609347	kilometers
square miles	2.590	square kilometers

1 Introduction

A coastal breach is a new opening in a narrow landmass such as a barrier spit or barrier island that allows water to flow between the water bodies on each side. Elevated water level, combined with larger and longer period waves during storms, and inadequate beach and dune volume promote breaching. Sometimes, a breach is open only at higher normal tide and is called a high-tide breach. Such a breach is prone to closure by sediment transported to it by the longshore current. If a breach remains open during all phases of the normal tide, then the possibility exists for the breach to become self-sustaining in the form of an inlet.

Every year around the United States coast, breaching takes place on barrier islands, barrier spits, and closed river mouths. Breaches occur naturally, or they can be purposefully dug or dredged, and such a breach may have positive or negative engineering and environmental consequences.

In December 1993, the south barrier spit at Grays Harbor, WA, experienced a breach adjacent to the south jetty, and from October to December 1994 the U.S. Army Engineer District, Seattle (hereafter Seattle District) closed it with sand dredged from the navigation channel. In 2001, breaching at the same location became imminent. In response, the Seattle District restored the breach fill by placing sand from an upland stockpile and planting native American dune grass to prevent wind and rain erosion of the restored area. This study investigates and quantifies breaching processes adjacent to the south jetty at Grays Harbor.

This chapter gives the purpose for the study, background on the Grays Harbor navigation project and 1993 breach, and an overview of the process of coastal breaching. Discussion of the study context within regional sediment processes concludes the chapter.

Purpose of Study

The purpose of this study was to analyze the December 1993 breach at Grays Harbor, WA, and assess the threat to the Federal Navigation Project had the breach not been filled the following fall. The study was conducted by quantifying evolution of breach morphology (Chapter 2); numerically simulating the ocean wave and water level conditions producing the current through such a breach, including investigation of wide-area implications for the current in Grays Harbor (Chapter 3); and numerical modeling breach evolution (Chapter 4). Conclusions are given in Chapter 5.

Breaching near or adjacent to a navigable coastal inlet holds potential for compromising the functioning of the navigation project and increasing its operation and maintenance cost. A breach increases the effective cross-sectional area of the combined inlet-breach system. Because the inlet and cross-sectional area and tidal prism of the back bay have a fixed relation, flows through the breach decrease the capacity of the channel to confine the tidal current and scour sediment. In some situations, the configuration of the bay and flood shoal may favor the breach as the main channel in directing tidal flow. Breach erosion near a jetty also allows for the presence of greater current velocities and wave action, and may threaten the stability of the structure (Kraus and Wamsley 2003).

In addition, the presence of a breach can alter regional hydrodynamic and sediment transport processes. Flow through a breach will change the balance of water surface elevation and current around the inlet and bay system. The new balance can alter flows, hence sediment transport, at considerable distance from the breach.

The evolution of the 1993 breach is analyzed with a Geographic Information System (GIS). The width of the breach and erosion of the adjacent shoreline are quantified from aerial photographs. Shoreline position and bottom configurations in the vicinity of the former breach are the basis of numerical modeling of wave- and tide-driven currents. Estimates are made of the wave and current climate at South Beach, Point Chehalis, and in Half Moon Bay under the assumption of a breach at the jetty. Hydrodynamics for various alternatives of further erosion of the breach are modeled to evaluate flow patterns in a developed breach condition. Sediment transport and evolution of the breach are modeled to assess the potential for continued breach growth and long-term assessment of breach stability. Study products are intended to assist the Seattle District in developing a long-term management plan for protecting Federal navigation project features.

Grays Harbor, Washington

Grays Harbor is located on the southwest Washington coast at the mouth of the Chehalis River, about 45 miles north of the Columbia River mouth. The harbor is 21 km wide at its broadest point, and 24 km long from Aberdeen, WA, to the entrance. The water surface area is 91 square miles¹ at mean higher high water (mhhw) and 38 square miles at mean lower low water (mllw). The estuary is enclosed on the ocean side by two spits, Point Brown on the north and Point Chehalis on the south. The spits are separated by a 2-mile-wide opening that forms the harbor entrance. Two convergent rock jetties, the north jetty and south jetty, extend seaward from the spit points. The jetties are part of the Grays Harbor Navigation Project, which is a federally constructed and maintained navigation channel that allows deep-draft shipping through the outer bar, Grays Harbor estuary, and the Chehalis River to Cosmopolis (Figure 1).

¹ This study involves analysis of historic and recent engineering documents and data with values expressed in American Customary (non-SI) units. To maintain continuity with the previous body of work, the original units are retained in their context. Measurements and calculations made as part of the present study are expressed in SI units. A table of factors for converting non-SI units of measurement to SI units is presented on page xv.

The Seattle District has conducted investigations of coastal and inlet processes at Grays Harbor, and the present study takes advantage of the modeling technology, data sets, and background information available from those recent studies. Osborne et al. (2003) compiled the engineering history and acting coastal processes at the south jetty of Grays Harbor. Kraus and Arden (2003, 2004) edited technical reports documenting numerical simulations, morphology change, sediment budget, and measurements at Grays Harbor, with emphasis on the north jetty and adjacent beach, but also covering the entire harbor and regional oceanographic processes. Cialone and Kraus (2001, 2002) and Cialone et al. (2002) discuss modeling of waves and circulation at and around Grays Harbor.

1993 Breach and Recent Breach Potential

In December 1993, persistent shoreline erosion near the south jetty culminated in the formation of a breach between the jetty and the adjacent South Beach. The city of Westport, Grays Harbor County, and the Port of Grays Harbor were alarmed by the rapid growth of the breach and expressed concern for further erosion of the South Beach, damage to water wells and a sewer treatment plant, and consequences for the Grays Harbor Navigation Project as the breach continued to grow during the winter storm season (Figure 2). In March 1994, the Seattle District was directed by the U.S. Department of the Army to close the breach. The Seattle District closed the breach between October and December 1994 with 600,000 cu yd of sand dredged from the navigation channel at a cost of \$3,730,000. The breach closure was considered a temporary measure to protect the Grays Harbor navigation project and to alleviate local concerns.

In 1997, the Seattle District completed a comprehensive study to determine the most appropriate long-term solution for protecting the Federal navigation project features and alleviate local concerns (U.S. Army Engineer District, Seattle 1997). Several alternatives were considered, and the study concluded that extending the south jetty to meet the existing Point Chehalis revetment, combined with beach nourishment, was the most appropriate solution. The Point Chehalis revetment extension and fill were constructed as the first phase from November 1998 to March 1999.

The second phase of the project was modified to incorporate a soft solution design. The plan consisted of construction of a wave diffraction mound to reduce wave-induced erosion of Half Moon Bay, a cobble transition beach designed to slow Half Moon Bay beach erosion directly adjacent to the jetty, and repair work to strengthen the landward end of the south jetty at the breach fill. Between December 1999 and February 2000, a wave diffraction mound was constructed and 11,600 cu yd of rounded cobble, and gravel was placed on the adjacent Half Moon Bay beach. The cobble placement did not extend as far eastward as originally designed because of environmental concerns. The eastern portion of the south jetty was also reinforced. In January of 2002, an additional 16,100 cu yd of cobble and gravel was placed to slow erosion of the breach fill.

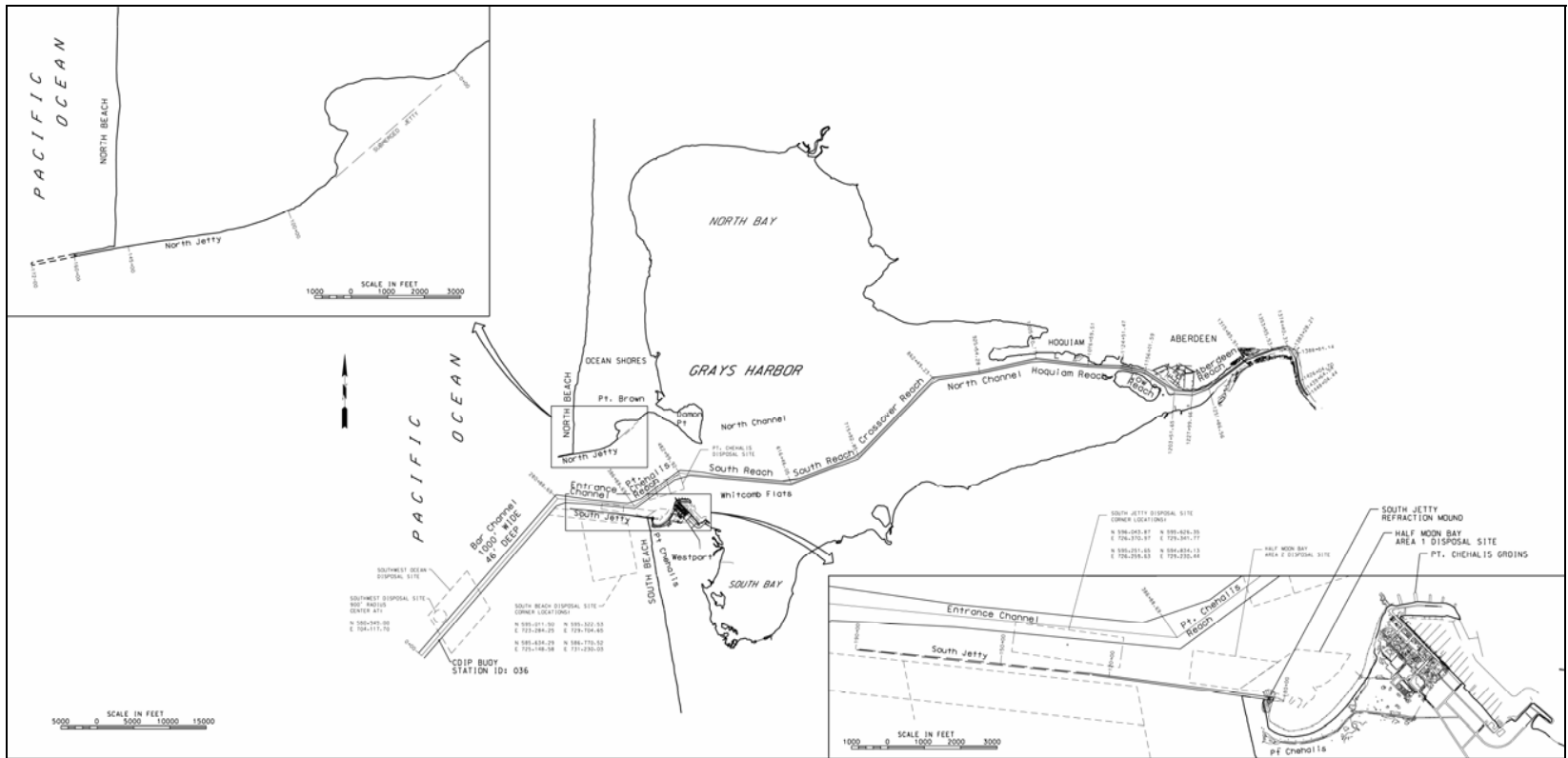


Figure 1. Grays Harbor Navigation Project (figure provided by Seattle District)



Figure 2. Breached area at Grays Harbor south jetty, 6 March 1994

In November 2001, a series of storms began to overtop the breach fill, again raising concern of local residents, industry, government, and the Seattle District. In response, in April 2002 approximately 125,000 cu yd of sand from an upland stockpile was placed at the breach fill to restore the breach fill. In November 2002, approximately 50,000 sprigs of native American dune grass were planted on 3 acres of the breach fill to resist wind and rain erosion (Arden 2003). The November 2001 weakened condition of the barrier spit is attributed to lack of sediment supply on the ocean side, recession of the shoreline in Half Moon Bay, heavy rainfall that created deep gullies that can serve as pilot channels for breaching, and multiple winter storms with high water level and large waves. An additional 27,000 cu yd of sand was placed in the southwest corner of Half Moon Bay in February 2004 to further protect the eroding breach fill.

Overview of Breaching Process

The processes of coastal breaching have received little study (Kraus et al. 2002) and, until recently, predictive models for describing the breaching process have been lacking. Breaching potential is maximized if the barrier is low and narrow. Narrowing of the barrier can be caused by erosion on either the beach or bay or estuary side. At inlets stabilized by jetties that terminate along a sandy beach, such as that at Grays Harbor, a phenomenon known as inner bank erosion is often observed. Seabergh (1999) investigated inner bank erosion with a physical model of an idealized inlet and found that the erosion is the result of wave action combined with tidal and wave-induced currents. The waves initially cut a trough at the intersection of the jetty and sandy shoreline, and then the trough gradually widens to allow diffracted waves to further erode the shore, both behind the structure and bayward. The tidal and wave-induced current then removes the sediment from the inner (bayside) shoreline. If the water level is held constant and a fixed control point such as the south jetty terminus exists, an equilibrium shape is reached similar to an open-coast crenulate bay (Krumbein 1944; Silvester 1960, 1970; Yasso 1965; Hsu and Evans 1989; Moreno and Kraus 1999). The erosion forms an embayment that narrows the barrier by cutting back the inner bank toward the ocean beach. Such crenulated bays are ubiquitous along the coast worldwide.

Lowering of the barrier is a consequence of dune degradation. Several causes of dune degradation can be identified, including fixed footpaths for beach access, seepage, undercutting and failure from wave attack, gullies formed by heavy precipitation, and wave overtopping. If a barrier is relatively narrow, seepage through the porous sediment can occur during periods of high water. Seepage may cause a sliding of a slope along a failure surface or piping. Piping undermines the dune and may collapse the dune body and lower the crest. Undercutting and subsequent failure of dunes is frequently observed (e.g., Carter et al. 1990). In small-scale wave tank experiments, Erikson et al. (2003) observed recession of the dune face as a two-step process described by notching and slumping or notching and toppling. Overtopping water lowers the dune crest by scour and infiltration. Infiltration leads to a decrease in dune slope stability due to saturation and air inclusion. The presence of waves increases the sediment mobilization and transport.

The narrowing and lowering of the barrier creates localized low profiles in the dune system. Such areas are called pilot channels. While the water level is elevated, inundation occurs, and water begins to flow through the pilot channels. Once the dune crest is submerged, erosion in the breach occurs rapidly. After complete wash out of the dune, the breach widens by erosion at the back and deepens as flow scours the breach channel. The processes active at the breach banks are similar to the processes and mechanisms of riverbank erosion.

Processes of bank erosion fall into two groups, fluvial entrainment, and subaerial/subaqueous weakening and weathering. Fluvial processes relate to the hydraulics of flow. Fluvial entrainment causes bank recession by entraining bank material and transporting it downstream or the flow may scour the bed and cause a gravitational failure of the bank. Weakening and weathering of the bank material is controlled by sediment properties, vegetation, and climate conditions. The most effective processes of weakening and weathering are associated

directly with soil moisture. These processes either operate within the bank to reduce its strength or act on the bank to loosen and detach sediment particles.

Erosion of a noncohesive bank is primarily attributable to the avalanching of individual particles that are dislodged by shear stresses at the bank. Sediment is transported as bed load laterally from the bank to the bed and is carried downstream by the flow. If there is excessive erosion at the bed adjacent to the bank, the bank may erode by mass failure and avalanching.

Breach evolution is determined not only by the destructive forces of breach opening (erosion), but also by the constructive forces of breach filling. Breach filling is analogous to the closure of tidal inlets and coastal lagoon entrances, which has been investigated by many researchers (e.g., Bruun and Gerritsen 1960; Oertel 1972; FitzGerald 1988, 1996; Hayes 1975, 1991; Gordon 1990; Komar 1998; Kraus et al. 2002). Breach closure processes can be classified into two categories. The most common is closure by longshore sediment transport, depending on the supply of sediment and its rate. The second mechanism is onshore transport and primarily operates on microtidal coasts where the longshore sediment transport rate is small (Ranasinghe et al. 1999).

A tidal inlet, or breach, interrupts the longshore sediment transport, and a spit forms updrift of the breach channel if there is an available supply of sediment from longshore transport. If the breach flow is sufficiently strong to remove any sand deposited in the breach channel, a spit will not elongate. If, however, the breach flow does not scour the littorally derived sediment, a spit will continue to elongate, impede tidal flow through the breach, and eventually fill the breach channel (Smith and Zarillo 1988).

If a breach captures a significant portion of the tidal flow, further opening of the breach through erosion of the barrier can be severe. During January 1980, a storm resulted in a breach formed at the narrowest section of the barrier island 300 m east of the east jetty at Moriches Inlet on Long Island, NY, a Federal navigation project. By fall of 1980, the breach had widened to 885 m (Figure 3) and had a maximum depth of about 3 m. The net longshore drift is from east to west at this site. Although the east jetty is on the updrift side of the inlet, the barrier beach narrowed because of erosion due to strong ebb flow currents in the east-west channel on the bay side of the barrier island, combined with erosion on the Atlantic Ocean side about 300 m east of the jetty. The barrier was narrowed by bay-side and ocean-side erosion, and a moderate extratropical storm overwashed the barrier, initiating the breach. The breach captured a portion of the tidal flow, which scoured sand deposited in the breach channel by the longshore transport. The U.S. Army Engineer District, New York (hereafter, New York District), was required to mechanically close the breach and did so in February 1981 through placement of approximately 1.2 million cu yd of dredged material.

The Moriches Inlet breach shares characteristics with the 1993 breach at Grays Harbor. Both breaches were on the updrift sides of a sediment-deprived barrier spit, occurred near jetties, and widened during the winter storm season. Also, both breaches were closed in response to the strong requests of local government and industry.

Central questions are: (a) will a breach occur for given hydrodynamic and barrier conditions, and (b) will a breach close once it is open? Modeling of breach processes is in its infancy. One published model is the morphologic-based incipient breaching model of Kraus (2003), which has recently been extended to include inlet hydrodynamics and infilling by longshore sediment transport (Kraus and Hayashi 2005). This model is described in Chapter 4. Another valuable means of examining the fate of a breach is to conduct a morphologic analysis, provided adequate data are available on the evolution of breach width and depth. Such is the case for the 1993 breach at Grays Harbor, as described in Chapter 2.

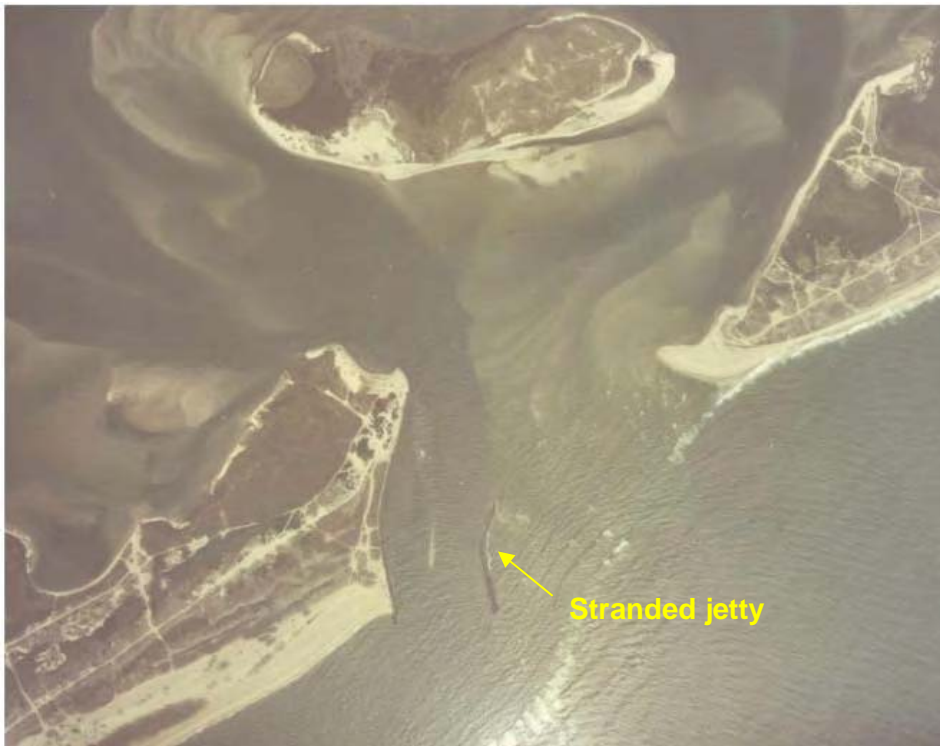


Figure 3. Breach at Moriches Inlet on 21 September 1980, 9 months after formation

Regional Processes

The U.S. Army Corps of Engineers (USACE) constructs, maintains, and operates Federal navigation projects within a regional sediment management (RSM) context. Regional sediment management recognizes that the consequences of navigation projects, intended and unintended, may extend beyond authorized physical limits. Martin and Rosati (2003) compiled civil works authorities and policies supporting implementation of regional sediment management. Among these policies, pursuant to Section 5 of the River and Harbor Act of 1935, "...each investigation on navigation improvements potentially affecting adjacent shorelines must include analysis of the probable

effects on shoreline configurations. A distance of not less than 10 miles on either side of the improvement should be analyzed” [USACE 2000; paragraph E-14(b)].

In addition, USACE actions at Federal navigation projects can be subjected to scrutiny under the Fifth Amendment of the United States Constitution, which states in part, “Private property [shall not] be taken for a public use, without just compensation.” The so-called takings amendment has been invoked against the USACE for alleged downdrift erosion induced by construction of jetties, as well for dredging of navigation channels.

An RSM analysis is both required by policy and prudent in identifying and avoiding possible detrimental impacts to private and local public property (that is considered as private) in the U.S. Court of Federal Claims. An RSM approach was followed in this study.

Independent Technical Review

The Seattle District convened an Independent Technical Review (ITR) of a draft of this report and a related draft report (Hughes and Cohen 2006) describing results of a movable-bed physical model of Half Moon Bay, located bayward of the south jetty. The ITR committee was composed of coastal experts outside of the USACE. The final version of these reports benefited from the ITR. The ITR and the response to reviewers is contained in Appendix C.

2 Analysis of December 1993 Breach

This chapter contains an analysis of the December 1993 breach adjacent to the south jetty at Grays Harbor. Observed shoreline recession that weakened the barrier spit and the storm wave conditions and associated water level that initiated the breach are discussed. A geomorphic analysis within a GIS is presented to document the evolution of the breach and adjacent shoreline.

Morphology Prior to Federal Navigation Project

Prior to jetty construction at Grays Harbor, inlet morphology was similar to other natural inlets. Shallow and extensive shoals existed adjacent to the beaches both north and south of the inlet. A large subaqueous spit south of the channel, called South Spit, controlled the orientation of the channel as it exited the estuary (Figure 4). The north spit penetrated into the inlet about 2 miles from Point Brown. The primary channel directed flow between the two spits and through the entrance from three secondary estuarine channels. See Byrnes and Baker (2003) for a complete discussion of Grays Harbor inlet and nearshore morphology both prior to and after construction of the Federal navigation project.

Similar to most unstructured inlets, Grays Harbor was dynamic, with large morphologic changes from year to year. Figures 5-9 illustrate the dynamic character of the inlet prior to jetty construction, both north and south of the inlet. In 1881 (Figure 5), a small marginal flood channel with a north-northeast orientation is evident near the landward terminus of the present day south jetty, in the vicinity of the 1993 breach location. Bathymetric information throughout the 1880s and 1890s indicates that the channel was ephemeral. In the 1883 and 1891 bathymetry, the channel had shoaled. The 1894 map shows the channel with the same north-northeast orientation. By 1898, the channel had nearly tripled in width, was oriented in a more northerly direction, and had deepened where it connected with the main inlet channel. Figure 10 is a plot of the bathymetry in 1900 after the south jetty had been constructed, cutting off the marginal channel. Sand was impounded south of the jetty.

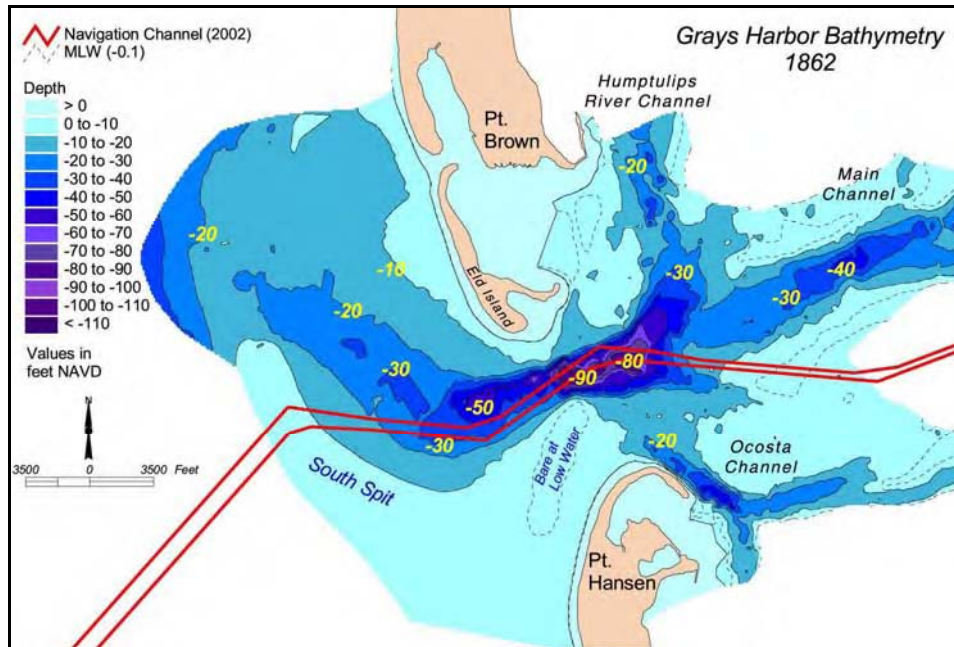


Figure 4. Bathymetric morphology for Grays Harbor entrance, 1862 (from Byrnes and Baker 2003)

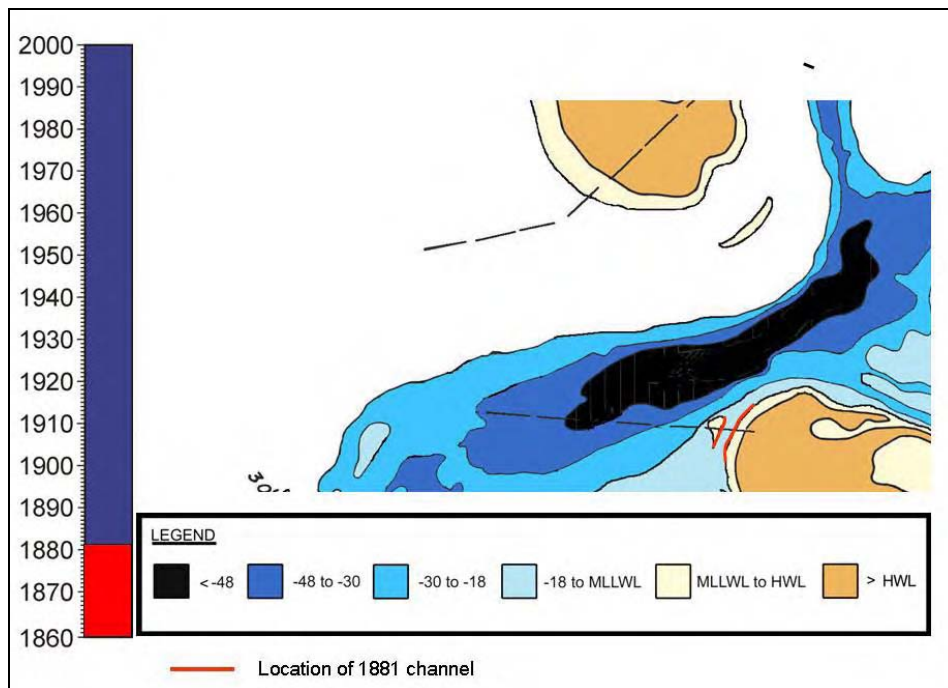


Figure 5. Bathymetric morphology for Grays Harbor entrance, 1881 (marginal flood channel exists)

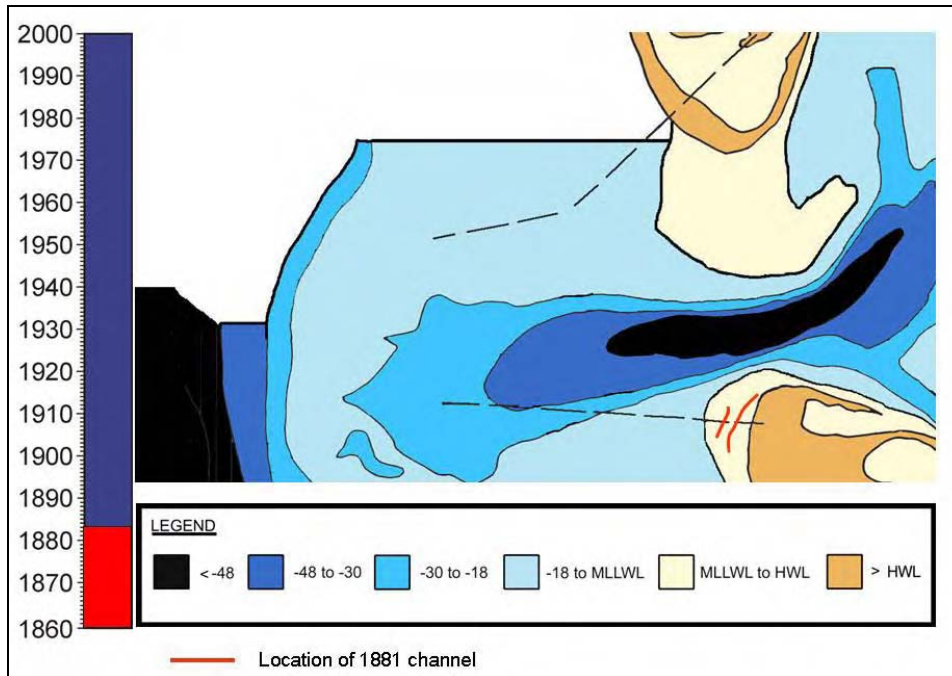


Figure 6. Bathymetric morphology for Grays Harbor entrance, 1883 (no marginal flood channel)

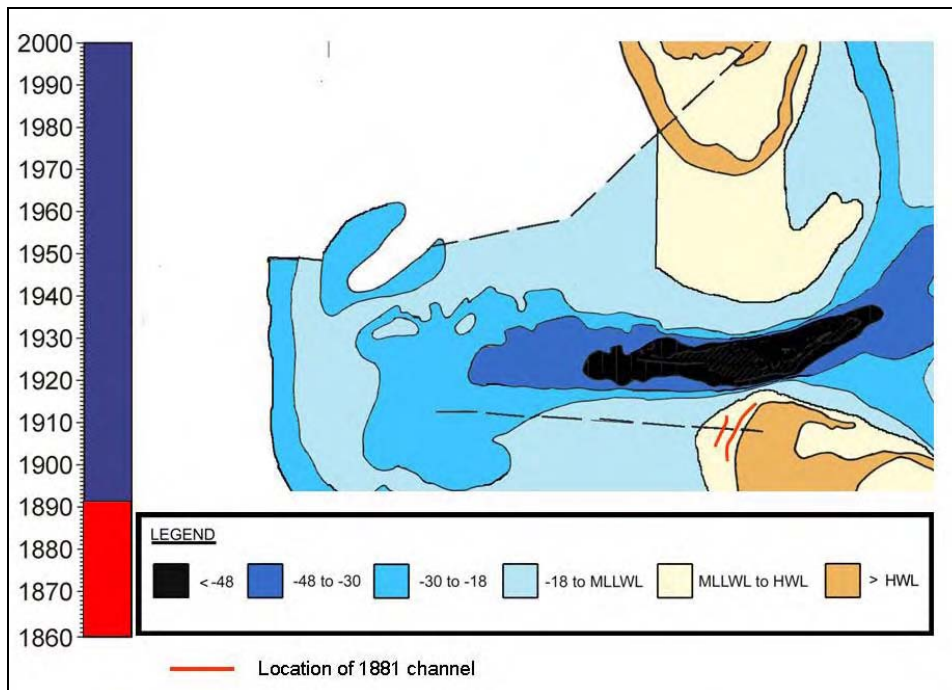


Figure 7. Bathymetric morphology for Grays Harbor entrance, 1891 (no marginal flood channel)

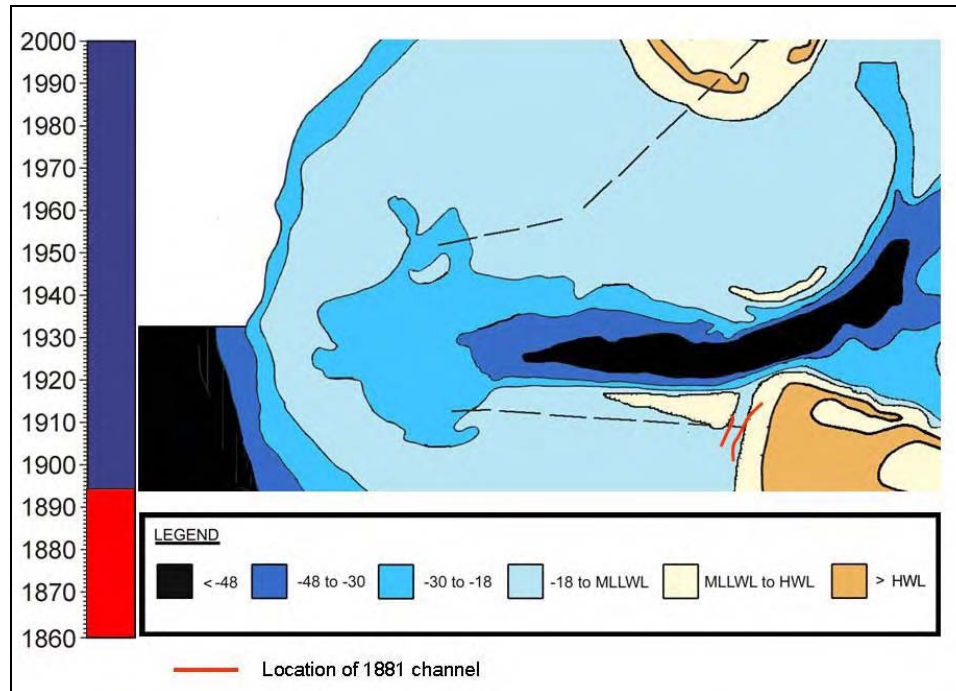


Figure 8. Bathymetric morphology for Grays Harbor entrance, 1894 (marginal flood channel exists)

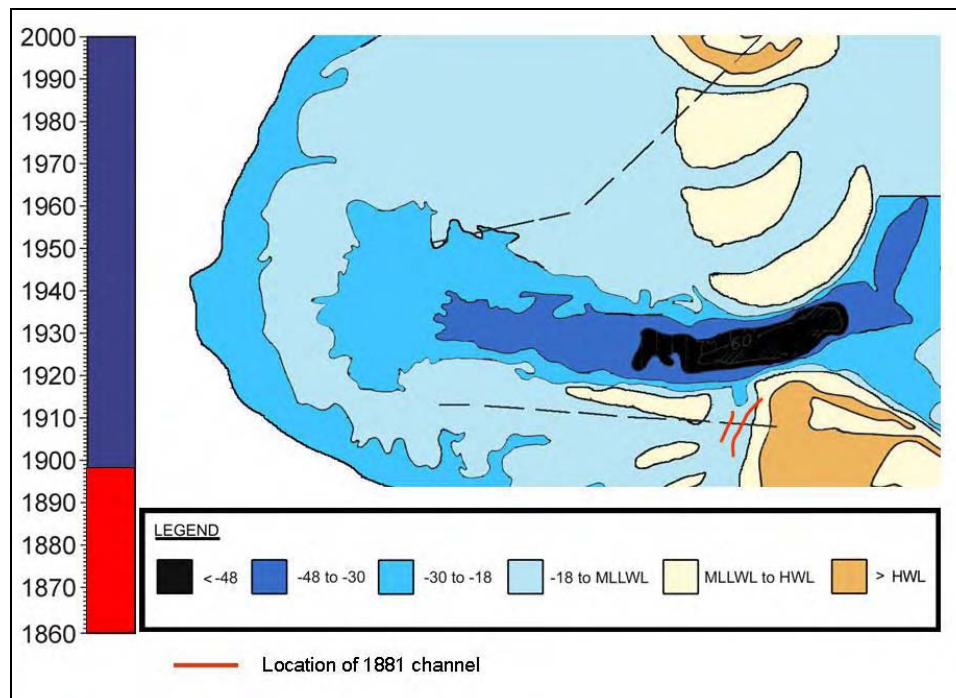


Figure 9. Bathymetric morphology for Grays Harbor entrance, 1898 (marginal flood channel exists)

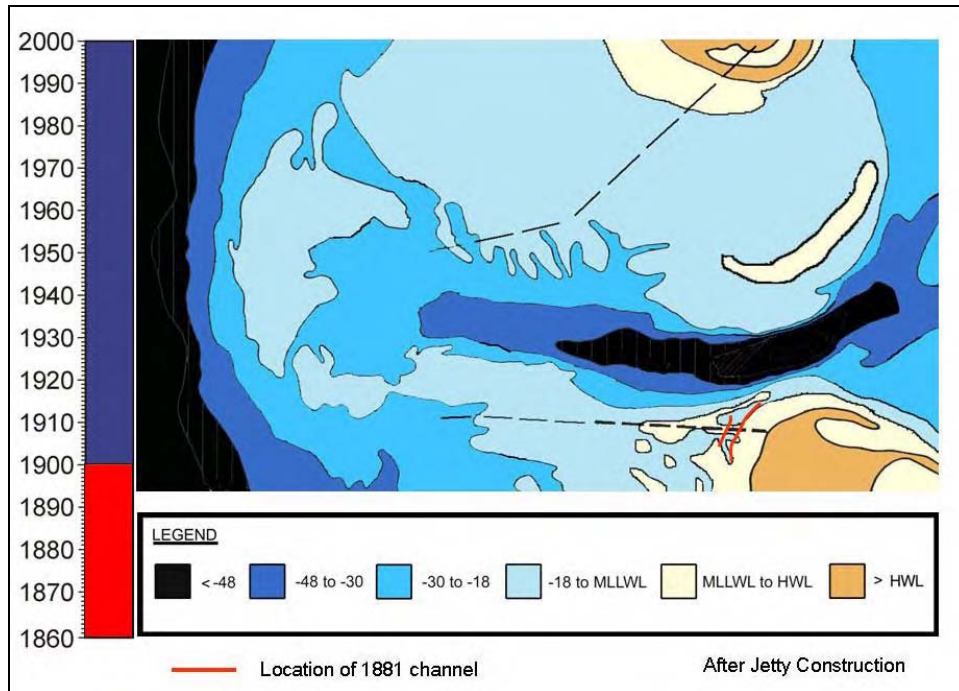


Figure 10. Bathymetric morphology for Grays Harbor entrance, 1900 (after jetty construction)

Because of their proximity, the breach and marginal flood channel have been compared. Although there are similarities, it may be misleading to directly compare a breach with the pre-navigation project marginal flood channel. The marginal flood channel differs from the breach channel in mode of formation and orientation. The marginal flood channel was formed by the scouring of flood tidal flow near the barrier beach. The breach formed as a result of storm waves and water levels cutting across the barrier. The two channels were also formed and evolved in different inlet environments, as the construction of the jetties significantly altered both the hydrodynamic and morphologic conditions at Grays Harbor.

The difference in the orientation of the two channels is shown in Figure 11. The 1894 bathymetry map shows the marginal flood channel, called the Canoe Channel, as well as the location of the landward terminus of the present day south jetty. The 2001 shoreline is plotted on the map to define the location of the marginal flood channel relative to the location of Half Moon Bay and the 1993 breach. The initial breach (December 1993) had an east-west orientation. By March 1994, the breach channel orientation had changed to a northeasterly direction. The breach channel was progressing to an orientation similar to the marginal flood channel, but the jetty acted as a barrier to westward growth or migration of the breach channel and constrained any further reorientation to the north.

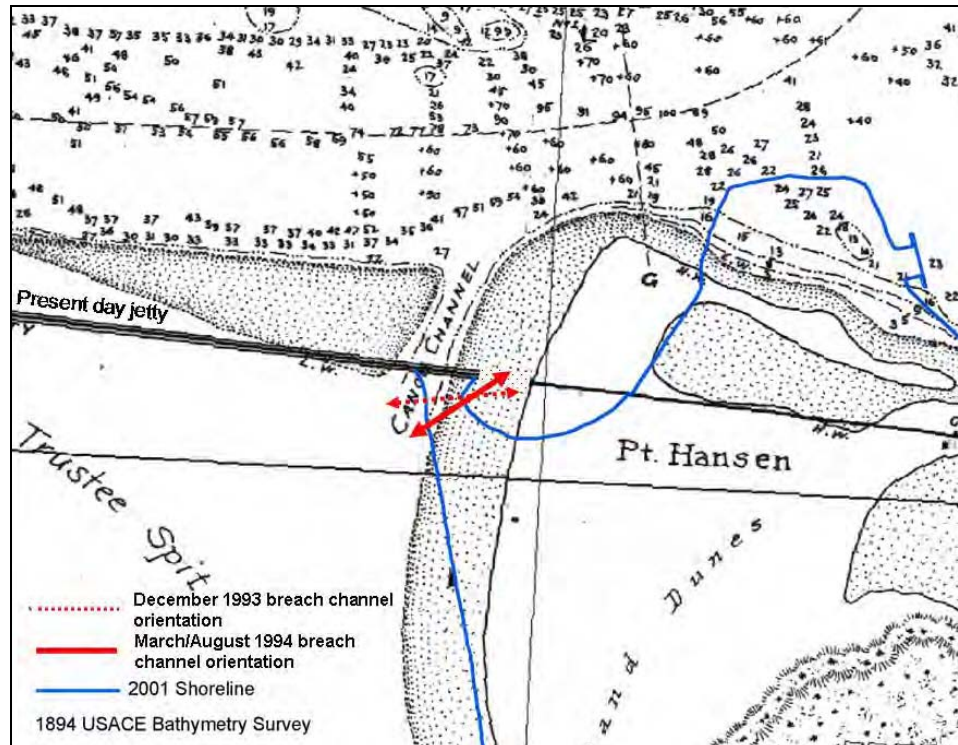


Figure 11. Location of marginal flood channel relative to 1993 breach

Shoreline Recession and Dune Lowering

The Grays Harbor breach resulted from persistent erosion on both the ocean (South Beach) and bay (Half Moon Bay) sides of Pt. Chehalis. Since 1967, the vegetation line at South Beach has receded at rates ranging from 2 to 62 ft/year. Shoreline recession rates increased during the mid- to late-1980s, with vegetation line recession rates ranging from 26 to 62 ft/year (Burch and Sherwood 1992). The USAED, Seattle (1997) estimated an average shoreline recession rate that varied from a low of 4 ft/year between 1973 and 1986, to a high of 54 ft/year between 1990 and 1992. For the period 1990 to 1996, which includes the December 1993 breach and subsequent fill, the USAED, Seattle (1997) computed an average recession rate of 36 ft/year. The recession, indicating volume loss of the beach, is greatest adjacent to the jetty, transitioning to a more stable shoreline position 3,500 ft south of the jetty (Sultan and Osborne 2004).

Volume losses in the nearshore region off South Beach have occurred as well. Burch and Sherwood (1992) analyzed bathymetric data from Seattle District surveys to compute sediment volume changes in the nearshore off South Beach through 1990, updating the earlier estimates of erosion and deposition from 1900 to 1960 provided in USACE, CTH (1967). The pattern of beach volume change in the nearshore area off South Beach was rapid erosion during the first third of the 90-year period, relative stability for the second third, and slow erosion during the last 30 years. Following jetty construction, approximately 36 million cu yd of sediment was lost from the area off South Beach until 1928. Between 1928 and 1943, net accretion occurred, and then the area remained relatively unchanged until about 1949. Beginning in 1949, the

area off South Beach has eroded almost continuously. The net loss from 1900 to 1990 was about 61 million cu yd (Burch and Sherwood 1992).

The offshore erosion at South Beach resulted when shoal migration and sand exchange between the entrance area and shelf seaward of South Beach was severed by the construction of the south jetty. Transport processes continue to mobilize and bypass sand from this area to the north side of the inlet. The littoral transport rates to South Beach were not sufficient to compensate for the natural sediment exchange processes at the inlet prior to jetty construction (Byrnes and Baker 2003).

The shoreline on the bay side of the spit has also receded as a result of inner bank erosion after the construction of the south jetty. After repairs to the landward portion of the south jetty were completed in 1939, cutting off the sediment supply from the south, erosion initiated formation of Half Moon Bay in 1946. The shoreline recession at Half Moon Bay before the breach occurred is plotted in Figure 12, taken from a general analysis of inner bank erosion at inlets (Seabergh 1999).

Burch and Sherwood (1992) examined shoreline change at Half Moon Bay by analyzing vegetation lines. From 1949 to 1967, Half Moon Bay grew with an average shoreline recession of 27 ft/year. The trend then reversed, and the shoreline advanced at a rate of about 13 ft/year from 1973 to 1977. From 1977 to about 1985, the movement of the vegetation line again reversed, and it receded at a slow average rate of about 3 ft/year. Analysis of high-water shorelines after 1985 indicates that recession rates have increased to an average of more than 10 ft/year. The USAED, Seattle (1997) estimated the long-term recession rate by measuring the change in shoreline position between 1957 and 1967, and between 1993 and 1996. The Half Moon Bay shoreline was found to have a long-term recession rate of between 5 and 10 ft/year. Similar to the behavior of South Beach, the Half Moon Bay shoreline data clearly demonstrate a long-term recessional (erosional) trend.

The persistent shoreline recession on both the ocean side and bay side at South Beach weakened the barrier and subjected the dune to wave attack. Damage to the dune system by ocean side wave attack and overtopping is evident in Figure 13a. An analysis of changes in the vegetation line was performed to quantify the shoreline recession that precipitated the breach. The analysis indicates that the barrier progressively deteriorated. Figure 13b is an aerial photograph of the breach taken on 17 December 1993 with the vegetation lines from July 1991, July 1992, and May 1993 overlaid. The progressive narrowing of the barrier spit is evident, including notching at the breach location. In July 1991, the vegetated dune system was approximately 170 m wide at the location where the barrier eventually breached. By July 1992, the vegetated barrier had narrowed to approximately 135 m, and in May of 1993 the vegetated barrier was only 30 m wide.

The barrier was predominantly narrowed due to shoreline recession and dune erosion on the ocean side. From July 1991 to July 1992, the vegetation line receded 25 m at South Beach and approximately 5 m at Half Moon Bay. From July 1992 to May 1993, a series of storms caused extensive shoreline recession and dune erosion. The vegetation line receded 100 m on the ocean, while

recession at Half Moon Bay was again about 5 m for this 10-month period that included winter storms.

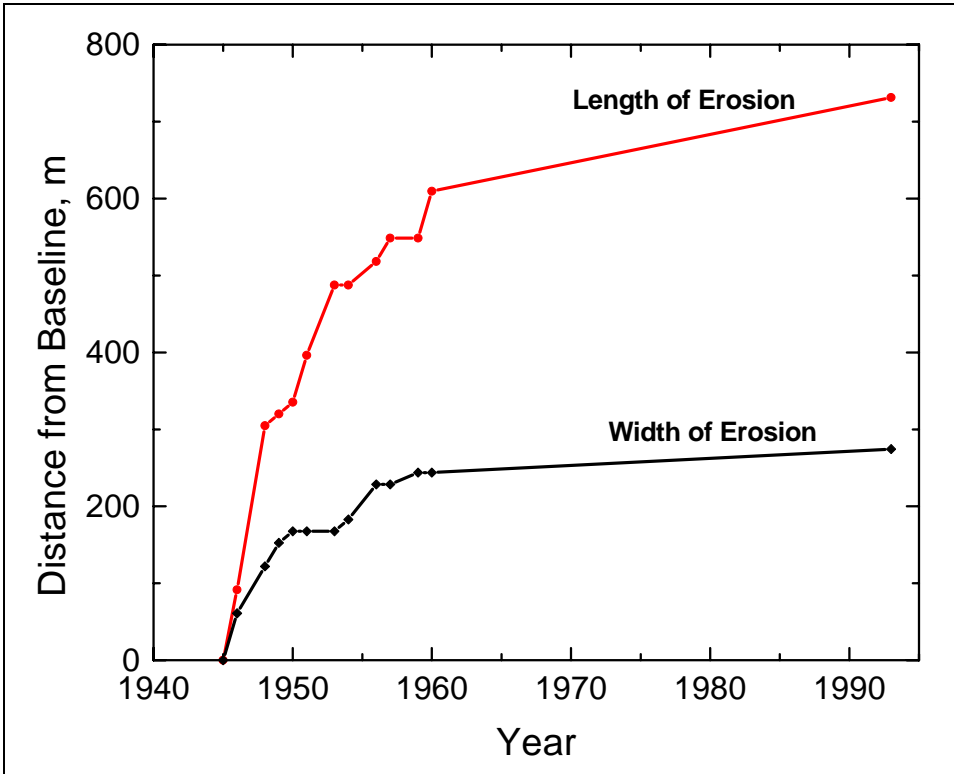


Figure 12. Measured shoreline position at Half Moon Bay 1946-1993 (from Seabergh 1999) (definition photograph January 2002)



Figure 13a. South Beach and Half Moon Bay, May 1993, tide elevation -0.5 m mllw



Figure 13b. Interpreted vegetation lines, July 1991 to May 1993

Waves

The wave climate of the northeastern Pacific Ocean has been extensively studied (e.g., Ruggiero et al. 1996; Tillotson and Komar 1997; Allan and Komar 2000a, 2000b, 2001, 2002a, 2002b). The northeastern Pacific wave climate exhibits strong seasonal variability. The average deepwater significant wave height H_s along the Washington coast is less than 2 m in the summer, and the average H_s during winter is approximately 3.7 m. Spectral peak wave period T_p is also seasonally variable, averaging less than 10 sec in summer months and increasing to greater than 12 sec in winter. Wave direction is also seasonally variable, with summer waves originating predominantly from the west-northwest and winter storms from the west-southwest.

Osborne (2003) provides an analysis of the Grays Harbor wave climate based on data from the Coastal Data Information Program (CDIP) Buoy 03601. The CDIP buoy is approximately 9.5 km southwest of the entrance to Grays Harbor in about 40 m of water. The buoy, whose operation is supported by the Seattle District, has been in operation since 1981, with directional measurements available since 1993. From 1994 to 2001, the average monthly H_s was between 1.2 and 1.7 m from May to September and ranged from 2.0 to 2.9 m from October to April. The monthly average T_p at Grays Harbor ranged from 8.1 to 10.1 sec in summer and 10.6 to 12.9 sec during winter months.

Wave incidence at Grays Harbor is predominantly from the west-northwest. However, most of the extreme waves (H_s greater than 5 m) originate from the west-southwest. Osborne (2003) performed an extremal analysis with the Automated Coastal Engineering System program (Leenknecht et al. 1992) based on the largest H_s measured each year at the CDIP buoy from January 1985 to December 2001 (17-year period). The results are listed in Table 1.

A storm on 10 December 1993 breached the weakened barrier spit at the south jetty. The storm persisted over 8-15 December. A time series of wave height, period, and direction is given in Figure 14. The maximum significant offshore wave height was 7.5 m, and the period was 13 sec. The direction of the offshore waves varied from south-southwest to west. In terms of peak significant wave height, the storm had only a 2-year return period (see Table 1), but was of relatively long duration. Waves much larger than those present when the barrier was breached have occurred in the years since this event.

Return Period (year)	Extreme Wave Height (m)
2	7.0
5	8.4
10	9.2
25	10.0
50	10.6

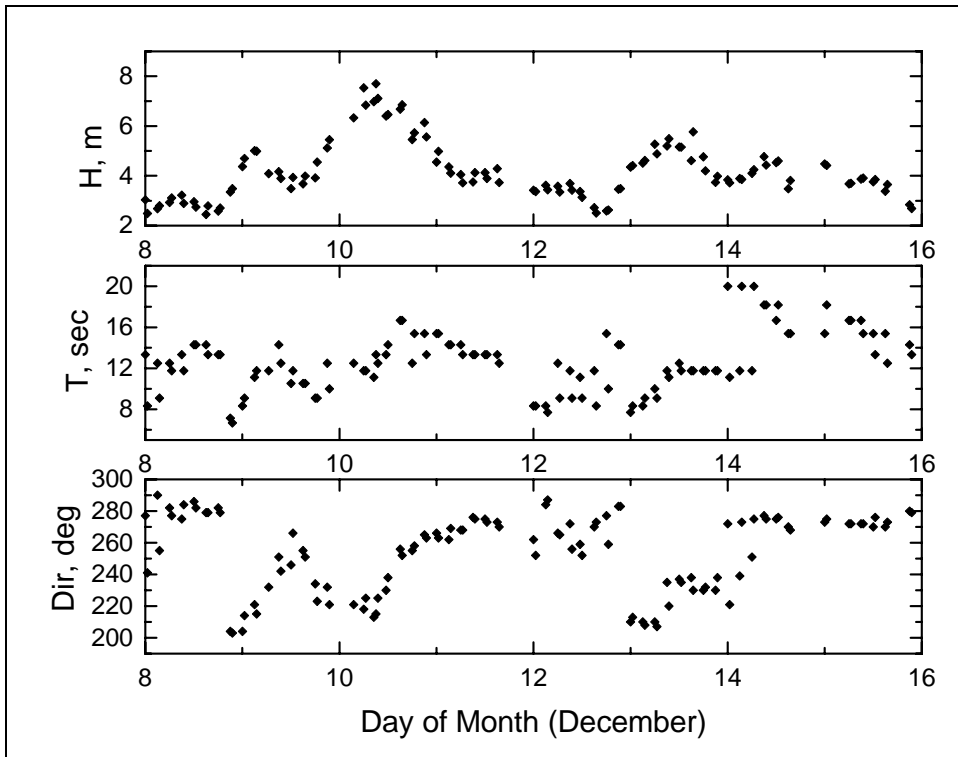


Figure 14. Time series of significant wave height, spectral peak period, and mean direction from which waves are incident at peak period, 8 December 1993 to 15 December 1993

Water Level

The tide at Grays Harbor is mixed and exhibits the diurnal inequality typical of the Pacific Northwest coast. The relatively large mean diurnal range at the entrance to Grays Harbor is 2.6 m. The mean spring range at the entrance is approximately 2.8 m. At Aberdeen, WA, where the Chehalis River empties into the Grays Harbor estuary, the mean tide range is 2.4 m and the spring tide range is 3.1 m. The tide range increases from the entrance to the upper reaches of the bay because of the constriction and shoaling of the tidal wave as it propagates into the bay. A summary of tidal datum planes is given in Table 2.

Table 2	
Tidal Datum Relationships Relative to mllw	
Datum	Adjustment (m)
Mean higher high water (mhhw)	2.79
Mean high water (mhw)	2.57
Mean sea level (msl)	1.50
Mean low water (mlw)	0.42
Mean lower low water (mllw)	0

Winter water level can be as much as 0.3 m higher than summer level. Tides along the southwest Washington coast are also characterized by interannual fluctuations. El Niño winters typically bring elevated water levels. At the National Ocean Service (NOS) tide gauge at Toke Point, WA, approximately 30 km south of Grays Harbor, observed water level was 0.25 m greater than normal during the 1982/83 El Niño and as much as 0.4 m greater than normal during the 1997/98 El Niño (Kaminsky et al. 1998).

A long-term water level record at the Grays Harbor inlet entrance does not exist, and there were no measurements for the December 1993 storm that breached the barrier. However, in the fall of 1999, a data collection program was sponsored by the Seattle District to measure waves, currents, suspended sediment concentration, and water level near the entrance of Grays Harbor. The methods to collect and process the data are described in Hericks and Simpson (2000). These Grays Harbor water level data were correlated to data measured at NOS water level measurement stations at Neah Bay, WA, and Astoria, OR, which are long-term records that include the December 1993 storm that breached the barrier. The correlation of the 1999 data is applied to construct an estimate of water level at Grays Harbor on both the ocean and bay sides at the time of the breach.

The data at Grays Harbor was collected at six stations that extended from the ocean side of the inlet through the throat and into the bay. Stations on both the ocean and bay sides were selected to estimate water level across the barrier. The Grays Harbor data were correlated to the Neah Bay and Astoria gauges with the simple linear expression:

$$y = Ax + B \tag{1}$$

where

y = measured water level at Grays Harbor

x = measured water level at Neah Bay or Astoria

A and B = correlation factors

The results for this analysis of the 1999 data are given in Table 3.

Table 3				
Water Level Correlation Factors				
	Neah Bay, WA		Astoria, OR	
	Grays Harbor, Ocean	Grays Harbor, Bay	Grays Harbor, Ocean	Grays Harbor, Bay
A	1.15	1.12	0.99	0.97
B	0.19	0.23	0.32	0.35

The final ocean-side and bay-side estimated water levels for Grays Harbor were obtained by averaging the estimates obtained from Neah Bay and Astoria. Figure 15 is a comparison of the measured and predicted water levels at Grays Harbor from October 1999 for both the ocean and the bay. The simple model estimates the water level reasonably well. The root-mean-square error between the measured and estimated water level for the entire 1999 data set was approximately 0.2 m for the ocean side and 0.14 m for the bay side.

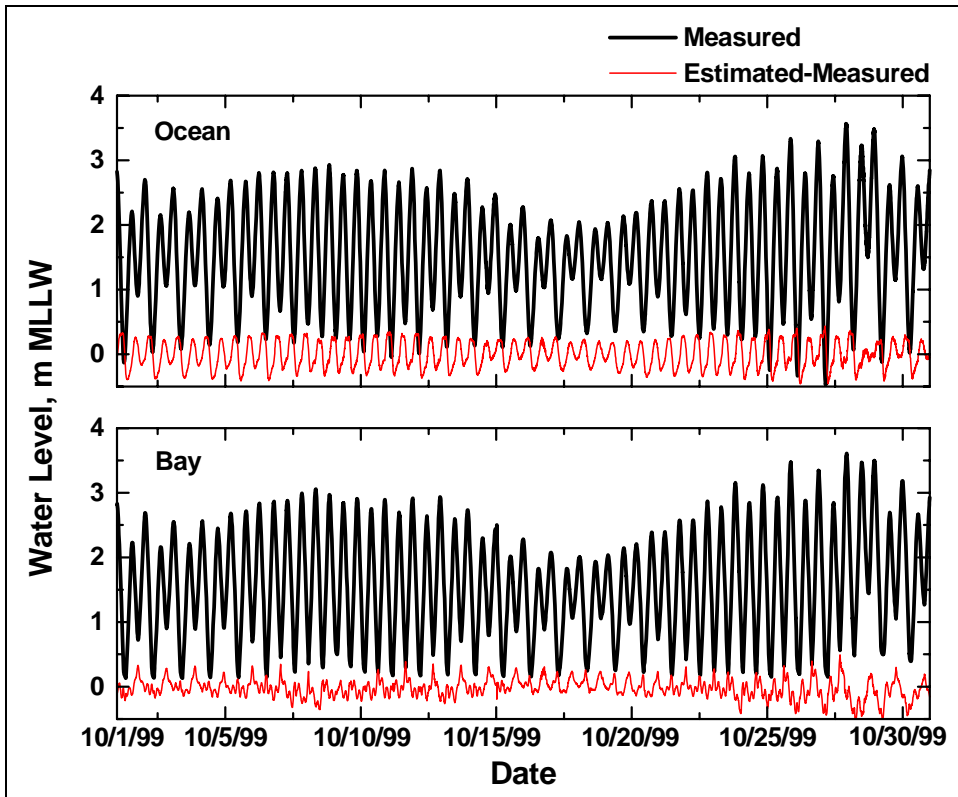


Figure 15. Comparison of measured and estimated October 1999 water levels at Grays Harbor on both ocean and bay sides

With the correlation factors determined from the 1999 data sets, an estimate of the water level in December 1993 was obtained. Figure 16 plots the water level for both the ocean side and the bay side. At the peak of the storm, the range was nearly 4 m, and maximum water elevations were 2.5 m above mean sea level (msl).

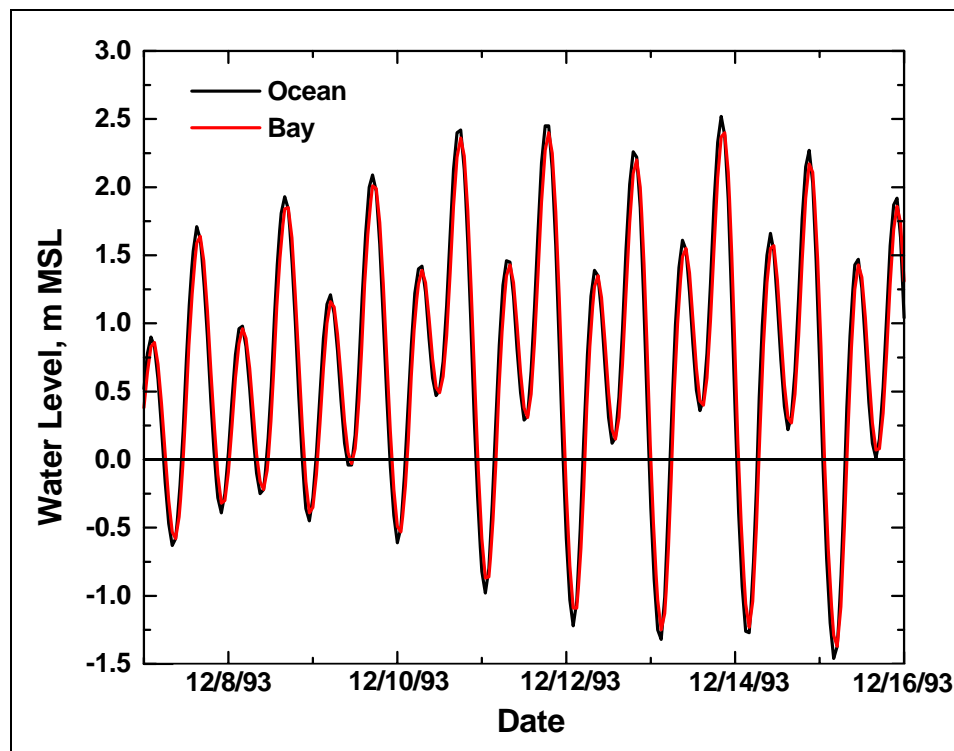


Figure 16. Estimated water level at Grays Harbor, 8-16 December 1993

Breach Evolution

The barrier spit at the Grays Harbor south jetty breached during the early morning on 10 December 1993 (Figure 17). By midday, the breach width was estimated by visual observation to be approximately 8 m. The breach widened rapidly, exposing the landward end of the jetty and eroding portions of the adjacent Westhaven State Park. Visual observations of the initial breach indicated a predominant flood flow through it for all tidal phases. The peak breach current velocity on 14 December was estimated by visual observation to be 1.5 to 2 m/sec.¹

¹ Hartman Associates, Inc. (1994). "Technical analyses of the shoreline breach at south jetty Grays Harbor, Washington," Report submitted to Public Works, City of Westport Washington, Hartman Associates, Inc., Seattle, WA.



Figure 17. Initial breach formation, looking seaward (west), 10 December 1993 (Seattle District photographs)

Breach formation is often associated with the formation of wing spits along the breach banks both on the Pacific (e.g., 1952 Bayocean Peninsula breach)¹ and Atlantic [e.g., 2003 Hatteras breach (Wamsley and Hathaway 2004)] coasts. The spits act to concentrate the flow and help maintain the breach channel. Flood and ebb shoals can also form as sediment carried through or eroded from the breach channel is deposited. Analyzing changes within a breach channel can be difficult because it is a dynamic feature, as are the adjacent wing spits and shoals.

¹ Henshaw, J. L. (1956). "The Bayocean breakwater," unpublished report, U.S. Army Engineer District, Portland, OR.

Breach width

The evolution of the breach and adjacent shorelines was analyzed within ArcView® GIS. The breach width was defined as the narrowest distance between barrier scarps or between the barrier scarp and south jetty. Initial erosion was rapid. By 17 December 1993, the breach had widened to 85 m (Figure 18). Approximately 1 month later, the lobe of vegetated barrier adjacent to the jetty had completely eroded. Table 4 summarizes the calculated breach widths from 17 December 1993 to 10 August 1994. The photographs from which the breach width estimates were calculated from January 1994 forward are compiled in Appendix A (Figures A1 to A4). From December 1993 to August 1994, the barrier spit receded 165 m from the south jetty.



Figure 18. Breach, 17 December 1993; tide elevation +2.0 m mllw

Table 4 Estimated Breach Width	
Date	Breach Width (m)
17 December 1993	85
January 1994	115
2 February 1994	120
6 March 1994	140
10 August 1994	165
NOTE: See Figure 19 and Appendix A, Figures A1-A4 for measurement locations.	

Breach depth

Depths in the breach are available from surveys conducted by the Seattle District in March and August 1994. These surveys and aerial photographs indicate that minimum elevations through the breach were between approximately 0.0 and +1.0 m mllw from breach inception through August 1994.

Figure 19 is a comparison plot of three cross-sectional transects through the breach channel for March 1994 and August 1994. In March, the breach channel had elevations of +1.0 to +1.5 m mllw. By August, the breach channel had deepened to elevations ranging between 0.0 and +1.0 m mllw. The widening of the breach at Transect 1 is also evident in Figure 19.

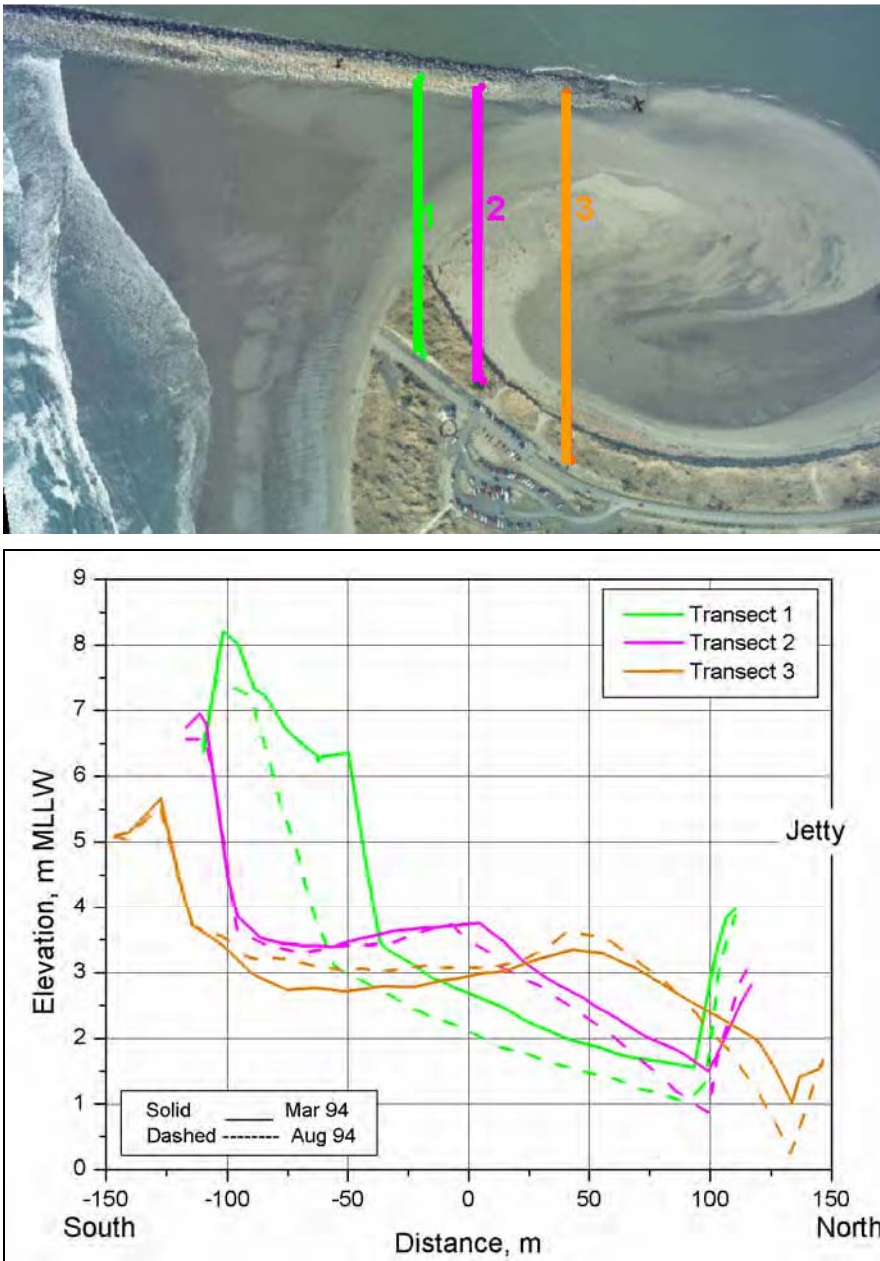


Figure 19. Comparison of breach channel cross section

The growth of the breach channel is also seen in the plot of bathymetric change from March to August 1994 (Figure 20). The warm colors indicate deepening, and the cool colors are areas of shoaling. The data show the growth of the wing spit/flood shoal area with accumulation of sand in these areas and the formation of a bar seaward of the breach channel near the south jetty. The growth of the breach channel is also evident and illustrates the weakened condition of the barrier in August as compared to March.

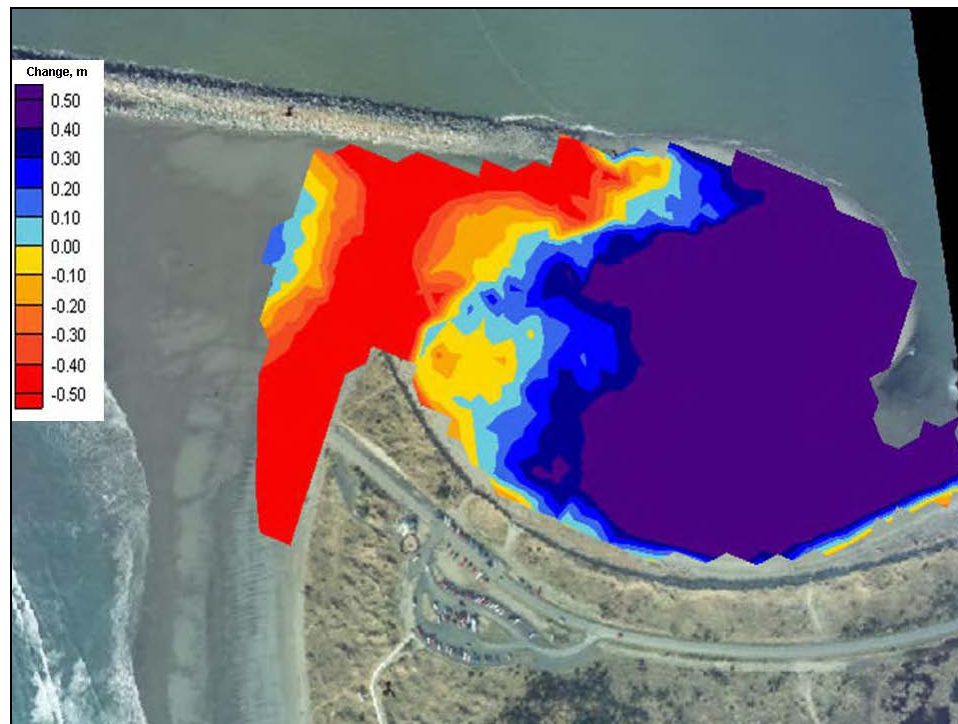


Figure 20. Difference plot of March 1994 and August 1994 breach bathymetry data sets

The volume of the flood shoal created in Half Moon Bay by the breach was estimated by comparing the March and August surveys to bathymetry in Half Moon Bay judged to be typical of a “no-breach” condition. By March 1994, approximately 75,000 cu m of sediment had deposited in Half Moon Bay, and by August 1994 the volume reached 210,000 cu m.

Observation of the breach in August 1994 indicated that tidal flow through it was constrained to a 40-m-wide channel adjacent to the jetty at all times except storms at high tide. On 23 August, approximately 1 hr before high slack tide, the current was flooding (eastward directed) at an estimated speed of 0.6 to 0.9 m/sec. One hour, 20 min. after high slack, an ebb flow (flow directed to the west) was observed visually be 0.6 to 0.9 m/sec.¹

¹ Nelson, E. (1994). “Trip report, site visit to Grays Harbor south jetty breach, 23 August 1994,” Memorandum for Record, U.S. Army Engineer District, Seattle.

South Beach Shoreline Recession

The shoreline within about 550 m of the south jetty underwent a rapid reconfiguration after the breach formed and before it was filled mechanically. Figure 21 is a plot of the vegetation lines from May 1993 to 10 August 1994. Recession of the vegetation line was calculated at five locations along South Beach and is tabulated in Table 5. A significant amount of erosion occurred from May 1993 to 17 December 1993. Recession of the vegetation line during the first 7 days after the barrier breached on 10 December 1993 is not known. Shoreline recession slowed with time.

Beach erosion is greatest near the jetty and decreases with distance to the south. Shoreline recession is less than 3 m from March to August 1994 at distances greater than 560 m south of the jetty. Total recession of the vegetation line 180 m south of the jetty (SB1) for the 8 months following the breach exceeded 120 m. The shoreline recession rate at SB1 under breach conditions (approximately 180 m/year) was much greater than the 0.6 to 19 m/year that had been documented since 1967 (Osborne et al. 2003).

The short-term rates documented in Table 5 are not indicative of long-term change rates in a breached condition. However, it should be noted that the beach loss occurred during a season typically associated with beach recovery on the southwest Washington coast. The Washington coast is characterized by seasonal variability in wave height and direction that generally results in northerly offshore sediment transport in the winter (beach erosion) and southerly onshore transport in the summer (beach accretion). This seasonal signal is evident in the data collected near the south jetty from 1997 to 2000 as part of regional monitoring program conducted jointly by the Washington Department of Ecology and the U.S. Geological Survey. The purpose of the program was to quantify the short- to medium-term beach change rates and morphologic variability in the study area. The survey near the south jetty documented beach lowering in the winter (surveys conducted in March) and recovery in the summer (surveys conducted in August). The magnitude of seasonal shoreline change was as much as 30 m (Ruggiero and Voigt 2000). The vegetation line recession in the breached condition from March to August 1994 was 15 to 30 m, a seasonal time period usually associated with beach recovery.

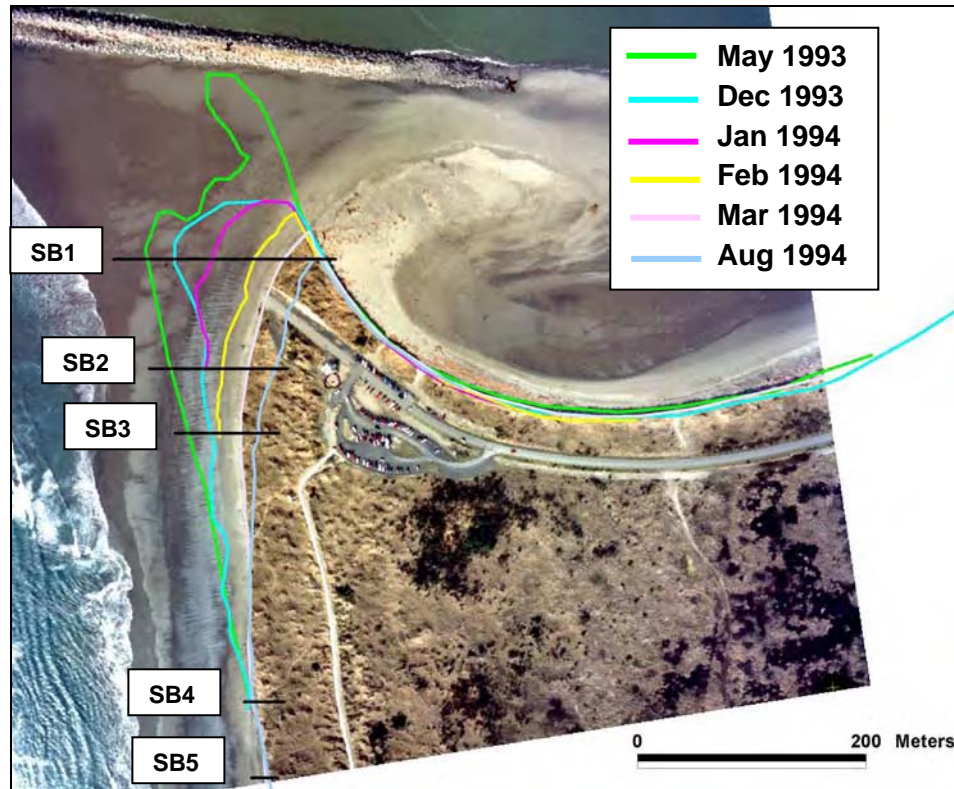


Figure 21. Recession of the vegetation line at South Beach under breach condition (photograph March 1994)

Table 5 South Beach Shoreline Recession					
Time Period	SB1 (m)	SB2 (m)	SB3 (m)	SB4 (m)	SB5 (m)
23 May 1993 to 17 December 1993	18	27	27	0	NA
17 December 1993 to January 1994	30	2	NA	NA	NA
January 1994 to 2 February 1994	40	10	NA	NA	NA
2 February 1994 to 6 March 1994	25	25	18	NA	NA
6 March 1994 to 10 August 1994	29	25	15	2	3
Total Recession after 17 December 1993*	123	62	43	5	NA

*Note: From 17 December 1993 to 10 August 1994.

Summary

Persistent shoreline recession on both the ocean and bay sides of Pt. Chehalis weakened the barrier and exposed the dune to wave attack. On 10 December 1993, a storm of 7-day duration produced elevated water level that breached the weakened barrier spit adjacent to the south jetty. In terms of peak significant wave height, the storm had a 2-year return period with a maximum significant offshore wave height of 7.5 m. The breach widened rapidly, exposing the landward end of the jetty and eroding portions of the adjacent Westhaven State Park. A predominant flood flow through the initial breach had maximum velocity estimated at 1.5 to 2 m/sec. By 17 December 1993, the breach had widened to approximately 85 m. The breach continued to grow at a slower rate, reaching a width of approximately 140 m by 6 March 1994 and 165 m by 10 August 1994. In August 1994, both ebb and flood flow were observed with an estimated velocity of 0.6 to 0.9 m/sec.

The breach channel not only grew laterally, but also deepened between March and August 1994. In March 1994, the breach channel elevations ranged from approximately +1.5 to +1.0 m mllw. By August of 1994, the channel had deepened by approximately 0.5 m to elevations ranging from +1.0 to 0.0 m mllw. Sediment eroded from and carried through the breach channel deposited in Half Moon Bay. By August 1994, approximately 210,000 cu m removed from the breach area had been deposited and remained in Half Moon Bay.

The South Beach experienced erosion before the breach was filled. Shoreline recession was greatest near the jetty and decreased with distance to the south. The shoreline recession rate at a location 180 m south of the jetty for the 8 months following the breach was approximately 180 m/year, much greater than the average 0.6 to 19 m/year experienced since 1967.

3 Numerical Modeling of Breach Hydrodynamics

This chapter describes numerical simulations of tidal and wave-induced flow to examine the hydrodynamic conditions during the December 1993 breach at the Grays Harbor south jetty. The simulations were performed for documented stages of breach development and for potential dimensions (width, depth) of a hypothetical breach under a selected set of hydrodynamic forcing conditions. These simulations are morphologically static in that the flow is through a breach channel that does not change. The simulations are intended to estimate the variation in flow: (a) as breach geometry evolved from December 1993 to August 1994, and (b) as hydrodynamic forcing conditions might change for a given breach configuration. A controlled set of forcing conditions was applied; therefore, differences observed in the hydrodynamic response are due to the changing bathymetric configuration of the breach.

Simulations of the existing condition prior to the December 1993 breach, referred to as “pre-breach” simulations, served as a basis for comparison. In addition, simulations with a Seattle District conceptual breach and a variation of that concept that exposes the base of the south jetty, referred to as the large breach, were made to examine hydrodynamics for a breach configuration that might occur after a series of winter storms. As discussed in Chapter 2, the December 1993 breach was closed before arrival of winter storms of the following year.

The models M2D (Militello et al. 2004) and Steady-State Spectral Wave (STWAVE) (Smith et al. 1999, 2001) were the primary hydrodynamic and wave models, respectively, implemented for this study and are described in the following paragraphs. The hydrodynamic model ADCIRC (Luetlich et al. 1992) previously applied at the site (Cialone et al. 2002; 2003) provided boundary forcing conditions for the local scale (M2D) hydrodynamic model (Militello and Zundel 2002).

The purpose of the simulations presented in this chapter was to determine, through examination of predicted current and water level, if a breach would have negative consequences for the Federal navigation project at Grays Harbor, in particular, as increased dredging of the deep-draft navigation channel and degradation of the south jetty. A regional perspective was taken in observing potential consequences in the far field of Grays Harbor, distant from the breach. Information on the expected change in the hydrodynamic environment is also available through the simulations.

Numerical Models

Models M2D, STWAVE, and Advanced Circulation (ADCIRC) are documented in technical reports and technical notes, as well as in the literature of study applications and engineering projects. A short description of the models is given for general understanding of the function of the models. For more details, the reader is referred to the references provided here and in the preceding section.

M2D

Model M2D is a finite-volume numerical representation of the two-dimensional depth-integrated continuity and momentum equations of water motion. The governing equations, numerical representation, bottom and surface stresses, grid scheme, boundary conditions, other model features, graphical interface, and study applications are documented in Militello et al. (2004). Cells are defined on a staggered, rectilinear grid and can have constant or variable side lengths. The momentum equations are solved for velocity first in a time-stepping manner, followed by solution of the continuity equation for water surface elevation, in which the updated velocities calculated by the momentum equations are applied.

Features of the M2D model include robust flooding and drying, time-varying wind-speed, spatially-varying bottom-friction, time- and space-varying wave-stress forcing, efficient grid storage in memory, representation of hard bottom (non-erodible areas), and hot-start option. M2D has been designed as a local-scale model that can be easily and quickly applied to engineering projects. The model has been developed to maximize flexibility in grid specifications and forcing. The flooding and drying capability is significant for the present study, which includes simulations of a breach with depths above the ambient water level.

STWAVE

STWAVE is a steady-state finite-difference model based on the wave action balance equation. The purpose of applying nearshore wave transformation models such as STWAVE is to describe quantitatively the change in wave parameters (wave height, period, direction, and spectral shape) between the offshore and the nearshore regions. STWAVE simulates depth-induced wave refraction and shoaling, current-induced refraction and shoaling, depth- and steepness-induced wave breaking, diffraction, wind-wave growth, and wave-wave interaction and whitecapping that redistribute and dissipate energy in a growing wave field.

In addition to individual model simulations, models STWAVE and M2D were coupled in the Surface-water Modeling System (SMS) Steering Module (Zundel 2000; Militello and Zundel 2003). The Steering Module method of coupling models is an efficient and accurate means of simulating the tidal hydrodynamics, wave-driven currents, setup and set down, and wave-current interaction in the nearshore, including at tidal inlets.

ADCIRC

The ADCIRC is a highly developed numerical model for solving the equations of motion for a moving fluid on a rotating earth. It serves as the USACE regional oceanographic and storm surge model as certified by the Federal Emergency Management Agency. The equations are formulated with hydrostatic pressure and are discretized in space with the finite-element method and in time with the finite-difference method. ADCIRC can be run either as a two-dimensional, depth-integrated (2DDI) model or as a three-dimensional (3D) model. Elevation is obtained from the solution of the depth-integrated continuity equation in the Generalized Wave-Continuity Equation form. Velocity is obtained from the solution of either the 2DDI or 3D momentum equations for shallow-water waves. All nonlinear terms are retained in these equations.

ADCIRC can be operated in either a Cartesian or a spherical coordinate system. ADCIRC boundary conditions include specified elevation (harmonic tidal constituents or time series), specified normal flow (harmonic tidal constituents or time series), zero normal flow, slip or no slip conditions for velocity, external barrier overflow out of the domain, internal barrier overflow between sections of the domain, surface stress (wind and/or wave radiation stress), atmospheric pressure, and outward radiation of waves (Sommerfeld condition). ADCIRC can be forced with elevation, normal flow, or surface stress boundary conditions, tidal potential, and earth load/self attraction tide. Recently, updated global-scale ADCIRC studies were completed on high-performance computers to provide accurate tidal constituents for the Atlantic Ocean coast, Gulf of Mexico coast, and Pacific Ocean coast of the United States to furnish reliable tidal constituents for project-scale simulations (Mukai et al. 2002; Spargo et al. 2004).

ADCIRC was applied in previous studies for the entire Grays Harbor inlet/bay system (Cialone et al. 2003). Measured current and water level (1999) served as comparisons to verify ADCIRC. The validated model has been proven to reproduce one month of field measurements through the inlet throat at six locations. The detailed breach bathymetry, fine grid resolution, small numerical time-step, and the large number of simulations for the present project made application of a local scale model preferable. The calibrated ADCIRC model was used to drive the local scale model M2D. Water surface elevation and velocity computed by the calibrated ADCIRC model on a regional scale grid were applied as boundary forcing conditions for the local scale M2D model for this project application. Results internal to the M2D domain were essentially identical to the ADCIRC results, but had more detail in the breach location. The SMS provides the capability for interpolating elevation and velocity results from the ADCIRC domain to the M2D boundary.

Note that ADCIRC is calibrated for known conditions. The capability of the model to predict water levels and velocities for known conditions leads to the capability to apply the model as a predictive tool for hydrodynamic behavior under other (bathymetry, wave, wind, tide) conditions. The breach is a modification to the bathymetry relative to known conditions. Therefore, the model is not calibrated for breach conditions, but is used to predict hydrodynamics that would occur during breach conditions. This is standard operating procedure.

Model Validation

The ADCIRC model was validated with field data collected in 1999, as documented in Kraus and Arden (2004). ADCIRC provided boundary forcing conditions for the local scale (M2D) hydrodynamic model. The Coastal Inlets Research Program (CIRP) conducted at the U.S. Army Engineer Research and Development Center's (ERDC's) Coastal and Hydraulics Laboratory (CHL) has linked ADCIRC and M2D for many study sites, with ADCIRC serving as a regional circulation model driving the project-level model M2D. The linkage has been implemented in SMS. Prudent development of model grids has shown that a local model will produce similar results as the regional model, with slight differences possible depending primarily on resolution between the models at the particular comparison point.

The M2D model was validated for the present study by comparing M2D results to the 1999 measurements and to ADCIRC results at the stations identified in Figure 22. Figure 23 compares water level at sta Tide 1, and Figures 24-26 compare velocity magnitude at sta 4, 2, and 5, respectively. Stations 2 and 5 are included in both the M2D outer and M2D inner grids. M2D calculations agree well with the measurements. Water level predictions by M2D and ADCIRC are nearly identical. Current speed calculated with M2D are in phase with the measurements, and the M2D results improve on the peak speed predictions relative to ADCIRC, attributed to finer resolution of the M2D mesh.

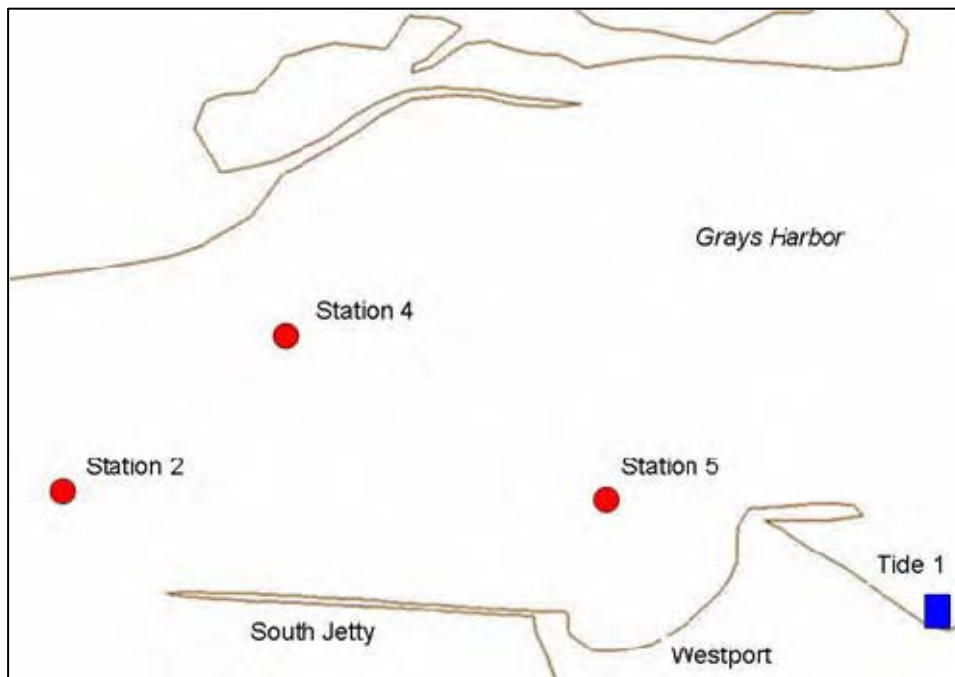


Figure 22. Field data collection station locations, 1999

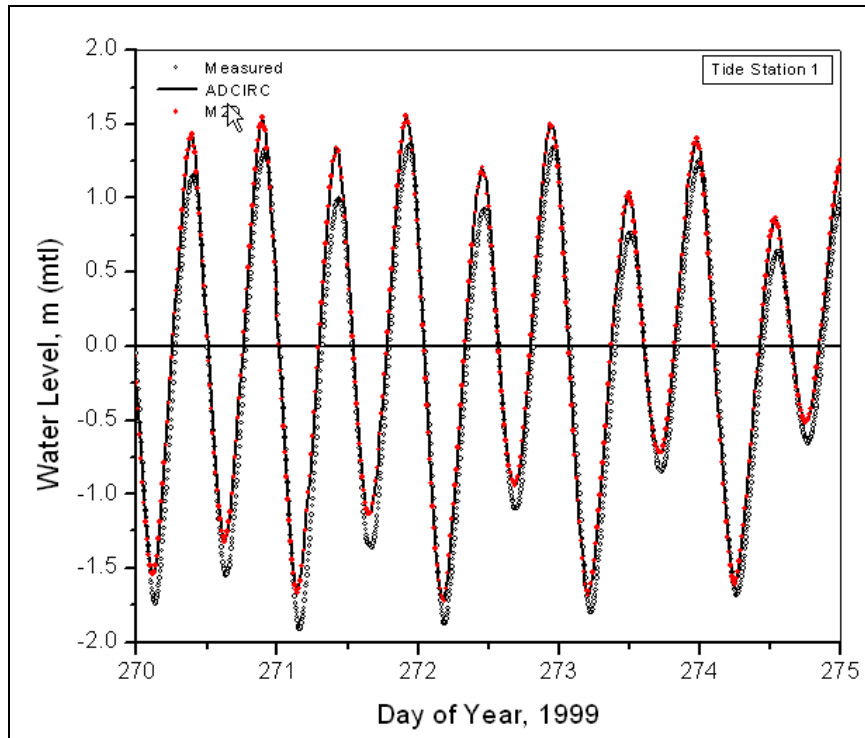


Figure 23. M2D water level results compared to ADCIRC calculations and measurements

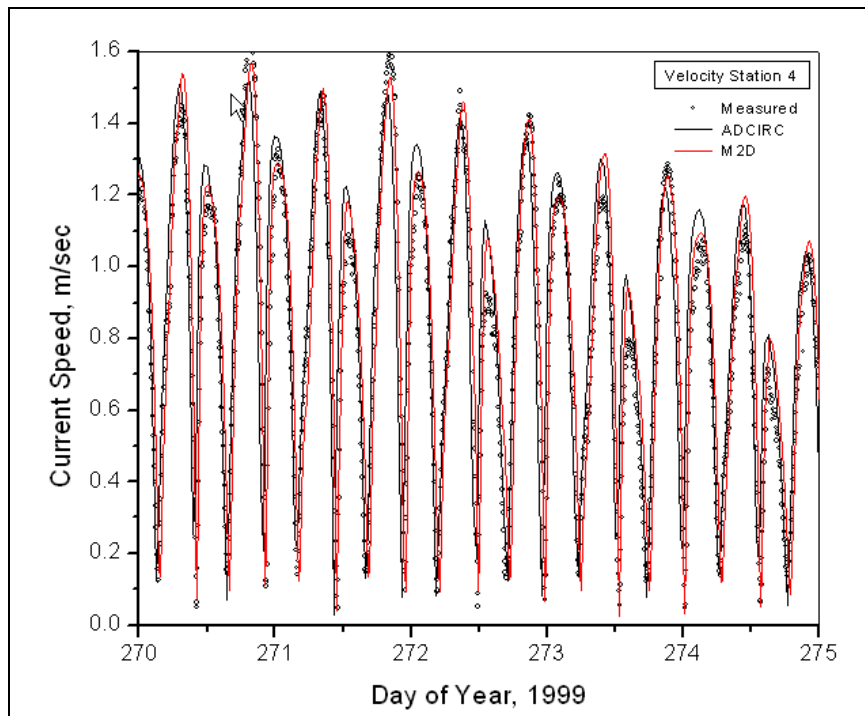


Figure 24. M2D current speed results compared to ADCIRC calculations and measurements at sta 4

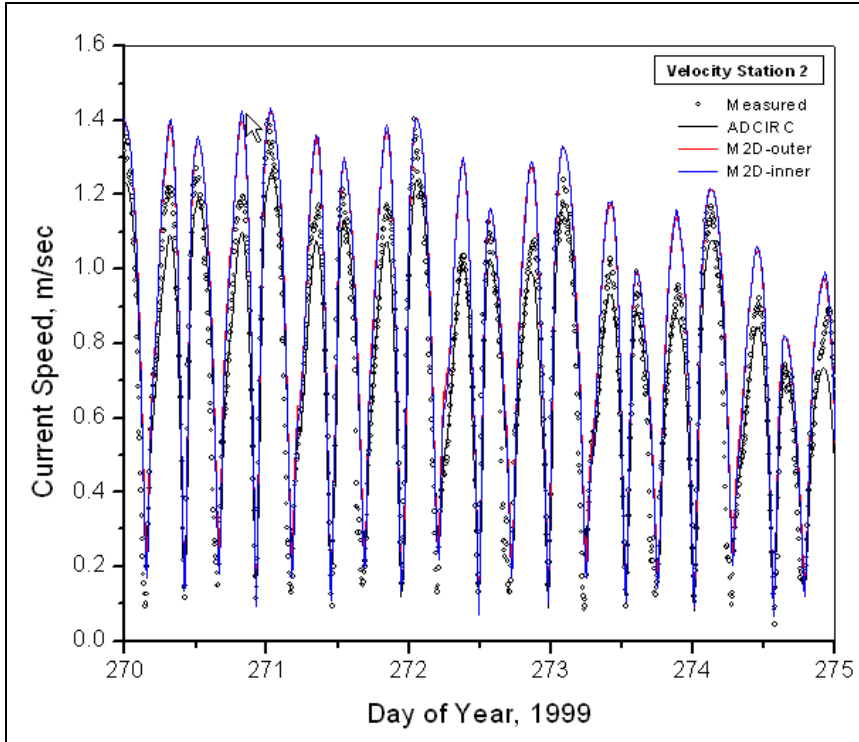


Figure 25. M2D current speed results compared to ADCIRC calculations and measurements at sta 2

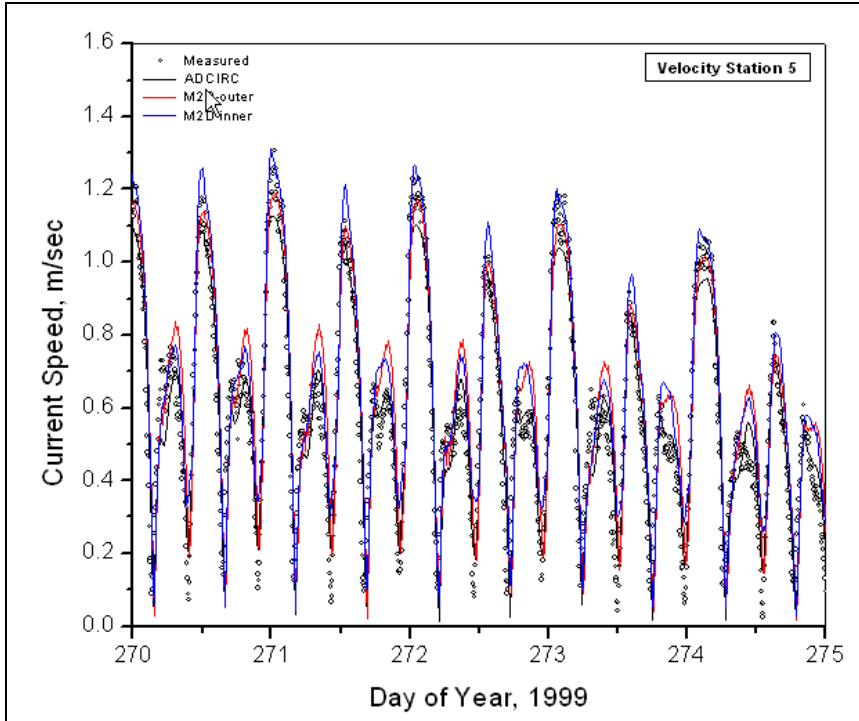


Figure 26. M2D current speed results compared to ADCIRC calculations and measurements at sta 5

The version of the STWAVE model applied in this study was also validated with field data collected in 1999 and is documented in Kraus and Arden (2004). This version of STWAVE simulates depth-induced wave refraction and shoaling, current-induced refraction and shoaling, depth- and steepness-induced wave breaking, diffraction, wind-wave growth, and wave-wave interactions and white capping that redistribute and dissipate energy in a growing wave field. The validation of the STWAVE model is presented for selected stations in Figures 27 to 29. The model calculations compare well to the measurements. To assess the sensitivity of the wave height estimates to bottom friction for Grays Harbor, the model was run with a bottom friction coefficient of 0.01 for a sandy bottom. Figures 27-29 show calculated wave heights with and without bottom friction for sta 2, 4, and 5, respectively, together with the measurements. The root-mean-square (RMS) differences between the with- and without-bottom friction results for each station and are listed in Table 6.

Station	RMS Difference (m)
2	0.07
4	0.07
5	0.04

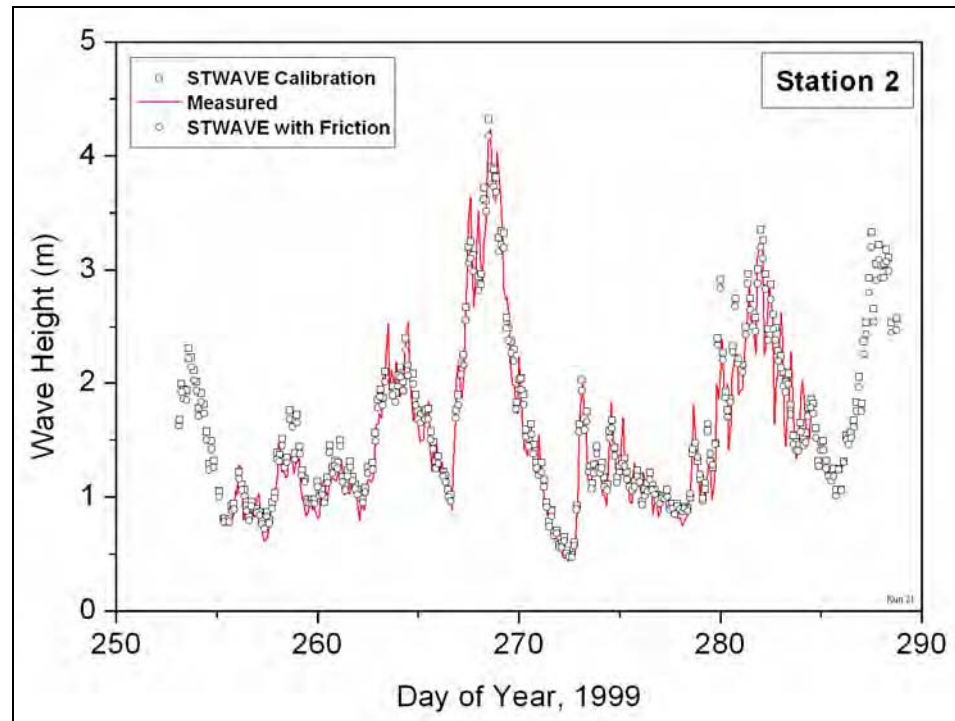


Figure 27. Calculated wave height with and without bottom friction at sta 2 compared to measurements

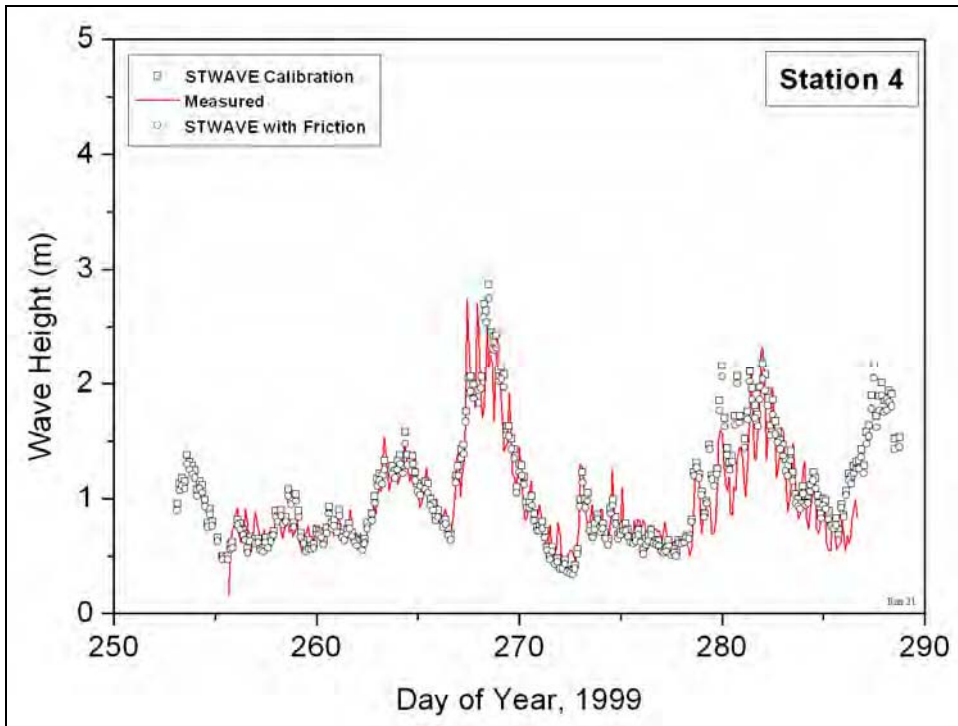


Figure 28. Calculated wave height with and without bottom friction at sta 4 compared to measurements.

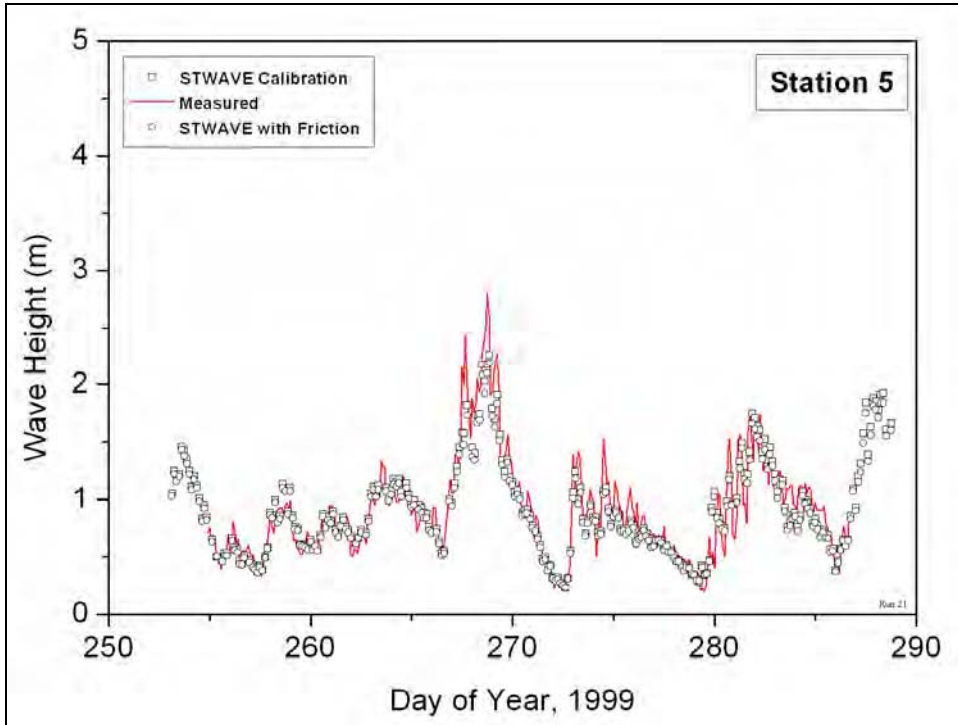


Figure 29. Calculated wave height with and without bottom friction at sta 5 compared to measurements.

Numerical Simulations

For this hydrodynamic study, seven bathymetric configurations were examined:

- a.* Prior to the December 1993 breach (denoted as existing or pre-breach condition).
- b.* Breach configuration in December 1993.
- c.* Breach configuration in March 1994.
- d.* Breach configuration in August 1994.
- e.* Large breach to simulate a breach after a storm season.
- f.* Large breach without a landmass next to the jetty.
- g.* Large breach without a landmass next to the jetty and the depth through the breach reduced as compared to the original large breach.

Each condition required development of numerical grids for hydrodynamic and wave model simulations (Figures 30-34). These conditions were selected to demonstrate the variation in flow as the breach developed and progressed over a 9-month period (December 1993 - August 1994) as compared to flows in the vicinity of the south jetty, Westport, and Half Moon Bay without a breach and with a hypothetical breach (large breach).

The existing-condition bathymetry prior to the December 1993 breach was developed from a composite of Seattle District 1993, 1994, 1999, and 2001 surveys. The Grays Harbor breach that occurred on 10 December 1993 was photographed on 17 December 1993. That aerial photograph was overlaid on the existing (pre-breach) bathymetry to approximate the width and extent of the breach in December 1993. In this manner, a breach was numerically represented in the existing-condition bathymetry. The locations of the wet-dry line, vegetation line, and other identifiable points were used to estimate depths through the breach. Bathymetric surveys of the breach in March and August 1994 gave the most accurate representation of breach conditions, and numerical grids were created from the data for those two time periods.

The minimum elevation through the breach in December 1993 was 1.5-1.6 m above mllw and then shifted to a more northward location by March 1994 (Chapter 2, Figure 20). The minimum elevations through the breach in March and August 1994 were 1.0 and 0.2 m above mllw, respectively. The large breach was considered representative of the bathymetry prior to jetty construction (1898-1902). This extreme condition was modeled to estimate hydrodynamic conditions had the breach been permitted to expand. The depth through the large breach was 6.1 m below mllw (7.6 m below mean tide level (mtl)), and the width was 370 m. Based on observations of breaching near other jetties (Schmeltz et al. 1982; Kraus and Wamsley 2003), the segment of land adjacent to the south jetty in the original Seattle District concept would likely have been eroded. Removal of this material was considered an alternative to the original large-breach concept, as was the reduction of breach depth to 3.05 m below mllw (4.55 m below mtl), to evaluate a less extreme breach. Bathymetric data sets were developed for these two variations of the large breach and are evaluated in this chapter. This, however, does not preclude a configuration similar to the one

suggested by the Seattle District. In fact, the August 1994 survey shows a submergent bar at the landmass location. A comparison of results for different configurations serves to improve the reader's understanding of the resulting hydrodynamics.

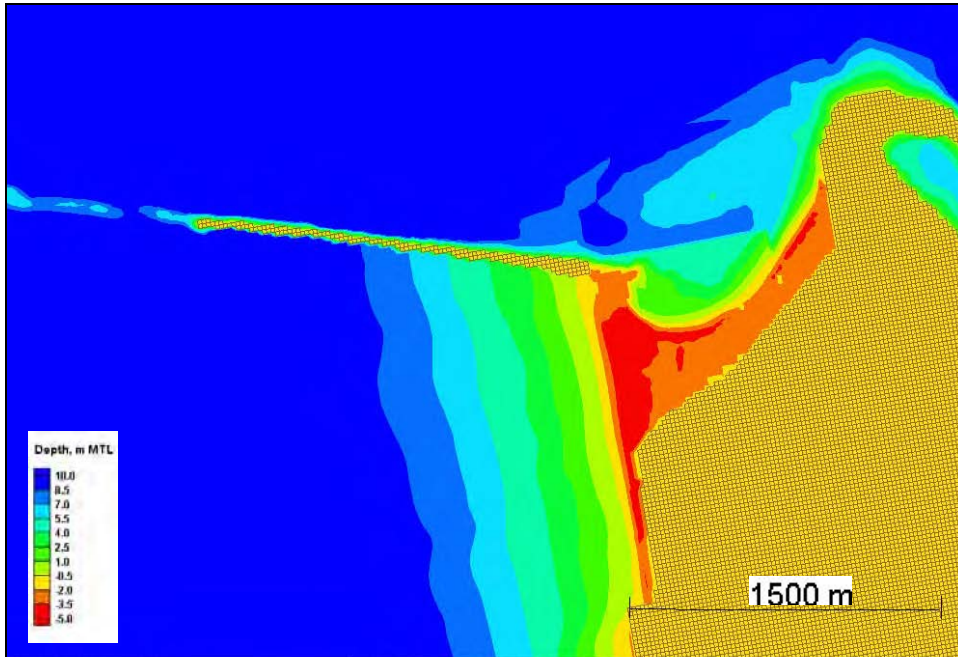


Figure 30. Existing condition bathymetry

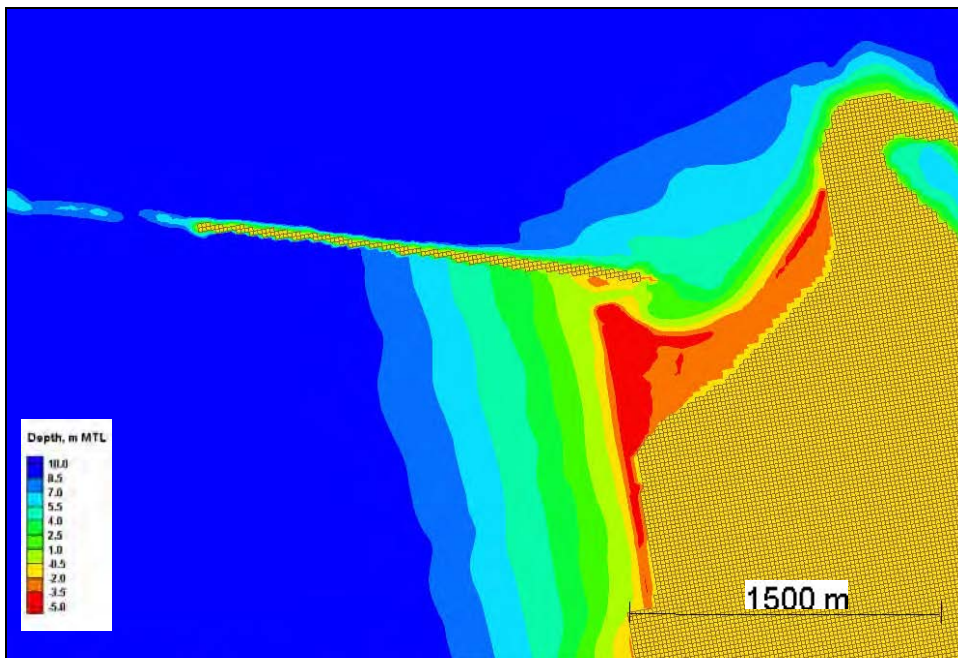


Figure 31. December 1993 bathymetry

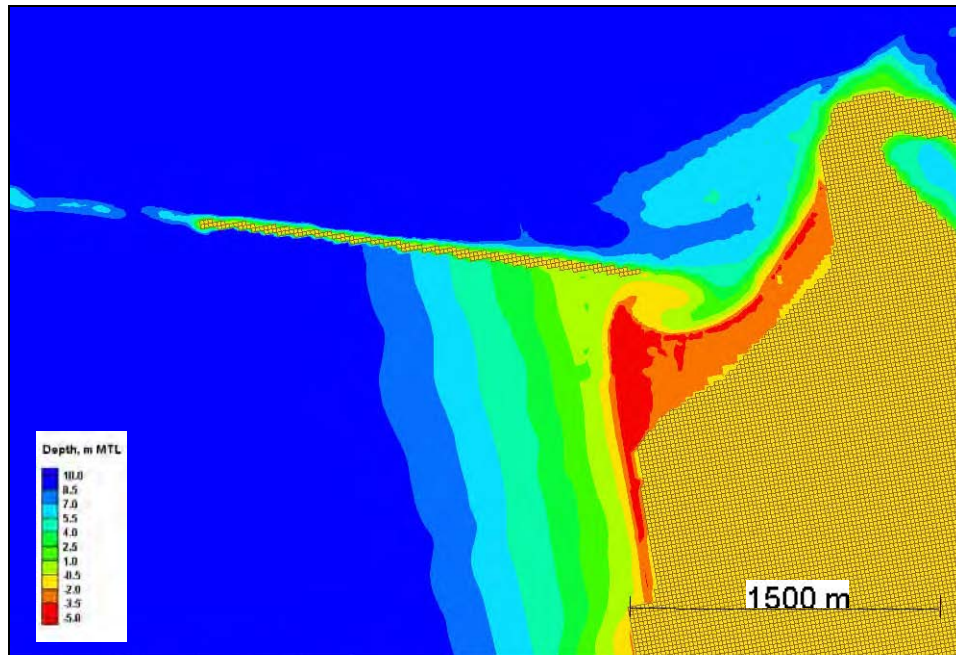


Figure 32. March 1994 bathymetry

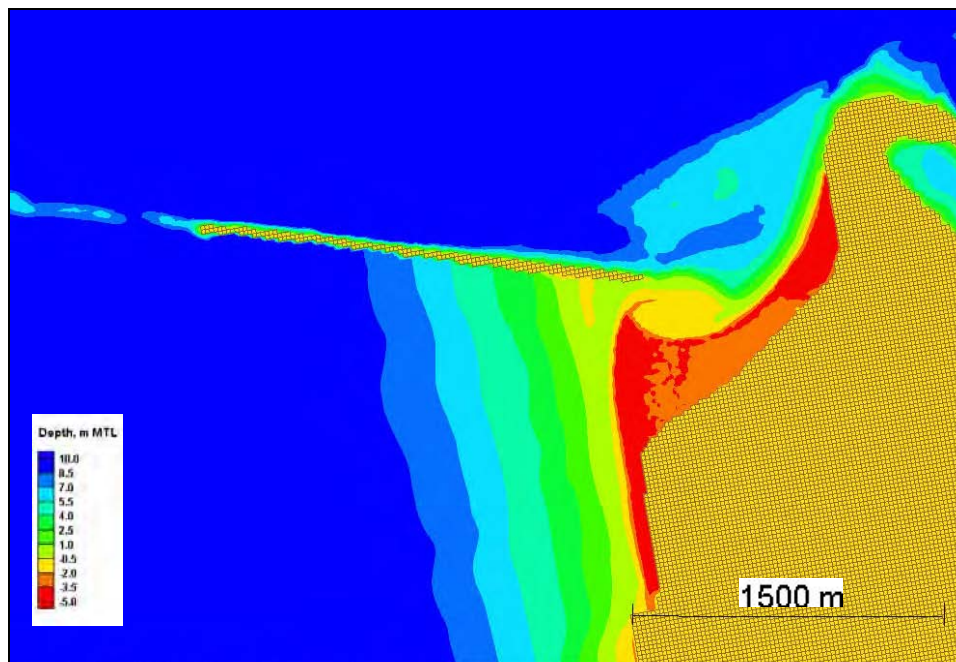


Figure 33. August 1994 bathymetry

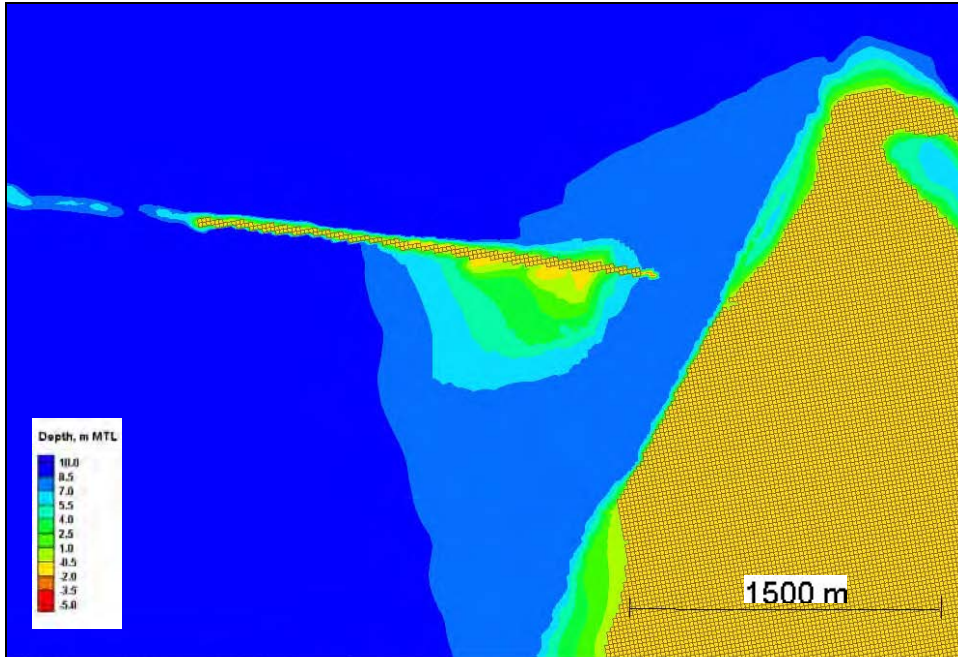


Figure 34. Large breach bathymetry

Numerical grids were developed for M2D and STWAVE for the five original bathymetric configurations and two variations of the large breach. Two grid resolutions were selected, resulting in 14 M2D grids and 14 STWAVE grids (seven bathymetric conditions times two grid resolutions). Grids were constructed at 100-m resolution and nested to 20-m resolution (Figures 35 and 36). The fine (20-m) resolution grids for STWAVE and M2D were identical in size. The coarse (100-m) resolution STWAVE grid was a subset of the M2D grid (Figure 37), with outer dimensions 800 m smaller than the M2D dimensions. The 14 M2D grids (seven coarse and seven fine) and 14 STWAVE grids (seven coarse and seven fine) generated were applied to tidal current and wave transformation simulations, respectively, and were coupled with the SMS Hydrodynamic Steering Module to calculate water level and wave-induced currents.

M2D hydrodynamic simulations were made for the seven bathymetric conditions to examine the magnitude, duration, and spatial extent of tidal flow through the breach for different bathymetry. These particular simulations did not include waves; therefore, the contribution of the wave-generated current through the breach was not simulated. Table 7 lists the hydrodynamic and wave model simulations performed for this study. Tide-only simulations are denoted by simulation numbers 101, 105, 109, 113, 117, 121, and 124.

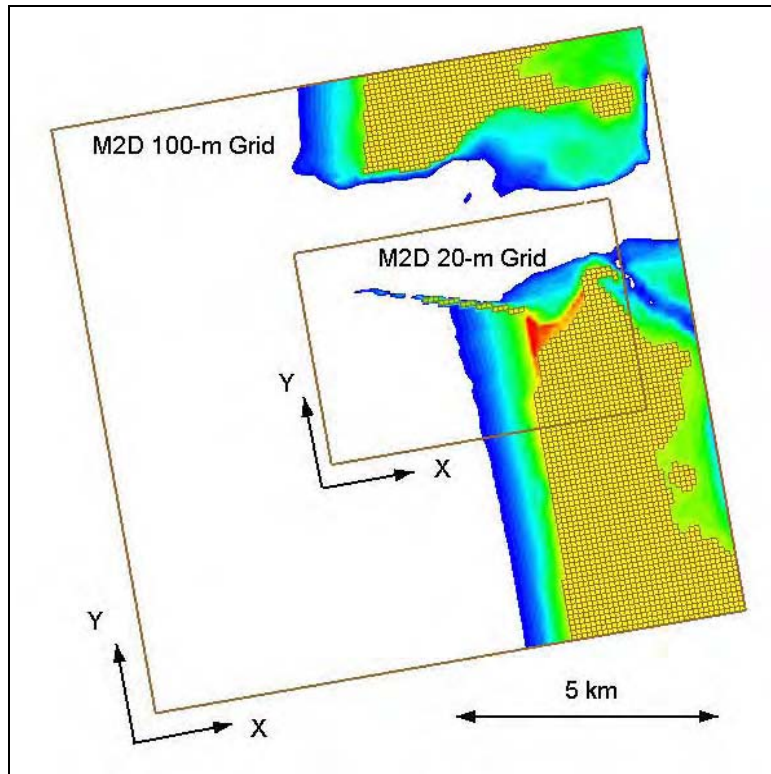


Figure 35. Nested M2D grids

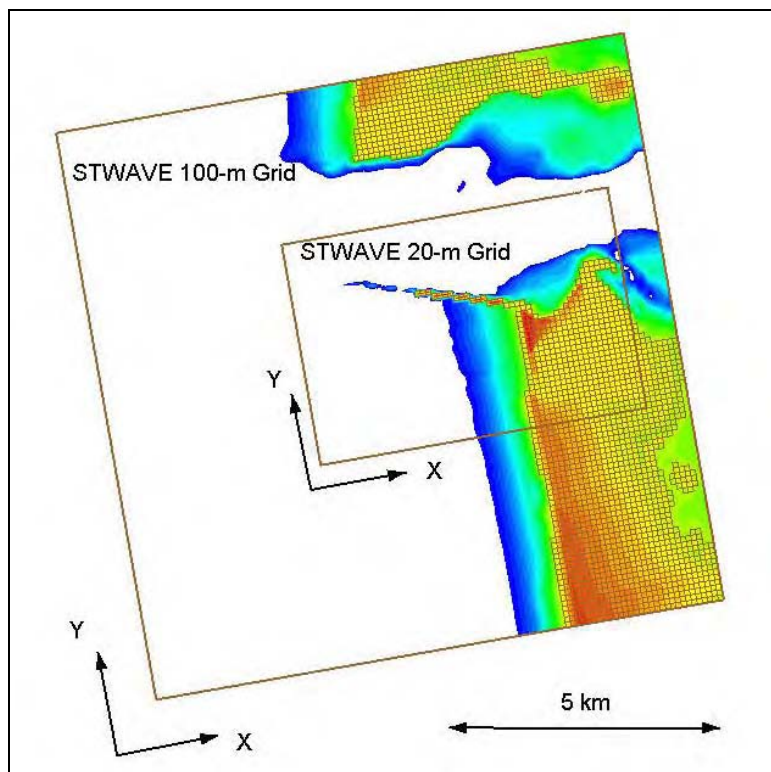


Figure 36. Nested STWAVE grids

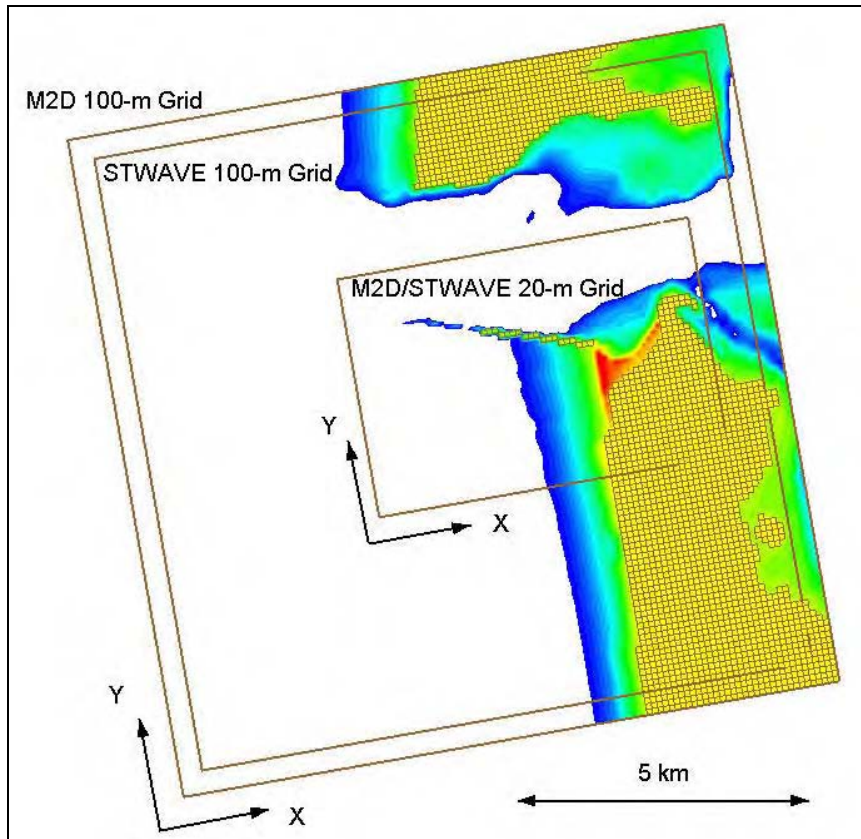


Figure 37. Nested M2D and STWAVE grids

M2D-STWAVE SMS Hydrodynamic Steering Module simulations were made for the seven bathymetric conditions to examine the magnitude, duration, and spatial extent of combined tidal and wave-induced flow through the breach for different bathymetry. The purpose of the simulations was to illustrate the relative change in circulation patterns and peak velocities at the breach, in the navigation channel, and in the inlet throat for a series of tide and wave conditions. Three wave conditions were simulated for each of the original five bathymetric conditions and two wave conditions were simulated for the two alternatives to the large breach for a total of 19 SMS Steering Module simulations (Table 6). The wave conditions represented typical waves (height of 1.5 m, period of 8 sec, and direction from 280 deg), a west-southwest high-energy condition (height of 6 m, period of 14 sec), and a west-northwest high-energy condition (height of 5 m, period of 13 sec). The simulations were morphologically static because the bathymetry was not changed during a given simulation (i.e., sediment transport and morphology change were not activated for these simulations). However, by modeling three bathymetric configurations of the breach, hydrodynamic response to temporal changes in bathymetry (breach development, scour, shoaling, wing spit development) is represented in the simulations. Observations and analysis of changes in hydrodynamics were made by comparing simulations with different bathymetry.

Table 7 Hydrodynamic-Wave Model Simulations				
Simulation No.	Bathymetry	Wave Condition		
		Height, m	Period, sec	Direction, deg
101	December 1993	Tide only		
102	December 1993	1.5	8	280.0
103	December 1993	6.0	14	247.5
104	December 1993	5.0	13	292.5
105	March 1994	Tide only		
106	March 1994	1.5	8	280.0
107	March 1994	6.0	14	247.5
108	March 1994	5.0	13	292.5
109	August 1994	Tide only		
110	August 1994	1.5	8	280.0
111	August 1994	6.0	14	247.5
112	August 1994	5.0	13	292.5
113	Existing	Tide only		
114	Existing	1.5	8	280.0
115	Existing	6.0	14	247.5
116	Existing	5.0	13	292.5
117	Large Breach	Tide only		
118	Large Breach	1.5	8	280.0
119	Large Breach	6.0	14	247.5
120	Large Breach	5.0	13	292.5
121	Large Breach without jetty protective landmass	Tide only		
122	Large Breach without jetty protective landmass	6.0	14	247.5
123	Large Breach without jetty protective landmass	5.0	13	292.5
124	Large Breach without jetty protective landmass Breach depth = 4.55 m, mtl	Tide only		
125	Large Breach without jetty protective landmass Breach depth = 4.55 m, mtl	6.0	14	247.5
126	Large Breach without jetty protective landmass Breach depth = 4.55 m, mtl	5.0	13	292.5

Hydrodynamic model simulations were made for each of the conditions listed in Table 6. Model simulation duration was 72 hr with a 0.5-sec time-step. For the coupled wave and hydrodynamic model simulations, the models were linked to pass wave information for calculating the wave-induced current and water-surface elevation change in the circulation model. Wave conditions were held constant during the hydrodynamic model simulation.

Analysis of Numerical Simulations

It was found that none of the breach configurations changed water level in the bay significantly. Therefore, subsequent material in this chapter concerns temporal and spatial changes in calculated current magnitude and horizontal circulation pattern.

Pre-breach simulations

Analysis of the pre-breach simulations was made to examine the circulation pattern in the vicinity of the south jetty and Half Moon Bay. These pre-breach condition simulations serve as a base for comparison to all of the breach simulations. Patterns with the breach in place are compared to the pre-breach conditions to indicate any change in hydrodynamics caused by the breach. Figures 38-45 show flood and ebb flow patterns for Runs 113-116 (pre-breach simulations). Run 113 is a hydrodynamic simulation with pre-breach bathymetry and tidal currents only. The flow is concentrated in the inlet throat and around the tip of the jetty leading to the inlet throat. An eddy is generated inside the inlet (north of the south jetty) on flood (Figure 38) and outside the inlet (south of the south jetty) on ebb (Figure 39). Velocity measurements made in the inlet throat (Hericks and Simpson 2000) indicate stronger flood currents on the north side of the inlet and stronger ebb currents on the south side of the inlet. Although the numerical model grid for the present study does not cover the entire inlet, the model is driven by results from the ADCIRC model that does have full inlet coverage. The horizontal circulation patterns in Figures 38 and 39 indicate stronger flood flow is on the northern side of the figure and an eddy near the south jetty. Ebb currents are stronger than flood currents at the south jetty. The vector pattern near the south jetty and breach area shows a northward and seaward current on flood and a seaward current on ebb. The red vectors indicate the general flow trend and show the longshore flood current directed seaward around the jetty tip and the inlet ebb current jetting seaward then spreading laterally.

Run 114 is a Steering Module simulation with pre-breach bathymetry and typical waves. Results from this simulation are similar to Run 113 results with the addition of a weak southward-directed longshore current and a rip current. This longshore current and rip pattern persists for both flood and ebb conditions (Figures 40 and 41).

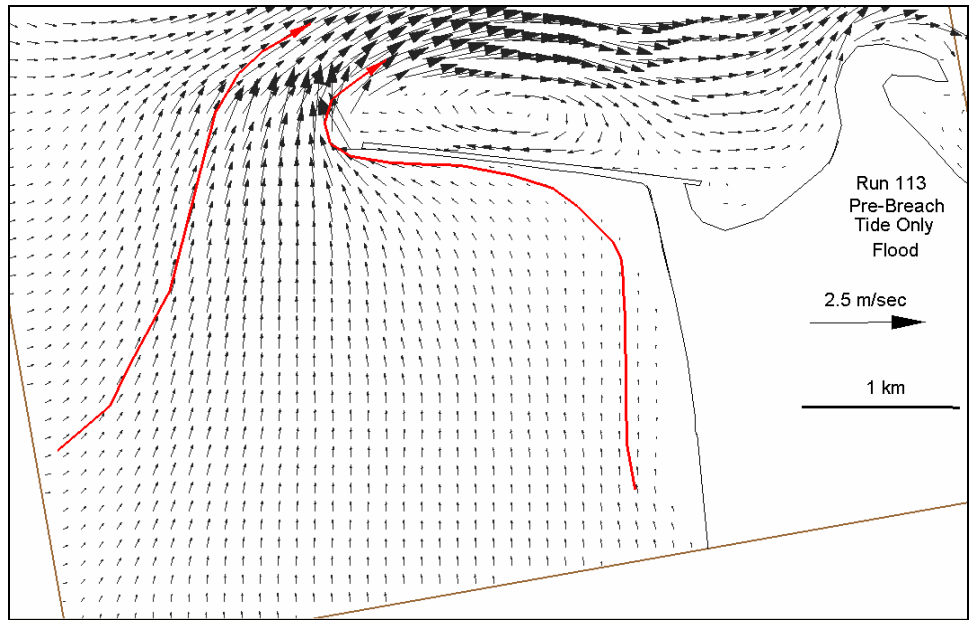


Figure 38. Flood flow for pre-breach, tide-only simulation (Run 113)

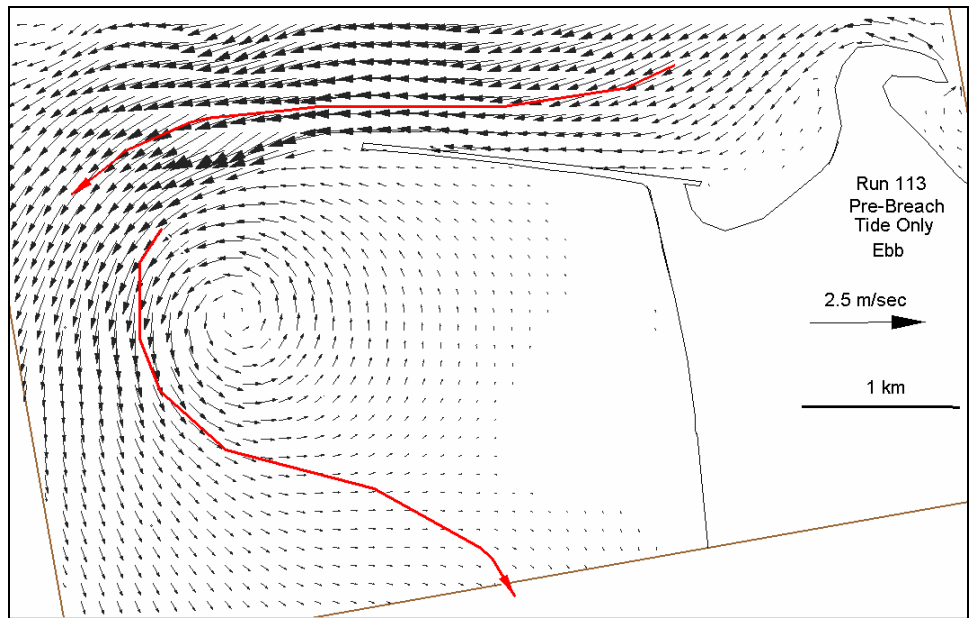


Figure 39. Ebb flow for pre-breach, tide-only simulation (Run 113)

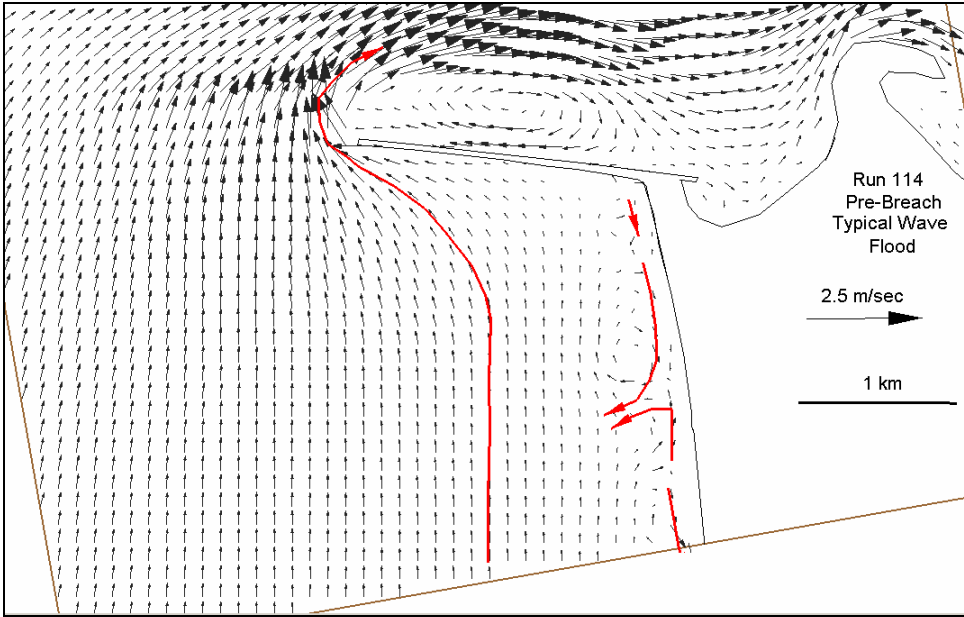


Figure 40. Flood flow for pre-breach, typical wave simulation (Run 114)

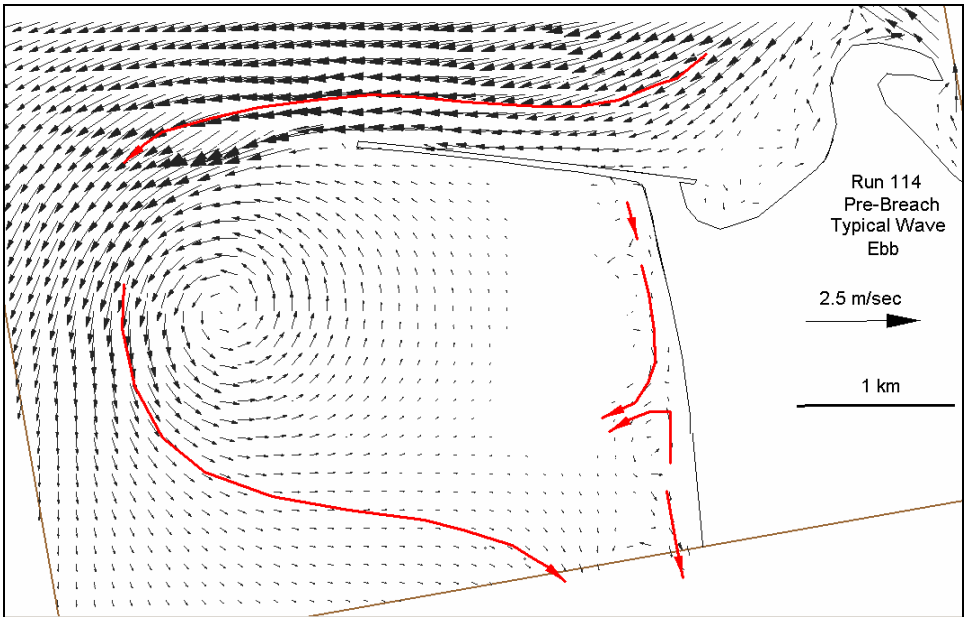


Figure 41. Ebb flow for pre-breach, typical wave simulation (Run 114)

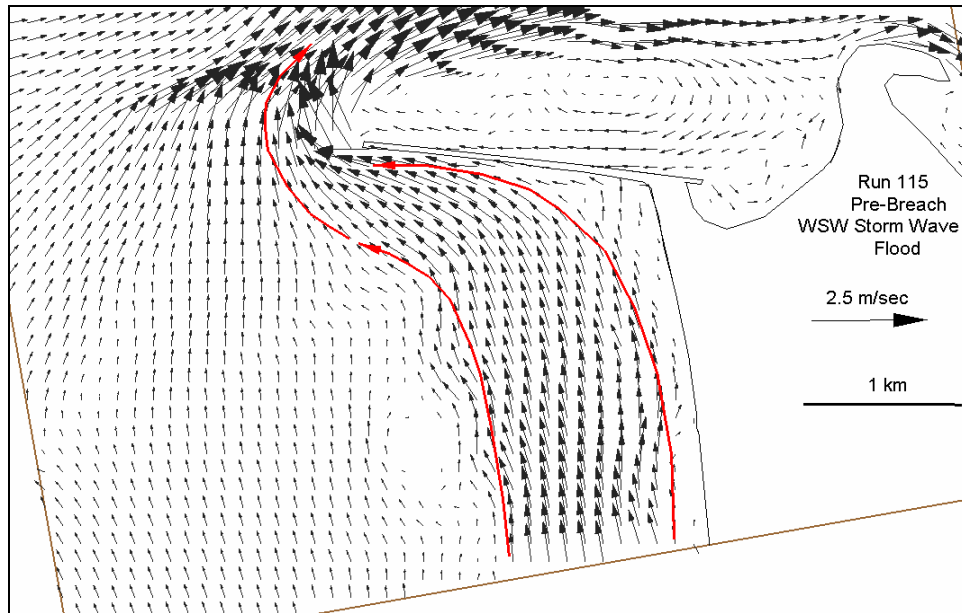


Figure 42. Flood flow for pre-breach, west-southwest storm wave simulation (Run 115)

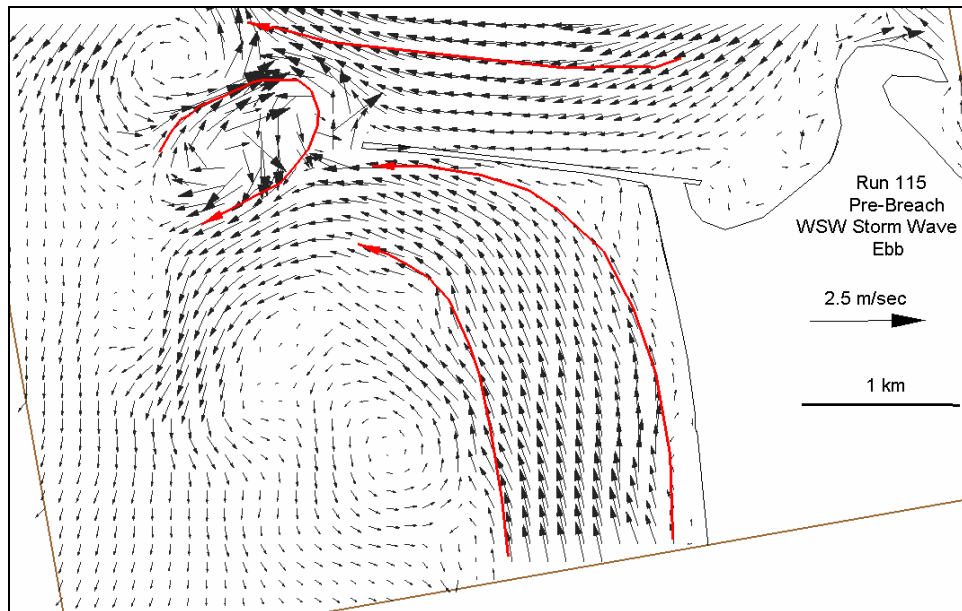


Figure 43. Ebb flow for pre-breach, west-southwest storm wave simulation (Run 115)

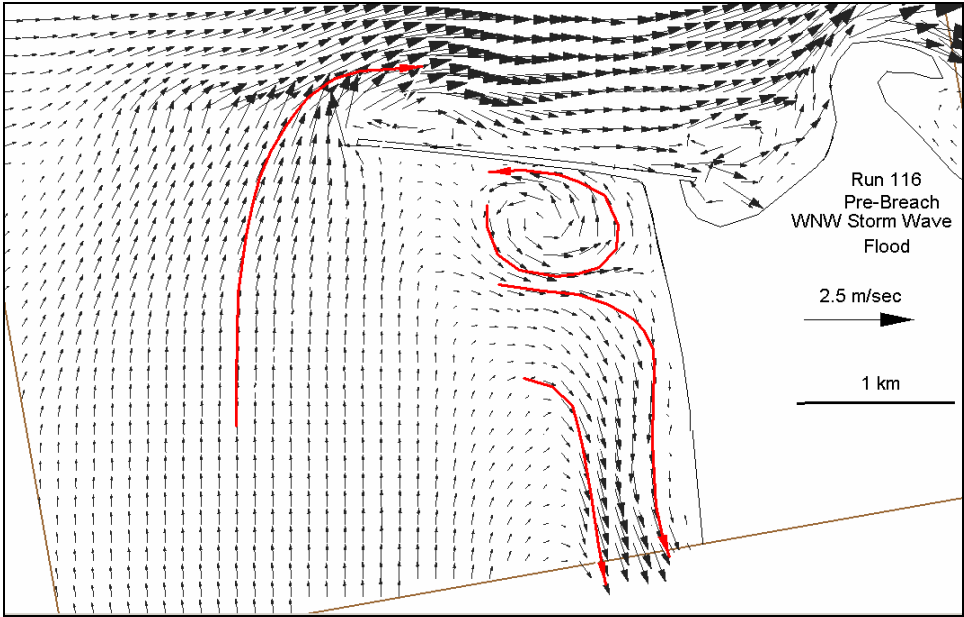


Figure 44. Flood flow for pre-breach, west-northwest storm wave simulation (Run 116)

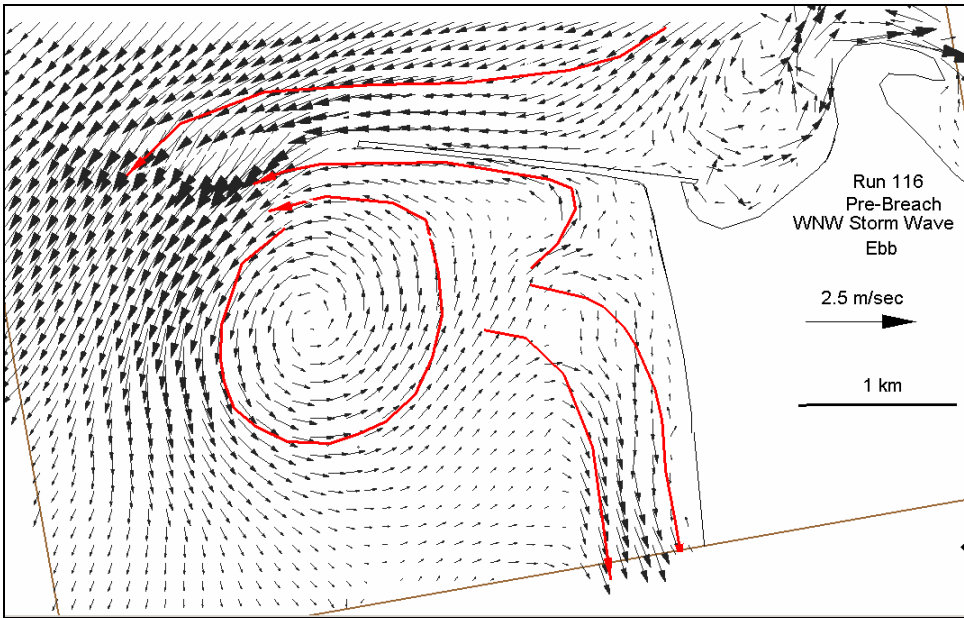


Figure 45. Ebb flow for pre-breach, west-northwest storm wave simulation (Run 116)

Run 115 is an SMS Steering Module simulation with pre-breach bathymetry and west-southwest storm waves. Results from this simulation are similar to Run 113 results with the addition of a strong northward-directed longshore current. The width of the longshore current is about two-thirds of the jetty length. The current sweeps seaward along the jetty and reinforced the tidal flood current near the jetty tip (Figure 42). The ebb current and the wave-driven longshore current interact near the jetty tip, and two opposite gyres form (Figure 43).

Run 116 is an SMS Steering Module simulation with pre-breach bathymetry and west-northwest storm waves. Results from this simulation are similar to Run 113 results with the addition of a strong southward-directed longshore current. The width of the longshore current is about one-half of the jetty length. The longshore current is established approximately 0.5 km south of the south jetty. Closer to the south jetty, an eddy develops, and a seaward-directed current is observed at the jetty on flood and ebb (Figures 44 and 45).

The simulations for the existing (pre-breach) condition show the basic horizontal circulation patterns for tidal and wave-induced currents. The flow in the inlet throat is strong and predominantly tidally driven. Structurally-induced eddies are also observed. With the coupling of the circulation and wave models, the circulation patterns show the establishment of longshore current, rip current, and eddies caused by the interaction of waves and currents. The general flow pattern near the south jetty and breach area shows a northward and seaward current on flood and a seaward current on ebb.

These calculated circulation patterns are consistent with sediment budget transport pathways presented in Byrnes and Baker (2003). The general hydrodynamic pattern of northward and offshore-directed transport near the south jetty is in accord with the comprehensive morphologic-based sediment budget. This pattern is supported by the absence of a fillet (sediment deficit) adjacent to the south jetty.

1993 breach simulations

An analysis of the 1993 breach simulations consisted of an examination of flood and ebb flow through the breach for 12 wave and bathymetry combinations (Table 6). December 1993, March 1994, and August 1994 bathymetries were selected for the model simulations. The selection was based on available aerial photography and bathymetric data.

December 1993. The breach in December 1993 was 85 m wide with a controlling elevation of near 2.0 m mllw (see Figure 18). This information was applied to generate the grid for hydrodynamic simulations of the December 1993 breach configuration. Flow through the breach was limited to periods when the water level was above the controlling elevation. Current speed at a selected point in the breach throat (Figure 46) was extracted from the model simulations (Figure 47). The time-series of current speeds at that location indicates that flow is observed in the breach for 37 percent of the tidal cycle. Peak tidal currents through the breach are generally 0.8-1.0 m/sec. Typical waves raise the flood peaks slightly and lower the ebb peaks slightly (0.7-1.1 m/sec). West-northwest storm waves raise the flood peaks more (1.2 m/sec) and lower the ebb peaks to 0.6 m/sec. West-southwest storm waves cause the greatest increase in current

speed at Point 1 in the breach, with a peak flood current of 2.0 m/sec and no observed ebb current.



Figure 46. Observation Point 1 overlaid on December 1993 aerial photograph of breach

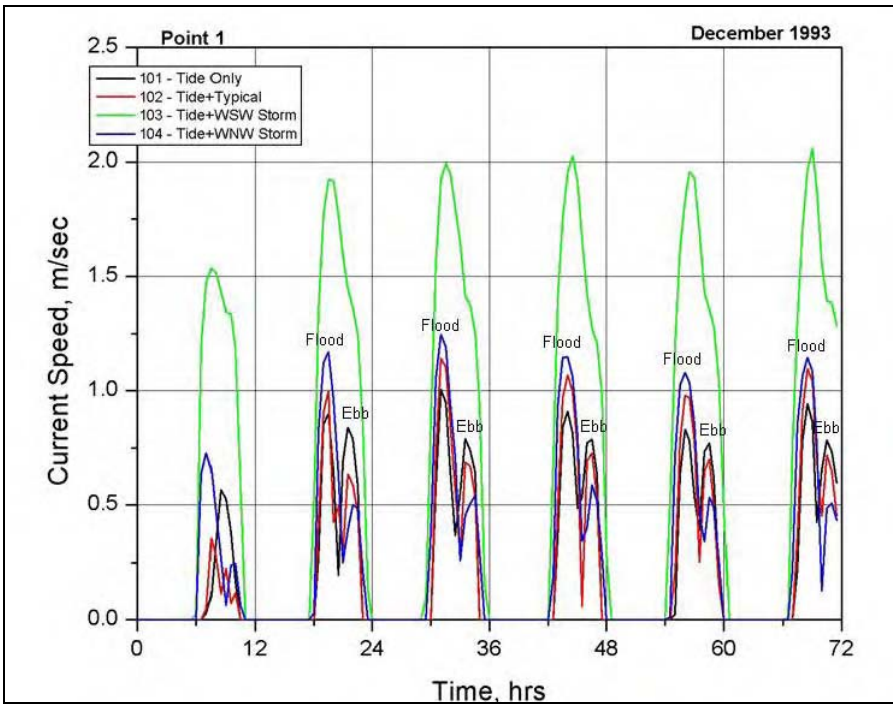


Figure 47. Time-series of current speed at Point 1 for December 1993 breach

Figures 48 and 49 show snapshots of peak flood and ebb-tidal flow patterns through the breach for the December 1993 bathymetry (Run 101). Flood and ebb flows are observed, with peak current speeds of 0.8-1.0 m/sec. An eddy on the north side of the south jetty creates a persistent seaward-directed flow observed in both the flood and ebb snapshots. [The current patterns of the M2D numerical model simulations in the eddy region are consistent with surface current patterns photographed from a physical model study of Grays Harbor (Brogdon 1972).] Also, flood flow through the breach sweeps north to join the ebb-flowing eddy (Figure 48).

Figures 50 and 51 show tidal-plus-wave-induced flow patterns through the breach for Run 102 (December 1993 bathymetry and typical waves). Results from this simulation are similar to Run 101 results; however, the flood current is enhanced, and the ebb current is reduced. Peak currents are 1.1 m/sec on flood and 0.7 m/sec on ebb.

Figures 52-54 show tidal-plus-wave-induced flow through the breach at its December 1993 bathymetry and west-southwest storm waves (Run 103). Results from this simulation are similar to Run 101 results; however, the flood current is further enhanced, and the ebb-tidal current is almost overcome by the opposing wave-induced current. Peak flood currents at hours 44-46 are 2.0 m/sec. The flood current at hour 44.5 jets through the breach (Figure 52), and at hour 45.5 the flood current is swept to the north, joining a seaward-directed eddy near the navigation channel (Figure 53). At hour 47, an ebb current is observed in the inlet throat, but a flood current persists through the breach throughout the ebb cycle (Figure 54).

Figures 55 and 56 show tidal-plus-wave-induced flow through the breach at its December 1993 bathymetry and west-northwest storm waves (Run 104). Results from this simulation are similar to Run 101 results; however, the flood current is enhanced, and the ebb current is reduced. Peak currents are 1.2 m/sec on flood and 0.6 m/sec on ebb.

March 1994. The March 1994 breach was measured to be 140 m wide, with the lowest point being +1.0 m mllw (Table 4). Flow through the breach was limited to periods when the water level was above the controlling elevation. Current speed at a selected point in the breach throat (Point 3, Figure 57) was extracted from the model simulations (Figure 58). As noted in Chapter 2, the lobe of material observed adjacent to the south jetty in the December 1993 aerial photograph (Figure 18) erodes by the time of the March 1994 aerial photograph and bathymetric survey. The primary flow through the breach at Point 1 in December 1993 shifted to Point 3 by March 1994. The time-series of current speeds at that location indicates that flow is observed in the breach for 56 percent of the tidal cycle.

Peak tidal currents through the breach are 0.8-0.9 m/sec for both flood and ebb. Typical waves raise the flood peaks to 1.0 m/sec and lower the ebb peaks slightly (0.8 m/sec). West-northwest storm waves raise the flood peaks more (1.2 m/sec) and lower the ebb peaks to 0.6 m/sec. West-southwest storm waves cause the greatest change to current speed at Point 3 in the breach. An ebb current is not observed. The peak flood current is 1.8 m/sec. (The current at Point 1 is less than 0.2 m/sec.)

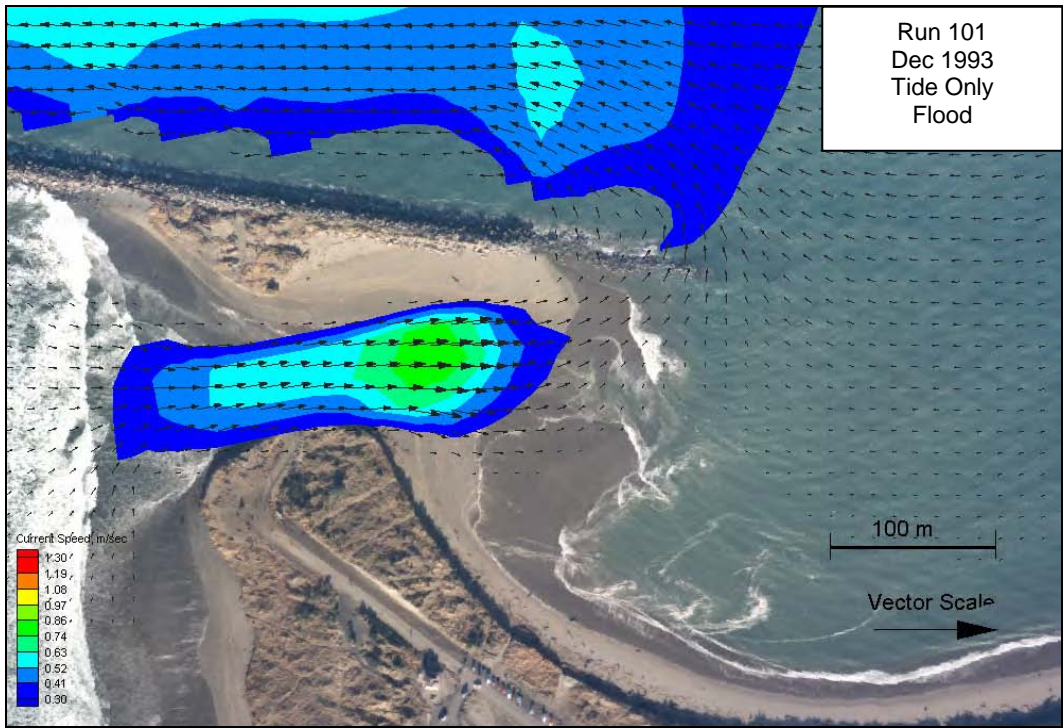


Figure 48. Flood flow for December 1993 breach, tide-only simulation (Run 101)

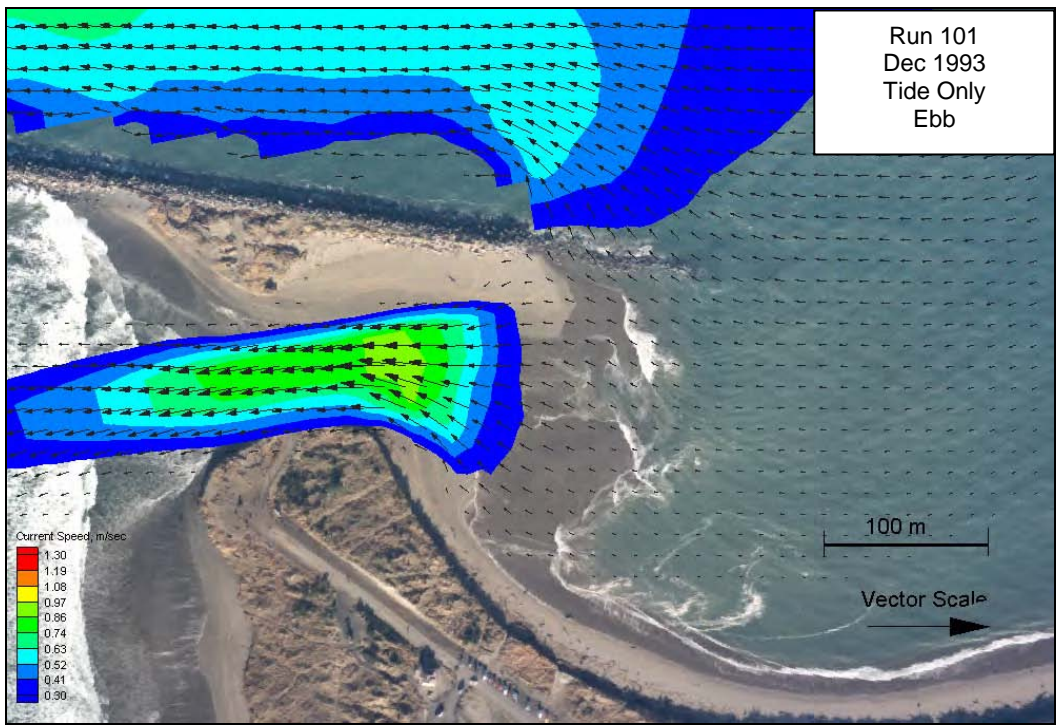


Figure 49. Ebb flow for December 1993 breach, tide-only simulation (Run 101)

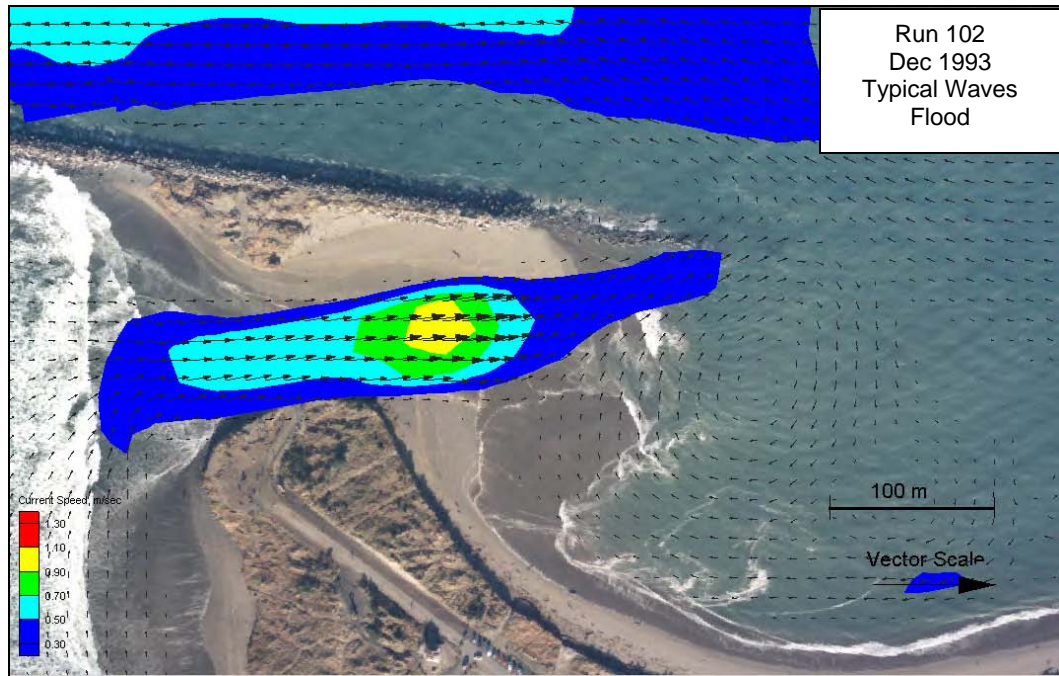


Figure 50. Flood flow for December 1993 breach, typical wave simulation (Run 102)

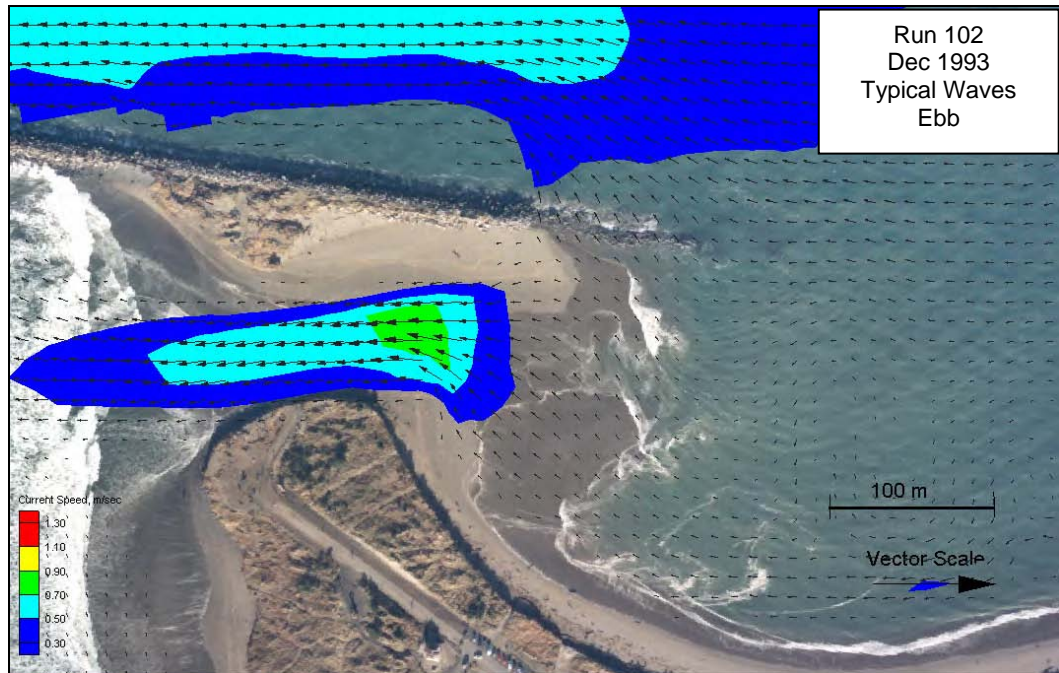


Figure 51. Ebb flow for December 1993 breach, typical wave simulation (Run 102)

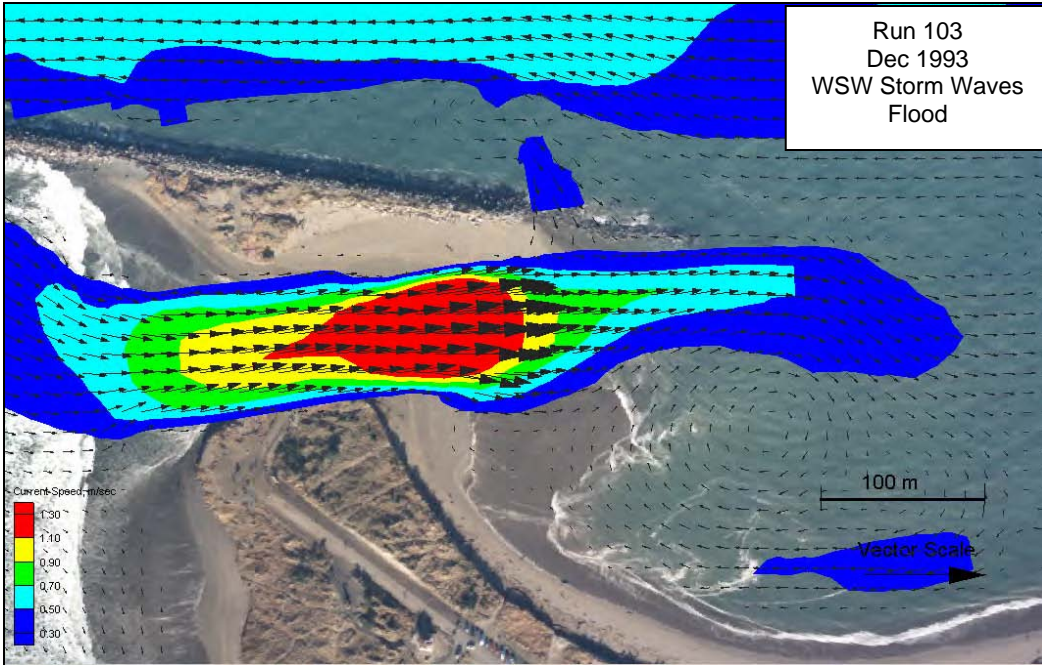


Figure 52. Flood flow at hour 44.5 for December 1993 breach, west-southwest storm wave simulation (Run 103)

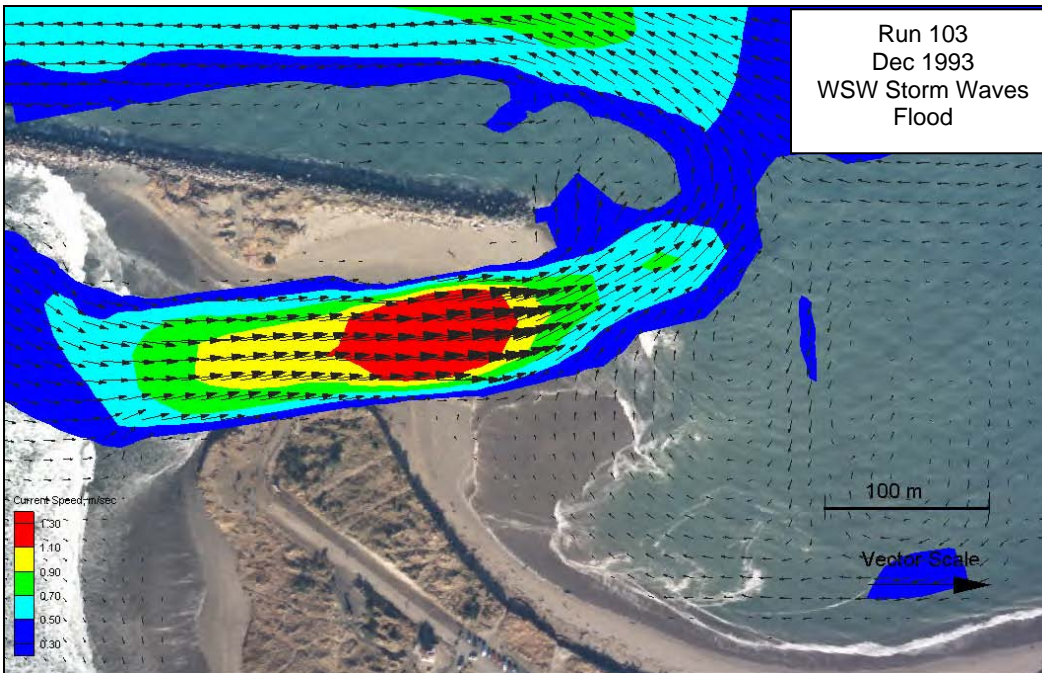


Figure 53. Flood flow at hour 45.5 for December 1993 breach, west-southwest storm wave simulation (Run 103)

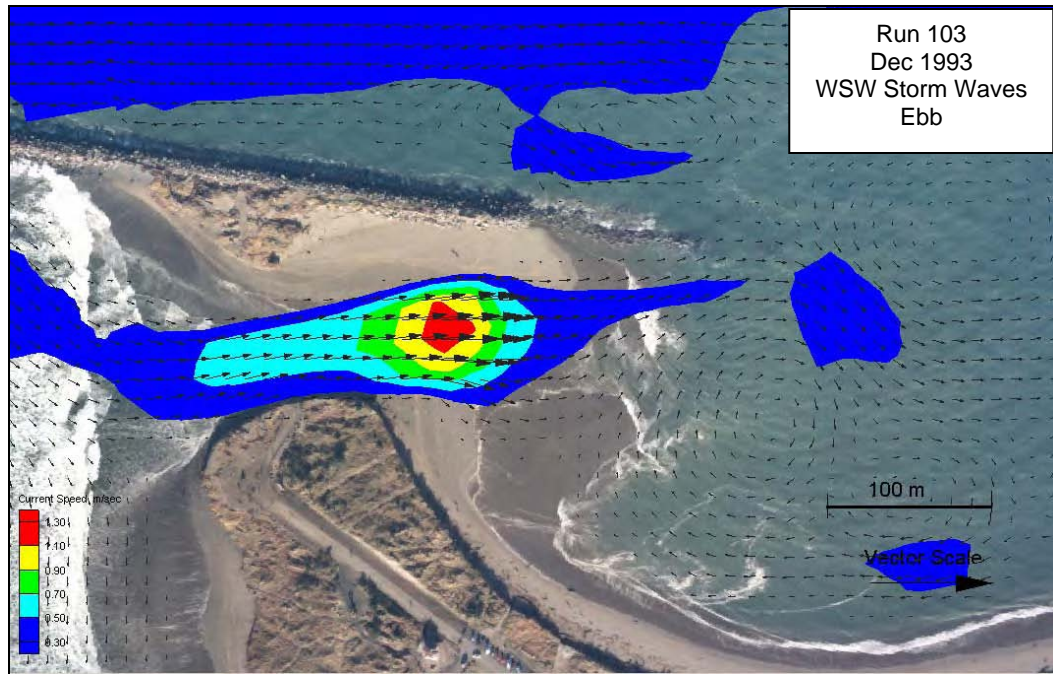


Figure 54. Ebb flow for December 1993 breach, west-southwest storm wave simulation (Run 103)

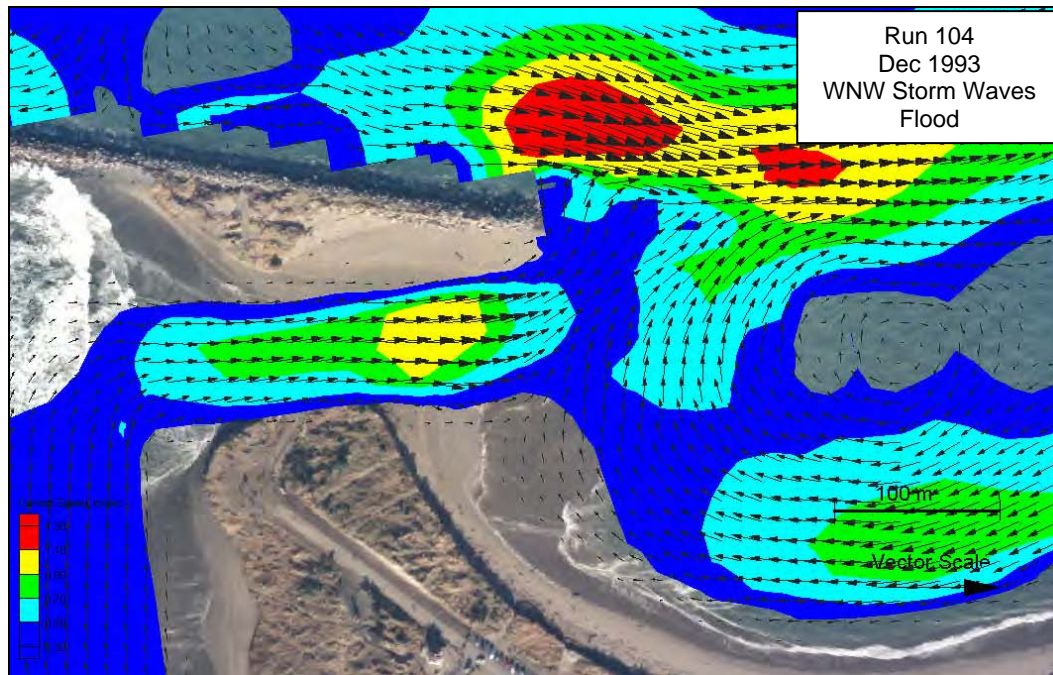


Figure 55. Flood flow for December 1993 breach, west-northwest storm wave simulation (Run 104)

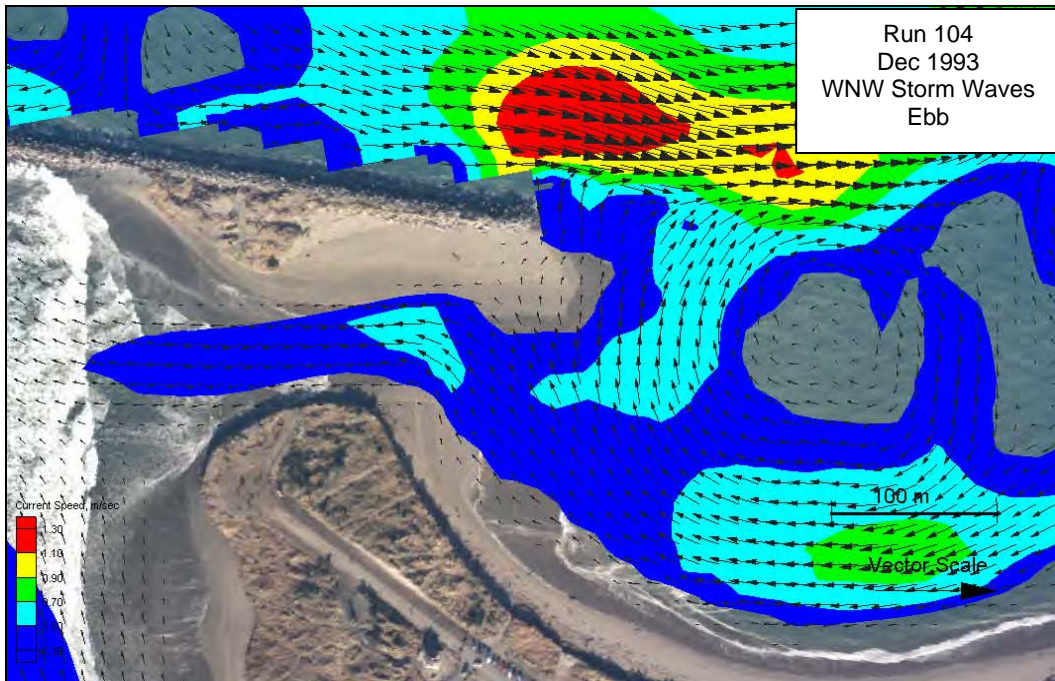


Figure 56. Ebb flow for December 1993 breach, west-northwest storm wave simulation (Run 104)



Figure 57. Observation points overlaid on March 1994 aerial photograph of breach

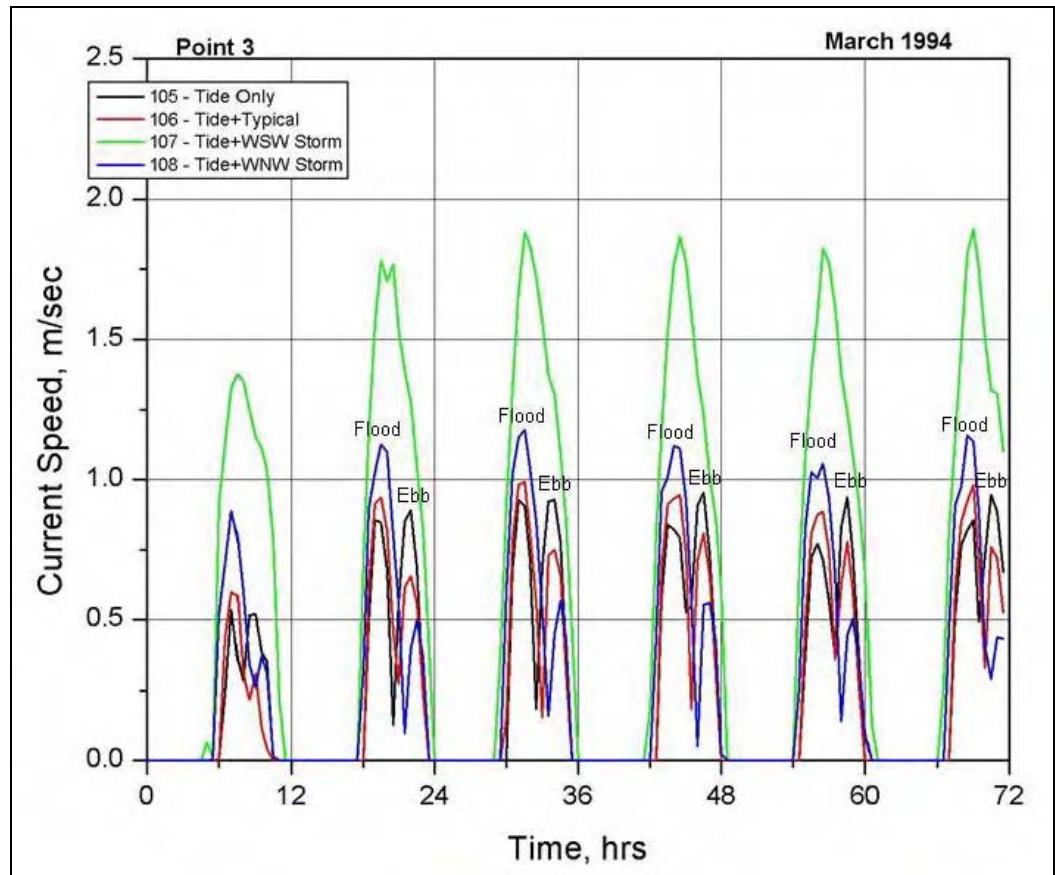


Figure 58. Time-series of current speed at Point 3 for March 1994 breach

Figures 59 and 60 show snapshots of peak flood and ebb-tidal flow patterns through the breach for March 1994 bathymetry (Run 105). Flood and ebb flows are observed, with peak current speeds of 0.7-1.0 m/sec. Figures 61 and 62 show tidal-plus-wave-induced flow patterns through the breach for Run 106 (March 1994 bathymetry and typical waves). Results from this simulation are similar to Run 105 results; however, the flood current is enhanced, and the ebb current is reduced. Peak currents are 1.0 m/sec on flood and 0.8 m/sec on ebb.

Figures 63 and 64 show tidal-plus-wave-induced flow through the breach at its March 1994 bathymetry and west-southwest storm waves (Run 107). Results from this simulation are similar to Run 105 results; however, the flood current is further enhanced, and the ebb-tidal current is weakened by the opposing wave-induced current. Peak flood currents are 1.8 m/sec. Figures 65 and 66 show tidal-plus-wave-induced flow through the breach at its March 1994 bathymetry and west-northwest storm waves (Run 108). Results from this simulation are similar to Run 105 results; however, the flood current is enhanced, and the ebb current is reduced. Peak current reaches 1.2 m/sec on flood and 0.6 m/sec on ebb.

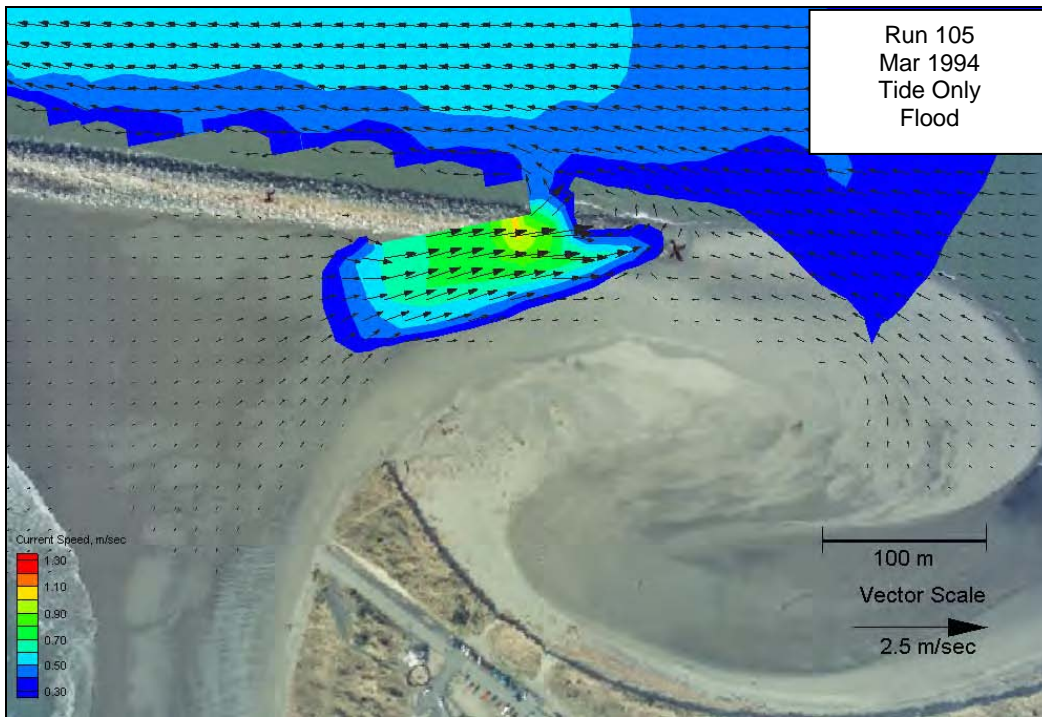


Figure 59. Flood flow for March 1994 breach, tide-only simulation (Run 105)

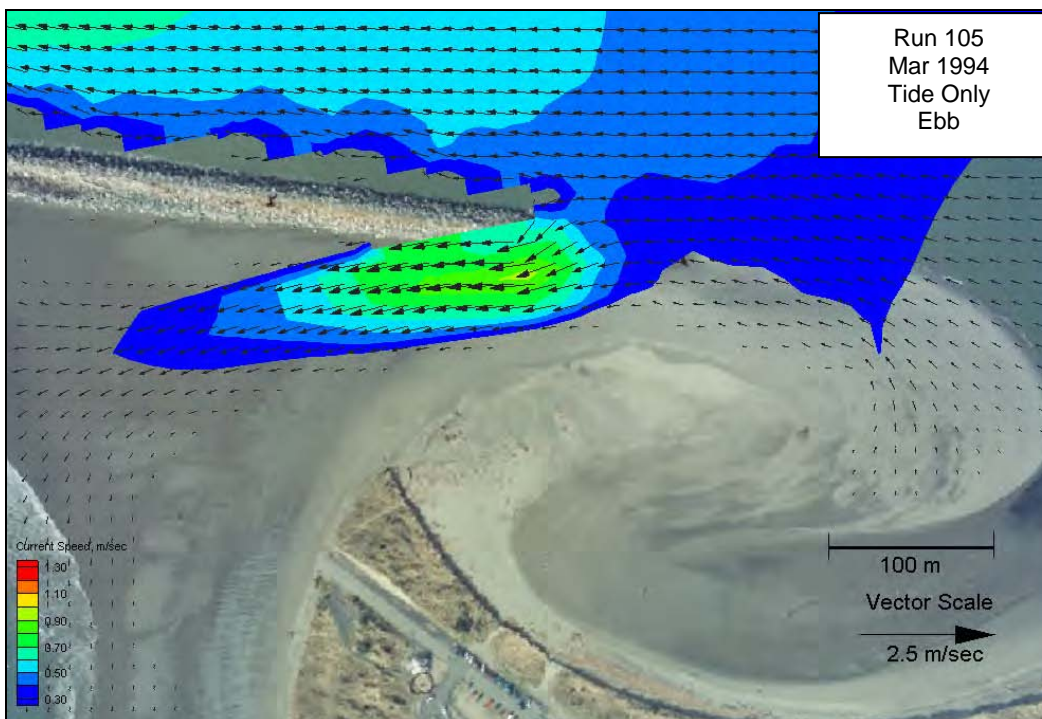


Figure 60. Ebb flow for March 1994 breach, tide-only simulation (Run 105)

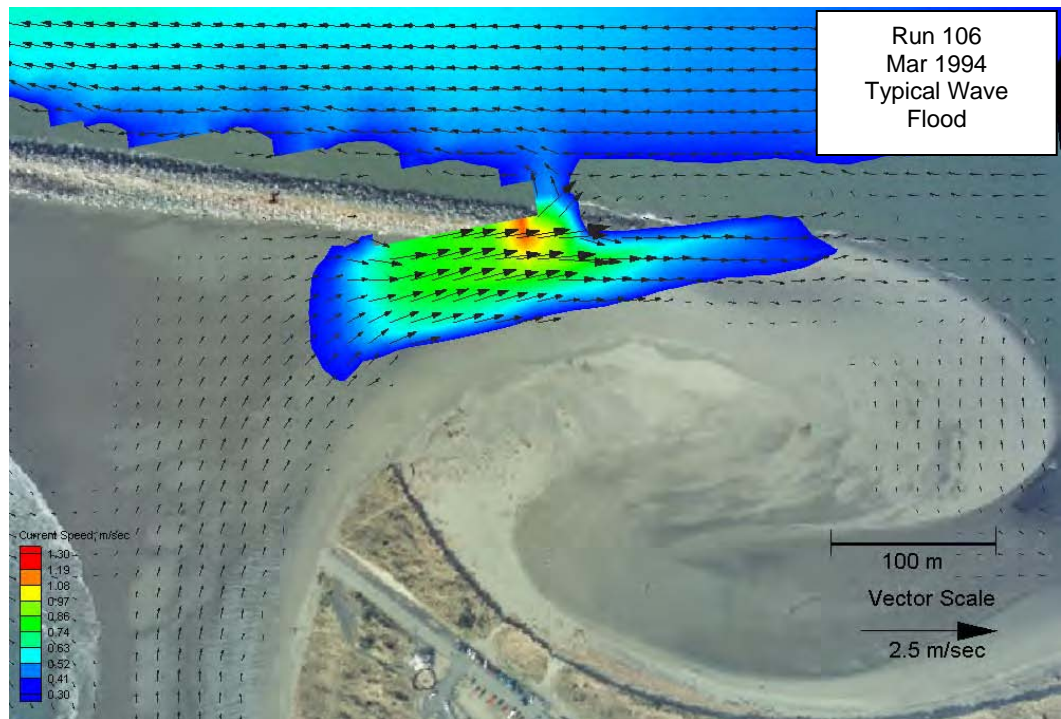


Figure 61. Flood flow for March 1994 breach, typical wave simulation (Run 106)

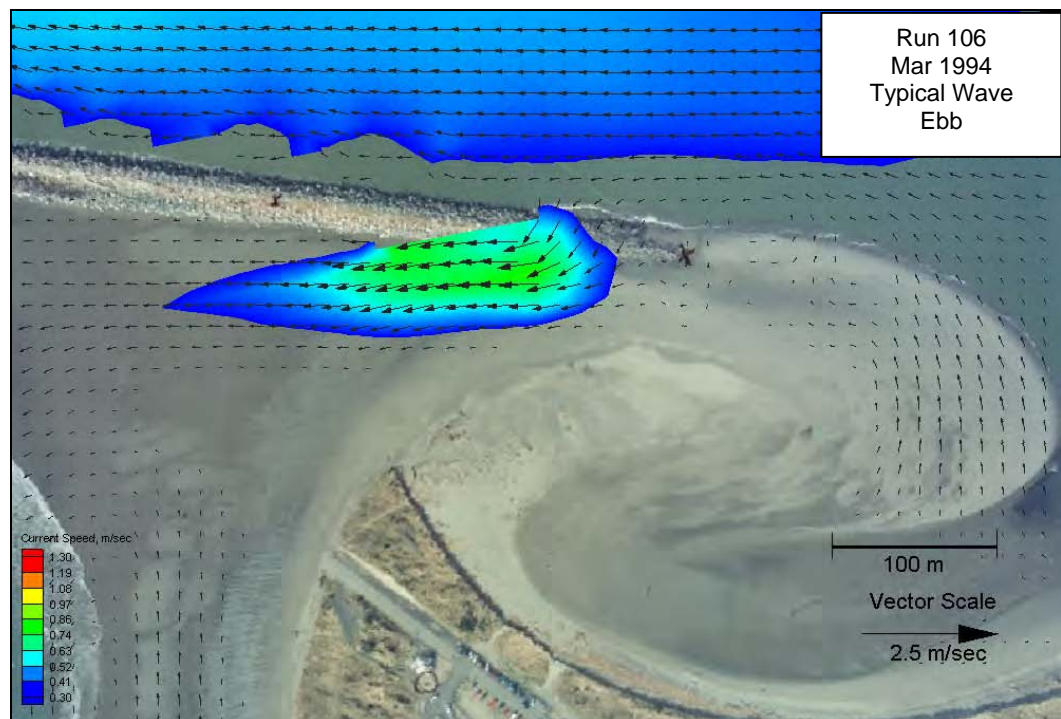


Figure 62. Ebb flow for March 1994 breach, typical wave simulation (Run 106)

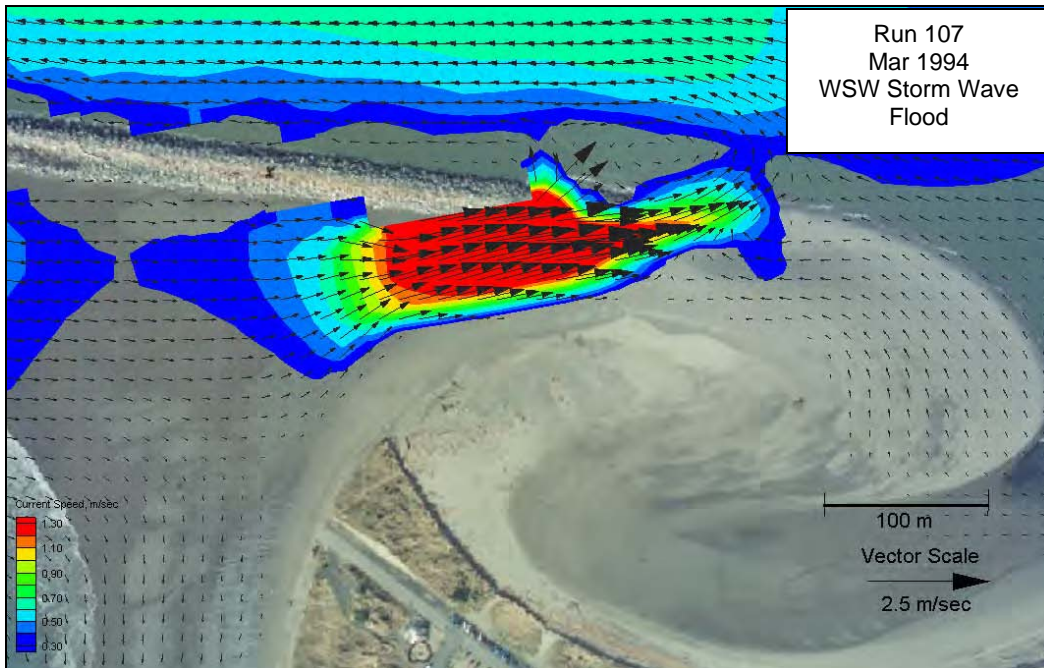


Figure 63. Flood flow for March 1994 breach, west-southwest storm wave simulation (Run 107)

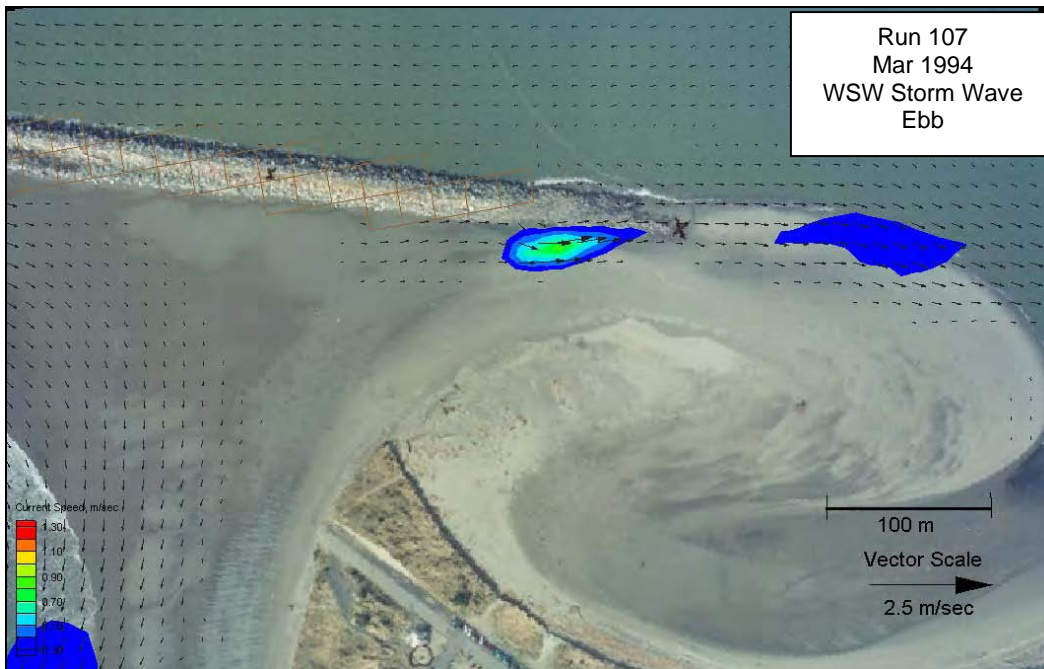


Figure 64. Ebb flow for March 1994 breach, west-southwest storm wave simulation (Run 107)

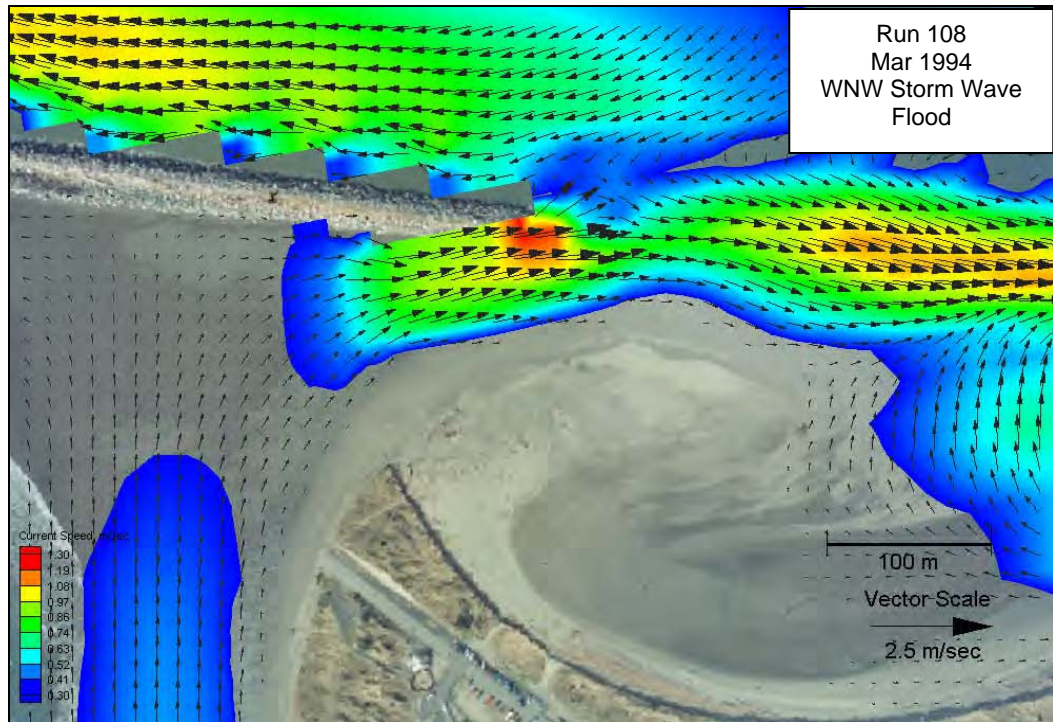


Figure 65. Flood flow for March 1994 breach, west-northwest storm wave simulation (Run 108)

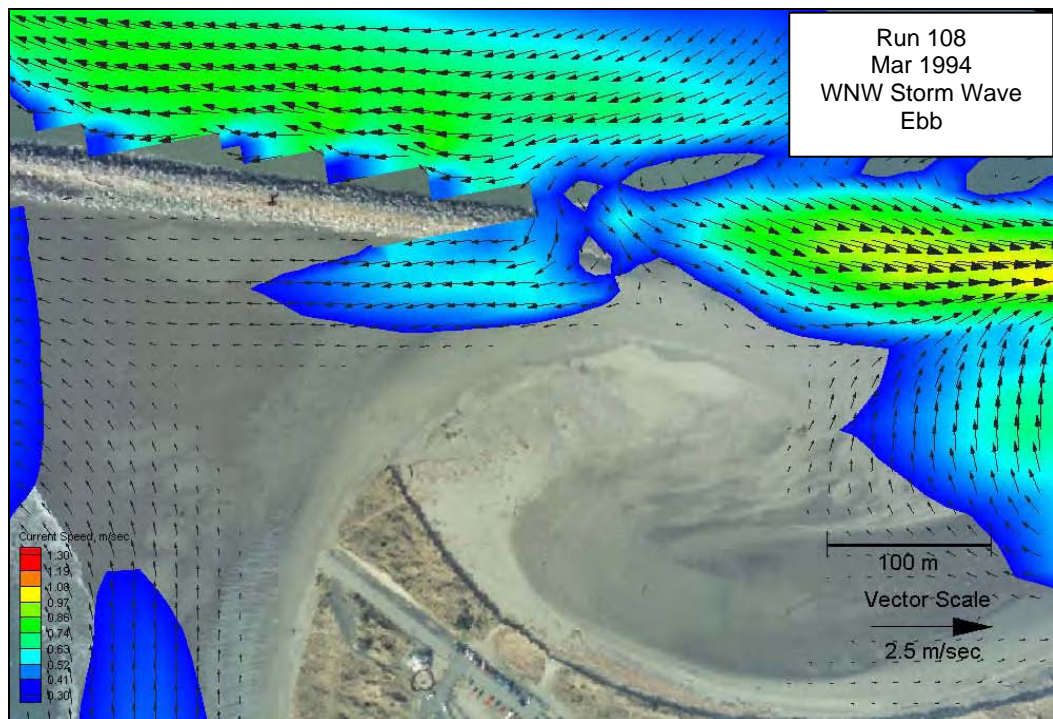


Figure 66. Ebb flow for March 1994 breach, west-northwest storm wave simulation (Run 108)

August 1994. In August 1994, the breach was 165 m wide with a minimum elevation of +0.2 m mllw (Figure 67). Flow through the breach was limited to periods when the water level was above minimum breach depth. Current speeds at four points in the breach throat (Points 1, 2, 3, and 5 in Figure 67) were extracted from the model simulations to illustrate that the current strength and spatial extent increased from December 1993 to August 1994 (Figure 68-71). The time-series of current speed at Point 3 indicates that flow occurs in the breach for 76 percent of the tidal cycle. This is a 39 percent increase (more than doubling) in flow time compared to the 37 percent flow time in the December 1993 condition.

The peak tidal current through the breach is typically 0.9-1.0 m/sec at Point 3 (Figure 68), 0.7-0.9 m/sec at Point 2 (Figure 69), 0.4 m/sec at Point 5 (Figure 70), and 0.3 m/sec at Point 1 (Figure 71). Considering Point 3, typical waves increase the flood current 0.2 to 1.2 m/sec and decrease the ebb current approximately 0.2 to 0.8 m/sec. These numerical observations are in accord with field observations made by Seattle District personnel during the August 1994 time period.

At Point 3, west-northwest storm waves raise the flood peaks more (1.25 m/sec) and decrease the ebb peaks to 0.6 m/sec. West-southwest storm waves increase the flood current to 2.2 m/sec. An ebb current is not observed. Note that west-southwest storm waves in August 1994 also cover a greater spatial extent. Peak flood currents at Point 2 are 1.5 m/sec, at Point 1 are 0.6 m/sec, and at Point 5 are 0.6 m/sec.



Figure 67. Observation points overlaid on August 1994 aerial photograph of breach

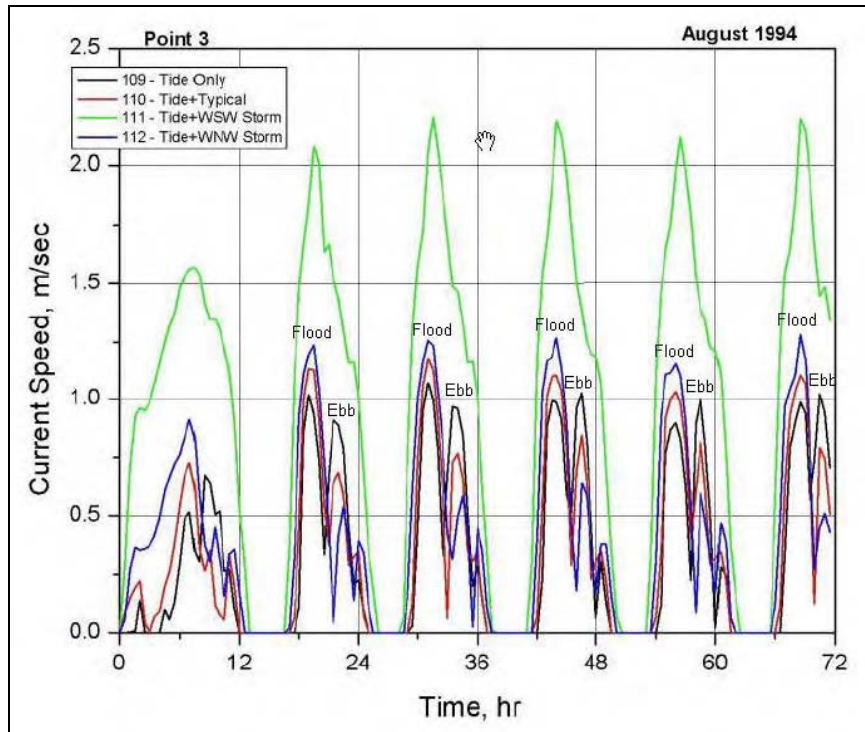


Figure 68. Time series of current speed at Point 3 for August 1994 breach

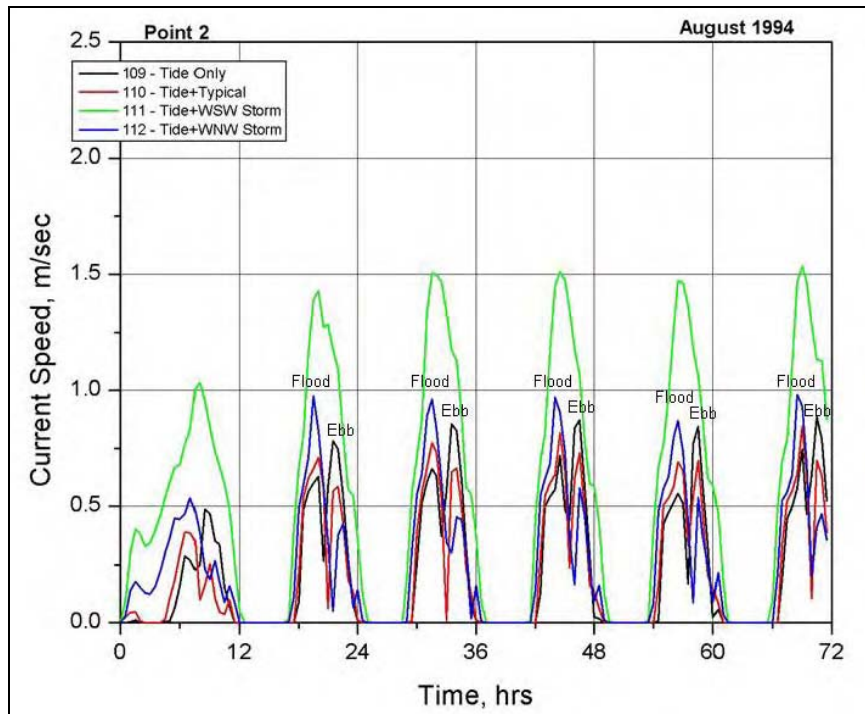


Figure 69. Time series of current speed at Point 2 for August 1994 breach

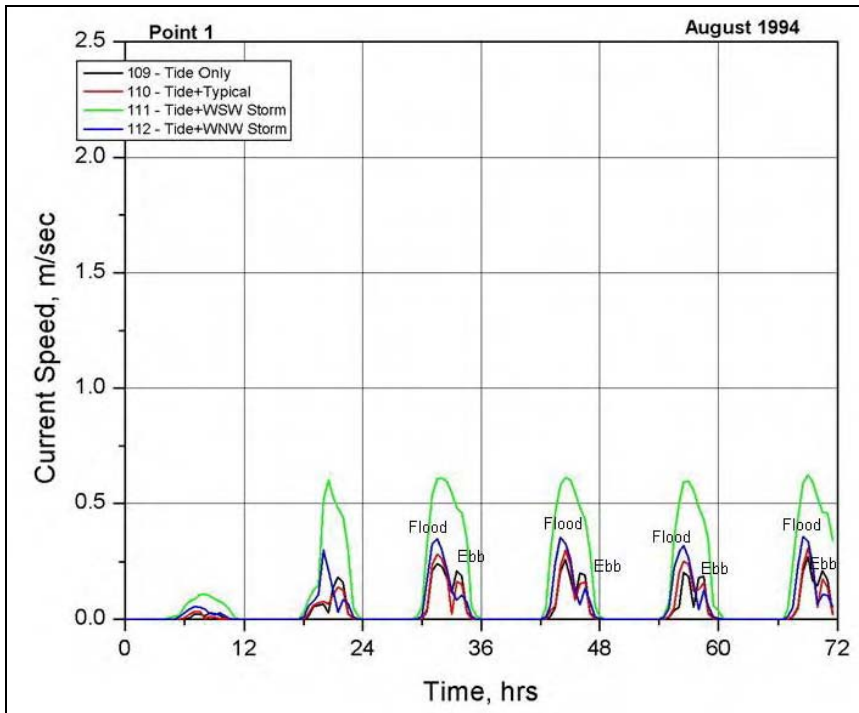


Figure 70. Time series of current speed at Point 1 for August 1994 breach

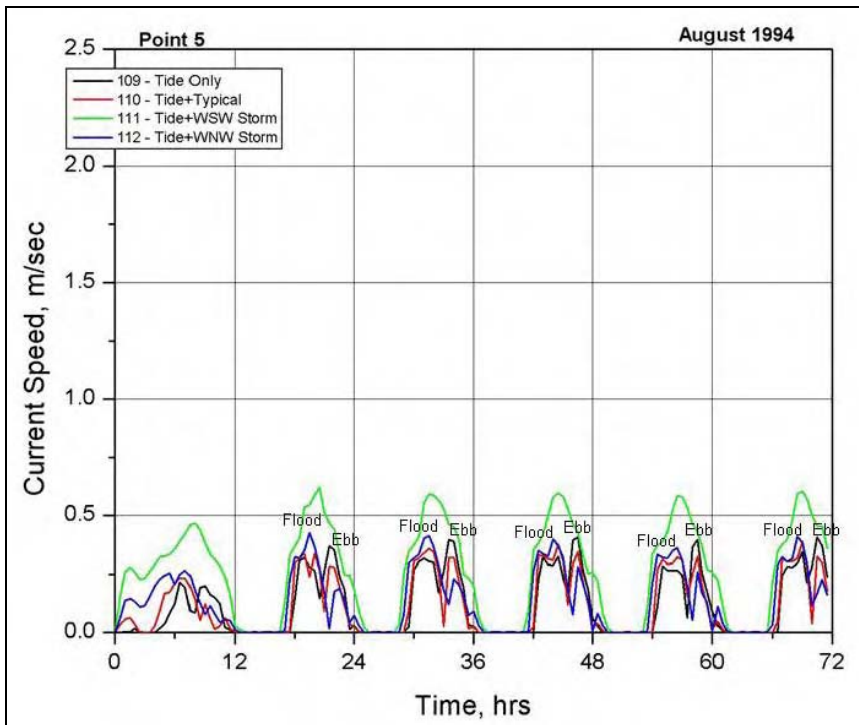


Figure 71. Time series of current speed at Point 5 for August 1994 breach

Figures 72 and 73 show snapshots of peak flood and ebb tidal flow patterns through the breach for the August 1994 bathymetry (Run 109). Flood and ebb flow is observed, with peak current speed of 0.7-1.0 m/sec. Figures 74 and 75 show tidal-plus-wave-induced flow patterns through the breach for Run 110 (August 1994 bathymetry and typical waves). Results from this simulation are similar to Run 109 results; however, the flood current is enhanced, and the ebb current is reduced. Peak currents are 1.2 m/sec on flood and 0.8 m/sec on ebb.

Figures 76 and 77 show tidal-plus-wave-induced flow through the breach in its August 1994 bathymetric configuration and west-southwest storm waves (Run 111). Results from this simulation are similar to Run 109 results; however, the flood current is further enhanced, and the ebb tidal current is weakened by the opposing wave-induced current. Peak flood currents are 2.2 m/sec. Figures 78 and 79 show tidal-plus-wave-induced flow through the breach for August 1994 bathymetry and west-northwest storm waves (Run 112). Results from this simulation are similar to Run 109 results; however, the flood current is enhanced (1.25 m/sec), and the ebb current is reduced (0.6 m/sec).

December 1993 to August 1994 changes

Figures 48, 59, and 72 show flood-tidal current patterns for the December 1993, March 1994, and August 1994 bathymetry, respectively. Figure 80 shows the general pattern of flow through the breach for the three time periods. Initially, the flood current passed through a confined east-west opening and was directed due east (Figure 48). By March 1994, the peak flood current is located closer to the south jetty and in an east-northeast orientation (Figure 59). In August 1994, the peak flood current covers a greater spatial extent, moving alongshore, through the breach area in an east-northeast direction, then to the north to join the main inlet current (Figure 72).

Figures 49, 60, and 73 show ebb-tidal current patterns for the December 1993, March 1994, and August 1994 bathymetry, respectively. Overall, the patterns are a reverse of the flood current patterns. Peak tidal currents are about 1.0 m/sec.

Figures 52, 53, 63, and 76 show flood current patterns with west-southwest storm waves for the December 1993, March 1994, and August 1994 bathymetry, respectively. (Note that the peak storm-induced current is 2.0-2.2 m/sec as compared to 1.0 m/sec for the tidal current.) In December 1993, the storm-induced flood current at hour 44.5 was in an easterly direction. At hour 45.5, the flood current through the breach sweeps northward and joins the inlet current. In March 1994, the storm-induced flood current is strong and flows adjacent to the south jetty in an east-northeast direction. In August 1994, the storm-induced flood current is even stronger adjacent to the south jetty in an east-northeast direction, then joins the inlet current.

The simulations were designed to illustrate relative change in currents from December 1993 to August 1994 for the same forcing conditions. From December 1993 to August 1994, peak current increased from 2.0 to 2.2 m/sec. In addition, the spatial extent of the strong current increased, and the flow time through the breach increased from 37 to 76 percent of the tidal cycle (more than doubling the flow time). The current magnitude, spatial extent, and temporal

length are indicators of increases in breach growth and potential for continued growth. However, if the current velocity in the breach were to fall below a critical velocity threshold for sediment transport, then sediment would deposit in the breach, and eventually it would close at a minimal elevation (mllw). Flows would return to the pre-breach trend of moving seaward at the jetty, and further deposition in the breach would be unlikely. The minimally healed breach would, however, be vulnerable to reopening by smaller and smaller storms.

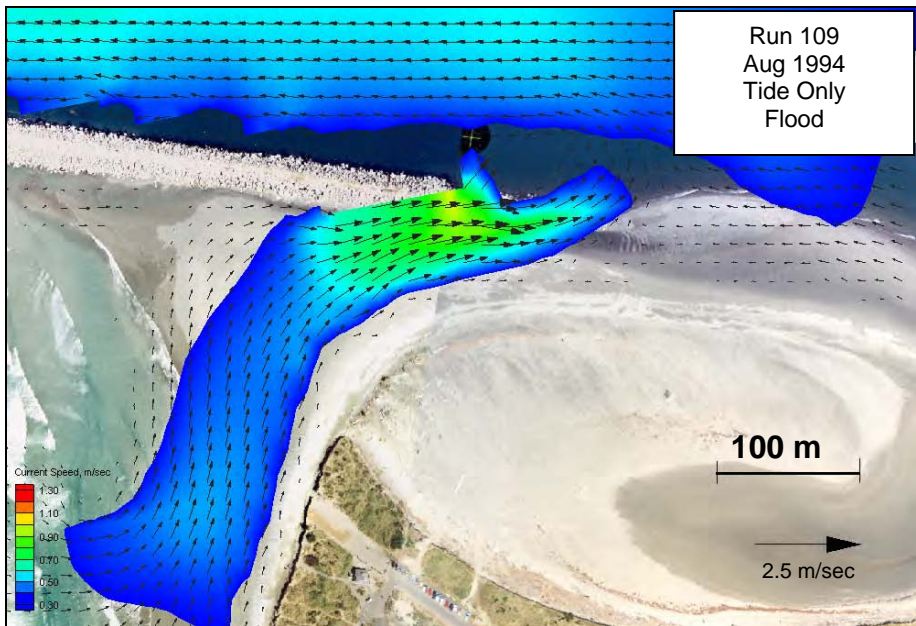


Figure 72. Flood flow for August 1994 breach, tide-only simulation (Run 109)

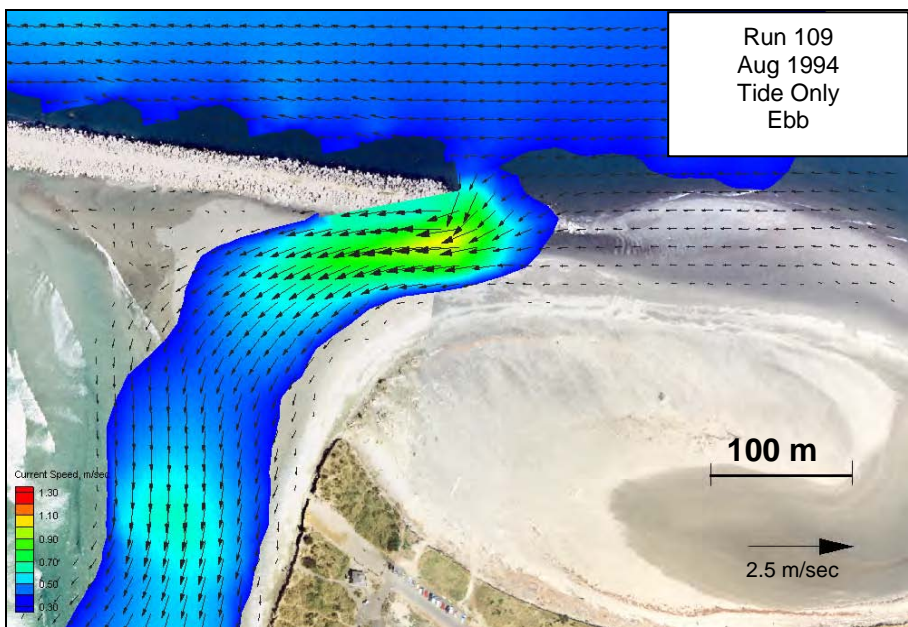


Figure 73. Ebb flow for August 1994 breach, tide-only simulation (Run 109)

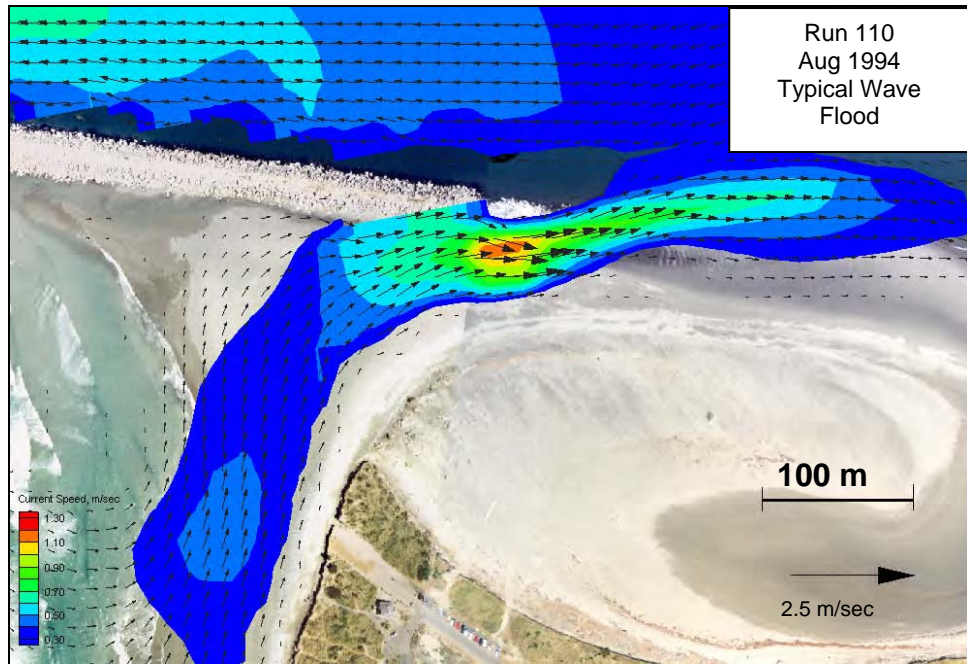


Figure 74. Flood flow for August 1994 breach, typical wave simulation (Run 110)

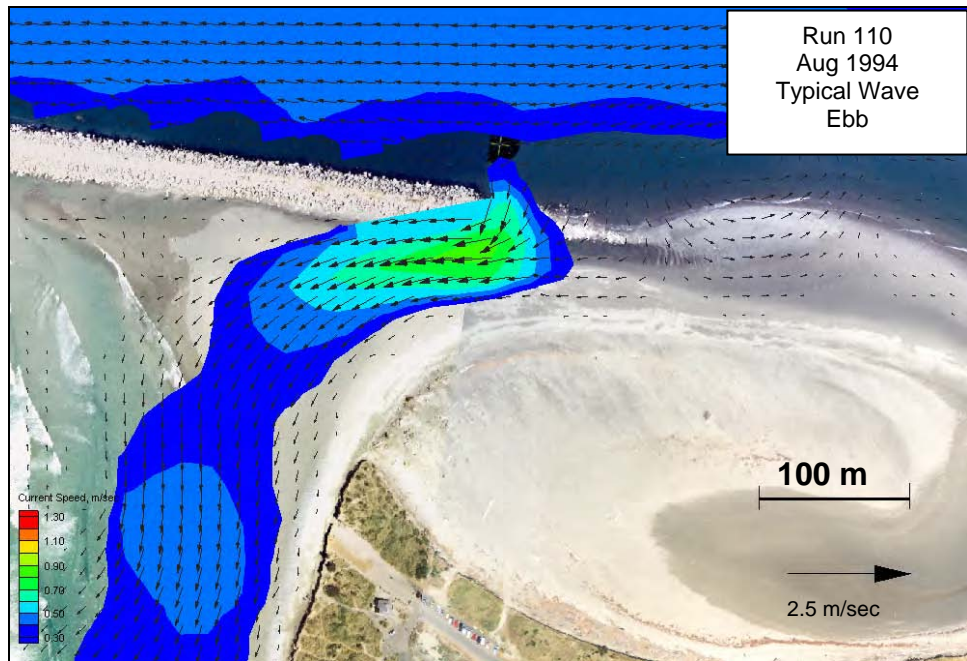


Figure 75. Ebb flow for August 1994 breach, typical wave simulation (Run 110)

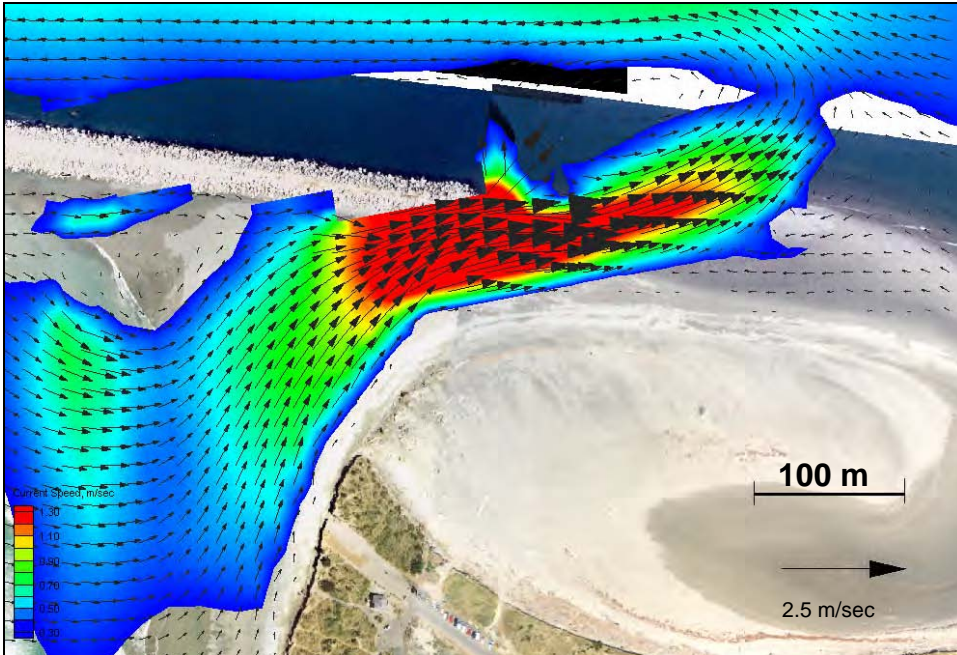


Figure 76. Flood flow for August 1994 breach, west-southwest storm wave simulation (Run 110)

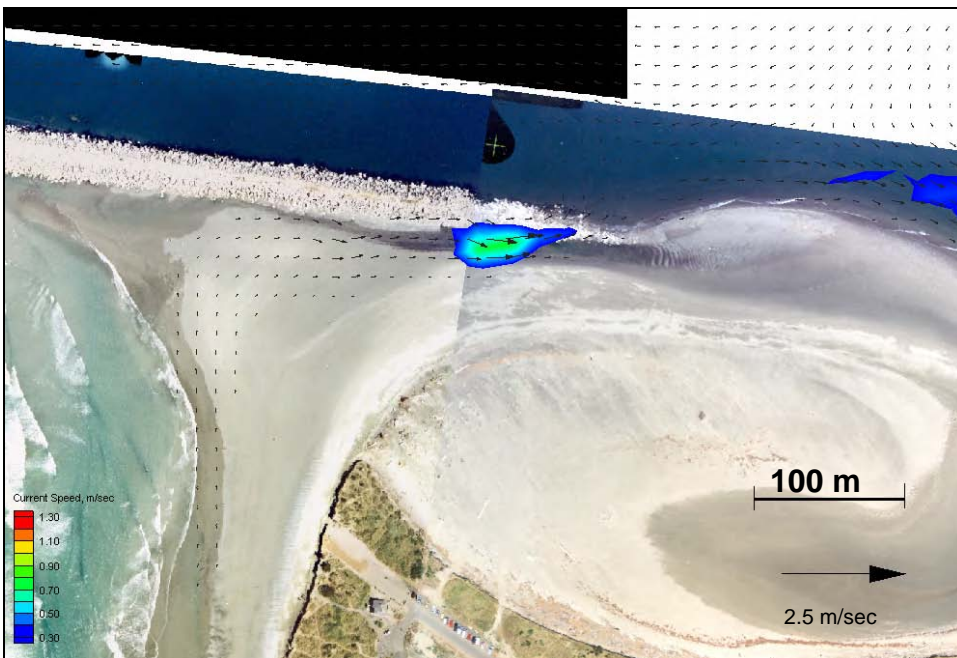


Figure 77. Ebb flow for August 1994 breach, west-southwest storm wave simulation (Run 110)

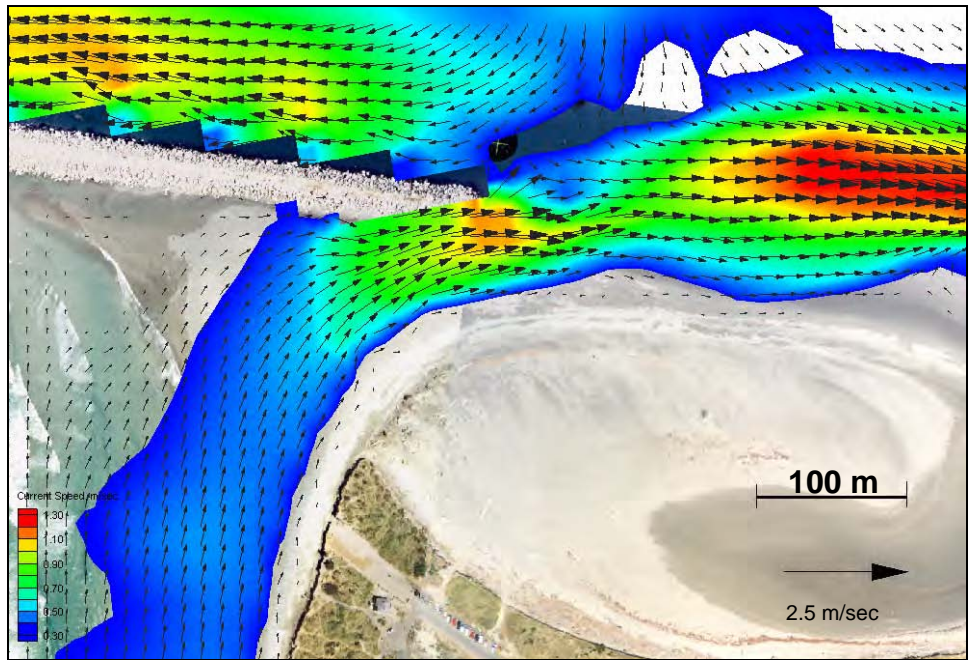


Figure 78. Flood flow for August 1994 breach, west-northwest storm wave simulation (Run 111)

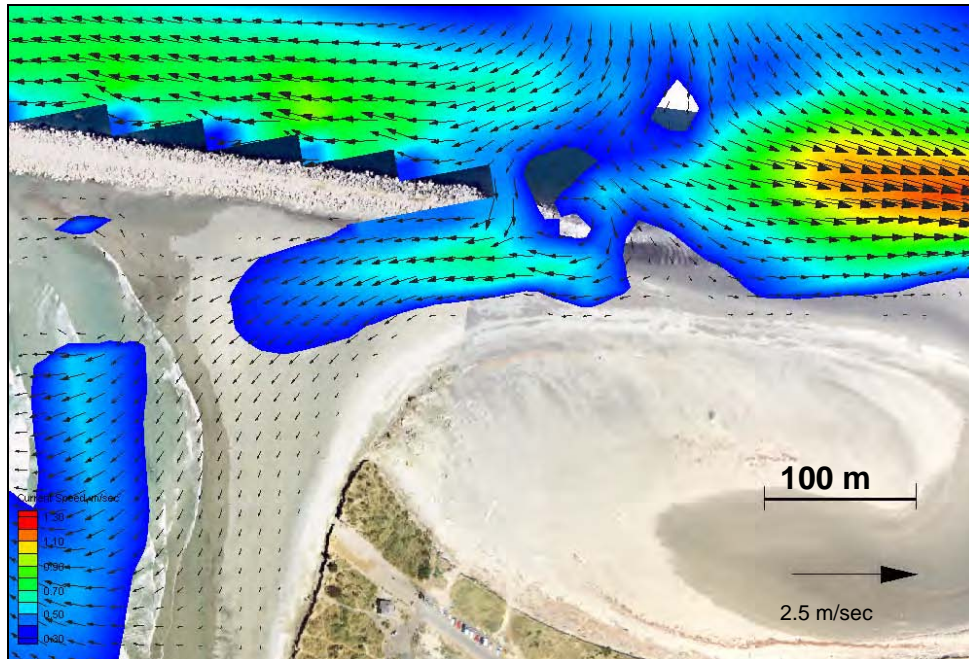


Figure 79. Ebb flow for August 1994 breach, west-northwest storm wave simulation (Run 111)

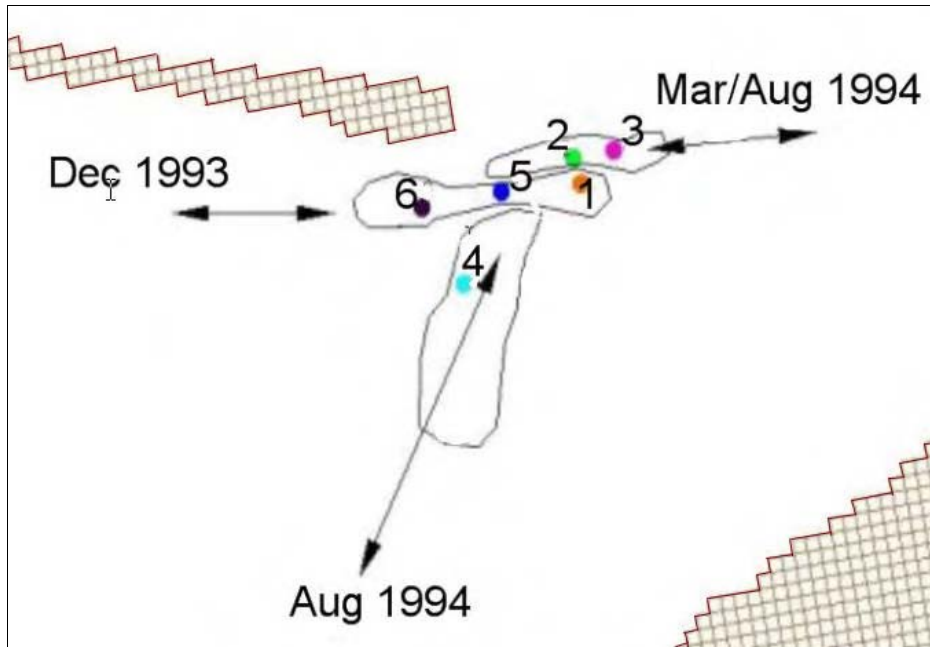


Figure 80. General flow patterns for December 1993, March 1994, and August 1994, and locations of calculation points discussed

Large-breach simulations

Analysis of the large-breach simulations consisted of an examination of flood and ebb flow through the breach for four tide and wave conditions (Table 6). The original large-breach configuration was 250 to 400 m wide, with a maximum depth of 6.1 m below mllw (Figure 81). At that depth, there was flow in the breach for the entire simulation period. Current speeds at four selected points in the breach were extracted from the model simulations (Figure 82).

The large breach was conceptualized by the Seattle District to represent the bathymetry prior to jetty construction (1898-1902). Based on observations of other breaches that have occurred near jetties, the segment of land adjacent to the south jetty in the large breach would likely be eroded. Removal of this material was considered an alternative to the original large breach. This, however, does not preclude a configuration similar to the one suggested by the Seattle District. In fact, the August 1994 survey shows a submergent bar at the landmass location. Another alternative was to reduce the breach depth to 4.55 m mtl to evaluate a less extreme breach. A comparison of results for different configurations serves to promote understanding of the resulting hydrodynamics. These alternatives to the large breach are presented in the next section.

Figures 83-86 are time series of current speed at Points A through D indicated in Figure 74 for the four wave and tide simulations (Runs 117-120). Peak tidal current through the breach is typically 0.8-1.5 m/sec (Run 117). Typical waves (Run 118) raise the flood peaks slightly and lower the ebb peaks slightly (0.6-1.55 m/sec) at Points B, C, and D. Point A is somewhat seaward of the breach throat and nearly in the surf zone where wave-induced currents and a gyre form. Typical waves at Point A show an increase on ebb due to these two processes. West-northwest storm waves (Run 120) raise the flood peaks more

(1.9 m/sec) and lower the ebb peaks to (0.5-1.1 m/sec). Again, at Point A there is an increase on ebb due to its location and exposure to other forcing. West-southwest storm waves (Run 119) cause the greatest increase in current speed at Points A through D. An ebb current is not observed except at Point A. Peak flood current is 1.8-2.2 m/sec.

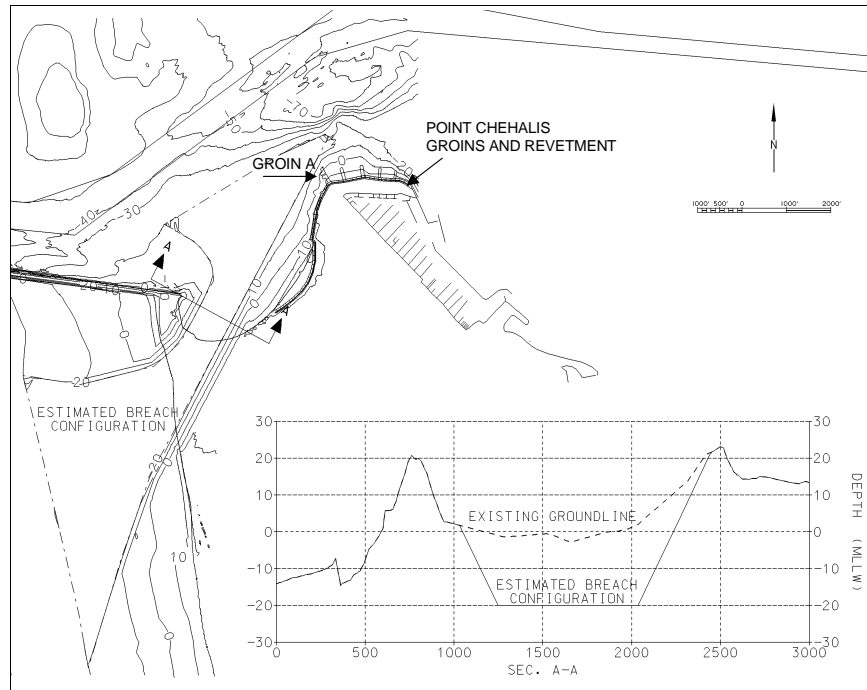


Figure 81. Original large-breach concept; distances and depths in feet (Source: Seattle District)

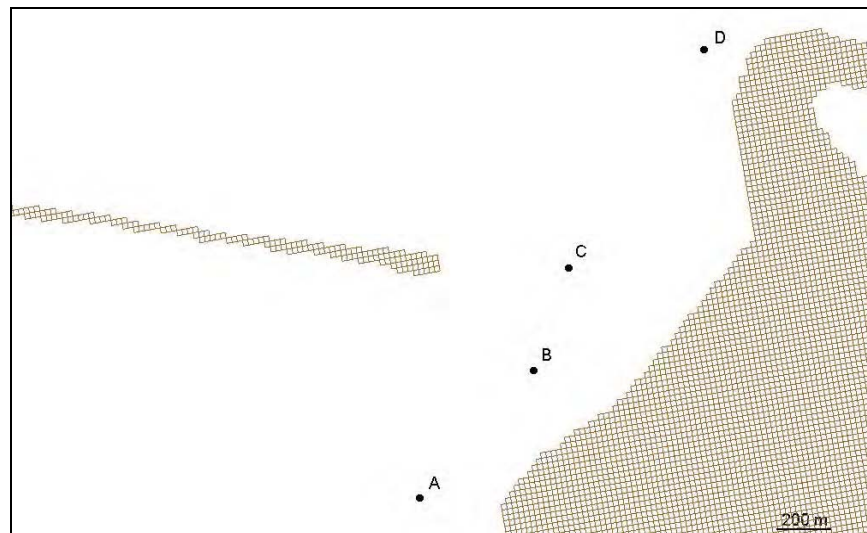


Figure 82. Observation points for large-breach simulations

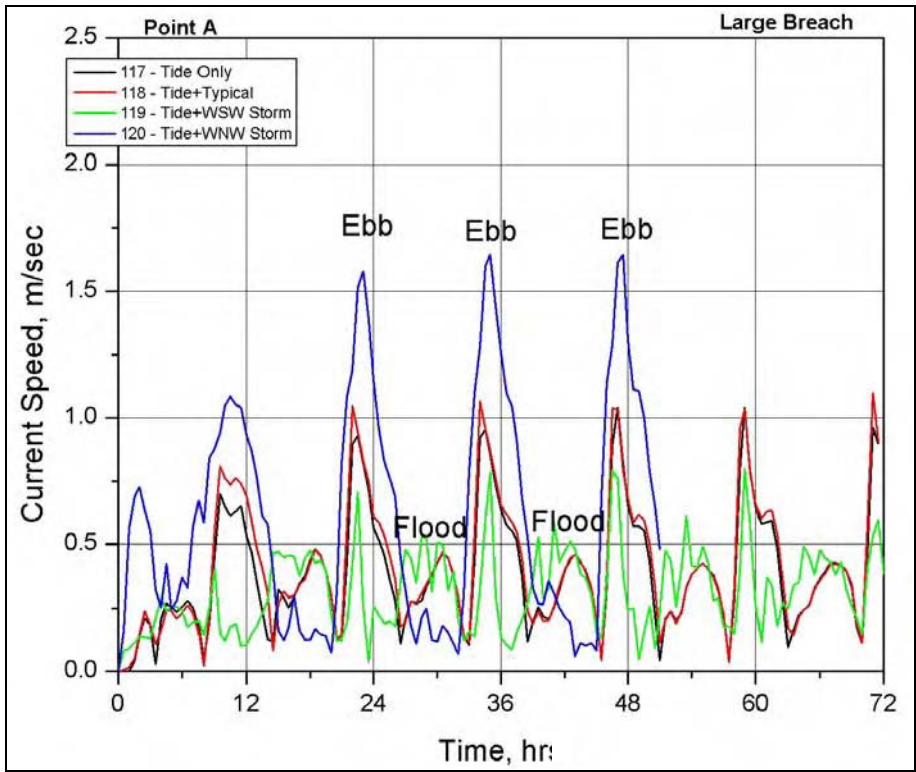


Figure 83. Time series of current speed at Point A for large breach

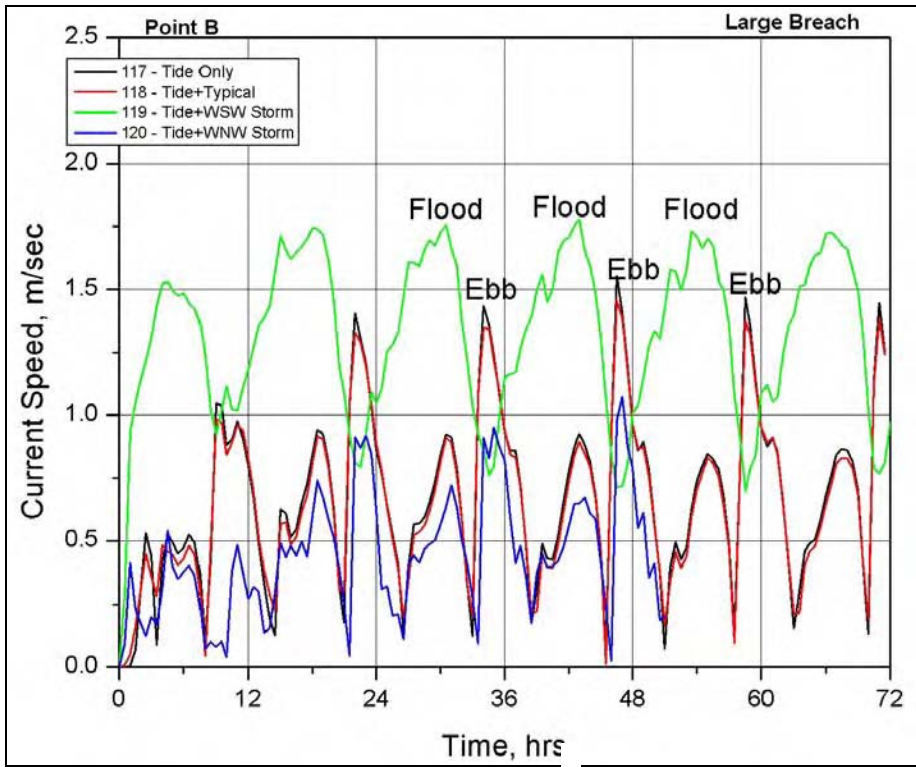


Figure 84. Time series of current speed at Point B for large breach

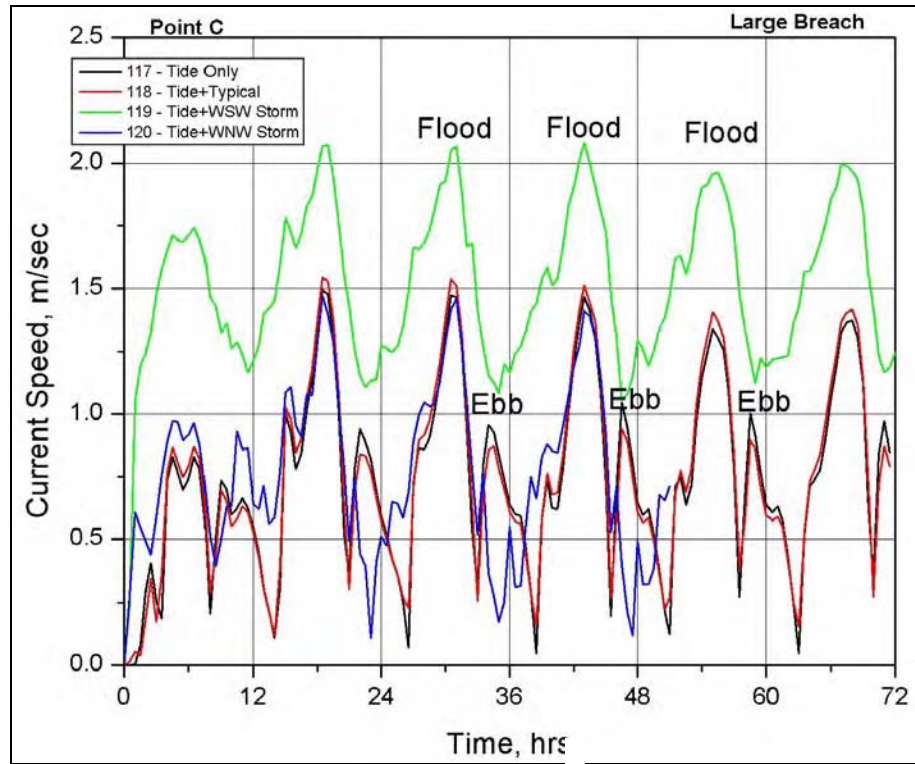


Figure 85. Time series of current speed at Point C for large breach

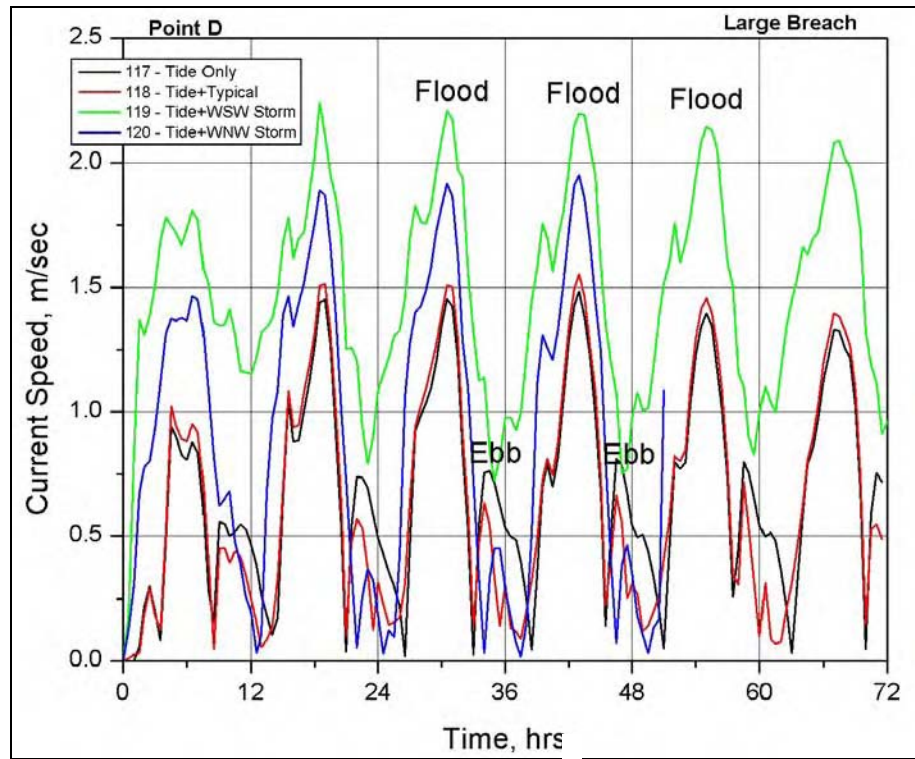


Figure 86. Time series of current speed at Point D for large breach

Figures 87 and 88 show snapshots of peak flood and ebb-tidal horizontal circulation patterns through the large breach (Run 117). Flood and ebb flow is observed, with peak current speed of 1.5 m/sec. An eddy on the north side of the south jetty creates a persistent effective ebb flow observed in both the flood and ebb snapshots. Also, flood flow joins the main flow in the vicinity of Point Chehalis. Figures 89 and 90 show tidal-plus-wave-induced flow patterns through the breach for Run 118 (typical waves). Results from this simulation are similar to Run 117 results; however, the flood current is slightly enhanced, and the ebb current is slightly reduced. Peak current is 1.6 m/sec on flood and 1.4 m/sec on ebb.

Figures 91 and 92 show tidal-plus-wave-induced flow through the large breach with west-southwest storm waves (Run 119). Results from this simulation are similar to Run 117 results; however, the flood current is further enhanced, and the ebb-tidal current is overcome by the opposing wave-induced current except for a small area in the surf zone. Peak flood current is 2.2 m/sec.

Figures 93 and 94 show tidal-plus-wave-induced flow through the large breach with west-northwest storm waves (Run 120). Results from this simulation are similar to Run 117 results; however, the flood current is enhanced and the ebb current is reduced in the breach throat. Peak current is 1.9 m/sec on flood and 1.1 m/sec on ebb. The ebb current at the seaward side of the breach throat is enhanced by a gyre formed between the ebb jet and the south jetty.

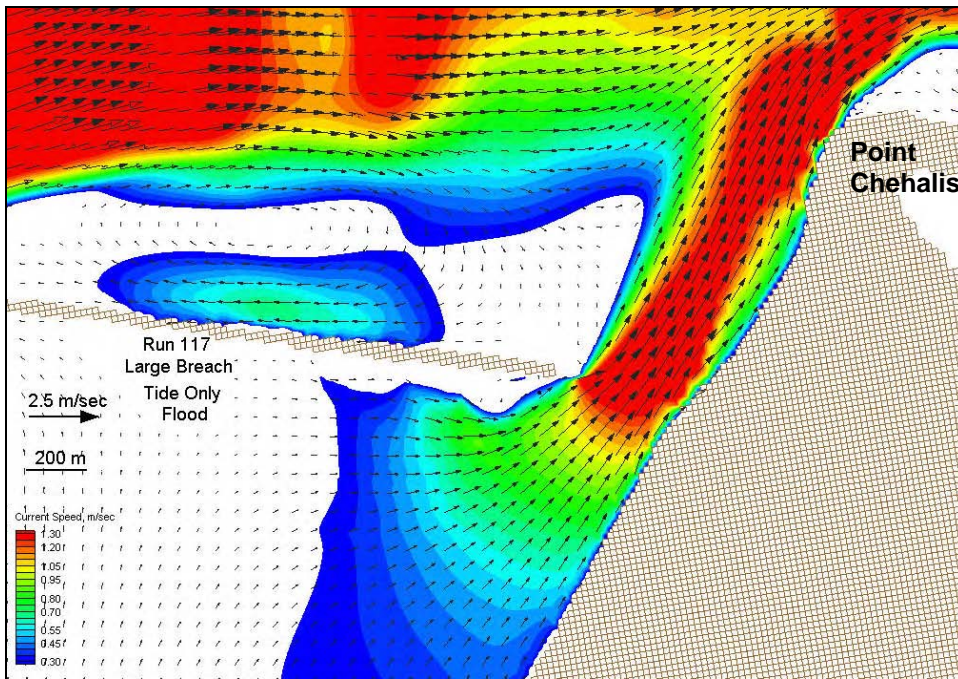


Figure 87. Flood flow for large breach, tide-only simulation (Run 117)

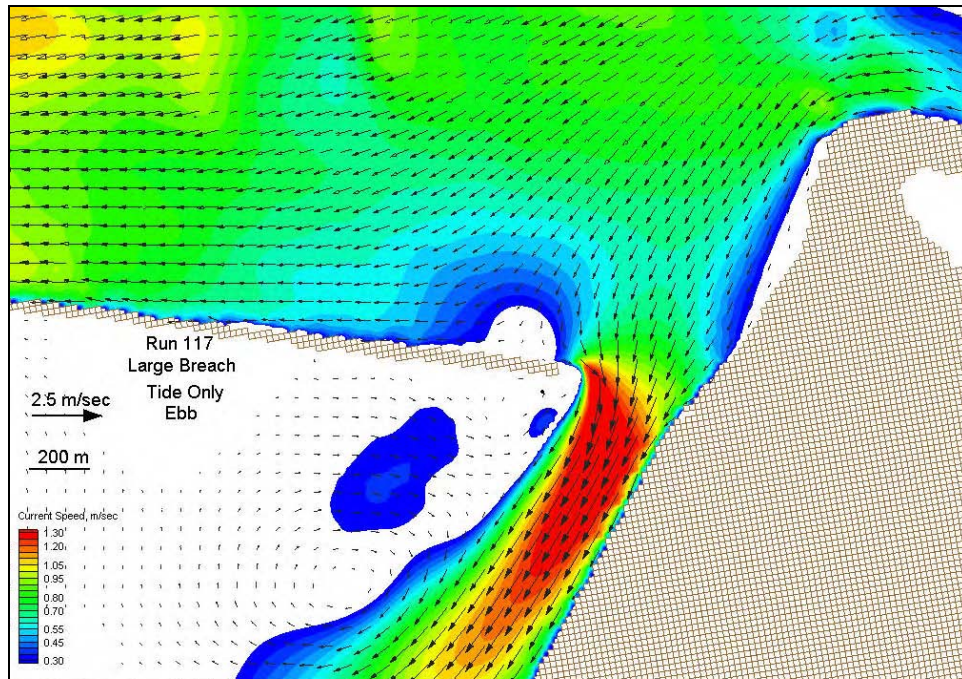


Figure 88. Ebb flow for large breach, tide-only simulation (Run 117)

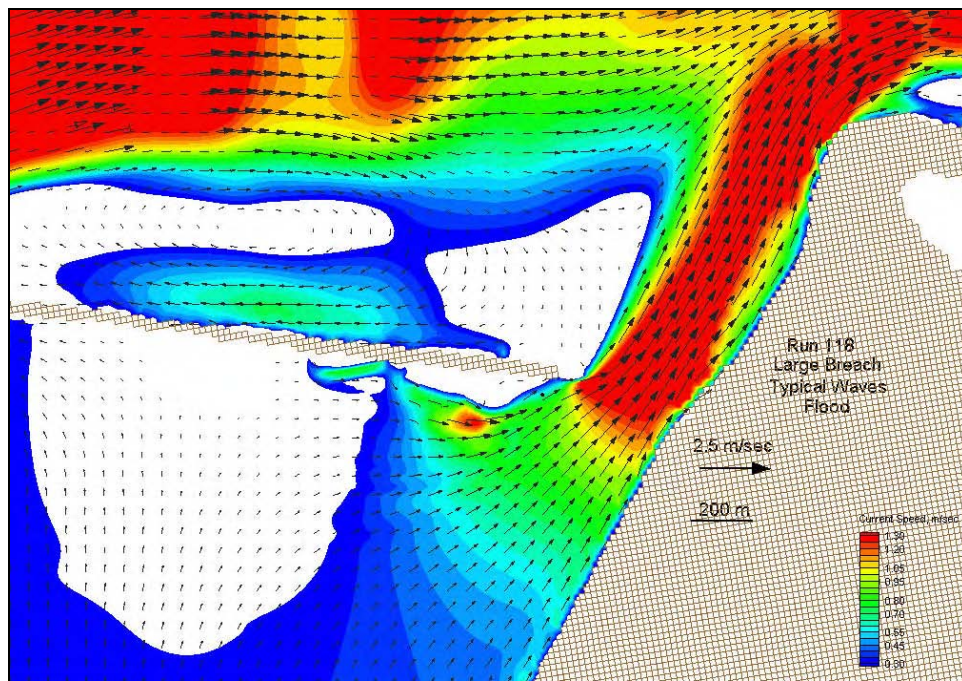


Figure 89. Flood flow for large breach, typical wave simulation (Run 118)

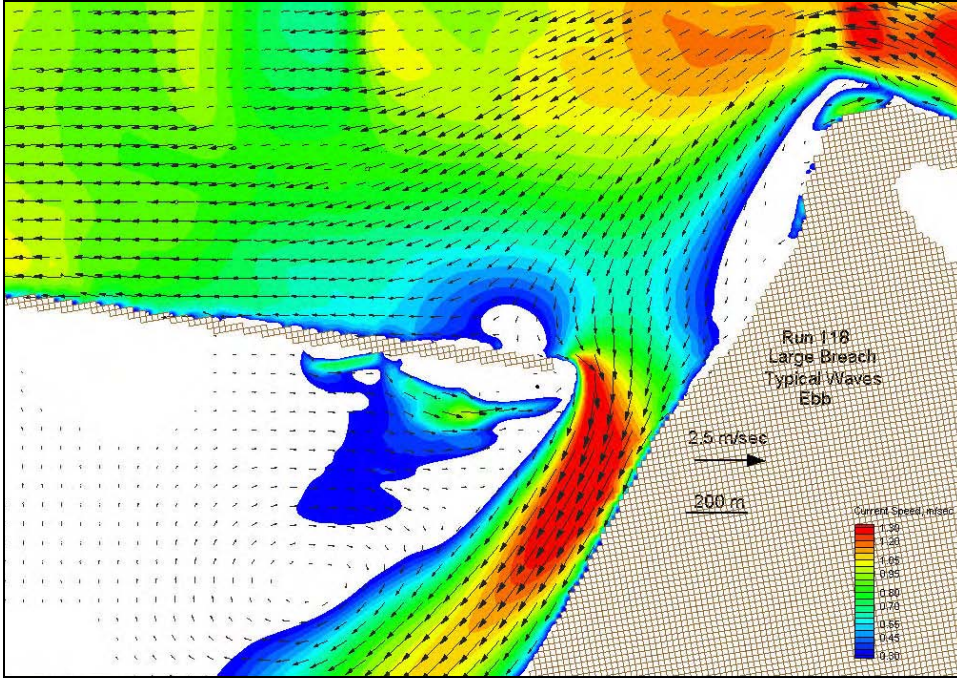


Figure 90. Ebb flow for large breach, typical wave simulation (Run 118)

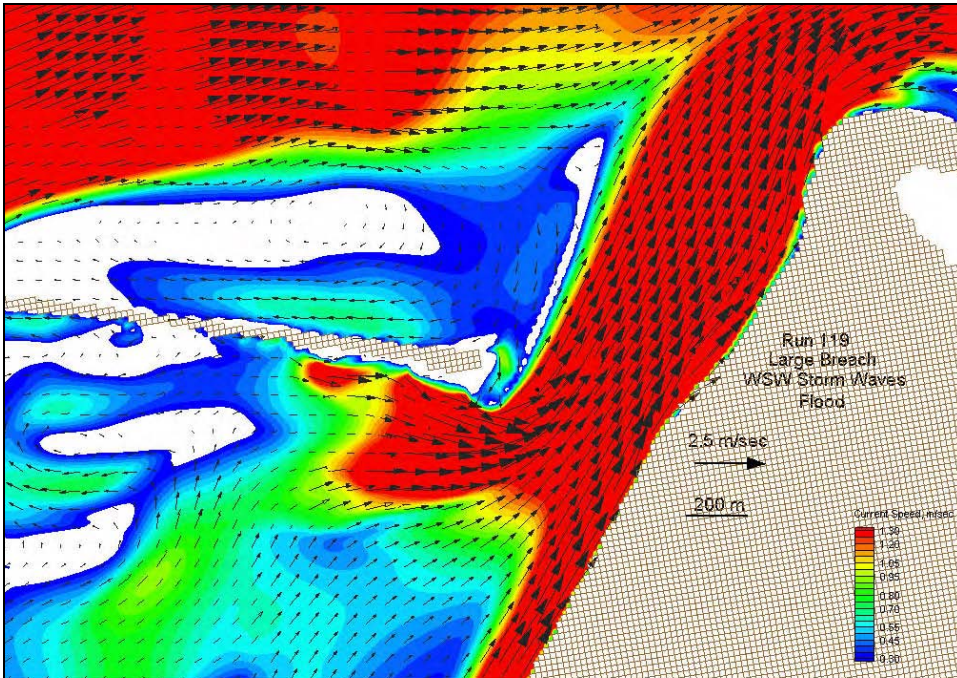


Figure 91. Flood flow for large breach, west-southwest storm wave simulation (Run 119)

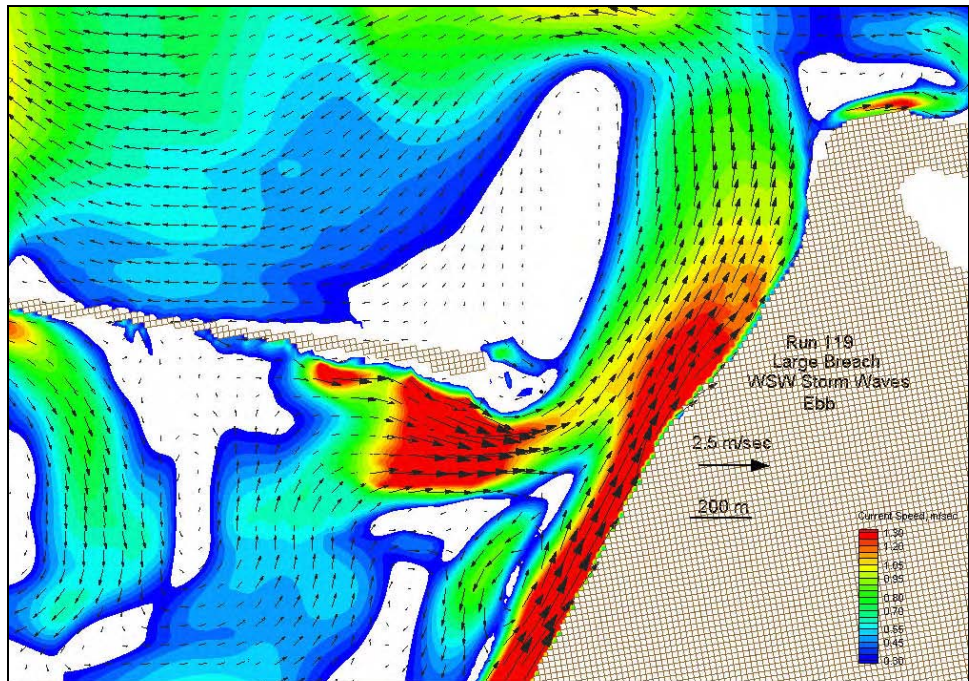


Figure 92. Ebb flow for large breach, west-southwest storm wave simulation (Run 119)

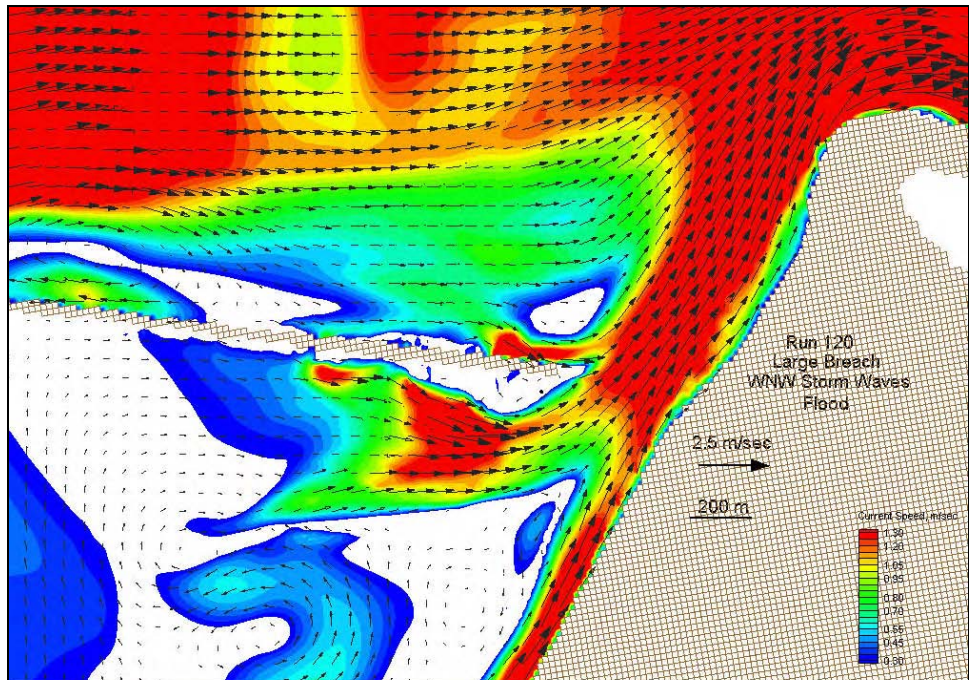


Figure 93. Flood flow for large breach, west-northwest storm wave simulation (Run 120)

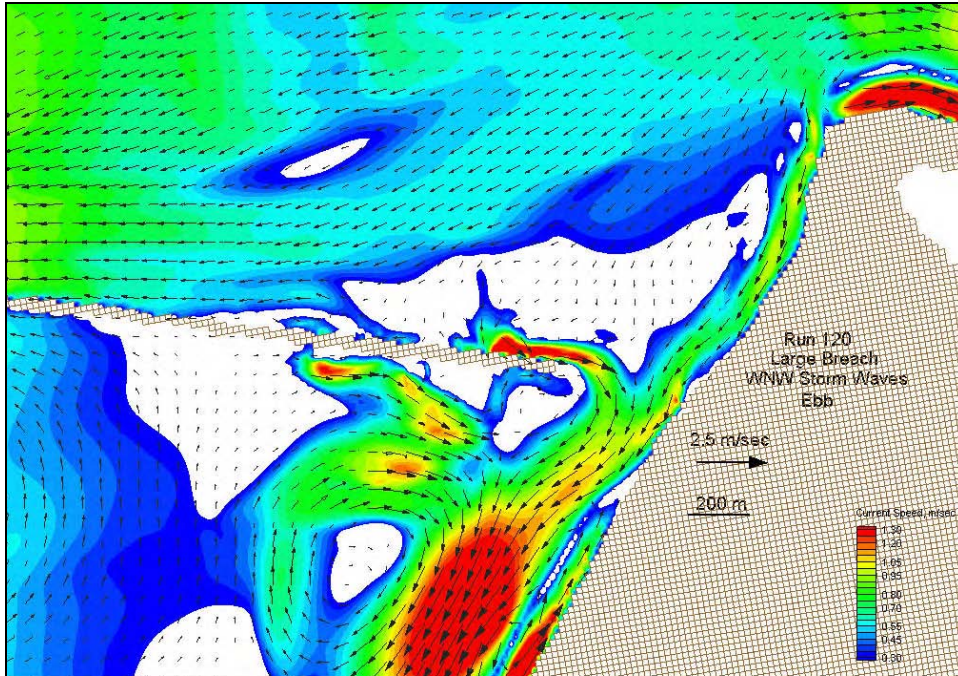


Figure 94. Ebb flow for large breach, west-northwest storm wave simulation (Run 120)

Alternative large-breach simulations

The configuration of the large breach was specified based on known bathymetry prior to jetty construction in 1898, when a channel was aligned on a southwest-northeast track in that general location. In addition, if breaching of a barrier island or spit occurs near a jetty, the segment of land adjacent to the structure is rapidly eroded, leaving a stranded jetty, as occurred at Moriches Inlet, NY, in 1980 (Schmeltz et al. 1982). As further evidence, the 1993 Grays Harbor breach showed a landmass adjacent to the south jetty in the December 1993 aerial photograph (Figure 46). The landmass was not emergent by the time of the March 1994 aerial photograph (Figure 57), leaving the south jetty in a more vulnerable state. For these reasons, the landmass adjacent to the south jetty in the large breach would likely be lost if this configuration were permitted to occur. Removal of this material provides a more realistic and more conservative alternative to the large breach, because it allows examination of the vulnerability of the south jetty to wave and current attack.

Another alternative to the original large breach was devised by reducing the breach depth to 4.55 m below mtl to evaluate a less extreme breach. Bathymetric data sets were developed for these two variations to the large breach (Figures 95 and 96). The black lines represent the location of the Federal navigation channel.

Simulations for the two large-breach alternatives represented three tide-and-wave conditions (Table 5). The typical-wave simulations were eliminated from the simulation series because the results were found to be similar to the tide-only simulations. Current speeds at 11 selected points in the breach, near the south jetty, and near the navigation channel were extracted from the model simulations for analysis and comparison (Appendix B, Figure B1).

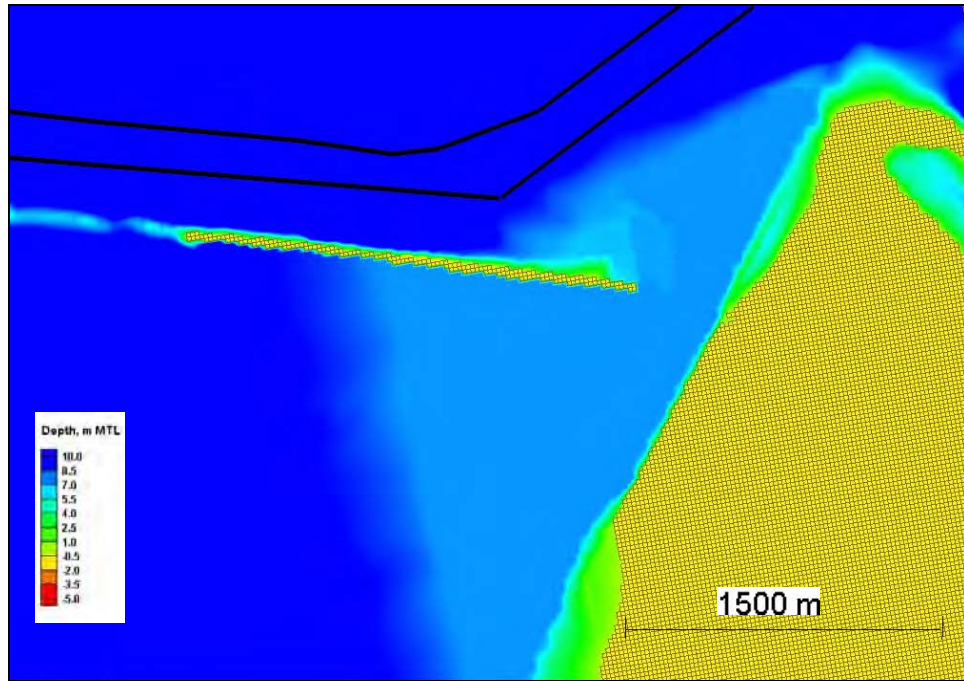


Figure 95. Large breach without jetty protective landmass

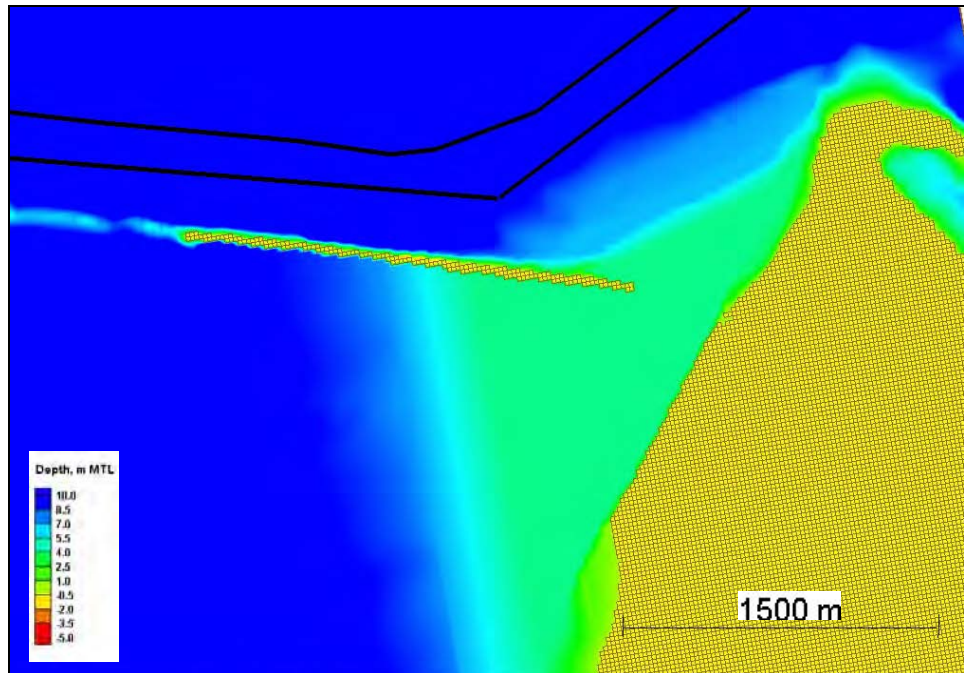


Figure 96. Large breach without jetty protective landmass and depth reduced to 4.55 m below mtl

To compare currents from the large-breach alternative simulations, time series of the three alternatives were plotted together at each of the 11 selected points. Graphs were generated for the tide-only, west-southwest storm wave, and west-northwest storm wave simulations, resulting in 33 time series (Figures B2-B34).

Tide-only simulations

Figures B2-B12 show time series comparisons at the 11 selected locations for the three large breach, tide-only simulations (Runs 117, 121, and 124). The original four observation locations (A-D) are in the main breach channel. For the tide-only simulations, the most notable change in current magnitude is at Point D (Figure B6). With the landmass removed and shallower water through the breach (Run 124), ebb current magnitude at hours 36, 48, and 60 is greatly reduced. This is largely due to the ebb current moving further from the Point Chehalis shoreline and bypassing Point D. (Figures B35-B58 and Figure 97 show snapshots of these flow patterns. Figure B42 (Run 117) and Figure B54 (Run 124) show the change in flow pattern at Point D.) Points E and F (near the south jetty) show an increase in current magnitude with the landmass removed (Figures B6 and B7). Peak current magnitudes at these locations are 0.9-1.2 m/sec with the landmass removed.

The original large breach produced peak current magnitudes of 0.2 m/sec at these locations. Point G shows an increase in current magnitude during ebb flow when the landmass is removed. The main ebb jet is south of Point G for the original large breach and moves through Point G when the landmass is removed (Figures B42 and B54). Points I through J are located near the inlet navigation channel. At these locations, a comparison was made to the existing (nonbreach) condition (Run 113), indicated in red in Figures B10-B12. Any change in flow magnitude or direction in these areas is an indicator of potential change in scour and deposition in the navigation channel. Point I shows little change in flow magnitude for the tide-only simulation (Figure B10). Points J and K show a large increase in ebb current magnitude at hours 23, 35, and 47 for Run 124. A portion of the ebb flow through the breach for the original large breach shifts to the navigation channel for the shallower depth breach (Run 124), causing stronger ebb currents at Points J and K.

West-southwest storm simulations

Figures B13-B23 show time series comparisons at the 11 selected locations for the three large-breach, west-southwest storm wave simulations (Runs 119, 122, and 125). For these simulations, current magnitude at Point B decreases with the landmass removed (Figure B14). At Point C, flood flow increases at hours 30, 43, and 54 for Run 125 due to the shallower water in the breach. Run 122 current magnitudes at hours 35, 47, and 59 are much less than the original concept currents at Point C. This decrease is largely due to the redirection of flow with the landmass removed (Figures B44 and B50).

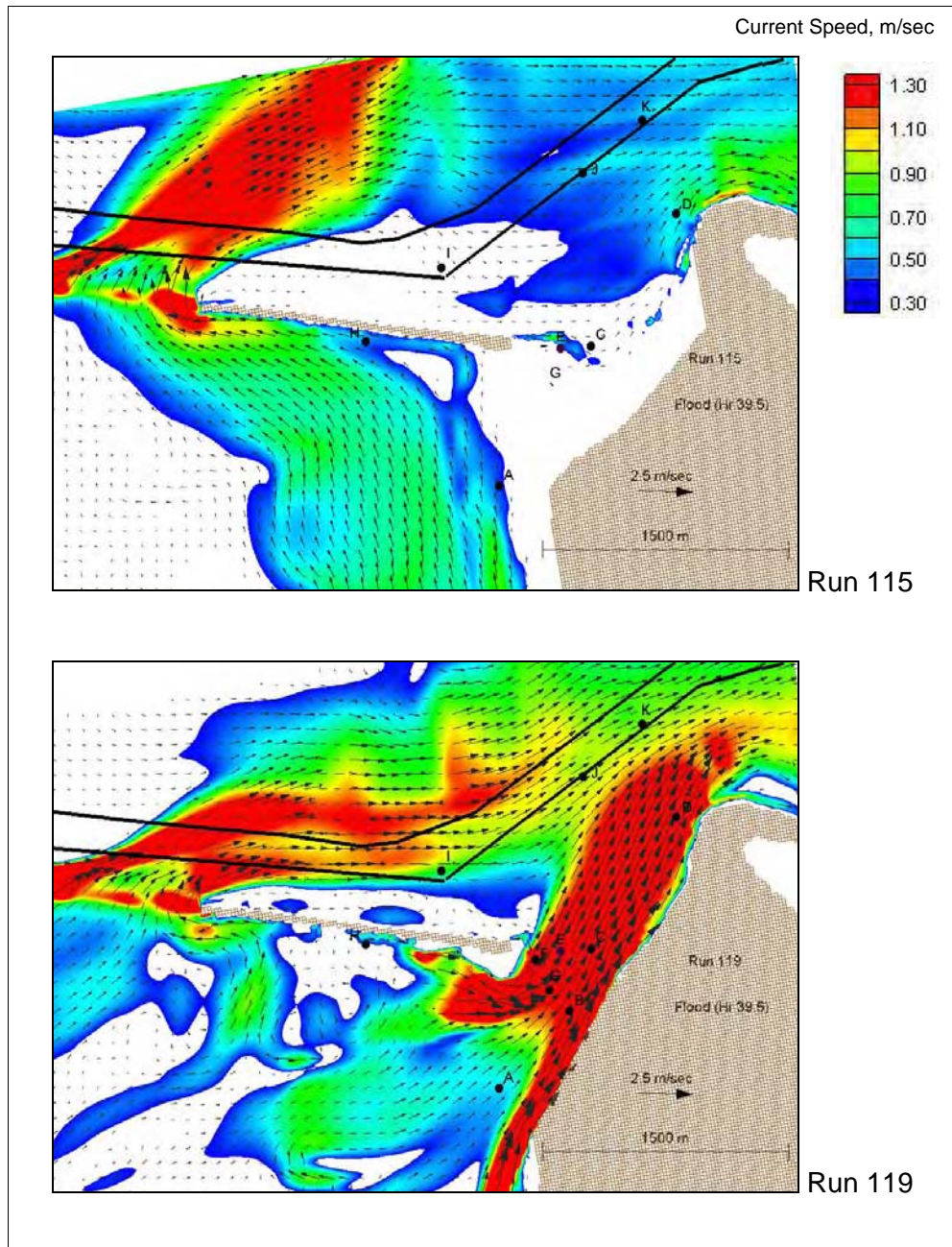


Figure 97. Change in flood flow characteristics at hour 39 with large breach (continued)

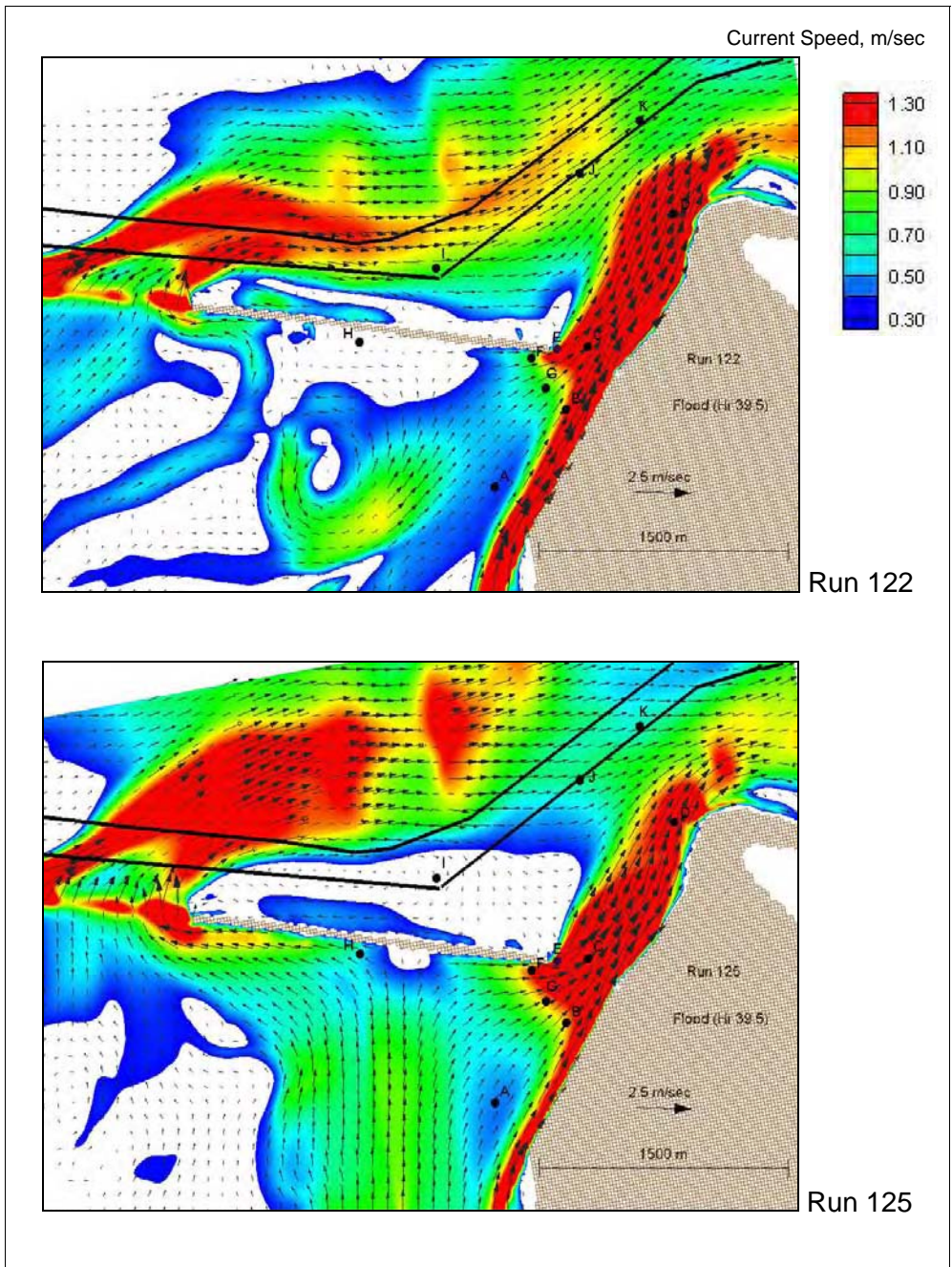


Figure 97. (Concluded)

Large variation in current magnitude time series at Point D was investigated, and potential concerns for maintenance of the navigation channel were revealed. At Point D, a comparison was made to the existing (nonbreach) condition indicated in red (Run 115), as well as to the original large breach (Run 119). Without a breach, current magnitude at Point D for a west-southwest storm wave is on the order of 0.5 m/sec. If a west-southwest storm occurred and the large breach existed, the flood current magnitude at Point D would increase to 2.2 m/sec. On ebb (hour 35), the current magnitude would decrease to 1.0 m/sec, but is still flooding at Point D. The direction of flow, however, shifts northward towards the navigation channel. This can be observed in the plan view snapshot (Figures B38 and B44). With the landmass removed (Run 122), flow is more concentrated along the shoreline, and there is an increase in current magnitude at Point D. With the shallower water of Run 125, the hour 36 current magnitude at Point D diminished to zero. In this case, the jet through the breach is diverted northward by the ebb current and bypasses Point D, heading directly into the navigation channel (Figure B56).

Points E, F, and G show Run 122 and 125 west-southwest storm current magnitudes are generally less than the original-concept currents (Run 119). This weakening is largely due to the redirection of flow with the landmass removed. At Point H, west-southwest storm conditions cause a 0.5 m/sec seaward-directed flow for Run 125 bathymetry.

Large variations in the current magnitude time series at Point I were investigated, and additional potential concerns for maintenance of the Federal navigation channel and flow dominance were discovered. At hour 35, the pre-breach simulation indicates a 0.7 m/sec ebb current at Point I. With the breach in place, the ebb current is deflected away from Point I, possibly reducing the scour potential for the navigation channel by the ebb jet. The duration of ebb flow is also reduced from 6 hr for Run 115 (hours 32.5 to 38.5) to 3 hr for Run 119 (hours 33.0 to 35.0). The significant change in ebb flow characteristics would likely reduce the scour potential in the Point I portion of the navigation channel.

Another notable difference in the Point I time series occurs at hour 39. The pre-breach simulation indicates a lack of strong flood flow. (Note that flood flow dominance on the north side of the inlet was indicated in Cialone et al. (2003); therefore, the lack of a strong flood flow at Point I is as expected.) With the large breach, the hour 39 flood current magnitude is 0.8 m/sec at Point I. Figure 97 shows the flood flow path for a west-southwest storm simulation shifts from the north side of the inlet for existing conditions, to the south side of the inlet with the large breach. The significant change in flood flow characteristics would likely increase deposition on the southern side of Grays Harbor (Whitcomb flats area), rather than the northern (Damon Point) side.

Differences in the current magnitude at hour 35 for pre-breach and large-breach simulations are also observed at Points J and K. The pre-breach simulation (Run 115) indicates a 0.9-1.0 m/sec ebb currents at hour 35 (Figures B22-B23). Figure B38 shows that current tends to align along the channel axis. The large-breach simulations (Runs 119, 122, and 125) show a reduction in current magnitude to 0.6-0.8 m/sec at hour 35 (Figures B22 and B23). However, Figures B44, B50, and B56 indicate that the direction of the current shifts from along the channel axis to across the channel axis. These

conditions have great potential for deposition of sediment in the navigation channel.

West-northwest storm simulations

Figures B24-B34 show time series comparisons at the 11 selected locations for the three large-breach alternative, west-northwest storm wave simulations (Runs 120, 123, and 126). For these simulations, current magnitude at Points A-C decreases with the landmass removed, mainly due to redirection of flow (Figure B24-B26). At Point D, the current magnitude at hours 24, 36, and 48 for Run 126 are 1.1 m/sec (flood) as compared to 0.5 m/sec (ebb) for the original large-breach simulation currents (Run 120). The change in current magnitude and direction for Run 126 is due to presence of an eddy that forms near Point D (Figure B58).

At Point E, the original large breach shows short intervals of strong (1.5 m/sec) ebb current (Figure B28). With the landmass removed (Runs 123 and 126), the duration of strong ebb flow at Point E is longer. All three large-breach simulations with west-northwest storm waves result in a 1.0-1.5 m/sec current for some portion of the tidal cycle.

Points F and G show changes in current magnitude that are related to redirection of flow with the landmass removed. The greater change is at Point G, which shows a strong (1.0 m/sec) flood current with the original large breach (Run 120) and a strong (1.5 m/sec) ebb current with the landmass removed (Run 123). At Point H, west-northwest storm conditions cause a 1.0 m/sec seaward-directed current for Run 123 bathymetry. West-northwest storm waves do not change the flood current at Points I, J, and K; however, there is a 0.2-0.4 m/sec reduction in ebb current magnitude, which could reduce the potential for ebb jet scouring of the Federal navigation channel.

Discussion

Hydrodynamic model simulations were made to examine the variation in current speed and water level as the breach evolved from December 1993 to August 1994. A large breach and two variations were also modeled. The purpose of the simulations was to determine, through inspection of predicted current and water level, if a breach would have negative consequences for the Federal navigation project at Grays Harbor, in particular, increased dredging of the deep-draft navigation channel and degradation of the south jetty through scour.

Consequences of the breach to the navigation channel and south jetty were evaluated by examining changes to current speed, direction, duration, and flow patterns at these locations. Calculated water level did not change significantly for the input hydrodynamic forcing conditions and breach alternatives examined. As a baseline for comparison, hydrodynamic simulations without a breach were made. These pre-breach or existing condition simulations show that current in the inlet throat is strong and predominantly tidally driven. The general flow pattern near the south jetty and breach area shows a northward and seaward current on flood and a seaward current on ebb. The pre-breach simulation flow

patterns are consistent with the sediment budget pathways developed by Byrnes and Baker (2003) and supported by the absence of a fillet near the south jetty. (For the present conditions, accretion of the south beach near the south jetty and the 1993 breach location is not expected.)

Simulation of historic breach

Hydrodynamic simulations of the December 1993, March 1994, and August 1994 breach configurations were made for four tide and wave forcing conditions. Initially (December 1993), the flood-tidal current passed through a confined east-west opening and was directed due east. By March 1994, the peak flood current was located closer to the south jetty and in an east-northeast orientation. In August 1994, the peak flood current covered a greater spatial extent, moving alongshore, through the breach area in an east-northeast direction, and then to the north to join the main inlet current. Overall, the ebb patterns are a reverse of the flood current patterns. These patterns indicate a trend toward the large-breach orientation of east-northeast/west-southwest, with persistent flood flow directed toward the Federal navigation channel.

From December 1993 to August 1994, peak storm current through the breach increased from 2.0 to 2.2 m/sec. The spatial extent of the strong current increased, and the duration of breach flow increased from 37 to 76 percent of the tidal cycle. This increase in current magnitude, spatial extent, and temporal duration are indicators of breach growth and potential for continued growth. Therefore, with the approaching autumn 1994 to winter 1995 stormy season, natural closure of the breach would have been unlikely.

The fact that the breach did grow in width and depth from December 1993 to August 1994, as documented in Chapter 2, indicates that the forcing conditions during that period were sufficiently strong to transport sediment away from the breach throat. Simulated tidal or typical waves produced flood and ebb currents on the order of 1.0 m/sec through the breach. Simulated storm waves nearly doubled peak current velocity, and flow was predominantly in the flooding direction through the breach.

If the current velocity in the breach were to fall below a critical velocity threshold for sediment transport, then material would deposit in the breach, and eventually it would close at a minimal elevation (e.g., mllw). Flow would return to the pre-breach trend of moving seaward at the jetty, and further deposition in the breach would be unlikely. The partially closed high-water breach would however, be vulnerable to reopening by smaller storms.

Simulation of conceptual large breach

The large breach was conceptualized by the Seattle District to represent the bathymetry prior to jetty construction at the turn of the twentieth century (1898). Based on observations of other breaches near jetties, the segment of land adjacent to the south jetty in the large breach would be eroded. Removal of this material was considered an alternative to the original large-breach concept. This removal of material, however, does not preclude a configuration similar to the one suggested by the Seattle District. In fact, the August 1994 survey shows a

submergent bar at the landmass location. Another alternative was to reduce the breach depth to 4.55 m mtl to evaluate a less extreme breach. A comparison of results for different configurations serves to improve the reader's understanding of the resulting hydrodynamics. Analysis of the large-breach simulations consisted of examination of flood and ebb flow through the breach for four tide and wave conditions. Current speeds at eleven selected points in the breach were extracted from the model simulations for analysis.

Points E and F (Figure 97), near the south jetty terminus, show an increase in current magnitude with the landmass removed, particularly for west-northwest storm waves. At Point E, the original large breach shows short periods of strong (1.5 m/sec) ebb current. With the landmass adjacent to the south jetty removed, the duration of strong ebb flow at Point E is much greater. All three large-breach simulations with west-northwest storm waves result in a 1.0-1.5 m/sec current for some portion of the tidal cycle. Exposure of the jetty terminus to a strong current and associated scour holds potential for destabilization of structure. According to the equilibrium scour depth potential formulation given by Hughes (2002), the maximum equilibrium scour depth that could be reached under mean (depth-averaged) currents of 1.5 m/sec is a depth of about 13 m for a mean sediment grain size of 0.5 mm, and a depth of 29 m for a mean grain size of 0.4 mm, representative of the winnowed sediments in Half Moon Bay. Estimated scour depth increases with decreasing grain size. The equilibrium scour depth estimates assume a fully-developed turbulent boundary layer and a sufficient number of tidal cycles to scour the bed to the equilibrium depth. Time to reach equilibrium scour depth is not predicted by the theory. Wave action would contribute to mobilizing sediment and increase potential for transport by the current. Wave action would accelerate scour during initial stages, but waves would have less effect as depth increases and orbital wave velocities become smaller near the bed.

Another area that could be potentially vulnerable with the large breach in place is the revetment at Point Chehalis (interrogation Point D is located near Groin A of the revetment, Figure 81). For existing (pre-breach) conditions, current magnitude at Point D for a west-southwest storm wave is on the order of 0.5 m/sec. If a west-southwest storm occurred and the large breach existed, the flood current magnitude at Point D would increase to approximately 2.2 m/sec.

On ebb tide, the current magnitude in the inlet at Point D for a west-southwest storm decreases to 1.0 m/sec, but is still flooding at that location. The direction of flow, however, shifts northward towards the navigation channel. The breach flood jet shifts in a counterclockwise, sweeping motion from the Point Chehalis revetment shoreline to the northeast, north, then northwest as the tide in the inlet changes (Figure B44). During this 4.5-hr time period, the Point Chehalis reach of the navigation channel from Point K, to Point J, to Point I, experienced cross-channel currents that could deposit sediment in the navigation channel.

Differences in the current magnitude at hour 35 (representing a typical peak ebb flow) for pre-breach and large-breach simulations are also observed at Points J and K. The pre-breach simulation indicates a 0.9- to 1.0-m/sec ebb current at hour 35 typically directed along the channel axis. The large-breach simulations show a reduction in current magnitude to 0.6-0.8 m/sec at hour 35. However, the direction of the current shifted from along-channel axis to across-

channel axis. These conditions have great potential for promoting sediment deposition in the Federal navigation channel. In addition, the cross current will change the flow at nearshore and open water disposal sites serving for placement of material dredged from the navigation channel.

Deposition and scour in the navigation channel is related to the strength of the ebb and flood flow through Grays Harbor entrance. Previous studies have shown that this inlet exhibits stronger flood flow on the north side of the entrance and stronger ebb flow on the south side of the entrance (near the navigation channel), indicating that the navigation channel is likely an exporter of sediment (Cialone et al. 2002, 2003). From the hydrodynamic simulations analyzed in this study, the large breach would change the flow dynamics of the inlet and navigation channel.

Large variations in the current magnitude time series at Point I (at edge of navigation channel, Figure 97) were investigated, and additional potential concerns for maintenance of the Federal navigation channel and flow dominance were revealed by the simulations. At hour 35, the pre-breach simulation indicates a 0.7 m/sec ebb current at Point I. With the large breach in place, the ebb current is deflected from Point I, possibly reducing the scour potential for the navigation channel by the ebb jet. The duration of ebb flow is also reduced from 6 hr for pre-breach conditions to 3 hr for the large-breach condition. At hour 39, the pre-breach simulation indicates a lack of strong flood flow, as would be expected for the south side of the inlet. With the large breach, the hour 39 flood current magnitude is 0.8 m/sec at Point I. The flood flow path for a west-southwest storm simulation shifts from the north side of the inlet for the existing condition, to the south side of the inlet with the large breach. The significant change in ebb flow characteristics would likely reduce the scour potential in the Point I portion of the navigation channel. The significant change in flood flow characteristics would likely increase deposition on the southern side of Grays Harbor (Whitcomb flats area), rather than the northern (Damon Point) side.

Example regional implications

A permanent breach, such as the large breach investigated here, holds potential regional implications for the flow distribution and sedimentation pattern at Grays Harbor. Without a breach, the strong longshore current from a west-southwest storm sweeps seaward at the south jetty and across to the north side of the inlet (Figure 97, Run 115). For west-southwest storms and with the large breach in place, the strong longshore current moves through the breach rather than around the south jetty (Figure 97, Run 119). Thus, the flow captured by the breach reduces flood flow that would otherwise cross to the north side of the inlet. The breach flow also opposes ebb flow near the south jetty and Half Moon Bay. These changes in inlet flow dynamics with the large breach in place would cause the flood current to shift from a northeasterly direction to a more easterly direction near the south jetty, and the ebb current would be reduced. Thus, the horizontal pattern of flood and ebb dominance would be changed by the presence of a permanent breach.

The changes in flow dynamics with a large, permanent breach will change the sediment dynamics and sediment bypassing pathways at Grays Harbor. The strong offshore-directed current at the south jetty for the existing condition and

the corresponding sediment bypassing to the north would be altered. The breach would cause sediment to enter Half Moon Bay and reduce sediment transport potential to the north, which is the direct and natural mechanism for sediment bypassing.

The increase in flood current and decrease in both the strength and duration of the ebb current are expected to increase sediment deposition and reduce sediment scouring in the navigation channel in the Point I to Point K reach. Increased flood flow on the south side of the inlet also may change the morphologic characteristics of Whitcomb Flats.

4 Morphologic Numerical Model of 1993 Breach

This chapter describes the application of a recently developed numerical model of barrier island breaching to examine evolution of the 1993 breach adjacent to the south jetty at Grays Harbor. Because the model is new, extensive background is given, including a proof of concept to simulate the 1980 breach that occurred adjacent to the east jetty at Moriches Inlet, NY. Measurements of the Moriches Inlet breach are available, and successful simulations at two sites demonstrate applicability of the model. The chapter begins with a discussion of breaching of barrier islands or spits adjacent to jetties.

Breaching Adjacent to Jetties

Jetties interrupt the natural pathway of sediment that is transported alongshore by obliquely incident waves and associated longshore current. As one geomorphic response, the shoreline adjusts through the redistribution of sediment both near the inlet and, possibly, for a considerable distance updrift and downdrift. The distance depends on the length of the jetties and dredged channel, wave height, and balance of net and gross longshore sediment transport, among other factors.

A breach located near an inlet will increase the effective channel cross-sectional area of the combined opening to the ocean, reducing the tidal current through the inlet and its scouring action, which can increase sediment shoaling in the navigation channel. Reduction of the tidal current in the inlet is an indirect cause of channel shoaling and increased channel maintenance dredging. Material entering the bay through the breach may be transported into the navigation channel, a direct cause of channel shoaling. Such was the concern for the deteriorating condition of the landward portion of the north jetty at Coos Bay, OR, where overwash was occurring on the adjacent beach and a breach was anticipated. Emergency action was initiated in December 2002 to repair the jetty by filling gaps to prevent sediment being transported through it, thereby increasing beach width and volume adjacent to the structure.¹

¹ Ms. Heidi P. Moritz, Hydraulics, Hydrology, and Geotechnical Design Branch, U.S. Army Engineer District, Portland, personal communication, 29 November 2004.

Breaching adjacent to a jetty isolates the structure from land. In addition to exposing the jetty to potential scouring currents and waves that could undermine the structure at the landward end, similar to tip scour common at the seaward ends of jetties, landward access to the structure is lost for inspection and repairs. Breaching produces an environmental change both locally and regionally through alteration of the horizontal pattern of the tidal and wave-induced current, as discussed in Chapter 3, which can change sedimentation patterns and, possibly, salinity.

Breaching of narrow barrier islands or barrier spits is possible at either the downdrift or updrift beach adjacent to jetties, and selected processes are discussed here, with examples.

Breaching downdrift of jetties

Chronic erosion is commonly observed on the downdrift side of stabilized inlets on coasts where there is a strong net direction of longshore sediment transport. The beach between the downdrift jetty and downdrift attachment bar can become isolated from sediment sources in severe cases (Hanson and Kraus 2001). This is the situation at Shinnecock Inlet, a federally maintained inlet on the eastern end of Long Island, NY, where potential breaching of the downdrift (west) beach has been imminent several times since jetty construction by the county in the 1950s.

Figure 98 shows Shinnecock Inlet in October 1996, with the western beach (left side of jetties) eroded to endanger the public road and the marina complex on the north (bay) side of the barrier island. Emergency measures have been taken by the county and township during severe storms to prevent breaching. The New York District places material dredged from the Federal channel onto the eroding beach segment.

As another example, a downdrift breach occurred at Mattituck Inlet, Long Island, NY, which faces the Long Island Sound. Regional net transport is from west to east on this coast. The Federal jetties at Mattituck were constructed in the early 1900s. The shoreline directly east of Mattituck Inlet receded rapidly during the 1920s and 1930s, and a landward breach at the base of the east jetty at Mattituck Inlet opened in or around 1935, resulting in the formation of a west-directed spit (Figure 99) at the base of the east jetty that encroached the navigation channel. In response to the breach, the New York District extended the east jetty landward in 1946, and material dredged during this time was placed onto the beach directly east of the inlet, the first known beach nourishment for this location (Morgan et al. 2005).



Figure 98. Shinnecock Inlet, NY, showing severely eroded downdrift beach adjacent to downdrift jetty

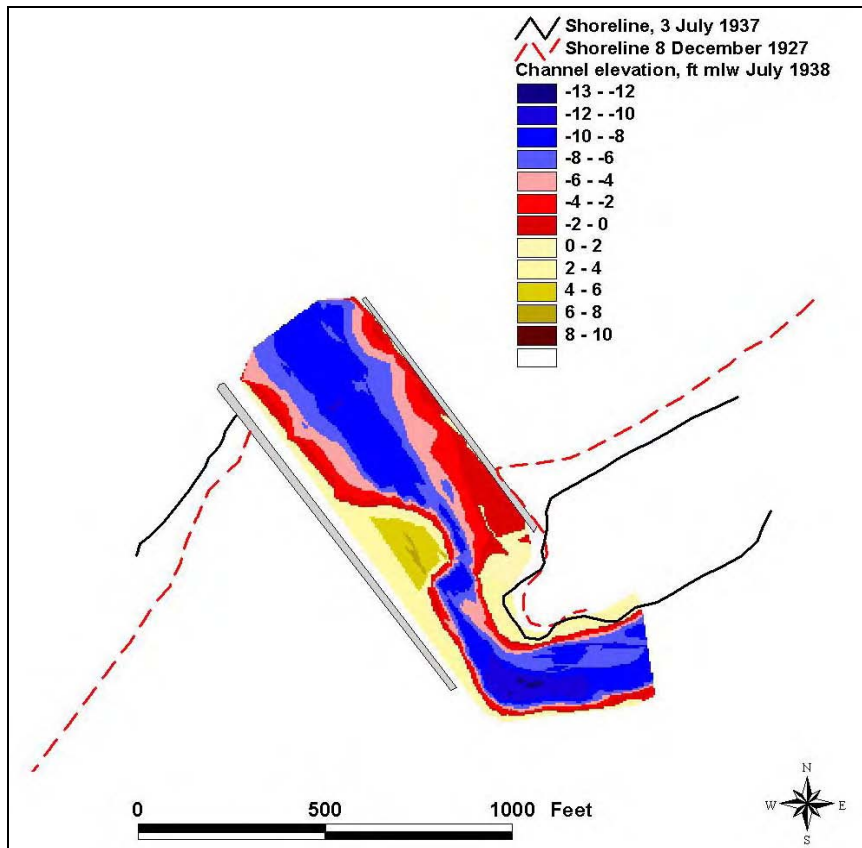


Figure 99. Mattituck Inlet, NY, with a spit encroaching from the east through a breach in the barrier island (from Morgan et al. 2005)

Breaching updrift of jetties

A porous or low jetty near the shore will promote erosion of the updrift beach by allowing sediment to enter the inlet through and over it. In such a situation, the inlet blocks sediment arriving to the updrift beach during times of reversals in longshore transport, and sediment brought to the beach from the dominant longshore transport direction passes through the porous jetty. A strong rip current adjacent to the updrift jetty can also remove material from the beach, acting similarly to a porous jetty in causing beach erosion. If the barrier island adjacent to the spit is narrowed by bank erosion in the tidal channel at the back bay, as was the case at Moriches Inlet, NY, or by formation of a headland bay beach as was the case at Grays Harbor in 1993, then breaching potential is increased during times of high water level and high storm waves.

In December 2002, the U.S. Army Engineer District, Portland, initiated emergency repairs of the updrift (north) jetty at Coos Bay, OR. The jetty and adjacent beach had been under observation because of gaps on the landward end of the jetty that were allowing sand to be transported off the beach, through the jetty, and into the inlet, increasing maintenance dredging of the Federal navigation channel. The condition of the jetty just prior to repairs is shown in Figure 100. A shore-parallel revetment had been proposed as a possible alternative or augmentation to prevent breaching, but this option was met by strong opposition because of anticipated environmental and recreational degradation, as well as in not addressing the root problem of loss of sand from the beach, a portion of which would enter the navigation channel.



Figure 100. Degraded north jetty at Coos Bay, OR, and inception of flanking channel expected to lead to a breach (December 2002; photograph by U.S. Coast Guard)

Breaching Model

Quantitative prediction of coastal breaching is a new area of research. In 2002, the CIRP, a research and development program conducted for Headquarters, U.S. Army Corps of Engineers, began study of coastal breaching to understand and evaluate the consequences of breaches for Federal navigation projects at inlets. The mission of the CIRP is to reduce the cost of design, operation, and maintenance of coastal inlets, and to preserve and promote the natural functioning of inlets and adjacent beaches as a sediment-sharing system. Ongoing applications of the developed breach simulation technology have expanded to design and evaluation of protective dunes for storm protection, while allowing overwash to replicate natural barrier island sediment processes to renew habitat. Work to date is documented by Kraus et al. (2002), Kraus and Wamsley (2003), Kraus (2003), and Kraus and Hayashi (2005).

The process of coastal breaching can be divided into two conceptual phases, incipient breaching and inlet development. Incipient breaching refers to breach growth during a short time after initial opening of a breach. Incipient breaching is characterized by a rapid increase in depth and width during and, possibly, shortly after the storm that opened the breach. Incipient breaching is primarily governed by strong cross-shore water flow from surge, wave setup, and tide that moves sediment either landward or seaward during storms. The inlet-development phase is characterized by a competition between the breach-sustaining sediment-transport forcing of the tidal or similar current through the breach and the closure process of infilling by the wave-induced longshore sediment transport that occurs under more typical waves. Growth of the breach in the inlet-development phase will be slow compared to the incipient breaching phase because of breach infilling by longshore sediment transport and because the breach will evolve toward equilibrium dimensions that are empirically known for permanent inlets.

A predictive breaching model must describe both the incipient breaching phase and the inlet-development phase of breach development. In doing so, it is necessary to account for the current through the breach and associated change in water level due to storm surge and tide; change in water level due to wave setup; longshore sediment transport; sediment transport in the breach by quasi-steady currents and waves; change in dimensions of the breach; interaction of the breach with other inlets opening to the same bay system shared with the breach; and time-dependent feedback from the breach to the acting hydrodynamics.

The incipient phase of a coastal breach depends on the initial condition of the barrier island (Kraus 2003), including the localized low area in the barrier island where the water can first flow, called the pilot channel. The inlet-development phase depends mainly on the local tidal hydrodynamics, nearshore wave climate determining the longshore sediment transport rate, and sediment grain size. A predictive model must be capable of describing the rapid changes in the incipient phase, which brings the requirement of relatively short time-step in a numerical model, while running for a long time period to simulate breach evolution over 1 year or more in the inlet-development phase.

The model developed in the CIRP represents both phases and the various acting and interacting processes. Its components are described next.

Hydrodynamic model

Water flowing through a breach moves primarily along the main axis of the opening, indicating that a one-dimensional (1-D) calculation approach represent the major process in the water and sediment movement. The classical depth-averaged 1-D inlet hydrodynamic equations (Keulegan 1967) are implemented in the CIRP morphologic breaching model as follows:

$$\frac{\partial U}{\partial t} + \frac{g}{L}(\eta_B - \eta_o) + \left(K_{en} + K_{ex} + \frac{2c_f L}{R_h} \right) \frac{|U|U}{2L} = 0 \quad (1)$$

for the momentum equation, and

$$A_C U = A_{Bay} \frac{d\eta_B}{dt} \quad (2)$$

for the continuity equation, in which

U = depth-averaged and inlet-length integrated current velocity

t = time

g = acceleration of gravity

L = width of breach through the barrier island

η_B and η_o = water-surface deviations from msl in the bay and in the ocean, respectively

K_{en} and K_{ex} = entrance and exit losses, respectively

c_f = bottom friction coefficient, represented here by Manning's formula, $c_f = gn^2 / h^{1/3}$, in which n = Manning's coefficient typically set as 0.025 sec/m^{1/3}, and h = water depth

R_H = hydraulic radius of the breach or inlet

A_C = breach or inlet channel cross-sectional area below msl and

A_{Bay} = surface area of the bay

Usual assumptions of an idealized Keulegan inlet apply, such as vertical walls in the bay, and sufficiently small bay area to allow the bay surface to move up and down uniformly in response to tidal flow. In the model, the breach cross-sectional area expressed in Equation 2 is time-dependent. Equations 1 and 2 are solved numerically for U and η_B , respectively.

Equation 1 contains a quadratic (nonlinear) friction term. An Euler explicit solution method and a trapezoidal solution method were compared to results from an iterative solution method with small tolerance that represented the exact solution of the nonlinear equation. Results showed that for a typical time-step necessary for field applications, $\Delta t = 10$ sec, the trapezoidal solution method gave good agreement with the iterative solution. Longer time-steps, for example, $\Delta t = 60$ sec, were also possible with the trapezoidal solution. However, physically generated transients can occur during the incipient breaching phase as

caused by rapid changes in water level, velocity through the breach, and growth of the breach. A 10- to 30-sec time-step was found to be necessary to resolve these transients.

After the velocity is obtained at a particular time-step, the morphology model calculates transport rates and breach response. The solution then proceeds forward again for the velocity and water surface elevation in the bay with the new breach geometry.

Breaking wave height and angle are calculated from conservation of wave energy flux, Equation 3, computed with linear wave theory, and by Snell's Law of wave refraction, Equation 4:

$$F_o = F_b \quad (3)$$

$$\frac{\sin \theta_b}{C_b} = \frac{\sin \theta_o}{C_o} \quad (4)$$

where

F_o, F_b = wave energy flux at deep water and breaking point, respectively

θ_o, θ_b = wave angle at deep water and breaking point, respectively

C_o, C_b = wave group celerity at deep water and breaking point, respectively

By linear wave theory, wave energy flux in deep water and the breaking point is:

$$F_i = \frac{1}{8} \rho g n_i C_i H_i^2 \cos \theta_i \quad (5)$$

where

ρ = density of water

n = group velocity parameter

H = wave height

i = location of computation as either deep water or the breaking point in the present analysis.

The relationship between wave height and water depth at breaking is $H_b = \gamma h_b$, where h_b is the water depth at the breaking point, and γ = ratio between wave height and water depth at breaking, taken as $\gamma = 0.78$. The breaking wave height and angle are determined by solving Equations 3 and 4 by the Newton-Raphson method.

If waves are present, they produce set up on a sloping beach and barrier island. Wave setup is estimated from the wave breaking condition at the given time-step. Wave setup during storms can significantly increase water level at the site of a potential breach. The magnitude of the wave setup in the surf zone is calculated by considering the energy dissipation equation in linear wave theory. A simple expression then relates wave height and mean water level in the surf zone. Initially, setup was estimated by an analytical relation based on the breaking wave condition developed by Bowen et al. (1968):

$$\eta_{setup} = \varepsilon \frac{3}{8} \gamma H_b \quad (6)$$

where

ε = empirical adjustment factor

γ = wave breaker index

H_b = wave height at breaking

This was modified for the Grays Harbor breach application in response to comments by the ITR. Based on the offshore wave condition, the maximum wave setup at the shoreline is estimated by an empirical equation (Stockdon et al. 2006):

$$\eta_{setup} = 0.35 \beta_f \sqrt{H_0 L_0} \quad (7)$$

where

β_f = beach foreshore slope

H_0 = deepwater wave height

L_0 = deepwater wave length

In the breach model, wave setup is added to the input water-surface elevation (tide plus surge) at the coastline according to the wave conditions at the particular time-step.

For the situation of multiple inlets and breaches, it is assumed that the openings do not directly interact, so that U and other parameters that are related to the opening in Equation 1 can be replaced by the parameters for the i^{th} opening among N total. Equation 1 is then written as:

$$\frac{\partial U_i}{\partial t} + \frac{g}{L_i} (\eta_B - \eta_o) + \left(K_{en,i} + K_{ex,i} + \frac{2c_{f,i} L_i}{R_{h,i}} \right) \frac{|U_i| U_i}{2L_i} = 0 \quad (8)$$

The continuity equation is generalized by replacing A_C and U by $(A_C)_i$ and U_i for the i^{th} opening among N total. Equation 2 becomes:

$$\sum_{i=1}^N (A_c)_i U_i = A_{Bay} \frac{d\eta_B}{dt} \quad (9)$$

This procedure is valid if the bay and multiple breach and inlet system obey the assumptions of the original Keulegan (1967) approach for a single inlet.

Sediment transport model

The rate of sediment transport along the bottom of the breach is calculated by the power law total-load formula of Watanabe et al. (1991):

$$q_B = \alpha \frac{(\tau_m - \tau_c)}{\rho g} U \quad (10)$$

in which

α = empirical coefficient typically of order 1 to 10

$\tau_m = c_f \rho \langle |U|U \rangle$, the time-averaged bottom shear stress

$\tau_c = (\rho_s - \rho)gd_{50}\Psi_c$ is the critical shear for sediment motion

ρ_s = density of sediment

d_{50} = median grain size diameter

Ψ_c = critical Shields parameter, set to 0.05 for fine to medium sand.

In the absence of waves, Equation 10 becomes:

$$q_B = \alpha \left[\frac{n^2}{h^{1/3}} U^3 - \left(\frac{\rho_s}{\rho} - 1 \right) d_{50} \Psi_c U \right] \quad (11)$$

In Equation 11, a Manning's friction coefficient is presently inserted in the shear stress as a representative value. If waves are present in the breach, the time-average bottom stress is evaluated by the square-wave approximation of Nishimura (1988), eliminating explicit wave-period time averaging at each time-step. Therefore, the bottom stress along a breach or inlet is expressed by:

$$\tau_m = c_f U \left(U_{wc} + \frac{\hat{w}_b}{U_{wc}} \cos \theta_b \right) \quad (12)$$

where

$$U_{wc} = \frac{1}{2} \left(\sqrt{U^2 + \hat{w}_b^2 + 2U\hat{w}_b \cos \theta_b} + \sqrt{U^2 + \hat{w}_b^2 - 2U\hat{w}_b \cos \theta_b} \right) \quad (13)$$

$$\hat{w}_b = \frac{\sigma H_b}{\pi \sinh k (h_b + \eta_{setup})} \quad (14)$$

$$k = \frac{2\pi}{T \sqrt{g (h_b + \eta_{setup})}} \quad (15)$$

Field observation of breaches indicates that the rapidly flowing water through them will remove material both by direct shear on the sides of the opening and by notching of the side, causing collapse of the slab of material above the notch. The process of shearing and notching of dunes and channel banks is not well known (Erikson et al. 2003). In the model, this complex process is simply represented as a fraction of the total transport at the bottom as:

$$q_s = \beta q_B , \quad (16)$$

where β is a calibration factor.

The longshore current can deposit sand into a breach, a portion of which may be transported out by waves and the longshore current. During a long-term simulation, it is feasible that the longshore sediment transport rate can exceed the total sediment transport rate through the breach, affecting closure. The total longshore sediment transport, Q_L is calculated from wave information at depth-limited breaking in a variation of the Coastal Engineering Research Center (CERC) formula as Komar (1998):

$$Q_L = 1.1 \rho g^{3/2} H_b^{5/2} \sin \theta_b \cos \theta_b \quad (17)$$

where Q_L has units of cubic meters per day. If it is assumed that, on average, the longshore sediment transport rate is uniform across the surf zone, the portion of sediment intercepting the breach can be estimated by the ratio of the distances from the shoreline adjacent to the breach and to the wave-breaking point at a given time-step. These distances are expressed through the equilibrium beach profile (Dean 1977) as:

$$x_b = \left(\frac{h_b}{A} \right)^{3/2} , \quad x_{Dtrap} = \left(\frac{h_{Dtrap}}{A} \right)^{3/2} \quad (18)$$

where

x_b = distance from shoreline to breaking point at depth h_b ,

x_{Dtrap} = distance from shoreline to the limit of trapping by the breach, which intersects the profile to the depth of the breach, h_{Dtrap} , and

A = shape parameter for equilibrium profile.

The longshore sediment transport rate Q_L is a computed estimate of a complex, time-dependent process. This calculated rate should be validated by comparing with known or published longshore sediment transport rates for the site, such as the annual net and gross rates.

Several investigations have reported on the distribution of longshore sediment transport across the surf zone. Kraus et al. (1982) found peaks in the swash zone and breaker zone in multicolor sand tracer field experiments, among four different observed distributions. Bodge and Dean (1987) measured the cross-shore distribution in short-term field experiments and in the laboratory, and they concluded that at least 5 to more than 60 percent of the total rate occurs in

the swash zone. Smith et al. (2003) concluded from mid-scale physical model experiments that swash zone transport contributes significantly to the total rate.

The cross-shore distribution of the longshore sediment transport rate depends on the breaking wave type, wave height and period, beach profile shape, and sediment size, among other factors. In the present version of the morphologic breaching model, an ad hoc distribution is specified for which at least 30 percent of the total rate in the inner surf zone enters the breach section. The trapped longshore sediment transport entering the breach is given by:

$$Q_{Dtrap} = \left(0.3 + \frac{x_{Dtrap}}{x_b} \right) Q_L = \left[0.3 + \left(\frac{h_{Dtrap}}{h_b} \right)^{3/2} \right] Q_L \quad (19)$$

All sediment entering the breach by longshore transport will not remain. Some portion will be resuspended and transported out to bypass the breach. The present version of the model contains an empirical coefficient r expressing the ratio of bypassed versus trapped sediment by the breach. Sensitivity tests indicate $r \sim 0.2$ to 0.5 provides reasonable results as a first approximation. The rate of longshore sediment transport entering and remaining in the breach is then expressed by:

$$Q_T = r Q_{Dtrap} \quad (20)$$

Therefore, the total bottom sediment transport rate at the breach section is calculated to be:

$$Q_B = q_B \times (\text{width of breach}) - Q_T \quad (21)$$

A positive sign means there is a net loss of sediment from the breach (breach grows in dimensions), whereas a negative sign means there is a net gain (breach decreases in size).

Morphologic model

The model proceeds from the continuity equation expressed for an assumed breach cross-sectional geometry. Because of the assumption of a specified cross-sectional geometry, the model is termed as a morphologic model. In the original model (Kraus 2003), the simple form of a rectangular barrier island was specified, as depicted in Figure 101. The rectangular barrier island has cross-shore width L , breach width x , and depth z measured from the crest of the barrier. A net transport rate at the bottom Q_B in time interval Δt erodes a bottom layer of uniform thickness Δz , and a transport rate Q_S on each side erodes each side as a layer of uniform thickness Δx .

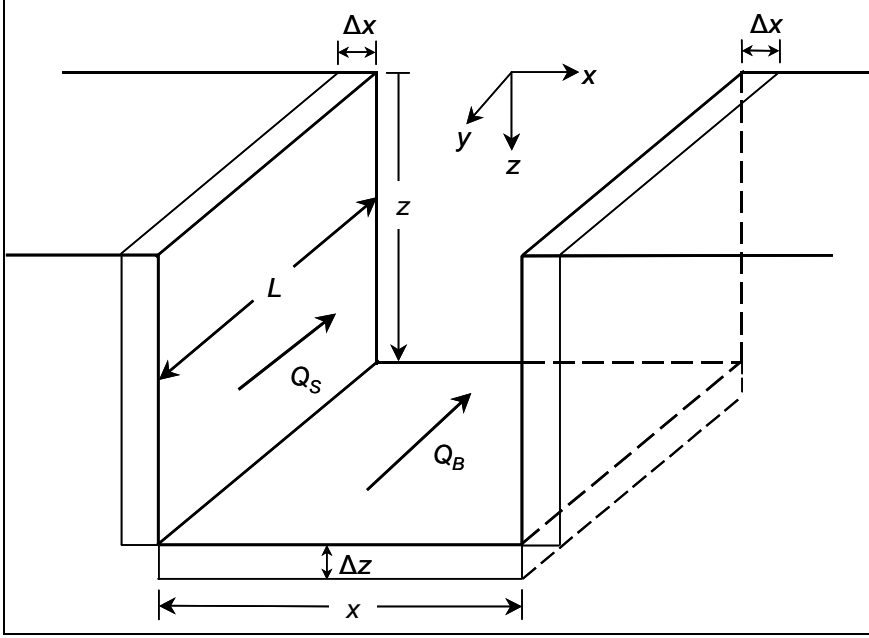


Figure 101. Definition sketch for rectangular barrier island

For such a rectangular barrier island, the continuity equation for sediment volume on one side and the bottom yields:

$$\frac{dx}{dt} = \frac{Q_S}{A_S}, \quad x_0 > 0, \quad (22)$$

and

$$\frac{dz}{dt} = \frac{Q_B}{A_B}, \quad z_0 > 0, \quad (23)$$

in which x_0 and z_0 are the initial width and depth of the region in the barrier island where the breach forms (the pilot channel), $A_S = Lz$, is the area of one side and $A_B = Lx$ is the area of bottom. Equations 22 and 23 are two coupled first-order nonlinear differential equations governing breach width and depth, respectively.

In the original morphologic model (Kraus 2003), the transport rates were parameterized as $Q_S = \hat{Q}_S(1 - x/x_e)$ and $Q_B = \hat{Q}_B(1 - z/z_e)$, in which \hat{Q}_S and \hat{Q}_B are constant maximum rates assumed to occur at the start of the breach, and x_e and z_e are values of the breach width and depth at equilibrium with the breach-forcing conditions. Closed-form solution of the two equations was found possible if \hat{Q}_B and \hat{Q}_S equaled a constant rate Q , leading to solutions of the form $x = x_e(1 - f(x)e^{-t/\tau})$ and $z = z_e(1 - g(z)e^{-t/\tau})$, in which $f(x)$ and $g(x)$ are complicated functions. These solutions describe exponential growth toward

equilibrium at a rate governed by the morphologic time scale $\tau = x_e z_e L / Q$.

Equations 22 and 23 possess characteristics of equations encountered in chaos theory. Therefore, the solution at early stages strongly depends on the initial condition, contained in the functions f and g , but eventually reaches the same value in exponential growth toward equilibrium. The exponential behavior of the analytical solution qualitatively agrees with the conceptual phases of breach growth, with rapid change at the incipient-breach phase transitioning to gradual change at the inlet-development phase.

The original morphologic model represents the macro-scale process of breach growth through specification of equilibrium morphologic conditions without consideration of the acting hydrodynamics and sediment transport. The solution indicates time-dependent breach dimensions are controlled by seven variables: initial width and depth of the breach, equilibrium width and depth of the breach, width of the barrier island, and maximum or initial net sediment transport rates at the bottom and sides of the breach. The original model has limitations in not depending on the current that transports sediment to and through the breach. Therefore, the model was enhanced by incorporating a 1-D inlet hydrodynamic model to calculate sediment transport together with other acting time-dependent processes, including longshore sediment transport.

Analytical solutions and numerical solutions were developed for the original breach model for a rectangular barrier island as depicted in Figure 101. Although a rectangle is a reasonable first approximation, barrier islands typically have a pyramidal or curved shape vertically, and may expand horizontally with distance from the jetty. In a numerical solution, such a shape can be represented by a series of stacked rectangles to give a vertical layered and horizontal sectioned barrier island shape (Figure 102).

In the numerical model, as the breach deepens and widens, new vertical layers and horizontal sections are opened, giving a new length L and surface area on the sides for calculating sediment transport. Figures 102 and 103 are definition sketches for simple vertical layer and horizontal section model. For vertical breach development, the side area of breach, A_s in Equation 22 is expressed by:

$$A_s = \sum_{i=1}^{N_L} z_i L_{Li} - \left[\left(\sum_{i=1}^{N_L} z_i \right) - z \right] L_{LN} \quad (24)$$

where the index i refers to the layer number, counting consecutively from the top of barrier island to N_L , the total number of layers, and L_{Li} is the length of layer i .

For horizontal breach development, the bottom area of breach, A_B in Equation 23 is expressed by:

$$A_B = \sum_{j=1}^{N_S} x_j L_{S,j} - \left[\left(\sum_{j=1}^{N_S} x_j \right) - x \right] L_{S,N_S} \quad (25)$$

where the index j refers to the section number, counting consecutively from the top of the barrier island to N_S , the total number of sections, and L_{Sj} is the length of section j .

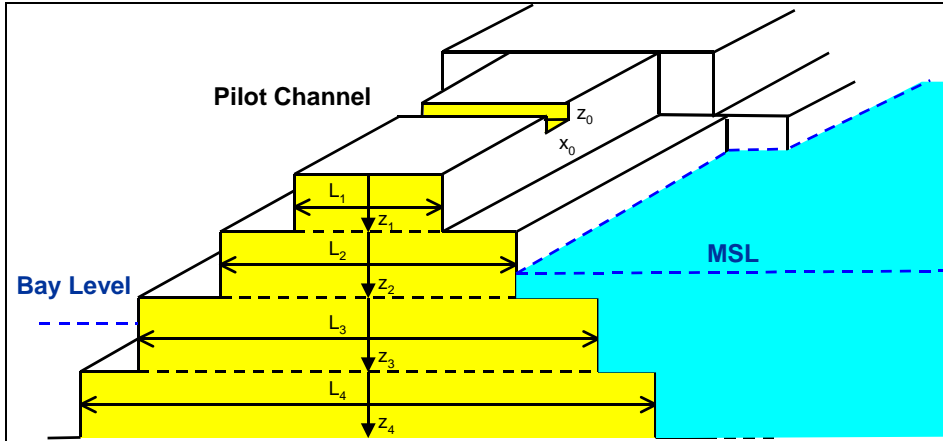


Figure 102. Definition sketch for layered barrier island cross section

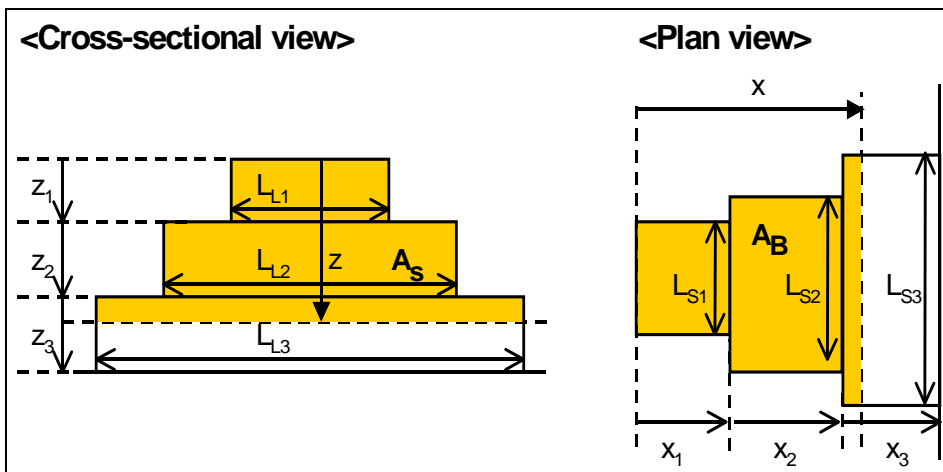


Figure 103. Definition sketch for vertical layers and horizontal sections

Tests of Breaching Model

Numerous tests of the breaching model were performed. This section summarizes a sensitivity test and comparisons of model results to laboratory data and to measurements at Moriches Inlet.

Semicircle barrier island

To test the layered barrier island numerical solution method, an analytical solution was developed for a semicircular-segment barrier island of constant horizontal width (Figure 104). For fixed breach width, the area of a side A_s is:

$$A_s = \left[\frac{\pi}{2} - \sin^{-1} \left(1 - \frac{z}{R} \right) \right] R^2 - (R - z) \sqrt{2zR - z^2} \quad (26)$$

where R = radius of the semicircular-segment.

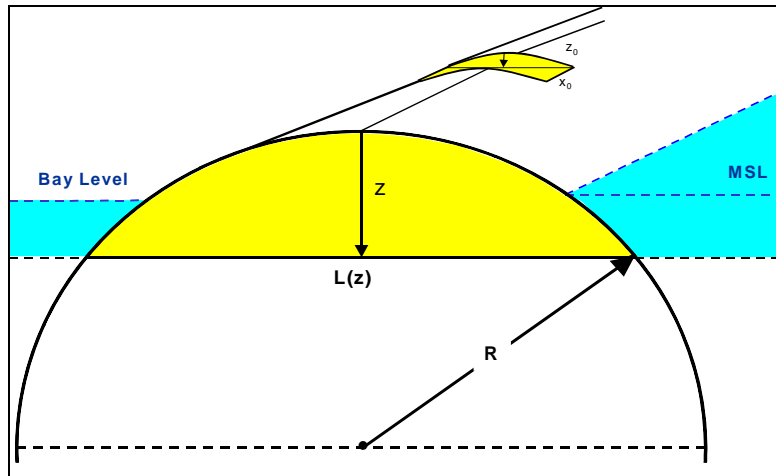


Figure 104. Definition sketch for semicircular-segment barrier island cross section

Example validation results for the layer model are displayed in Figure 105, for which the original morphologic breach model was run. Simulations were performed with 1, 3, and 5 layers specified in the layer model for the same total elevation of the barrier island crest of 6 m. Dimensions of the pilot channel were the same in both models. As expected, a single rectangle and small number (3, 5) of rectangular layers produce an underestimate of the breach width, because the volume to be removed is greater than contained in the semicircular segment. As the number of layers increases, the semicircular segment analytical solution is approached. For the specified dimensions, the plotted line for seven layers overlays the analytical solution.

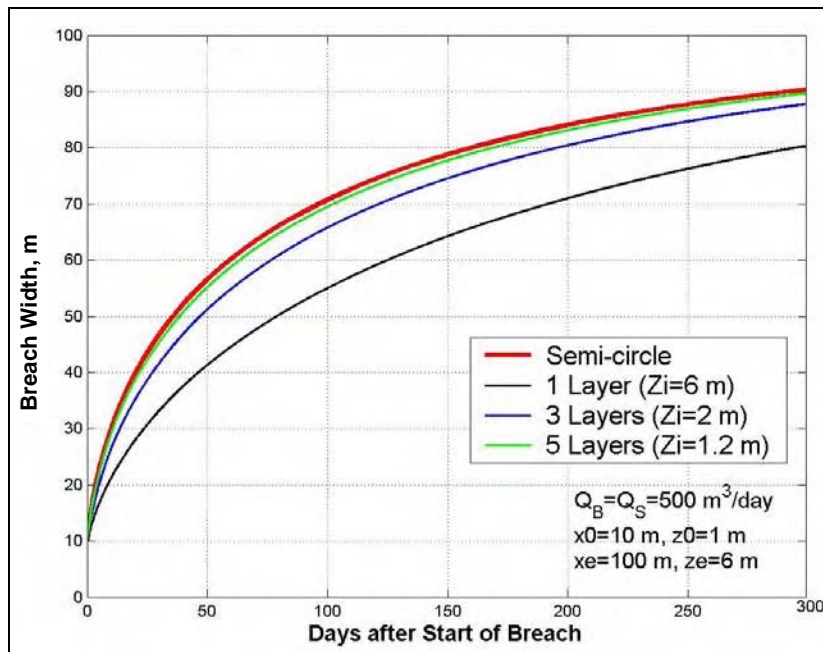


Figure 105. Validation of layer breach model algorithms by comparison to semicircular-segment analytical solution

Dutch laboratory study

De Looff et al. (1996) report results of a physical model of a sand dike installed in a wave basin to investigate breach width for various dike configurations. The breach was initiated by opening a small pilot channel at the top of the dike. Breach width, upstream water level, and surface-water velocity were recorded, and eight cases with different cross sections were reported. Data on breach depth were not obtained. In the present study, three cases (T2, T4, and T7) were examined to investigate the sensitivity of the numerical model to initial sand volume. Figure 106 shows the initial cross sections for T2, T4, and T7. Several layers were defined to represent the dike.

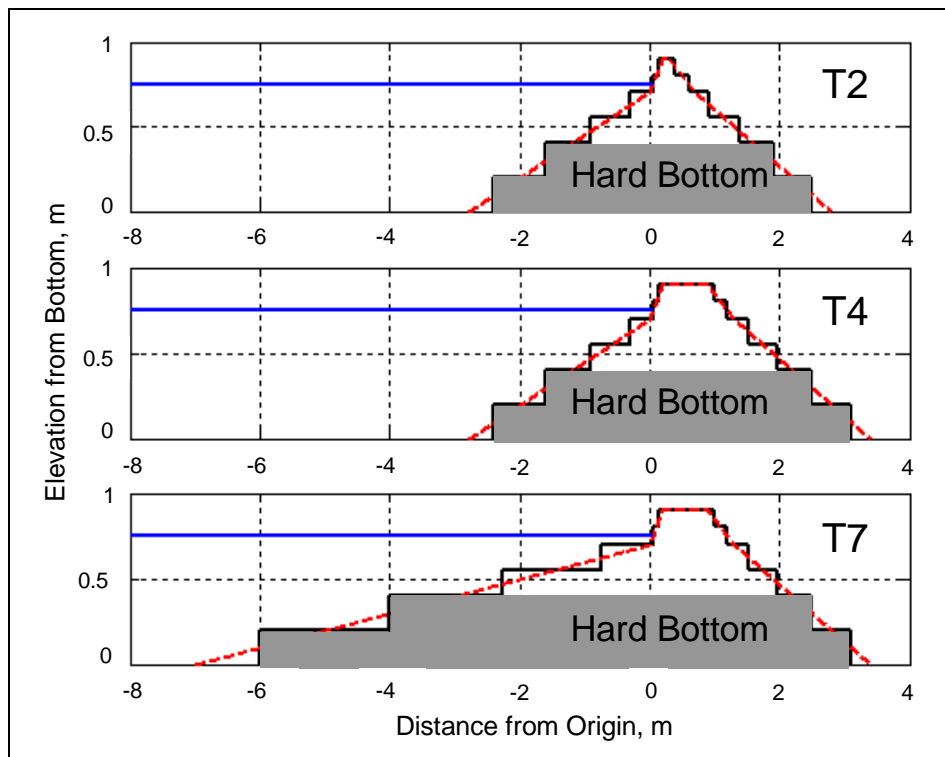


Figure 106. Initial cross-sectional profiles for Cases T2, T4, and T7

With T4 as the standard dike, Case T2 had a smaller sand volume, whereas T7 had a larger volume than T4. In the experiment, the upstream and downstream water levels were kept as constant as possible by a recirculation system with optional pump capacity up to $1.0 \text{ m}^3/\text{sec}$. When the breach started, the head-difference was 0.75 m for all tests. In the breach model simulation, the measured upstream water level served as the head-difference forcing (Figure 107).

Calibration was performed by adjusting the sediment transport parameters for Case T4, which yielded $\alpha = 2.5$ and $\beta = 0.5$ for a best fit to the measurements. This value of α is within the range typically found in field simulations. With these parameters fixed, simulations were run for Cases T2 and T7.

Model calculations shown in Figure 108 follow the qualitative trends in observations in which breach width increased faster for smaller dike volume. The calculations approach equilibrium slower than the observations under the imposed constant head in the numerical model, which may indicate the head was not completely constant in the laboratory (water was probably impounded on the downstream side). Unknowns exist in this data set that precludes optimization of the calculations, including ambiguous dimensions of the pilot channel, lack of information on breach depth, and possible non-constant hydraulic head. Computed velocities through the breach (Figure 109) approach 1 m/sec, a value observed in the laboratory at the final stage of the experiments.

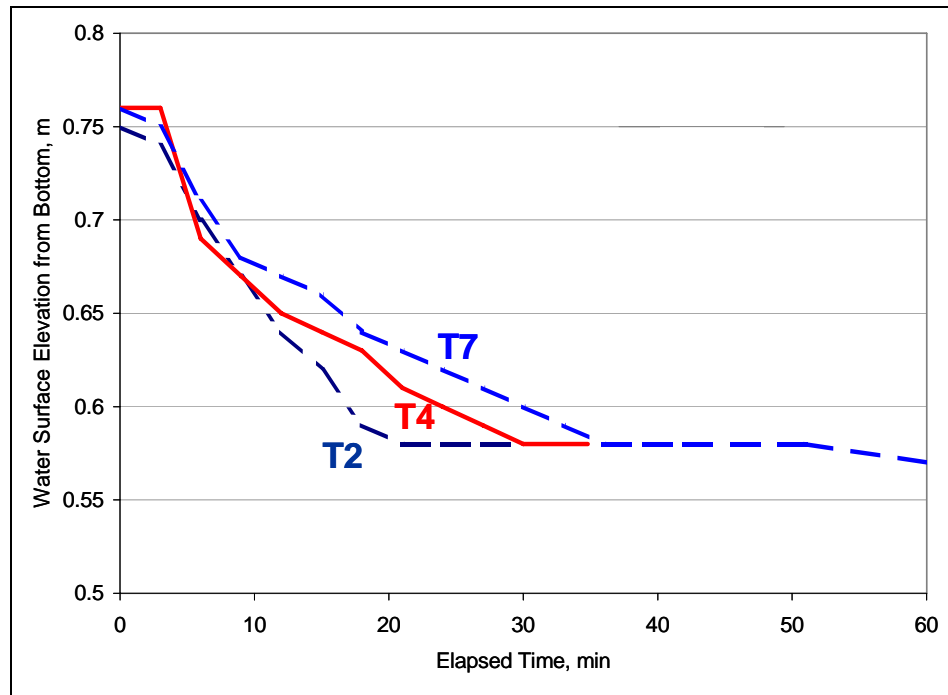


Figure 107. Measured water-surface elevation from bottom for Cases T2, T4, and T7

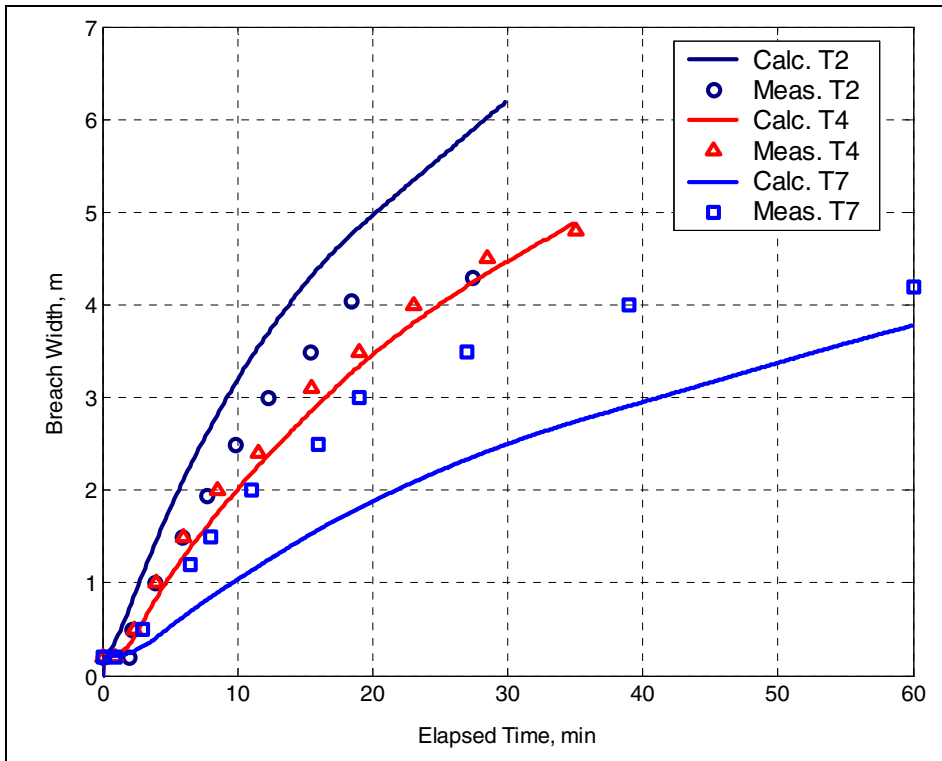


Figure 108. Measured and calculated width of dike breach, laboratory experiment

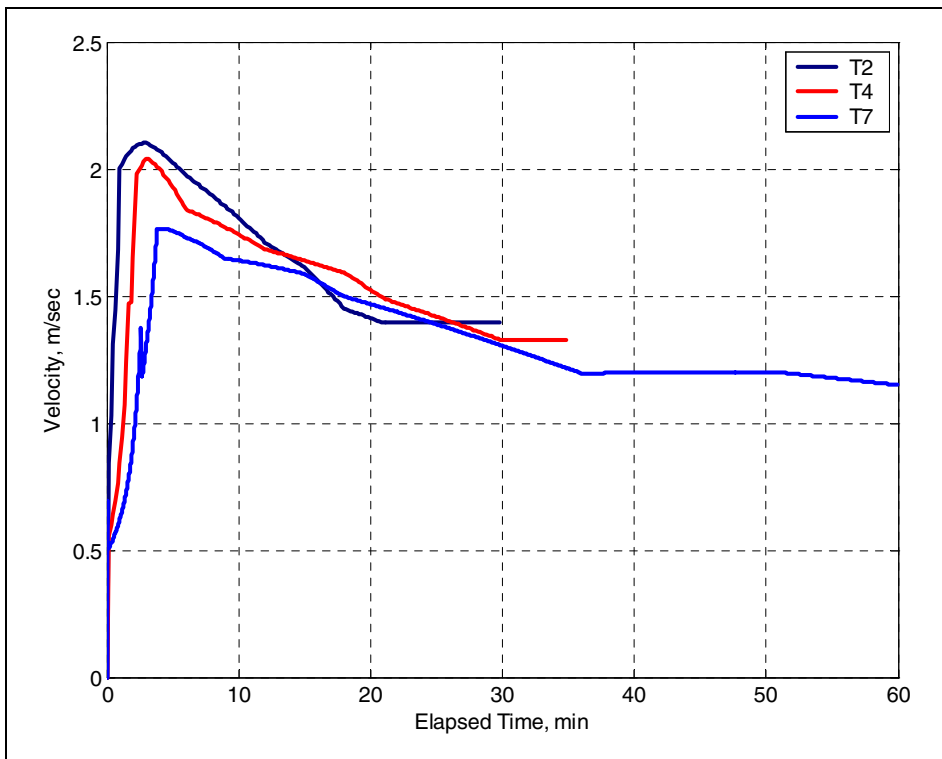


Figure 109. Calculated velocity in breach, laboratory experiment

USACE laboratory study

Two large-scale moveable-bed physical model experiments of barrier island breaching were conducted in August and September 2005 at ERDC CHL. The experiments were conducted in a 64-m long, 3-m wide wave flume with an idealized, sand-substrate barrier island. A pilot channel was cut in the barrier to initiate flow through the breach. The barrier (Figure 110) was constructed with a 1:10 foreshore slope, a level plateau, and a 1:7 backshore slope. Breaching was initiated both without waves (Case BR1) and with waves (Case BR2). BR1 was forced by a head difference sustained by elevated water levels on the offshore side of the barrier and depressed water levels on the bay side, controlled by pumping water from the bay to the ocean. BR2 was similar to BR1 with the addition of 10-cm monochromatic waves with 3.1-sec period. Breach morphologic evolution (Figure 111) was measured with timed topographic surveys at transects A, B, C, and D. Breach evolution was also captured with six overhead orthogonal video cameras and one overhead oblique video camera. Water level was measured in both the offshore and inshore basins with capacitance water level gauges. Current velocity was measured with an Acoustic Doppler Velocimeter (ADV) within the breach channel for BR1. The ADV failed for the case with waves, and current velocity measurements are not available for BR2. Waves were measured in BR2 with a wave gauge located offshore of the breaking point.

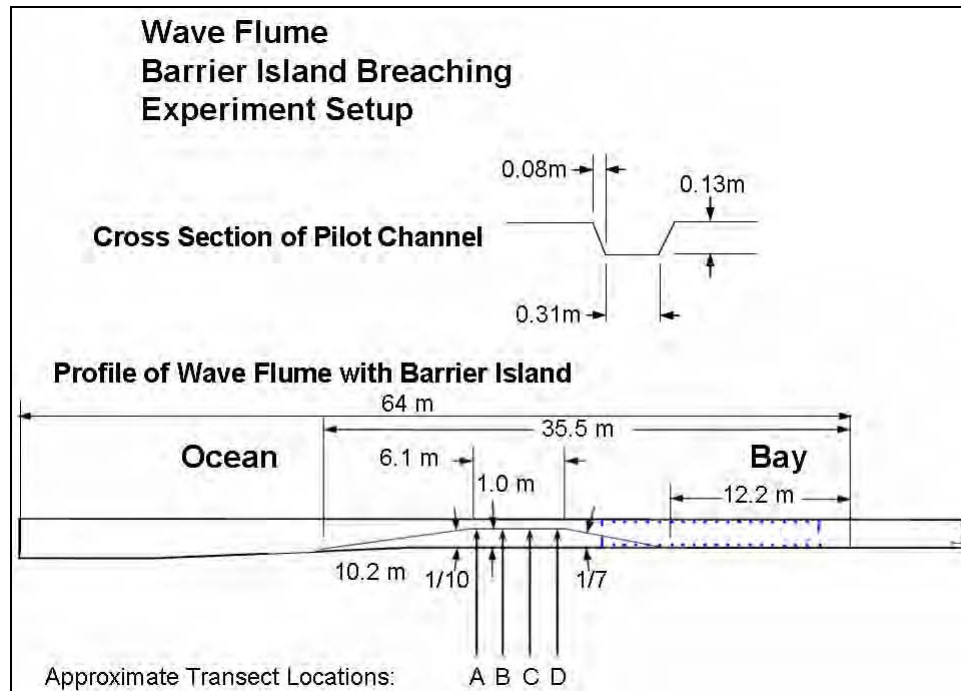


Figure 110. USACE breaching laboratory experiment schematic

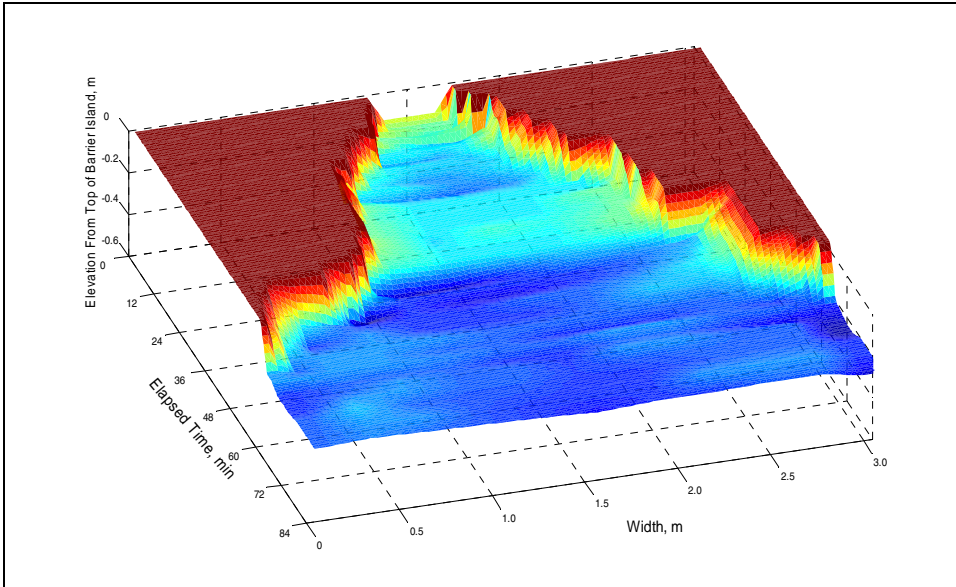


Figure 111. Measured morphologic evolution at transect D during BR1 laboratory experiment

Measured offshore and inshore basin water levels were input to the numerical morphologic breaching model, and several calibration runs were conducted. The breaching model was calibrated to the BR1 experiment by adjusting α and β in the transport equations to fit predicted current velocity, breach elevation, and breach width to measured values. The optimal values for this experiment were $\alpha = 0.5$ and $\beta = 1.5$.

The adjustment factor for sediment transport was held at $\alpha = 0.5$ for the remaining model simulations to verify results of BR1 and BR2. Adjustments were made to the β factor to simulate results of BR2 to compensate for increased sediment transport in the swash zone at the breach banks in the presence of waves.

Model calculations of velocity and breach depth (Figure 112) demonstrate good correlation. However, times of channel infilling due to shoaling and wall notching and collapse do not correlate well. The numerical breaching model does not presently have avalanching capability, and shoaling will also not occur. These new experiments have highlighted this limitation of the breaching model, projecting directions for its further development.

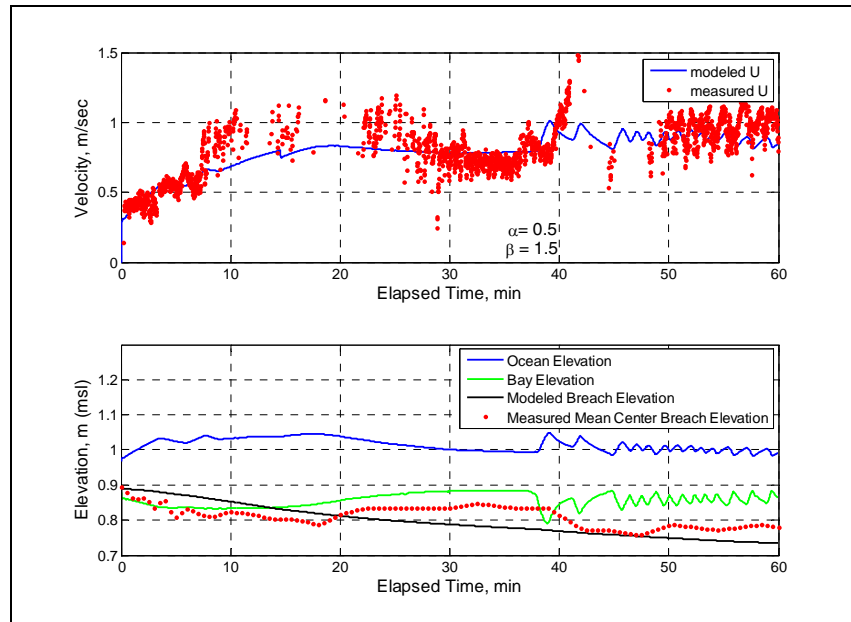


Figure 112. Measured and modeled channel velocity and elevation relative to water-surface elevation for BR1

The breach BR1 (Figure 113) widens at a slower rate and deepens at a greater rate compared to BR2 (Figure 114). Evolution of cross-sectional areas of the two cases (BR1 and BR2) is similar. Wave action with large transport in the swash zone at the breach banks flattens the channel walls and initially accelerates channel widening. The material eroded from the bank is deposited in the channel, slowing channel deepening. Evolution of the channel in BR2 as a wider and shallower channel also decreases the velocity (Figure 115) through the breach channel, because the frictional surface area along the channel bottom increased.

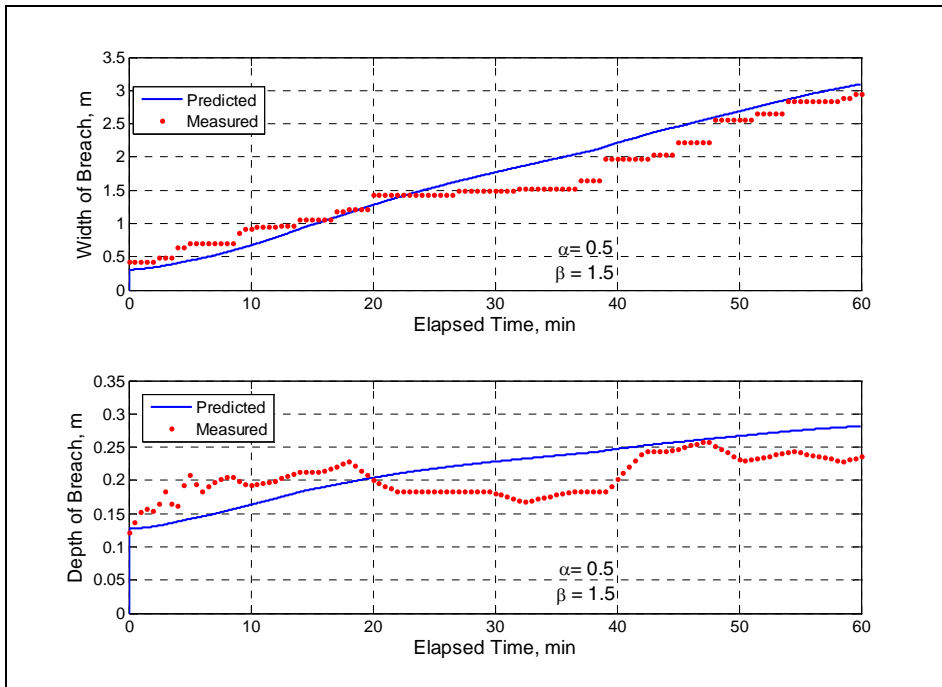


Figure 113. Breach width and depth, BR1

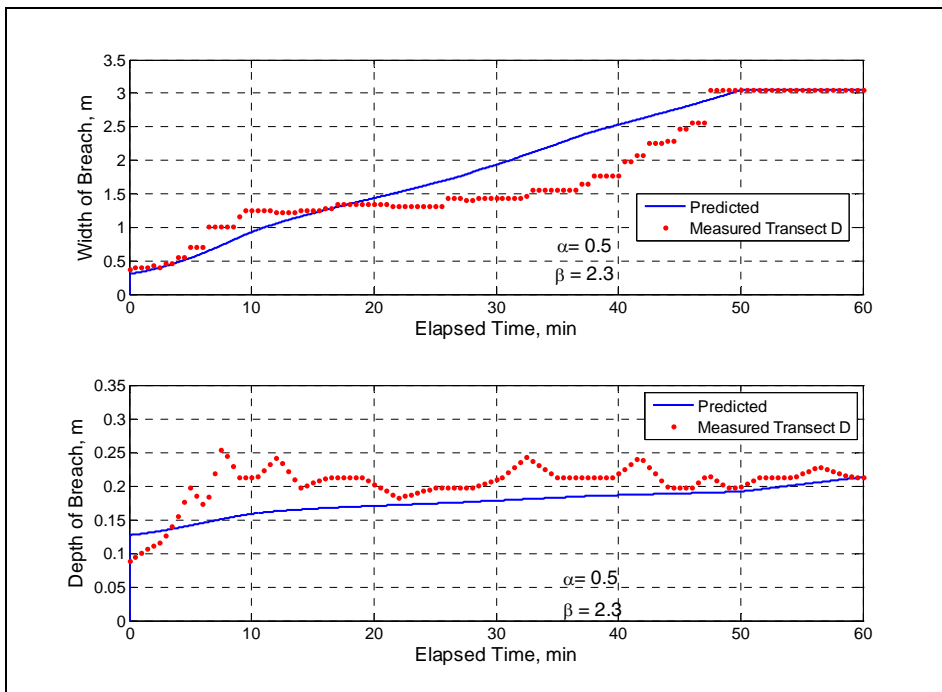


Figure 114. Breach width and depth, BR2

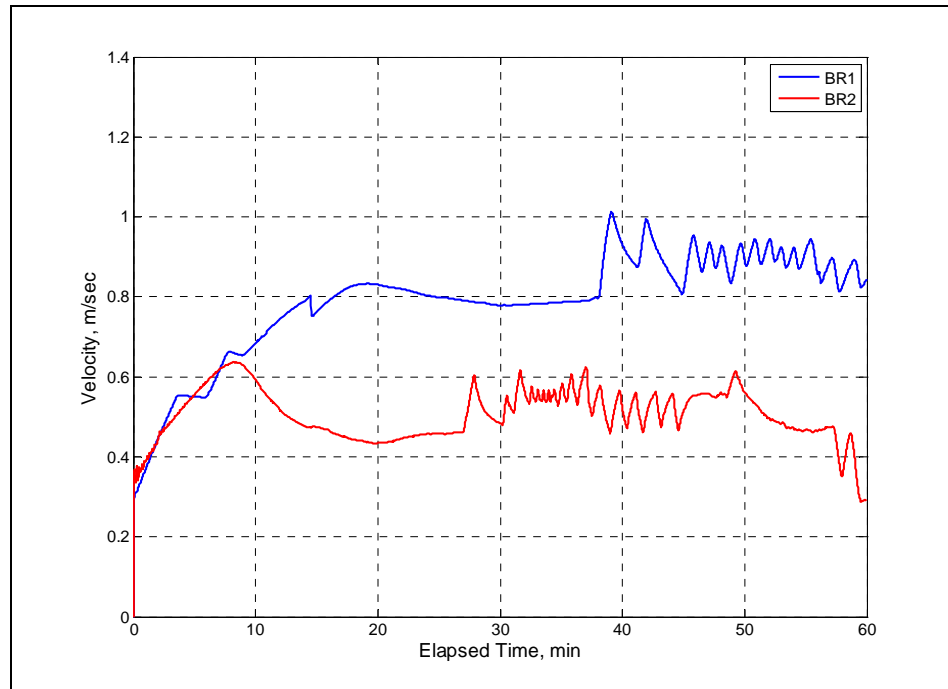


Figure 115. Calculated breach channel velocity in BR1 and BR2

1980 breach at Moriches Inlet, NY

Moriches Inlet is a federally maintained entrance located on the southeastern shore of Long Island, NY, connecting Moriches Bay (part of Great South Bay) to the Atlantic Ocean (Figure 116). Without stabilization by structures, inlet channels on eastern Long Island tend to migrate westward and have maximum depth of about 3 m with respect to mean lower low water. The ocean mean tide range at Moriches Inlet is about 1 m, and grain size on this glacially influenced coast is 0.35 mm. Moriches Inlet has a well-documented history of opening and closing in the past century (Czerniak 1977; Schmeltz et al. 1982). The modern inlet was opened by a storm in 1953, striking the coast during construction of dual jetties by local government. The jetties are spaced 245 m apart.

After the inlet opened in 1953, the barrier island on the eastern (updrift) side of Moriches Inlet gradually narrowed, primarily due to erosion at the jetty and shoreline or bank recession in the back bay, adjacent to an ebb-current channel. Sorensen and Schmeltz (1982) indicate the adjacent beach was about 100 m wide in 1972. During 14-16 January 1980, a storm opened a breach at the narrowest point in the barrier island, about 300 m east of the east jetty. Schmeltz et al. (1982) plot survey cross sections of the inlet after breach closure that shows the inlet becoming deeper once the breach was closed. It can be concluded that the inlet was filling in with the breach open.

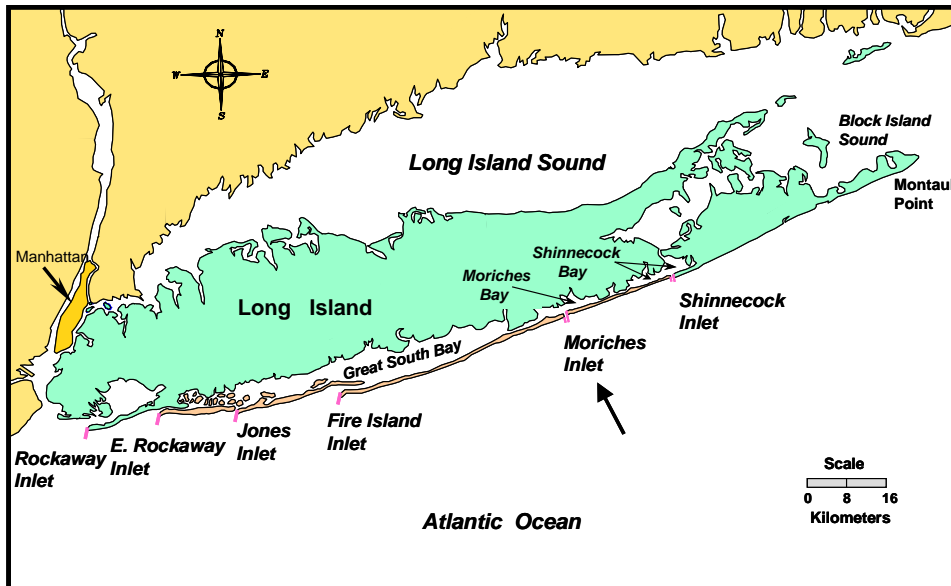


Figure 116. Location map for Moriches Inlet, Long Island, NY

Kraus (2003) summarizes previously reported and additional measurements of this breach. To obtain the additional data, Kraus and Hayashi (2005) analyzed seven aerial photographs, taken after the breach opened, in a GIS (Figure 117). The measured breach widths are summarized in Table 8. In this table, the initial pilot channel is assumed to have been 50 m wide and 0.25 m deep (from the top of the barrier island). Based on the analysis, the date when the breach reached the east jetty was estimated to be the beginning of May 1980, and the maximum breach width was achieved sometime between 18 July and 25 August, because the vegetation line remained at the same location after 25 August 1980.

If the maximum breach width is taken to be the distance from the east jetty to the vegetation line, it is estimated as 850 m, or 3-1/2 times the width between the jetties. After the maximum width was achieved, the breach narrowed slightly. The narrowing is attributed to longshore sediment transport from the east, the predominant direction of transport at the site, which began spit growth to the west. It is difficult to specify a single value for breach depth based on the available bathymetric surveys because of the highly irregular bottom. Therefore, the area-averaged depth and the maximum depth are listed in Table 8.

For the simulation, the barrier island was divided into three horizontal sections. The narrowest initial cross-sectional barrier island profile was specified according to discussions with the former Senior Coastal Engineer, New York District, who was familiar with Moriches Inlet during the time of the breach.¹ Other information on barrier width was estimated from an aerial photograph taken April 1976 (Figure 117). Wave data were taken from the Wave Information Study hindcast, sta 111. Based on the hindcast, the longshore sediment transport rate was calibrated by reference to an accepted value for the eastern Long Island area to give a net annual longshore sediment transport rate of 250,000 cu m/year. Water level measured at the NOS Battery, NY

¹ Private communication, Mr. Gilbert K. Nersesian, Senior Coastal Engineer (retired), U.S. Army Engineer District, New York, April 2004.

(sta 8518750), served to represent the storm surge and tide. The sediment transport calibration factors were determined to be $\alpha = 0.05$ and $\beta = 50$, and the adjustment factor for wave setup was $\varepsilon = 0.30$ in Equation 6.

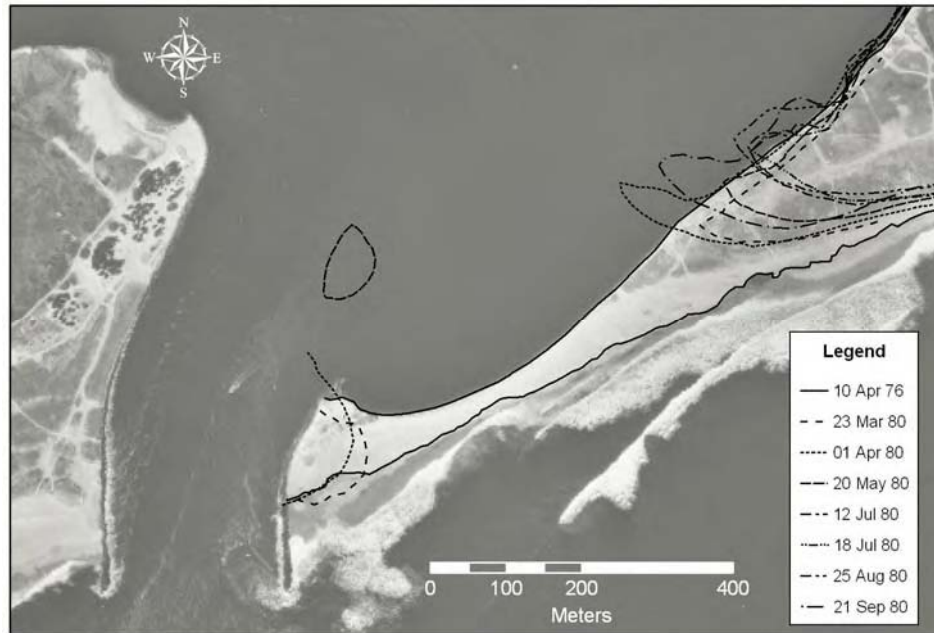


Figure 117. Moriches Inlet breach development

Table 8			
Dimensions of 1980 Breach at Moriches Inlet, NY (Compiled from Schmeltz et al. (1982), and Aerial Photograph Analysis in This Study)			
Date 1980	Estimated Elapsed Time, Days	Breach Width, m	Breach Depth from Assumed Elevation of Barrier Island Crest, m
13 January	0	50 (assumed)	0.25 (assumed)
16 January	3	90	2.35
20 January	7	215	2.75
23 March	70	560	N/A
01 April	79	571	N/A
01 May (day assumed)	109	620	N/A
23 May	131	740	N/A
12 July	181	800	N/A
18 July	187	812	N/A
25 August	225	810	N/A
21 September	252	720	N/A
27 September	258	Not Available	3.55 (Ave.), 5.62 (Max)
04 October	265	Not Available	3.95 (Ave.), 5.05 (Max)

The breach model was run to simulate 280 days, starting 13 January 1980, prior to the storm that opened the breach. Several days after start of the run, a breach opened at the pilot channel, indicating correct behavior of the model in predicting the breach. Figure 118 shows the calculated current velocity in Moriches Inlet and in the breach. At inception of the breach, the velocity exceeded 2.5 m/sec. After the storm subsided, tidal exchange between ocean and bay continued to enlarge the breach cross-sectional area, and the velocity through it decreased. Velocities in both the inlet and the breach became smaller, because the breach functioned as a second inlet, sharing the flow. It appears from the calculated velocity that Moriches Inlet was becoming unstable due to the presence of the breach, because the velocity through it frequently fell below 1 m/sec, an empirically known threshold for inlet stability. The velocity through the breach approached an apparent dynamic equilibrium exceeding 1 m/sec.

For the period of calculation in Figure 118, the inlet was ebb-biased with mean of -0.30 m/sec, and the breach was flood-biased with mean of 0.13 m/sec. The breach grew to have larger cross-sectional area than the inlet, so the discharges have equal magnitude. PRC Harris, Inc. (1980) measured the current velocity in the breach to be in the range of 1.5 to 2.1 m/sec during two site visits believed to be relatively soon after breach opening (no date was given for the visits). Model results are in qualitative agreement with those observations.

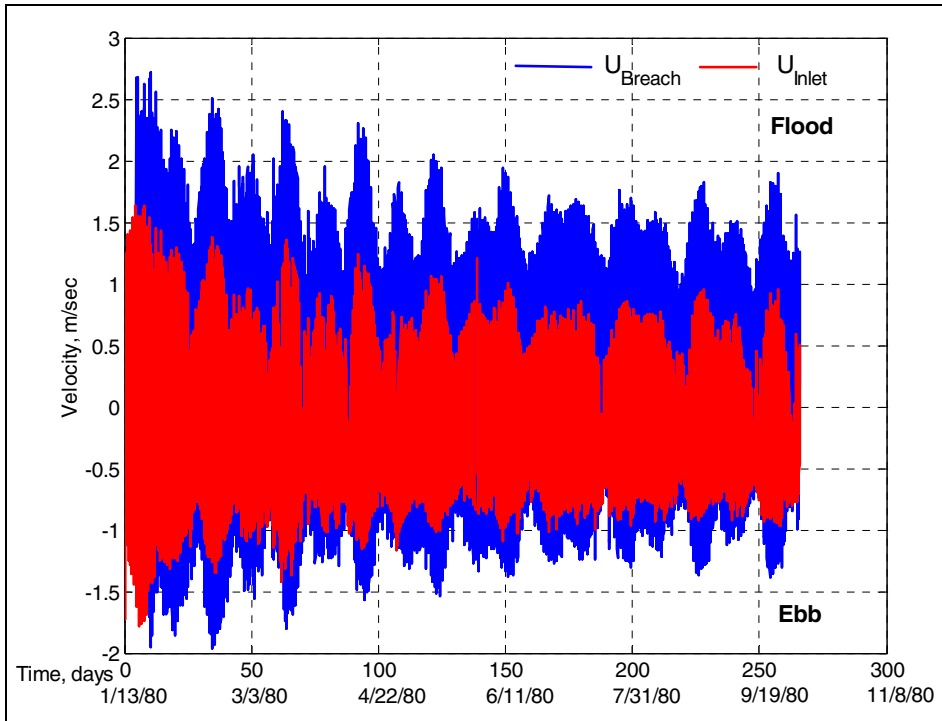


Figure 118. Velocity in Moriches Inlet breach and inlet during breach growth

Calculated breach width and depth for the 1980 Moriches Inlet breach are plotted in Figures 119 and 120, together with available measurements. The breach was calculated to reach the east jetty in May. The model reproduces the characteristic behavior that has been observed at many breaches, that is, rapid initial growth over approximately 50 days (incipient breaching phase), followed by a trend toward equilibrium at a much lower rate of growth (inlet-development phase). The calculated breach width and depth are in agreement with the data for trends and magnitude.

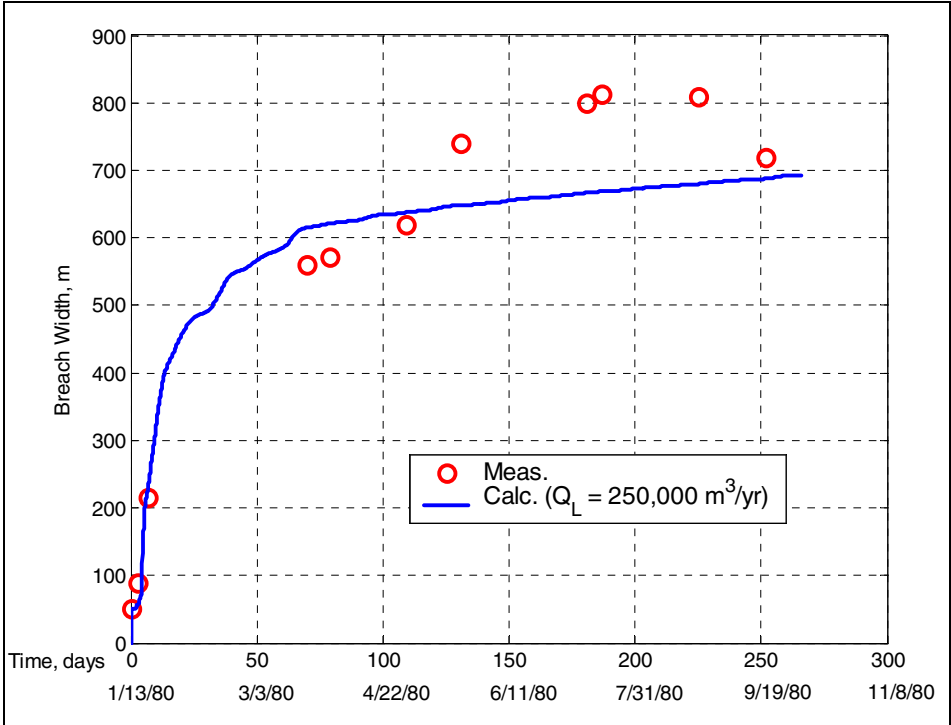


Figure 119. Calculated breach width and observations, 1980, Moriches Inlet

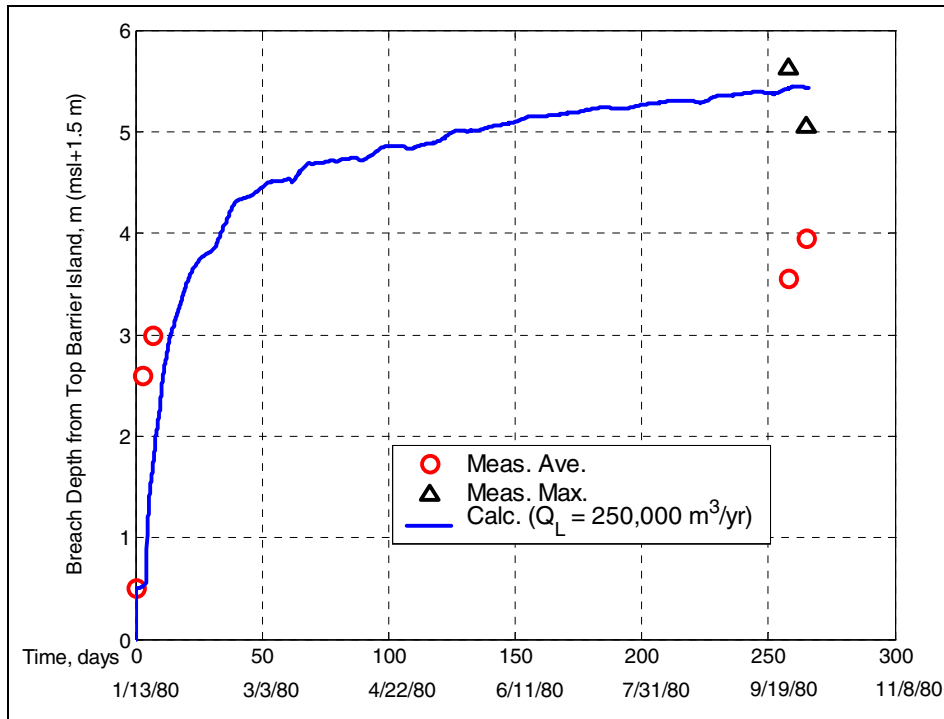


Figure 120. Calculated breach depth and observations, 1980, Moriches Inlet

Application to Grays Harbor

Based on success of the model in sensitivity tests, in comparisons to laboratory data, and in realistic simulation for the 1980 breach at Moriches Inlet, the breach model was applied to simulate the 1993 breach at Grays Harbor.

Available data

Wave measurements offshore of Grays Harbor are available from CDIP Buoy 03601. The CDIP buoy is located approximately 9.5 km southwest of the entrance to Grays Harbor in about 40 m of water. The buoy, whose operation is supported by the Seattle District, has been deployed since 1981, with directional measurements available since 1993. The wave data employed for the simulation run from December 1993 to March 1995.

Water level at Grays Harbor, both inside and outside the bay, was estimated by correlating with measurements from NOS water-level measurement stations at Neah Bay, WA, and at Astoria, OR, as discussed in Chapter 2. Storm surge is minor on the Pacific Coast as compared to the Atlantic Coast and Gulf Coast of the United States because of the steep continental shelf on the Pacific Coast. Wave setup is probably the dominant mechanism initiating breaching on the Pacific Coast. Infragravity waves (surf beat) likely play a role on the Pacific Coast in elevating water level at the shore, but this potential contribution was not included because of significant unknowns at present.

Because competent data sets could be developed for the bay tide and ocean tide at Grays Harbor for the time period of interest, 480 days, the model was forced with both water levels, eliminating the continuity equation (Equation 2) from the calculation. This procedure allowed calculation without representation of the Grays Harbor entrance, as the breach occupied only a small percent of the cross-sectional area of the entrance, in contrast to the situation at Moriches Inlet.

Topographic and bathymetric survey data are not available for the time immediately before the breach in 1993. Therefore, the initial cross section was estimated by reference to an aerial photograph taken in May 1993 (Figure 121) and the surveys of March and August 1994. From inspection of the aerial photograph, the area was divided laterally into two horizontal sections. Section 1 is the narrowed and lowest area adjacent to the south jetty. The length is estimated to be about 100 m. Section 2 is about 200 m long, starting from the end of Section 1. In the breaching model, these sections were represented by 16 vertical layers ranging from +3 to -5 m (msl), based on numerical model grid data estimated for December 1993 (Chapter 3). Figure 122 shows the two initial vertical cross-sectional profiles for each horizontal section. The profile below the +0.5 m (msl) in Section 1 was assumed to be the same as for Section 2.

The aerial photographic record indicates that a significant volume of sediment entered Half Moon Bay through the breach (Chapter 2). Therefore, in the model, once the breach was calculated to reach the south jetty, the effective length of Section 2 in the hydrodynamic model was increased to 1.5 times the calculated width of the breach to simulate an effectively longer breach and correspondingly greater friction resisting the flow.



Figure 121. Location of lateral sections, Grays Harbor

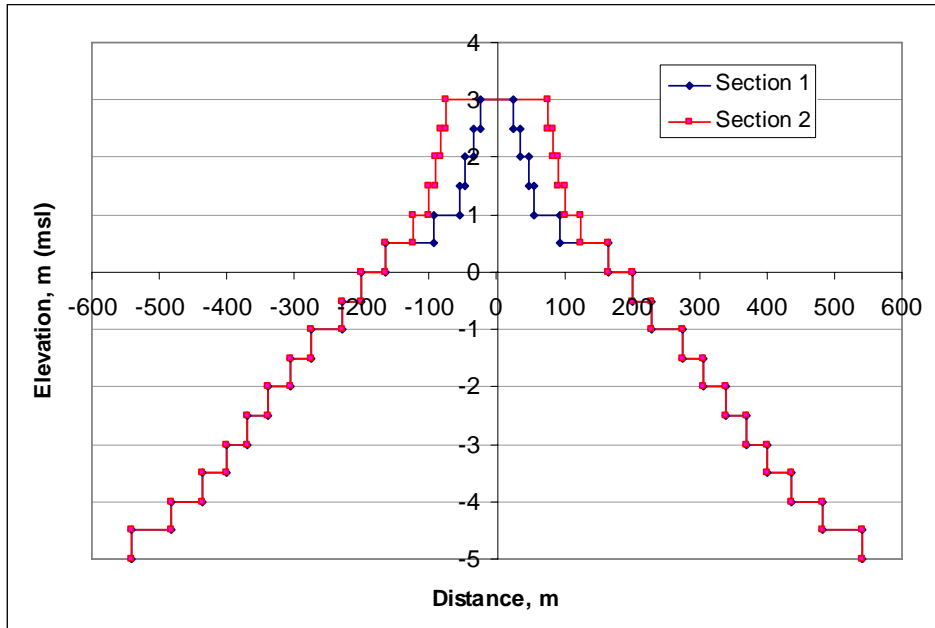


Figure 122. Estimated cross-sectional profiles for Sections 1 and 2, Grays Harbor

Dimensions of the pilot channel are significant factors in a breaching model, but these are not known for the 1993 breach. Therefore, pilot channels of different width and depth were created and run as part of an iterative model calibration process. The pilot channel producing the best overall agreement was found to be 50 m wide and at an elevation of 3 m mllw (i.e., 1.5 m deep, measured from the top of the barrier spit). The breach width and depth data are discussed in Chapter 2. For breach depth, analysis of additional transect lines was performed for the simulation. Measurements of depth were recalculated and plotted in two ways; the average depth (Meas. Ave.) and maximum depth (Meas. Max.).

Early tests comparing wave setup results from the breaching model to Coastal Modeling System (CMS) M2D setup results at Grays Harbor (Chapter 3) with offshore wave conditions: wave height = 6 m, wave period = 14 sec, and southwest wave angle = -6 deg suggested that Equation 6 was overpredicting setup at Grays Harbor. An adjustment factor, $\epsilon = 0.15$, was applied to the analytical setup equation to scale setup to the Grays Harbor study site.

It has been suggested that foreshore slope and wave steepness alter setup (Holman and Sallenger 1985; Hanslow and Nielsen 1993; Stockdon et al. 2006). Many of the empirical wave setup formulations do not include variables for bottom slope, but slope is implicit in the formulations from the beaches where the data were obtained to develop the parameterization. Stockdon et al. (2006) recommend beach foreshore slope be incorporated to parameterize wave setup in the relation given by Equation 7.

This formulation for setup was implemented in the breaching model. Several of the sites examined by Stockdon et al. (2006) included beaches along the

Oregon and California coasts which likely exhibit similar morphology and wave climate as the Grays Harbor site.

The beach profile in the vicinity of Grays Harbor was examined and the beach slope in the surf zone was determined to be approximately 0.01 (1:100), the average beach slope to be 0.02 (1:50), and the beach foreshore slope to be 0.029 (1:35). The foreshore is defined as the gradient between the 1.5- and 3.5-m (mllw) topographic contours. The slope calculation was conducted by averaging the foreshore slope of 51 cross-sections of the Digital Terrain Model of Grays Harbor at 20-m intervals for 1-km of the beach in the region immediately south of the breach. This slope is similar to the foreshore slope of 0.025 obtained along this stretch of beach by Ruggiero et al. (2005).

The foreshore slope of 0.029 was applied to the implemented setup formula, and a new breaching model simulation was executed with steady state 6-m waves with 14-sec period. A wave setup of 44 cm was calculated and added to the input water-surface elevations (Figure 123). Setup closely corresponds to the setup obtained by an independent CMS-M2D simulation with the same input forcing (Figure 124). Note that some cell drying occurs at the troughs in the CMS-M2D simulation. Linear regression analysis of this setup comparison (Figure 125) produces $R^2 = 0.997$, total RMS error = 15 cm, and RMS error over the range of observation = 6.6 percent. The first four values collected during the 0.1-day M2D ramp-up period were omitted from this analysis. The range of observation is reduced by the drying of M2D cells. Therefore, this percentage is higher than would be if no drying were to occur.

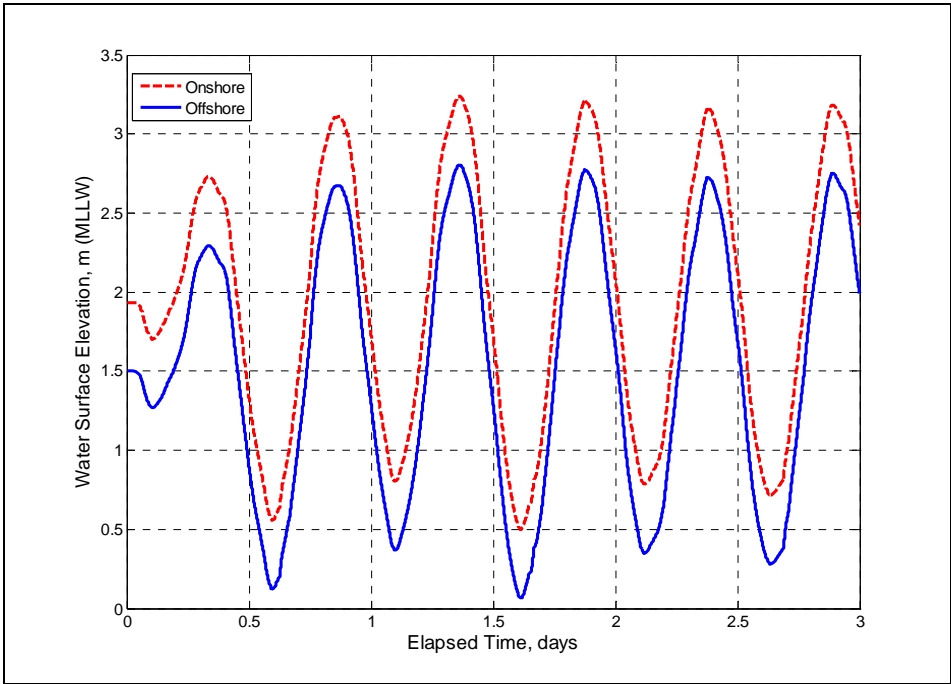


Figure 123. Wave setup calculated added to input water level

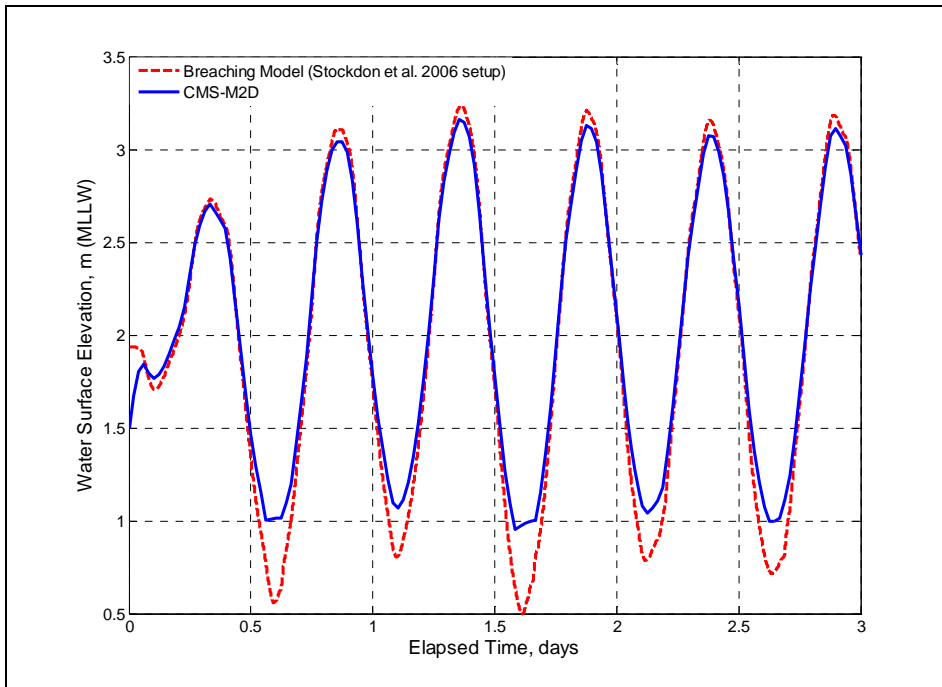


Figure 124. Comparison of calculated wave setup with results from CMS-M2D Grays Harbor

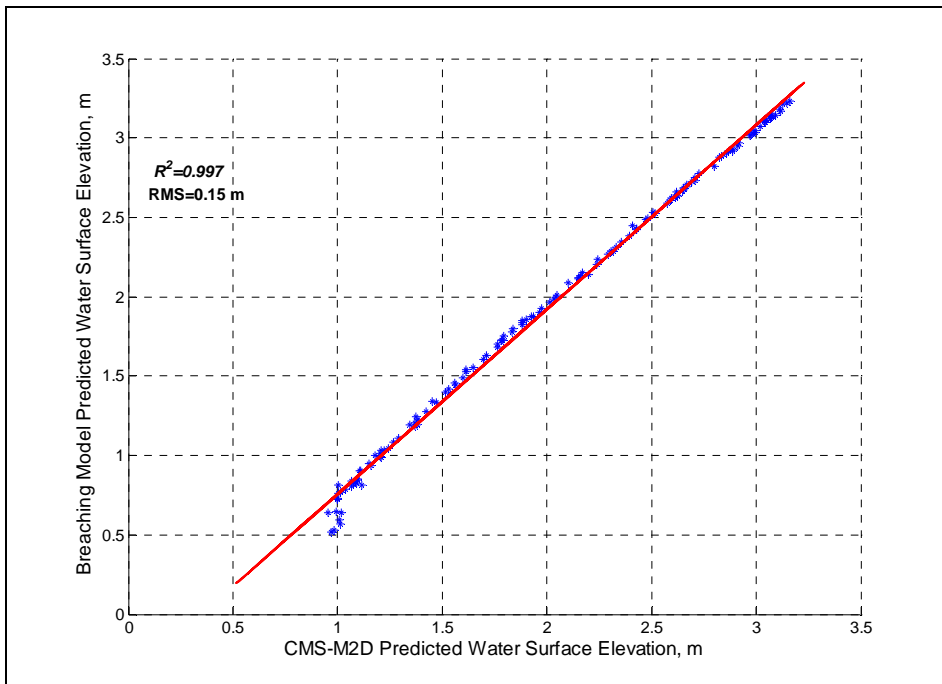


Figure 125. Linear regression of wave setup comparison shown in Figure 2

The breach was close to the south jetty, so longshore sediment transport could approach it only from the south. Northward-directed sediment transport was calculated and calibrated by comparing with the long-term annual net longshore sediment transport rate, 400,000 cu m/year (base value), estimated from a regional sediment budget (Byrnes et al. 2003). This value served as a base, and additional runs were done with net rates of 200,000 and 600,000 cu m/year to determine calculated breach response to a decrease and an increase, respectively, in sediment supply. For example, the question might arise as to whether a greater-than-average longshore transport in a given year might close such a breach.

Results

The breach model was first established by comparison to available measurements or estimates of breach width and depth. The calibration factors were determined to be $\alpha = 0.23$ and $\beta = 15$. The model was then run for approximately half a year after the actual breach was mechanically closed to estimate evolution of the breach through the next winter had it not been closed. As described in the model sediment transport section, it is possible for a breach to decrease in dimensions and even close if the longshore sediment transport dominates tidal transport through the breach.

In Figures 126 through 130, the dotted lines denote the prediction from the model if the breach had not been closed mechanically. Figures 126 and 127 show the calculations for breach width and depth. The simulation spans 480 days, and the time-step was 15 sec. The calculated breach width describes the trend in measurements, especially during the first 3 months, the incipient breaching phase.

After the first month, the breach reached the jetty (width of breach of about 100 m); thereafter, breach width growth in the model was determined by erosion only on the south side. The breach enlarges during the 1994 summer season, and the predicted rate of growth increases during the storms in the autumn and winter of 1994-1995. The calculations indicate that the breach would have continued to grow in width and depth had it not been closed mechanically.

An increased longshore transport rate of 600,000 cu m/year did not close the inlet, but did decrease breach depth substantially as compared to the 400,000 cu m/year base case. For the smaller-than-average longshore transport of 200,000 cu m/year, the breach grew more as compared to the base case. However, this growth is marginal compared to the change between the 600,000 cu m/year transport case and the base case. For the smaller longshore transport rate, the calculations were terminated when the depth reached 6.5 m below mhhw, which represents an approximate depth in Half Moon Bay.

Calculated velocity in the breach is plotted in Figure 128. During the incipient breaching phase, the velocity through the opening exceeded 2 m/sec. After the winter season, the velocity decreased in summer and then increased the next winter. At this time, the breach had already been open and become hydrodynamically efficient, so the velocity increased as compared to the preceding year. The mean of the calculated current for the 480-day period was

0.42 m/sec, indicating a strong flood bias, and in qualitative agreement with the 2D hydrodynamic calculations described in Chapter 3.

Figure 129 displays the sediment transport rate at the bottom and sides of the breach, and alongshore. In winter 1995, the rate of longshore sediment transport entering the breach increases substantially, because the more mature deep breach traps more sand as compared to the shallower breach of the previous winter.

The ratio of cross-sectional areas of the calculated breach and Grays Harbor entrance to msl is plotted in Figure 130. The entrance cross-sectional area at Grays Harbor Inlet is 26,000 sq m. The ratio remains small. A breach of this size is not expected to influence bay water-surface elevation, as found in Chapter 3.

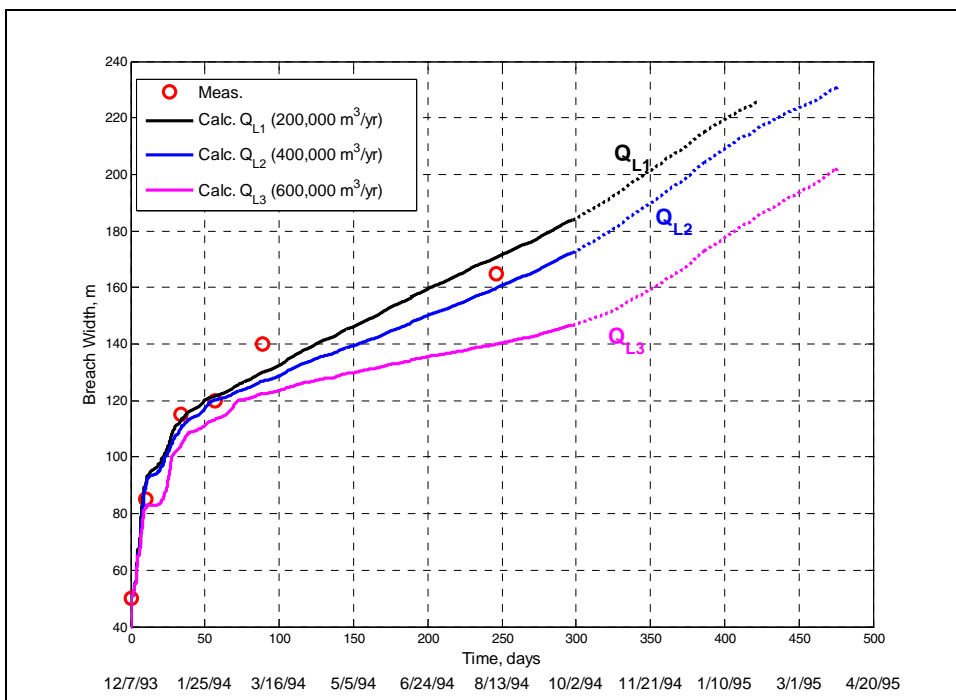


Figure 126. Calculated breach width and observations, 1993-1995, Grays Harbor

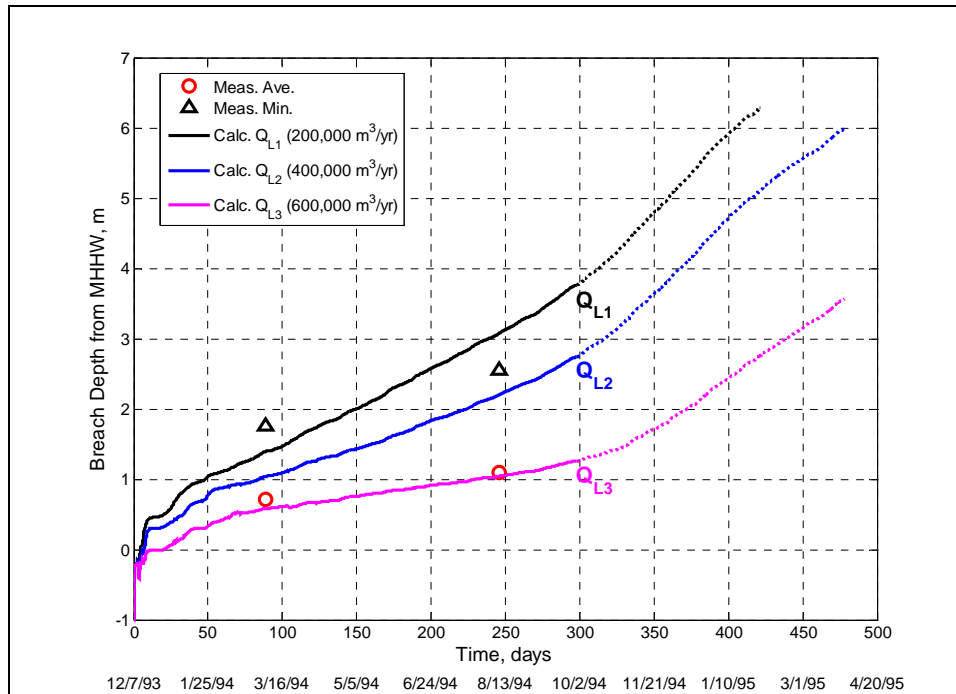


Figure 127. Calculated breach depth and observations , 1993-1995, Grays Harbor

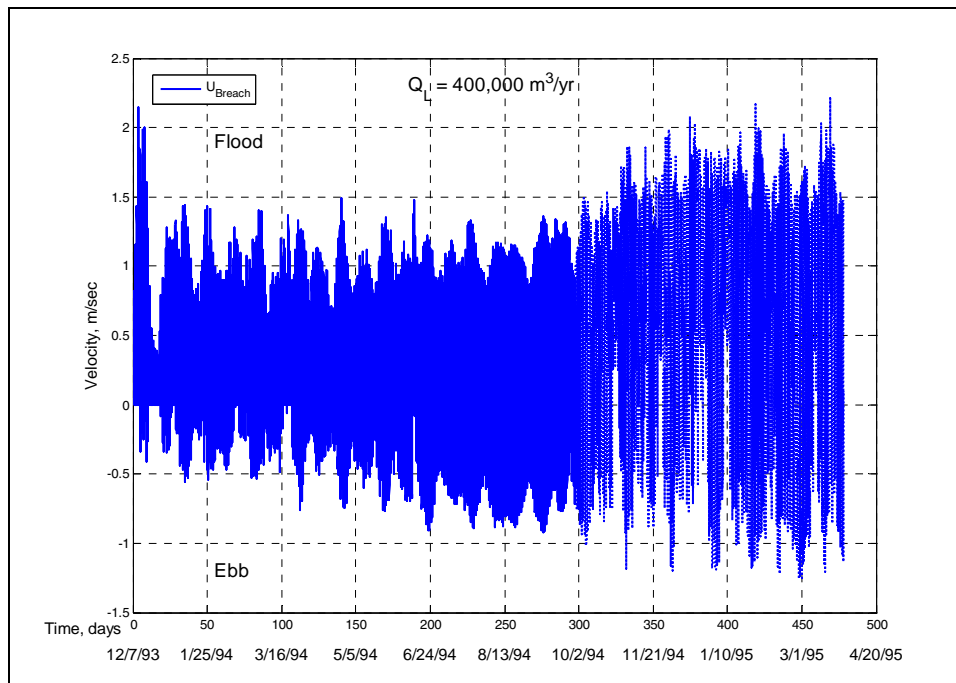


Figure 128. Calculated current velocity in breach, 1993-1995, Grays Harbor

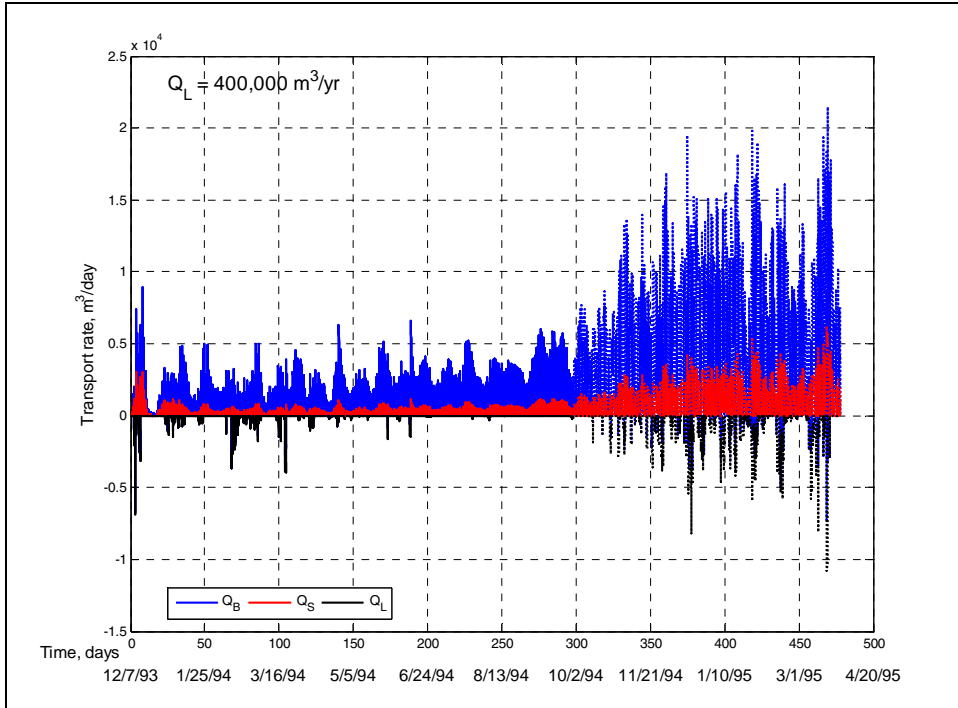


Figure 129. Sediment transport rates at bottom and side of breach, and alongshore, 1993-1995, Grays Harbor

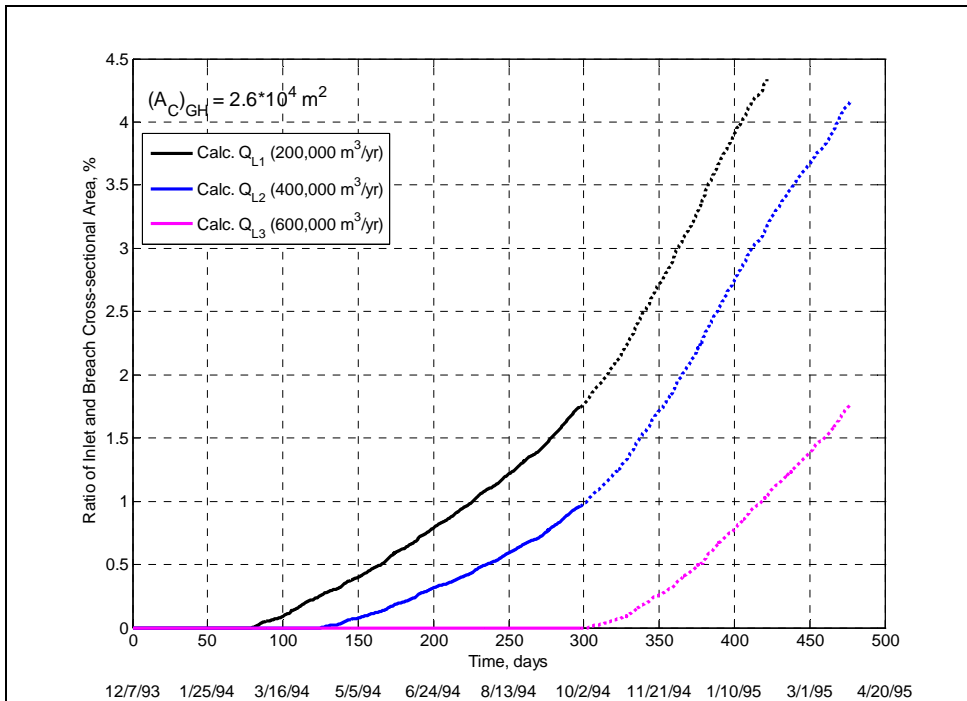


Figure 130. Ratio of calculated cross-sectional breach area 1993-1995 and inlet entrance area, Grays Harbor

Summary of Breach Simulations

A new morphologic model of breach inception and growth was applied to simulate the 1993 breach at the South Beach of Grays Harbor. The purpose of the modeling was to investigate evolution of the breach had it not been closed mechanically in the autumn of 1994. Prior to application at Grays Harbor, the model was tested with success in simulations of the qualitative behavior of laboratory sand dike breaching and the quantitative behavior of the 1980 breach at Moriches Inlet, NY.

The model was calibrated against measurements of breach width and depth at Grays Harbor. The incipient-breaching phase was well reproduced, with reasonable agreement with the measurements during the inlet-development phase. Continued running of the model for approximately 180 days after the mechanical closing of the breach indicated that the breach would have continued to grow in width and depth through the winter of autumn and winter of 1994 and 1995. The current in the breach was calculated in the model to be flood biased, in agreement with comprehensive 2D hydrodynamic simulations described in Chapter 3.

By April 1995, the end of winter storm season, width and depth of the breach were predicted to be approximately 230 m and 4.5 m msl, respectively. A sensitivity test with a greater-than-average annual longshore sediment supply did not close the breach, although depth in the breach was reduced.

5 Concluding Discussion

Preceding chapters in this report document analysis of the December 1993 breach at Grays Harbor, WA. This chapter integrates the results of the GIS analysis, hydrodynamic simulations, and breach morphology modeling to provide information for developing a long-term management plan for the Federal navigation project at Grays Harbor.

Synopsis of Study

After reconstruction of the south jetty in the late 1930s, the areas of South Beach and Half Moon Bay consistently eroded. The persistent shoreline recession on both the ocean and bay sides of Point Chehalis weakened the barrier spit and exposed the dune to wave attack. By May 1993, aerial photographs show that the dune adjacent to the south jetty had become severely degraded. The weakened barrier spit was breached by a storm that, in terms of peak significant wave height, had only a 2-year return period. The breach initially widened rapidly, exposing the landward end of the jetty and eroding portions of the adjacent Westhaven State Park.

By March 1994, the breach was approximately 140 m wide, with a maximum depth of +1.0 m mllw. GIS analysis indicated that from March to August 1994, the breach channel continued to grow laterally and deepen. Sediment eroded from and carried through the breach channel deposited in Half Moon Bay. By August 1994, approximately 210,000 cu m of sediment removed from the breach area had been deposited and remained in Half Moon Bay. Additional material may have been transported out of the historically eroding Half Moon Bay. The beach along the barrier spit (South Beach) also experienced erosion before the breach was filled. Shoreline recession was greatest near the jetty and decreased with distance to the south.

Susceptibility of a barrier island or spit to breaching is determined by its lowest elevation. The breach at the south jetty continued to deepen and widen, even during the summer months when breach healing, if it were to occur, is expected to take place. The data show that the barrier continued to weaken and would have been subject to further breach erosion with the onset of the elevated water levels and high waves of the winter storm season had the breach not been mechanically closed.

Hydrodynamic model simulations were performed to examine the variation in current speed and water level as the condition of the 1993 breach progressed

from December 1993 to August 1994. A hypothetical large breach, representing a probable maximum breach condition, and two variations to the large breach were also modeled. The purpose of the simulations was to determine if a breach would have negative consequences for the Federal navigation project at Grays Harbor, in particular navigation channel shoaling and scour at the south jetty. Consequences of the breach to the navigation channel and south jetty were evaluated by examining changes to current speed, direction, duration, and flow patterns at these locations. Calculated water level did not change significantly for the input hydrodynamic forcing conditions and breach alternatives examined.

As a baseline for comparison, hydrodynamic simulations without a breach were made. These pre-breach or existing-condition simulations show that current in the inlet throat is strong and predominantly tidally driven. The general flow pattern in the vicinity of the south jetty and breach area shows a northward and seaward current on flood and a seaward current on ebb. The pre-breach simulation flow patterns are consistent with the sediment budget pathways developed by Byrnes and Baker (2003), which indicate sediment is bypassed to the north, a conclusion supported by the absence of a fillet near the south jetty. For the present condition, accretion of South Beach near the south jetty is not expected.

A newly developed morphologic model of breach inception and evolution was applied in this study. The purpose of the morphologic modeling was to estimate evolution of the breach had it not been mechanically closed to determine if the breach would have closed, been reduced in size through infilling by longshore sediment transport, or widened in the subsequent winter. The model was first tested by comparison to laboratory data and to measurements of the 1980 breach adjacent to the (updrift) east jetty at Moriches Inlet, NY. With good performance obtained in the tests, the model was applied to simulate the 1993 breach at Grays Harbor.

The morphologic model includes a sediment supply by longshore transport that can close a breach. The morphologic model was validated with measurements from the GIS analysis, reproducing both the rapid growth of the incipient breach phase and then more gradual growth of the breach, including in the summer of 1994. The model predicted that the breach would have continued to grow considerably in the autumn and winter of 1994-1995, and that a larger than average longshore sediment supply would not have halted widening and deepening of the breach.

Hydrodynamic Simulation of Historic Breach

Hydrodynamic simulations of the December 1993, March 1994, and August 1994 breach configurations were conducted for four tide and wave forcing conditions. Initially (17 December 1993), the flood tidal current passed through a confined east-west opening and was directed due east. By March 1994, the peak flood current was located closer to the south jetty and in an east-northeast orientation. In August 1994, the peak flood current covered a greater spatial extent, with water moving alongshore, through the breach area in an east-northeast direction, and then to the north to join the main inlet current. Overall,

the ebb patterns are a reverse of the flood current patterns. These patterns indicate a trend toward the large breach orientation of east-northeast and west-southwest, with flow directed toward the Federal navigation channel.

A comparison of hydrodynamic model simulations for the three historic configurations of the breach indicates the relative current strength in the breach channel. Inferences about the growth or closure of the breach can be made by comparing the relative current strength. Between December 1993 and August 1994, the peak storm current through the breach increased slightly, from 2.0 to 2.2 m/sec. The spatial horizontal extent of strong current increased, and the duration of breach flow increased from 37 to 76 percent of the tidal cycle. The increases in current magnitude, spatial extent, and temporal duration are consistent with breach growth and potential for continued growth. Therefore, with the approaching fall 1994 to winter 1995 storm season, extensive coupled wave and current simulations indicate natural closure of the breach would have been unlikely.

The fact that the breach grew in width and depth from December 1993 to August 1994 indicates that the forcing conditions during that period were sufficiently strong to transport sediment away from the breach throat. Simulated tidal or typical waves produced flood and ebb currents on the order of 1.0 m/sec through the breach. Simulated storm waves nearly doubled the peak current speed, and flow was flood-directed through the breach during most of the tidal cycle.

If the water velocity in the breach were to fall below a critical threshold for sediment transport, then material would deposit in the breach, and it would eventually close at a minimal elevation (e.g., mllw). Flow would return to the pre-breach trend of moving seaward at the jetty and further deposition in the breach would be unlikely. The partially closed high-water breach would be vulnerable to reopening by smaller and smaller storms.

The sediment transported from the breach throat was initially deposited in Half Moon Bay. Half Moon Bay was created by erosion in the 1940s after jetty repairs were made, and it has continued to be a chronically eroding area, particularly during winter storms. From 1996 to February 2002, more than 950,000 cu m of dredged sand was disposed of in inner Half Moon Bay (see Figure 131) and an additional 175,000 cu m was placed directly along the Half Moon Bay shoreline. A sediment budget for the same time period presented by Osborne et al. (2003) indicates that the inner Half Moon Bay cell has had a net positive volume change of only approximately 100,000 cu m, suggesting a natural sediment loss from this area. The area depicted as outer Half Moon Bay in Figure 131 had a net gain of sediment from 1996 to February 2002 of about 1.1 million cu m. This sediment is likely a combination of material eroded from inner Half Moon Bay and the coarser fraction of the more than 3 million cu m of dredged material placed at the Point Chehalis disposal site from 1996 to 2001.

The overall sediment transport pattern is erosion along the shoreline to the northeast and north at Half Moon Bay. Sediment is transported from Half Moon Bay toward the inlet throat. Half Moon Bay, therefore, is an exporter of sediment in its present condition, and the hydrodynamic simulations indicate that there is an increased capacity for transport from Half Moon Bay in a breached condition, as discussed in the following paragraphs.

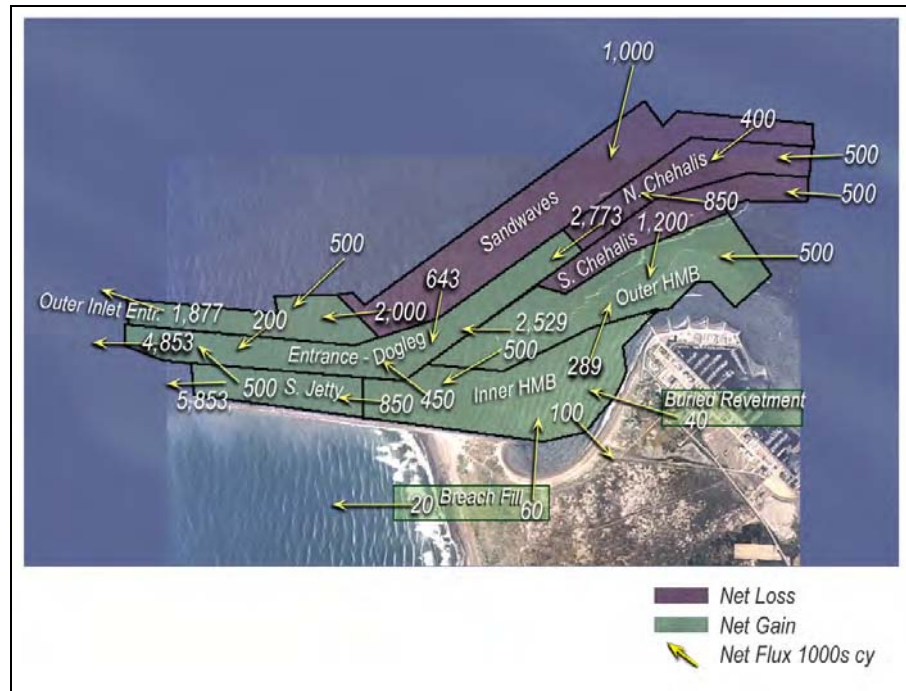


Figure 131. Sediment budget for the Half Moon Bay and south jetty area developed from net morphology change between 1996 and 2002 (from Osborne et al. 2003)

Hydrodynamic Simulation of Conceptual Large Breach

The large breach was conceptualized by the Seattle District to represent bathymetric conditions prior to jetty construction (1898). Based on observations of other breaches near jetties, the segment of land adjacent to the south jetty in the conceptualized large breach would be eroded. Removal of this material was considered an alternative to the Seattle District concept. Another alternative was to reduce the breach depth to 4.55 m mtl to evaluate a less extreme breach. Analysis of the large-breach simulations consisted of an examination of flood and ebb flow through the breach for four tide/wave conditions. Current speeds at 11 points in the breach were extracted from the model simulations for analysis.

Deposition and scour in the navigation channel is related to the strength of the ebb and flood flow through Grays Harbor entrance. Previous studies have shown that this inlet exhibits stronger flood flow on the north side of the entrance and stronger ebb flow on the south side of the entrance (near the navigation channel), indicating that the navigation channel is likely an exporter of sediment (Cialone et al. 2002, 2003). From the hydrodynamic simulations performed in this study, the large breach would change the flow dynamics of the inlet and navigation channel. For the existing condition, the ebb-tidal current on the south side of the inlet is generally strongest along the navigation channel axis. With a large breach, a portion of the ebb flow passes through the breach for tide-only, typical waves, and west-northwest storm simulations. Ebb flow in the navigation channel is thus reduced under those conditions. With west-southwest storm

waves, flow through the breach is continually flooding. The strong flood flow through the breach during ebb tide in the inlet pushes the ebb jet to the north, reducing the ebb current in the navigation channel.

Points E and F (Figure 97), near the south jetty terminus, show an increase in current magnitude with the land mass removed, particularly for west-northwest storm waves. At Point E, the original large breach shows short periods of strong (1.5 m/sec) ebb current. With the land mass adjacent to the south jetty removed, the duration of strong ebb flow at Point E is much greater. All three large-breach simulations with west-northwest storm waves result in 1.0-1.5 m/sec current for some portion of the tidal cycle. Exposure of the jetty terminus to a strong current and associated scour holds potential for destabilization of the structure. According to the equilibrium scour depth potential formulation given by Hughes (2002), a maximum equilibrium scour depth of 13 m could be reached under sustained mean (depth averaged) current of 1.5 m/sec mean sediment grain size of 0.5 mm, and a depth of 29 m for a mean grain size of 0.4 mm. Estimated scour depth increases with decreasing grain size.

Another area that could be potentially vulnerable with the large breach in place is the revetment at Point Chehalis (model Point D is near Groin A of the revetment, Figure 81). The hydrodynamic simulations with the large breach also show an increased potential for erosion in the revetment area. For existing (pre-breach) conditions, current magnitude at Point D for a west-southwest storm wave is on the order of 0.5 m/sec. If a west-southwest storm occurred and the large breach existed, the flood current magnitude at Point D increases to 2.2 m/sec.

The current at the revetment and along the Half Moon Bay shoreline would also transport sediment toward the navigation channel. Current velocity along the Half Moon Bay shoreline increases by 1.0 m/sec or more in the breached condition. The increased velocity increases the transport potential from the Half Moon Bay area toward the navigation channel. These results support the position of the Seattle District in the 1997 Evaluation Report (USAED, Seattle, 1997) that in a breached condition “material carried along the shoreline toward Point Chehalis will ultimately be deposited into the navigation channel.”

On ebb tide, with the breach in place, the current magnitude in the inlet at Point D for a west-southwest storm decreases to 1.0 m/sec, but is still flooding at that location. The direction of flow, however, shifts northward towards the navigation channel. The breach flood jet shifts in a counterclockwise, sweeping motion from the Pt. Chehalis revetment shoreline to a northeast, north, and then to northwest direction as the tide in the inlet changes. During this 4.5-hr time period, the Pt. Chehalis reach of the navigation channel from Point K, to Point H, to Point I (see Figure 97), experienced cross-channel current that would promote deposition of sediment in the navigation channel.

Differences in the current magnitude at hour 35 (representing a typical peak ebb flow) for pre-breach and large breach simulations are also observed at Points J and K. The pre-breach simulation indicates a 0.9-1.0 m/sec ebb current at hour 35 and is typically directed along the channel axis. The large breach simulations show a reduction in current magnitude to 0.6-0.8 m/sec at hour 35. Significantly, the direction of the current has shifted from along the channel axis to across the channel axis. This condition has potential for promoting sediment

deposition in the Federal navigation channel. In addition, the presence of a cross current holds implications for changing the dynamics of six nearshore and open-water disposal sites for placement of dredged material.

Large variations in the current magnitude time series at Point I were investigated, and revealed additional potential concerns for maintenance of the Federal navigation channel and flow dominance. At hour 35, the pre-breach simulation indicates a 0.7-m/sec ebb current at Point I. With the large breach in place, the ebb current is deflected away from Point I, possibly reducing the scour potential for the navigation channel by the ebb jet. The duration of ebb flow is also reduced from 6 hr for pre-breach conditions to 3 hr for the large-breach condition. At hour 39, the pre-breach simulation indicates a lack of strong flood flow, as would be expected for the south side of the inlet. With the large breach, the hour 39 flood current magnitude is 0.8 m/sec at Point I. The flood flow path for a west-southwest storm simulation shifts from predominantly on the north side of the inlet for the existing condition, to the south side of the inlet with the large breach. This significant change would likely alter the potential for scour and deposition in the navigation channel.

Example Regional Implications from Hydrodynamic Calculations

A permanent breach, such as the large breach, holds potential regional implications for the flow distribution and sedimentation pattern at Grays Harbor. Without a breach, the strong longshore current from a west-southwest storm sweeps seaward at the south jetty and across to the north side of the inlet (Figure 97, Run 115), holding potential to bypass sediment to the north. For west-southwest storms and with the large breach in place, the strong longshore current moves through the breach rather than around the south jetty (Figure 97, Run 119). Thus, the flow captured by the breach reduces flow that would otherwise cross to the north side of the inlet. The breach flow also opposes ebb flow near the south jetty and Half Moon Bay. These changes in inlet flow dynamics with the large breach in place will cause the flood current to shift from a northeasterly direction to a more easterly direction near the south jetty, and the ebb current will be reduced. Thus, the horizontal pattern of flood and ebb bias in that location would be altered by the presence of a permanent breach.

The changes in flow dynamics with a large, permanent breach will alter the sediment dynamics and sediment bypassing pathways at Grays Harbor. The strong offshore-directed current at the south jetty for the existing condition and the corresponding sediment bypassing to the north would change with a breach in place. The breach would transport sediment into Half Moon Bay and reduce sediment transport potential to the north, which is the direct and natural mechanism for sediment bypassing.

The increase in flood current and decrease in both the strength and duration of the ebb current on the south side of the inlet are expected to increase sediment deposition and reduce sediment scouring in parts of the navigation channel passing this area. Increased flood flow on the south side of the inlet also may change the morphologic characteristics of Whitcomb Flats. Other possible regional implications could be explored with the existing model technology.

Breach Morphology Modeling

The morphologic model of breaching (Chapter 4) represented contributions from a large number of inlet and coastal processes, including changes in water level, wave setup, tidal hydrodynamics, nonlinear bottom friction, sediment transport through the breach, and infilling of the breach by a longshore sediment transport supply. Also included were realistic descriptions of the barrier island geometry for both its cross section and lateral configuration, and infilling of the Half Moon Bay by sediment was represented by increasing frictional stress in the model that would retard flow and act to close the breach.

The 1-D hydrodynamic model in the morphology model produced a flood-flow bias through the breach, similar to that found in the more advanced combined wave and current modeling described in Chapter 3. Simulations with of breach evolution with the average-annual rate of longshore sediment supply to the north and with reduced and increased supplies all indicated that the breach would have continued to grow in depth and width had it not been mechanically closed in early autumn of 1994. Winter storms of 1994-1995 would have opened the breach significantly. By April 1995, the end of winter storm season, width and depth of the breach were predicted to be approximately 230 m and 4.5 m msl, respectively, for the breach receiving a typical average-annual rate of longshore sand supply.

Summary

The December 1993 breach at the south jetty caused extensive beach erosion along the South Beach and was a threat to many upland facilities and the bay environment through changes in current and wave exposure, as well as through increased sediment deposition. Measurements show that the breach continued to widen and deepen, even during the summer of 1994. Simulations of the hydrodynamics by a combined wave and current model and by a morphologic model of breaching indicate that the breach would have grown during the subsequent winter storms had it not been closed mechanically.

The hydrodynamic simulations show that under a breached condition there is an increased capacity for sediment transport out of Half Moon Bay toward the navigation channel and a decrease in both the strength and duration of the ebb current in the area of the breach, which would reduce sediment scouring in the navigation channel and increased scour potential at the landward terminus of the south jetty. Much of the sediment eroded from the barrier island when the breach opened and which was transported subsequently through the breach was deposited in Half Moon Bay, a historically erosional area. A portion of the sediment removed from Half Moon Bay would enter the navigation channel.

The results presented in this report support the conclusion of the USAED, Seattle (1997), that “based on the severity of the 1993 breach of the south jetty and the jetty-induced shoreline erosion of the Point Chehalis and Half Moon Bay shoreline, the no action alternative of not maintaining the Federal navigation project (including not closing the next breach between the South Jetty and the adjacent shoreline) is not acceptable.”

Considerable modeling technology has been developed in this and related studies performed for the Seattle District to analyze hydrodynamic, sediment transport, and morphology-change processes at Grays Harbor. This technology could be readily applied to examine alternatives for protecting the South Beach and preventing a future breach.

References

- Allen, J. C., and Komar, P. D. (2000a). "Spatial and temporal variations in wave climate of the North Pacific," Report to the Oregon Department of Land Conservation and Development, 46 pp.
- Allen, J. C., and Komar, P. D. (2000b). "Long-term and climate-related increases in storm wave height in the North Pacific," *EOS Transactions* 47, AGU, 561-567.
- Allen, J. C., and Komar, P. D. (2001). "Wave climate change and coastal erosion in the U.S. Pacific Northwest," *Proceedings Waves '01*, American Society of Civil Engineers (ASCE), 680-690.
- Allen, J. C., and Komar, P. D. (2002a). "The wave climate of the eastern North Pacific: Long-term trends and an El Niño/La Niña dependence," *Southwest Washington Coastal Erosion Workshop 2000*, G. Gelfenbaum and G. M. Kaminsky (eds.), Open-File-Report 02-229.
- Allen, J. C., and Komar, P. D. (2002b). "Extreme storms on the Pacific Northwest Coast during the 1997-98 El Niño and 1998-99 La Niña," *Journal of Coastal Research* 18(1), 175-193.
- Arden, H. (2003). "South jetty breach fill at Grays Harbor, Washington: Doing the right thing with dredged material," *Shore & Beach* 71(1), 3-5.
- Bodge, K. R., and Dean, R. G. (1987). "Short-term impoundment of longshore transport," *Proceedings Coastal Sediments '87*, ASCE, 468-483.
- Bowen, A. J., Inman, D. L., and Simmons, V.P. (1968). "Wave 'set-down' and set-up," *Journal of Geophysical Research* 73(8), 2,569-2,577.
- Brogdon, N. J. (1972). "Grays Harbor Estuary Washington; Report 4: South jetty study hydraulic model investigation," Technical Report H-72-2, U.S. Army Engineer Waterways Experiment Station, Vicksburg, MS.
- Bruun, P., and Gerritsen, F. (1960). *Stability of coastal inlets*. North-Holland, Amsterdam.
- Burch, T. L., and Sherwood, C. R. (1992). "Historical bathymetric changes near the entrance to Grays Harbor, Washington," Battelle/Marine Sciences Laboratory, Pacific Northwest Laboratory, Richland, WA.

- Byrnes, M. R., and Baker, J. L. (2003). "Inlet and nearshore morphodynamics," in North Jetty Performance and Entrance Navigation Channel Maintenance, Grays Harbor, Washington, N. C. Kraus and H. T. Arden (eds.), Coastal and Hydraulics Laboratory Technical Report ERDC/CHL TR-03-12, U.S. Army Engineer Research and Development Center, Vicksburg, MS.
- Byrnes, M. R., Baker, J. L., and Kraus, N. C. (2003). "Coastal sediment budget for Grays Harbor, Washington," *Proceedings Coastal Sediments '03*, CD-ROM, East Meets West Productions, Corpus Christi, TX, ISBN-981-238-422-7, 10 pp.
- Carter, R. G., Hesp, P. A., and Nordstrom, K. F. (1990). "Erosional landforms in coastal dunes," in *Coastal dunes: Form and process*, K. F. Nordstrom, N. Psuty, and B. Carter, eds., John Wiley and Sons, Inc., 217-250.
- Cialone, M. A., and Kraus, N. C. (2001). "Engineering study of inlet entrance hydrodynamics: Grays Harbor, Washington, USA," *Proceedings Coastal Dynamics 01*, ASCE, 413-422.
- Cialone, M. A., and Kraus, N. C. (2002). "Wave transformation at Grays Harbor, WA, with strong currents and large tide range," *Proceedings Waves 01*, ASCE, 794-803.
- Cialone, M. A., Militello, A., Brown, M. E., and Kraus, N. C. (2002). "Coupling of wave and circulation models at Grays Harbor Entrance, Washington, USA," *Proceedings 28th Coastal Engineering Conference*, World Scientific, 279-291.
- Cialone, M. A., Davies, M. H., and Osborne, P. D. (2003). "Wave, circulation, and sediment transport modeling," in North Jetty Performance and Entrance Navigation Channel Maintenance, Grays Harbor, Washington, N. C. Kraus and H. T. Arden (eds.), Coastal and Hydraulics Laboratory Technical Report ERDC/CHL TR-03-12, U.S. Army Engineer Research and Development Center, Vicksburg, MS.
- Czerniak, M. T. (1977). "Inlet interaction and stability theory verification," *Proceedings Coastal Sediments '77*, ASCE, 754-773.
- De Looff, H., Steetzel, H. J., and Kraak, A. W. (1996). "Breach growth: Experiments and modeling," *Proceedings 25th Coastal Engineering Conference*, ASCE, 2,746-2,755.
- Dean, R. G. (1977). "Equilibrium beach profiles: U.S. Atlantic and Gulf Coast," Ocean Engineering Technical Report No. 12, Department of Civil Engineering and College of Marine Studies, University of Delaware, Newark, DE.
- Erikson, L. H., Larson, M., Hanson, H., Kraus, N. C., and Nishi, R. (2003). "Prediction of notching and mass failure of dunes," *Proceedings Coastal Sediment '03*, CD-ROM, East Meets West Productions, Corpus Christi, TX, ISBN-981-238-422-7, 14 pp.
- FitzGerald, D. M. (1988). "Shoreline erosional-depositional processes associated with tidal inlets," in *Hydrodynamics and Sediment Dynamics of Tidal Inlets*, D. G. Aubrey and L. Weishar (eds.), Springer-Verlag, 186-225.

- FitzGerald, D. M. (1996). "Geomorphic variability and morphologic and sedimentologic controls on tidal inlets," *Journal of Coastal Research* SI 23, 47-72.
- Gordon, A. D. (1990). "Coastal lagoon entrance dynamics," *Proceedings 22nd Coastal Engineering Conference*, ASCE, 2,880-2,893.
- Hanslow, D. J., and Nielsen, P. (1993). "Shoreline set-up on natural beaches," *Journal of Coastal Research* SI 15, 1-10.
- Hanson, H., and Kraus, N. C. (2001). "Chronic beach erosion adjacent to inlets and remediation by composite (T-head) groins," Coastal Engineering Technical Note CHETN-IV-36, U.S. Army Engineer Research and Development Center, Vicksburg, MS.
- Hayes, M. O. (1975). "Morphology and sand accumulations in estuaries," *Estuarine Research* Vol. 2, L. E. Cronin (ed.), Academic Press, 3-22.
- Hayes, M. O. (1991). "Geomorphology and sedimentation patterns of tidal inlets," *Proceedings Coastal Sediments '91*, ASCE, 1,343-1,355.
- Hericks, D. B., and Simpson, D. P. (2000). "Grays Harbor estuary physical dynamics study: Final data report," PI Engineering for Offshore and Coastal Technology, Inc.
- Holman, R. A., and Sallenger, A. H. (1985). "Setup and swash on a natural beach," *Journal of Geophysical Research* 90(C1), 945-953.
- Hsu, J. R. C., and Evans, C. (1989). "Parabolic bay shapes and applications," *Proceedings of the Institution of Civil Engineers* 87(2), 557-570.
- Hughes, S. A. 2002. "Equilibrium cross sectional area at tidal inlets, *Journal of Coastal Research* 18(1), 160-174.
- Hughes, S. A., and Cohen, J. (2006). "Half Moon Bay, Grays Harbor, WA: Moveable-bed physical model study," U.S. Army Engineer Research and Development Center Technical Report ERDC/CHL TR-06-xx, Vicksburg, MS.
- Kaminsky, G. M., Ruggiero, P., and Gelfenbaum, G. (1998). "Monitoring coastal change in southwest Washington and northwest Oregon during the 1997/98 El Nino," *Shore and Beach* 66(3), 42-51.
- Keulegan, G. H. (1967). "Tidal flow in entrances: Water level fluctuations of basins in communication with the seas," Committee on Tidal Hydraulics Technical Bulletin No.14, U.S. Army Engineer Waterways Experiment Station, Vicksburg, MS.
- Komar, P. D. (1998). *Beach processes and sedimentation*. 2nd edition, Prentice-Hall, NJ, 544 pp.
- Kraus, N. C. (2003). "Analytical model of incipient breaching of coastal barriers," *Coastal Engineering Journal* 45(4), 511-531.

- Kraus, N. C., and Arden, H. T. (eds.). (2003). "North jetty performance and entrance navigation channel maintenance, Grays Harbor, Washington: Volume I, main text," Coastal and Hydraulics Laboratory Technical Report ERDC/CHL TR-03-12, U.S. Army Research and Development Center, Vicksburg, MS, 492 pp.
- Kraus, N. C., and Arden, H. T. (eds.). (2004). "North jetty performance and entrance navigation channel maintenance, Grays Harbor, Washington: Volume II, appendices," Coastal and Hydraulics Laboratory Technical Report ERDC/CHL TR-03-12, U.S. Army Research and Development Center, Vicksburg, MS, 746 pp.
- Kraus, N. C., and Hayashi, K. (2005). "Numerical morphologic model of barrier island breaching," *Proceedings 29th Coastal Engineering Conference*, World Scientific Press, 2,120-2,132.
- Kraus, N. C., Isobe, M., Igarashi, H., Sasaki, T. and Horikawa, K. (1982). "Field experiments on longshore sand transport in the surf zone," *Proceedings 18th Coastal Engineering Conference*, ASCE, 969-988.
- Kraus, N. C., Militello, A., and Todoroff, G. (2002). "Barrier breaching processes and barrier spit breach, Stone Lagoon, California," *Shore & Beach* 70(4), 21-28.
- Kraus, N. C., and Wamsley, T. V. (2003). "Coastal barrier breaching, Part 1: Overview of breaching processes," Coastal and Hydraulics Engineering Technical Note ERDC/CHL CHETN-IV-56, U.S. Army Engineer Research and Development Center, Vicksburg, MS. <http://chl.wes.army.mil/library/publications/chetn/pdf/chetn-iv-56.pdf>.
- Krumbein, W. C. (1944). "Shore processes and beach characteristics," *Beach Erosion Board, Technical Memorandum No. 3*, U.S. Army Corps of Engineers, Washington, DC.
- Leenknecht, D. A., Szuwalski, A., and Sherlock, A. R. (1992). "Automated coastal engineering system," Computer Program, Coastal Engineering Research Center, U.S. Army Engineer Waterways Experiment Station, Vicksburg, MS.
- Luetlich, R. A., Westerink, J. J., and Scheffner, N. W. (1992). "ADCIRC: An advanced three-dimensional circulation model for shelves, coasts, and estuaries; Report 1: Theory and methodology of ADCIRC-2DDI and ADCIRC-3DL," Dredging Research Program Technical Report DRP-92-6, U.S. Army Engineer Waterways Experiment Station, Vicksburg, MS.
- Martin, L. R., and Rosati, J. D. (2003). "Authorities and policies supporting implementation of regional sediment management," ERDC/RSM-TN-8, U.S. Army Engineer Research and Development Center, Vicksburg, MS, <http://www.wes.army.mil/rsm/pubs/pdfs/rsm-tn-8.pdf>.
- Militello, A., Reed, C. W., Zundel, A. K., and Kraus, N. C. (2004). "Two-dimensional depth-averaged circulation model M2D: Version 2.0, Report 1: Technical documentation and user's guide," Coastal and Hydraulics Laboratory Technical Report ERDC/CHL TR-04-2, U.S. Army Engineer Research and Development Center, Vicksburg, MS.

- Militello, A., and Zundel, A. K. (2002). "Coupling of regional and local circulation models ADCIRC and M2D," Coastal and Hydraulics Laboratory Technical Note CHETN-IV-42, U.S. Army Engineer Research and Development Center, Vicksburg, MS.
- Militello, A., and Zundel, A. K. (2003). "SMS steering module for coupling waves and currents, 2. M2D and STWAVE," Coastal and Hydraulics Engineering Technical Note ERDC/CHL CHETN-IV-60, U.S. Army Engineer Research and Development Center, Vicksburg, MS.
- Moreno, L. J., and Kraus, N. C. (1999). "Equilibrium shape of headland-bay beaches for engineering design," *Proceedings Coastal Sediments '99*, ASCE, 860-875.
- Morgan, M., Kraus, N. C., and McDonald, J. (2005). "Geomorphic analysis of Mattituck Inlet and Goldsmith Inlet, Long Island, New York," Coastal and Hydraulics Laboratory Technical Report ERDC/CHL-05-2, U.S. Army Engineer Research and Development Center, Vicksburg, MS.
- Mukai, A. Y., Westerink, J. J., Luettich, R. A., and Mark, D. (2002). "Eastcoast 2001, A tidal constituent database for Western North Atlantic, Gulf of Mexico, and Caribbean Sea," Coastal and Hydraulics Laboratory Technical Report ERDC/CHL TR-02-24, U.S. Army Engineer Research and Development Center, Vicksburg, MS.
- Nishimura, H. (1988). "Computation of nearshore current," in *Nearshore Dynamics and Coastal Processes*, K. Horikawa, (ed.), University of Tokyo Press, Tokyo, Japan, 271-291.
- Oertel, G. F. (1972). "Sediment transport on estuary entrance shoals and the formation of swash platforms," *Journal of Sedimentary Petrology* 42, 858-868.
- Osborne, P. D. (2003). "Oceanographic setting, field data collection, and analysis," in *North Jetty Performance and Entrance Navigation Channel Maintenance, Grays Harbor, Washington, Volume I*, N. C. Kraus and H. T. Arden (eds.), Coastal and Hydraulics Laboratory Technical Report ERDC/CHL TR-03-12, U.S. Army Engineering Research and Development Center, Vicksburg, MS.
- Osborne, P. D., Wamsley, T. V., and Arden, H. T. (2003). "South jetty sediment processes study, Grays Harbor Washington: Evaluation of engineering structures and maintenance measures," Coastal and Hydraulics Laboratory Technical Report ERDC/CHL TR-03-4, U.S. Army Engineering Research and Development Center, Vicksburg, MS.
- PRC Harris, Inc. (1980). "Moriches Inlet closure report on construction methods," Report to Lizza Industries, Inc., Lake Success, NY.
- Ranasinghe, R., Pattiaratchi, C., and Masselink, G. (1999). "A morphodynamic model to simulate the seasonal closure of tidal inlets," *Coastal Engineering* 37, 1-36.
- Ruggiero, P., Kaminsky, G. M., Gelfenbaum, G., and Voigt, B. (2005). "Seasonal to interannual morphodynamics along a high-energy dissipative littoral cell," *Journal of Coastal Research* 21(3), 553-578.

- Ruggiero, P., Komar, P. D., and McDougal, W. G., and Beach, R. A. (1996). "Extreme water levels, wave runup and coastal erosion," *Proceedings 25th Coastal Engineering Conference*, ASCE, 2,793-2,805.
- Ruggiero, P., and Voigt, B. (2000). "Beach monitoring in the Columbia River littoral cell, 1997-2000," Department of Ecology Publication No. 00-06-26, Washington Department of Ecology, Olympia WA.
- Seabergh, W. C. (1999). "Inner-bank erosion at jetty-shoreline intersection," *Proceedings Coastal Sediments '99*, ASCE, 2,235-2,248.
- Schmeltz, E. J., Sorensen, R. M., McCarthy, M. J., and Nersesian, G. (1982). "Breach/inlet interaction at Moriches Inlet," *Proceedings 18th Coastal Engineering Conference*, ASCE, 1,062-1,077.
- Silvester, R. (1960). "Stabilization of sedimentary coastlines," *Nature* 188, 467-469.
- Silvester, R. (1970). "Growth of crenulate shaped bays to equilibrium," *Journal of the Waterways and Harbors Division* 96(2), 275-287.
- Smith, G. L., and Zarillo, G. A. (1988). "Short-term interactions between hydraulics and morphodynamics of a small tidal inlet, Long Island, New York," *Journal of Coastal Research* 4, 301-314.
- Smith, J. M., Resio, D. T., and Zundel, A. K. (1999). "STWAVE: STEady-state spectral WAVE model, Report 1: User's manual for STWAVE Version 2.0," Coastal and Hydraulics Laboratory Instructional Report CHL-99-1, U.S. Army Engineer Waterways Experiment Station, Vicksburg, MS.
- Smith, J. M., Sherlock, A. R., and Resio, D. T. (2001). "STWAVE: STEady-state spectral WAVE model: User's manual for STWAVE Version 3.0," Coastal and Hydraulics Laboratory Supplemental Report ERDC/CHL SR-01-1, U.S. Army Engineer Research and Development Center, Vicksburg, MS.
- Smith, E. R., Wang, P., and Zhang, J. (2003). "Evaluation of the CERC Formula using large-scale model data," *Proceedings Coastal Sediments '03*, CD-ROM Published by World Scientific Press and East Meets West Productions, Corpus Christi, TX ISBN-981-238-422-7, 13 pp.
- Sorensen, R. M., and Schmeltz, E. J. (1982). "Closure of the breach at Moriches Inlet," *Shore & Beach* 50(4), 22-40.
- Spargo, E. A., Westerink, J. J., Luettich, R. A., and Mark, D. J. (2004). "ENPAC 2003: A tidal constituent database for the Eastern North Pacific Ocean," Coastal and Hydraulics Laboratory Technical Report ERDC/CHL TR-04-12, U.S. Army Engineer Research and Development Center, Vicksburg, MS.
- Stockdon, H. F., Holman, R. A., Howd, P. A., and Sallenger, A. H. (2006). "Empirical parameterization of setup, swash, and runup," *Coastal Engineering* 53(7), 573-588.
- Sultan, N. J., and Osborne, P. D. (2004). "South Beach shoreline change analysis," report prepared for the Southwest Washington Coastal Communities, PI Engineering, Edmonds, WA.

- Tillotson, K. J., and Komar, P. D. (1997). "The wave climate of the Pacific Northwest (Oregon and Washington): A comparison of data sources," *Journal of Coastal Research* 13, 440-452.
- U.S. Army Corps of Engineers. (2000). "Planning guidance notebook," Engineer Regulation 1105-2-100, Headquarters, U.S. Army Corps of Engineers, Washington, DC.
- U.S. Army Engineer Committee on Tidal Hydraulics. (1967). "Grays Harbor, Washington," report submitted to U.S. Army Engineer District, Seattle, U.S. Army Engineer Waterways Experiment Station, Vicksburg, MS.
- U.S. Army Engineer District, Seattle. (1997). "Long-term maintenance of the South Jetty at Grays Harbor, Washington," Evaluation Report, U.S. Army Engineer District, Seattle, Seattle, WA.
- Wamsley, T. V. and Hathaway, K. K. (2004). "Monitoring morphology and currents at the Hatteras breach," *Shore and Beach* 72(2), 9-14.
- Watanabe, A., Shimuzu, T., and Kondo, K. (1991). "Field application of a numerical model of beach topography response," *Proceedings Coastal Sediments '91*, ASCE Press, 1,814-1,928.
- Yasso, W. E. (1965). "Plan geometry of headland-bay beaches," *Journal of Geology* 73, 702-714.
- Zundel, A. K. (2000). "Surface-water modeling system reference manual," Brigham Young University, Environmental Modeling Research Laboratory, Provo, UT.

Appendix A Supplemental Photographic Documentation

This appendix includes photographs of the breach and Half Moon Bay. The photographs provide supplementary documentation to Chapter 2.



Figure A1. Breach, January 1994



Figure A2. Breach, 2 February 1994, tide elevation +2.0 ft mllw



Figure A3. Breach, 6 March 1994, tide elevation +1.3 ft mllw



Figure A4. Breach, 10 August 1994, tide elevation +2.3 ft mllw

Appendix B

Figures of M2D-STWAVE Model Simulation Results

This appendix contains figures of documented model results from the large-breach alternative simulations of M2D-STWAVE discussed in Chapter 3. Time-series of current speeds at 11 selected points in the breach, near the south jetty, and near the navigation channel were extracted from the model simulations for analysis and comparison (Figure B1). (To compare currents from the large-breach alternative simulations, time series of the three alternatives were plotted together at each of the 11 selected points.) Graphs were generated for the tide-only, west-southwest storm wave, and west-northwest storm wave simulations, resulting in 33 time series (Figures B2-B34). Figures B35-B58 show snapshots of horizontal circulation patterns.

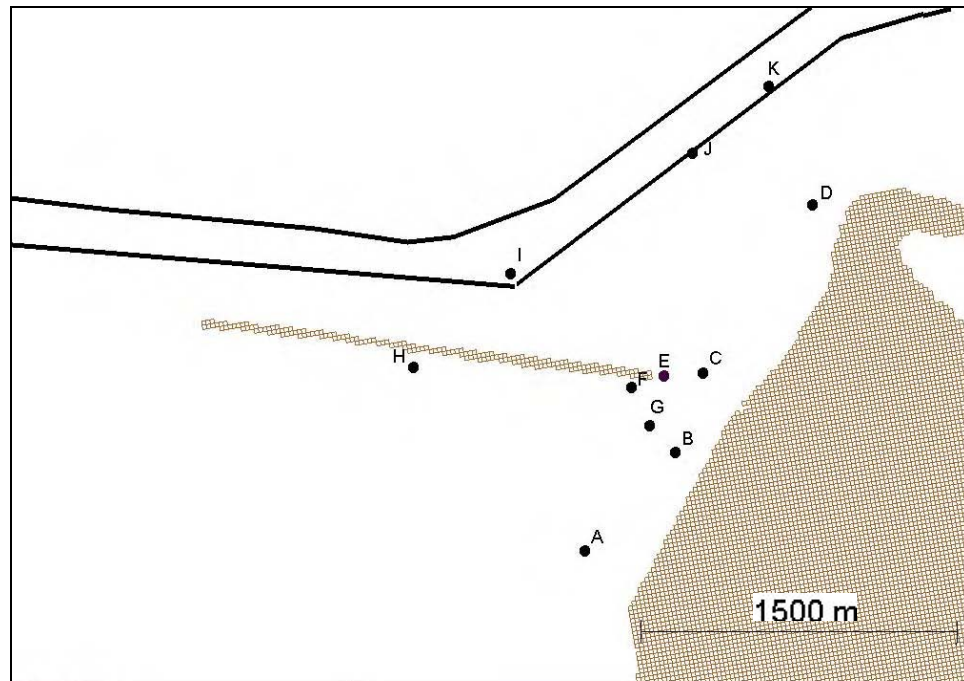


Figure B1. Observation points for large-breach alternatives

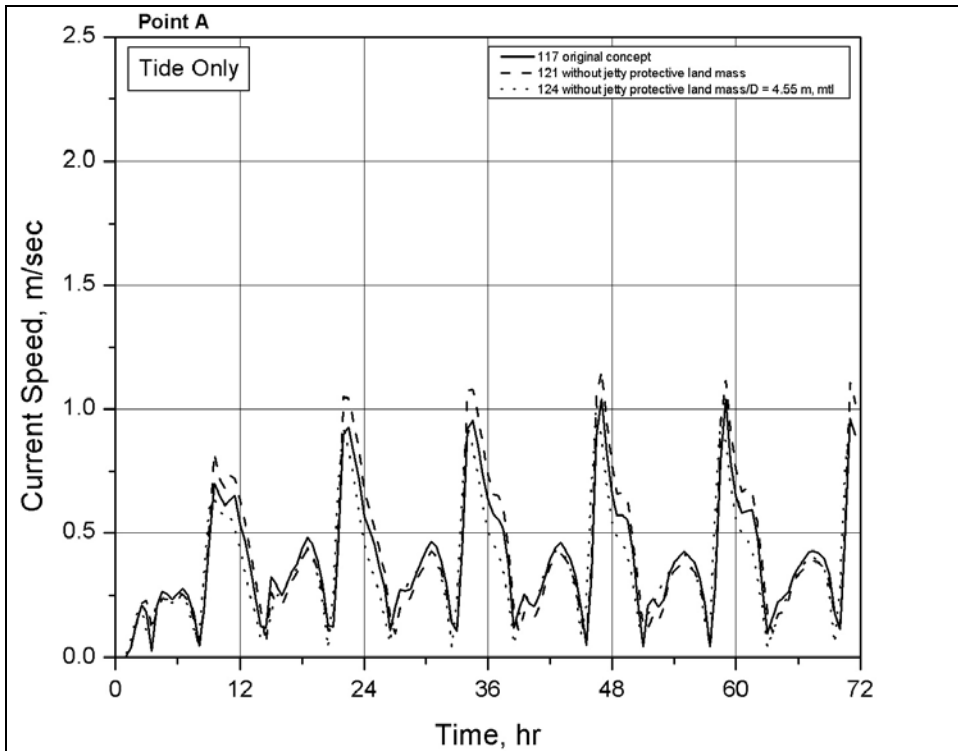


Figure B2. Time series of current speed at Point A for large-breach alternatives, tide only

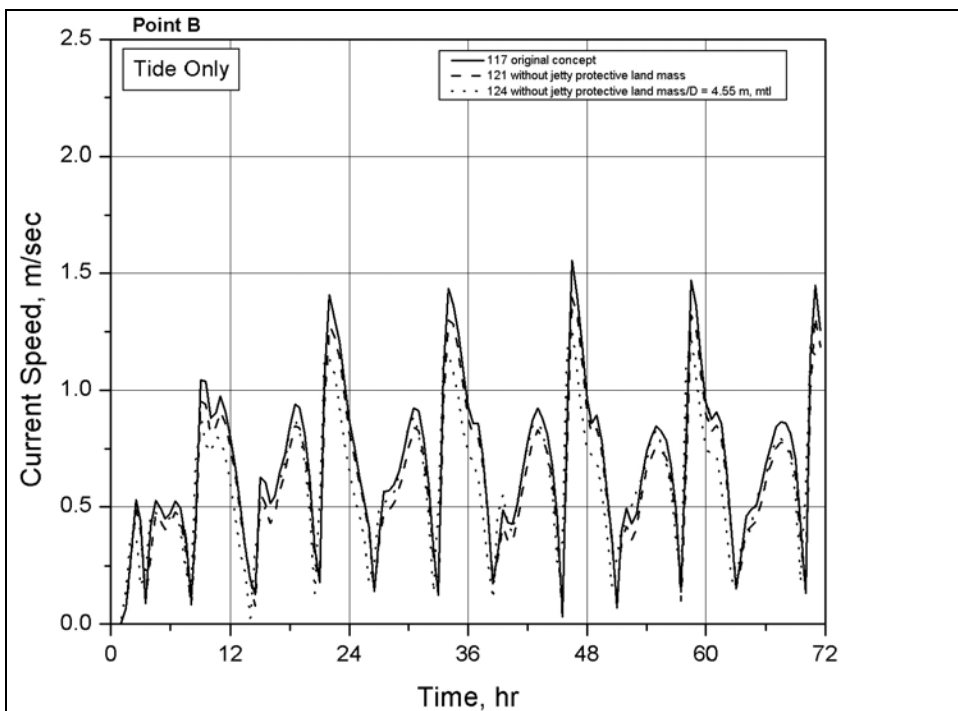


Figure B3. Time series of current speed at Point B for large breach alternatives, tide only

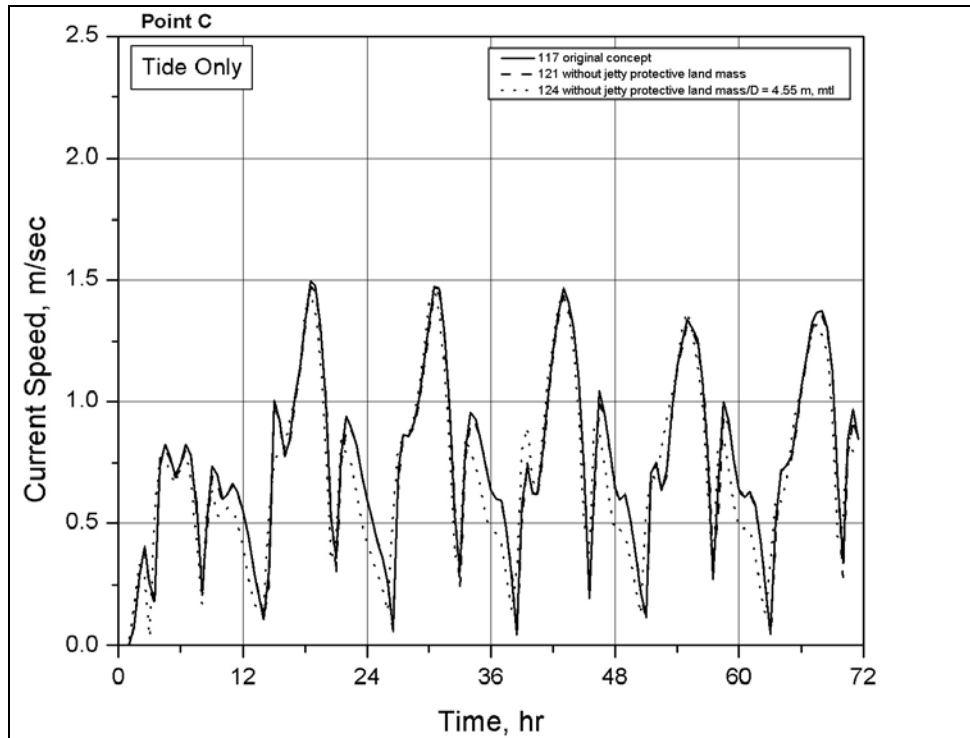


Figure B4. Time series of current speed at Point C for large-breach alternatives, tide only

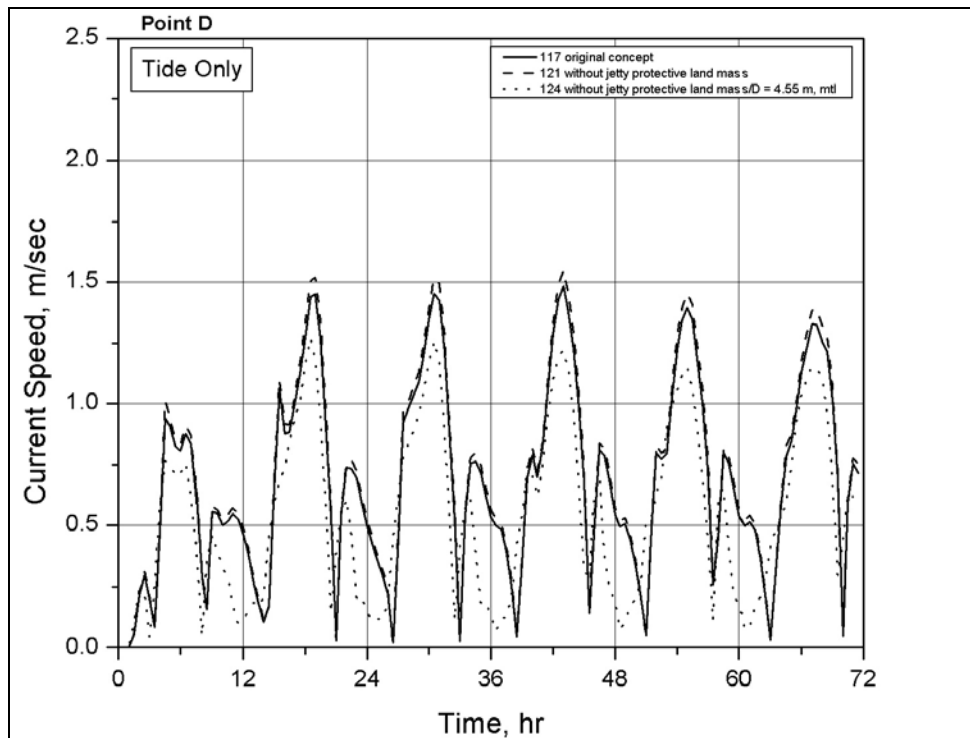


Figure B5. Time series of current speed at Point D for large-breach alternatives, tide only

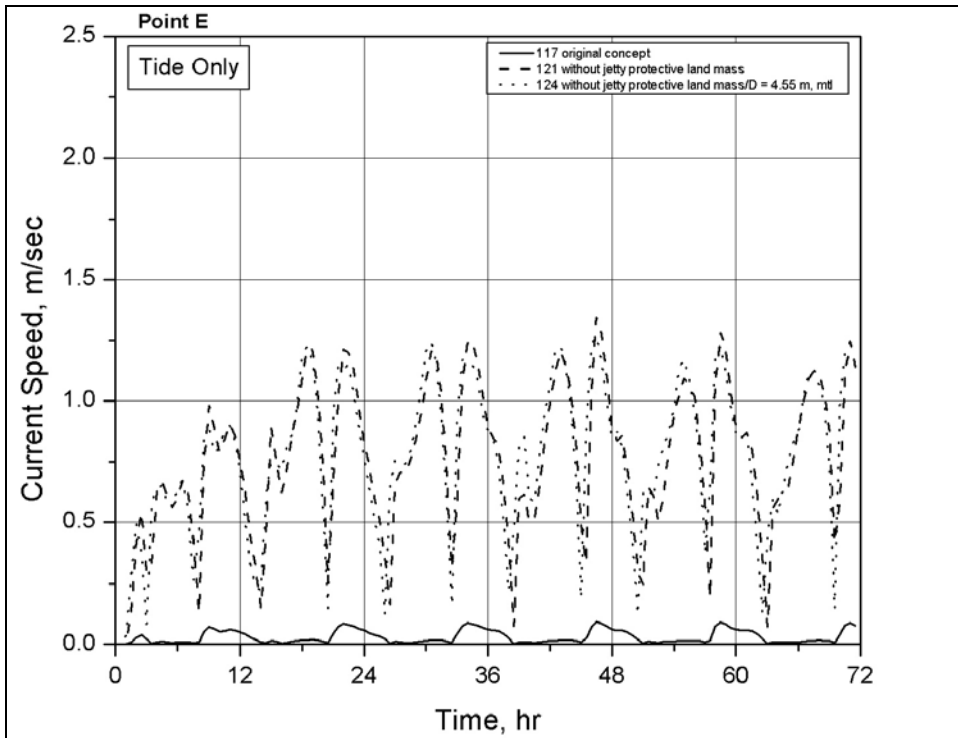


Figure B6. Time series of current speed at Point E for large-breach alternatives, tide only

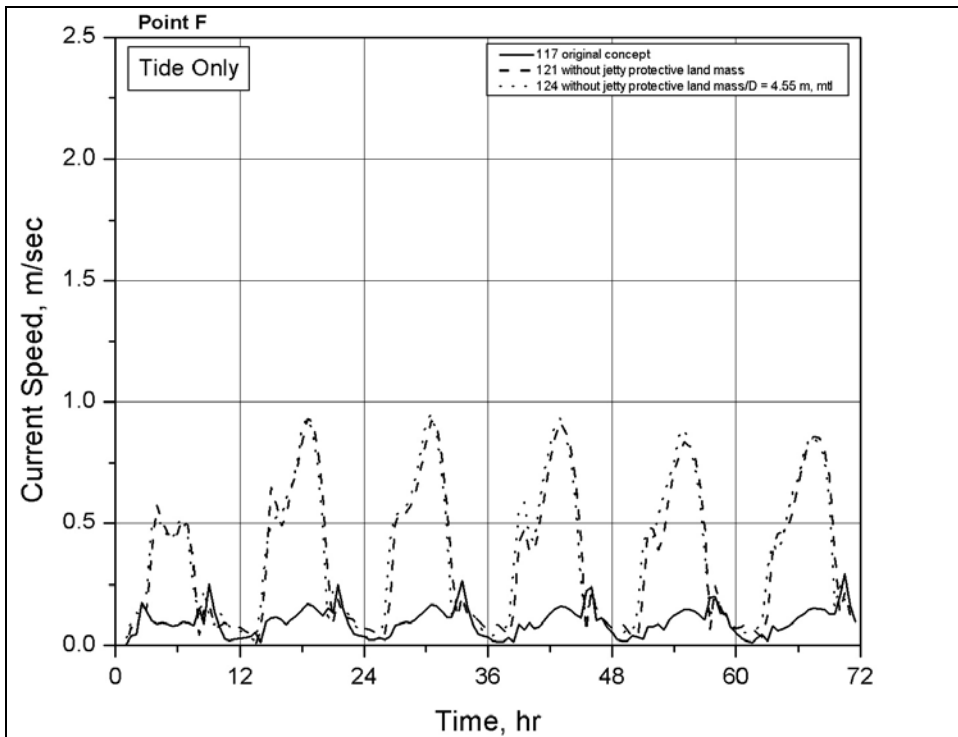


Figure B7. Time series of current speed at Point A for large-breach alternatives, tide only

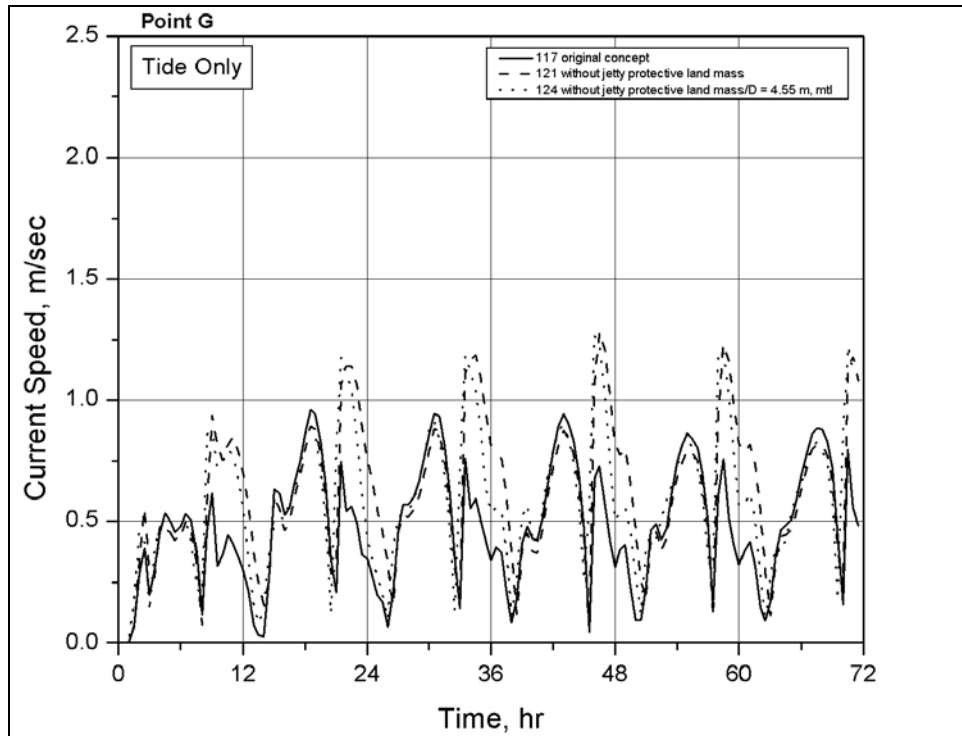


Figure B8. Time series of current speed at Point G for large-breach alternatives, tide only

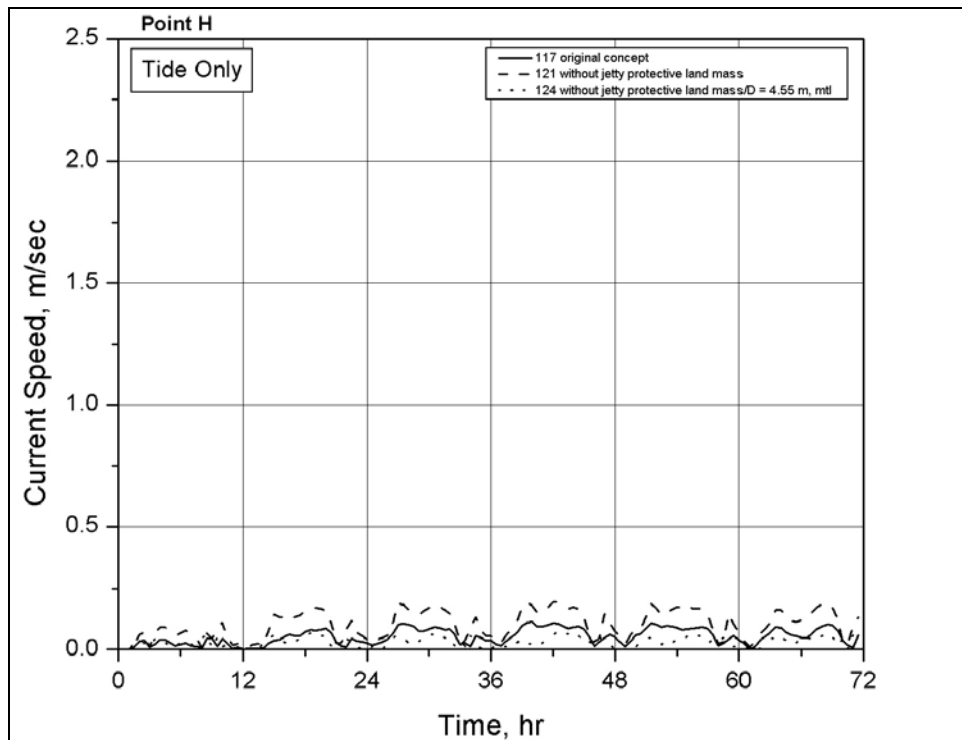


Figure B9. Time series of current speed at Point H for large-breach alternatives, tide only

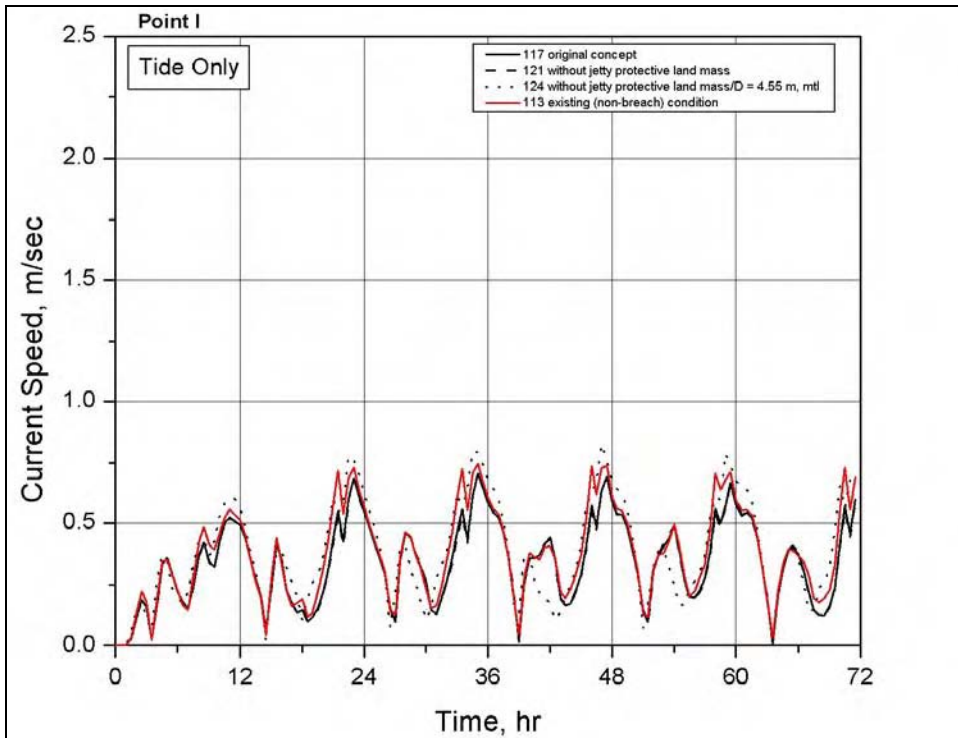


Figure B10. Time series of current speed at Point I for large-breach alternatives, tide only

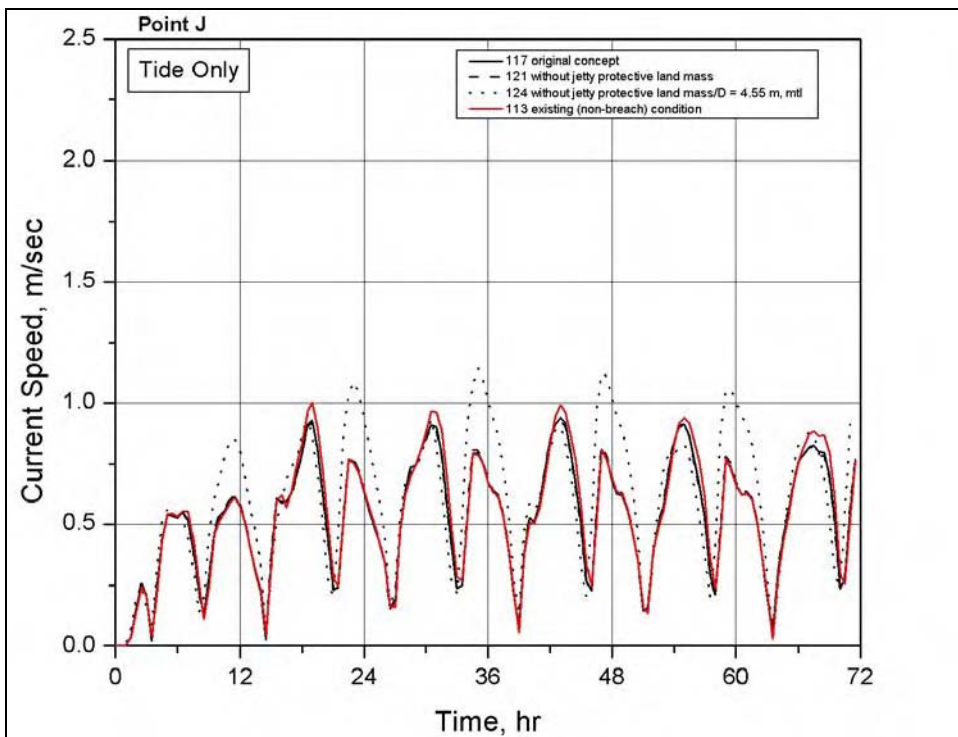


Figure B11. Time series of current speed at Point J for large-breach alternatives, tide only

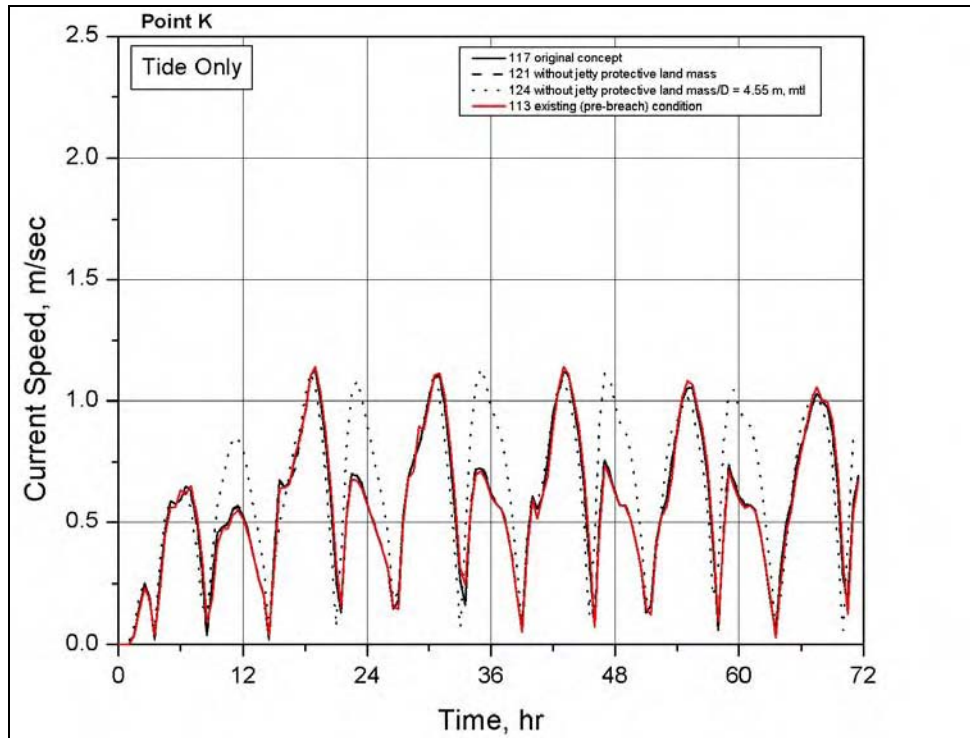


Figure B12. Time series of current speed at Point K for large-breach alternatives, tide only

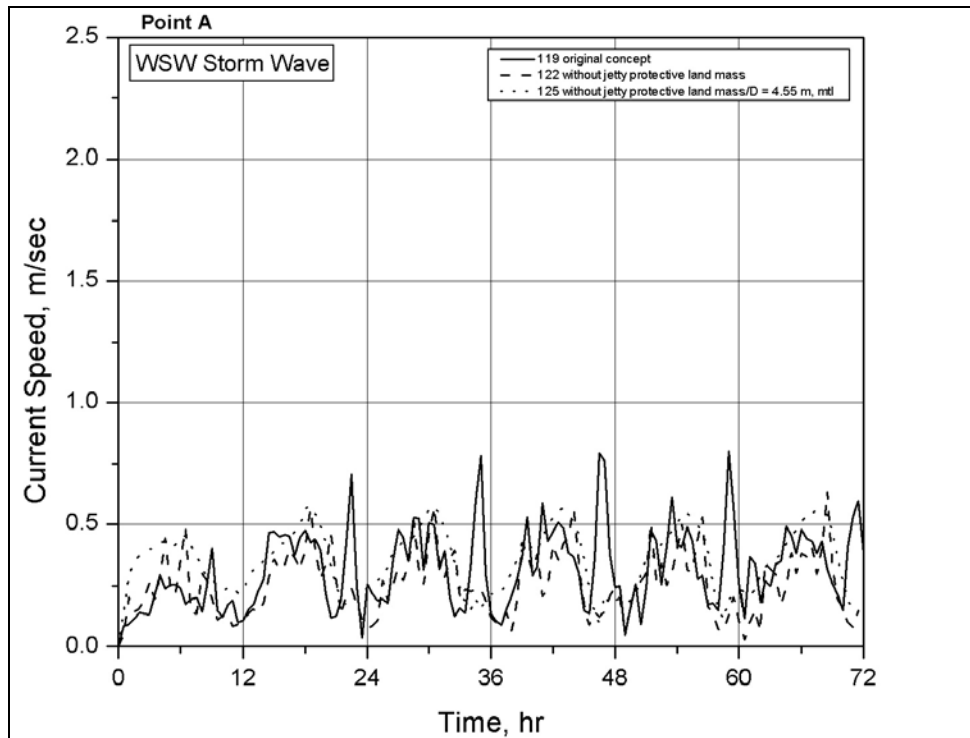


Figure B13. Time series of current speed at Point A for large-breach alternatives, west-southwest storm simulations

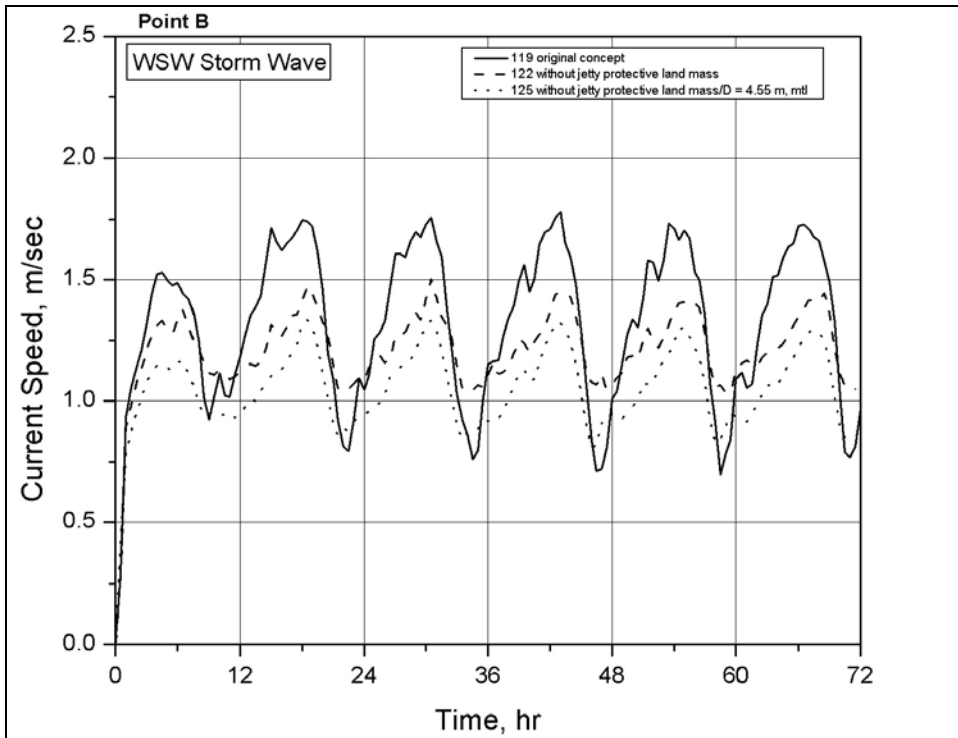


Figure B14. Time series of current speed at Point B for large-breach alternatives, west-southwest storm simulations

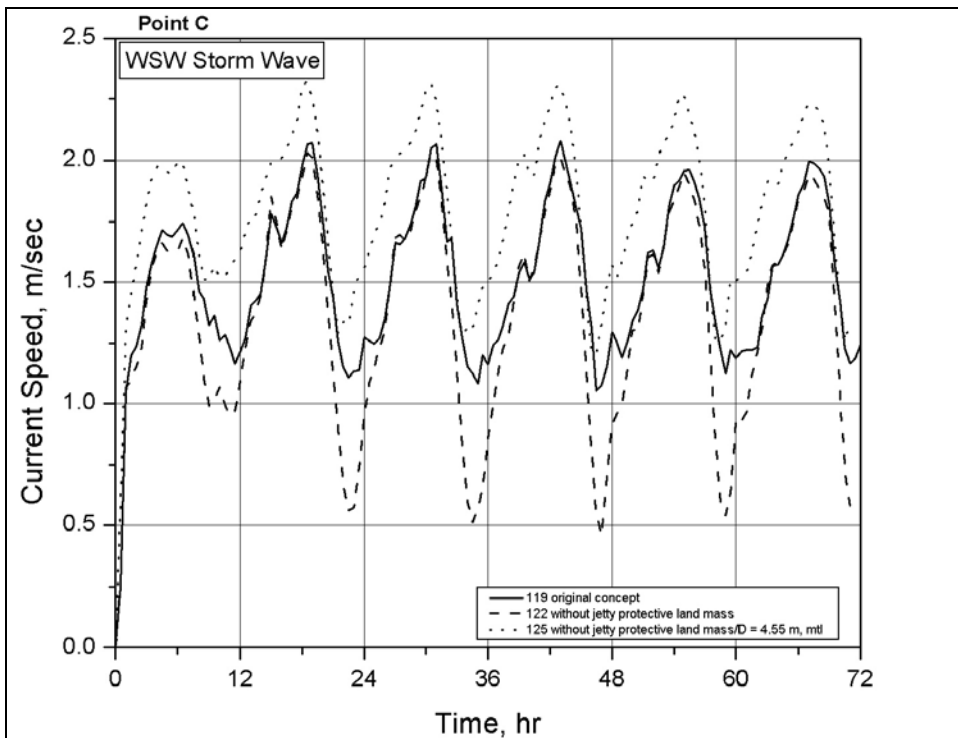


Figure B15. Time series of current speed at Point C for large-breach alternatives, west-southwest storm simulations

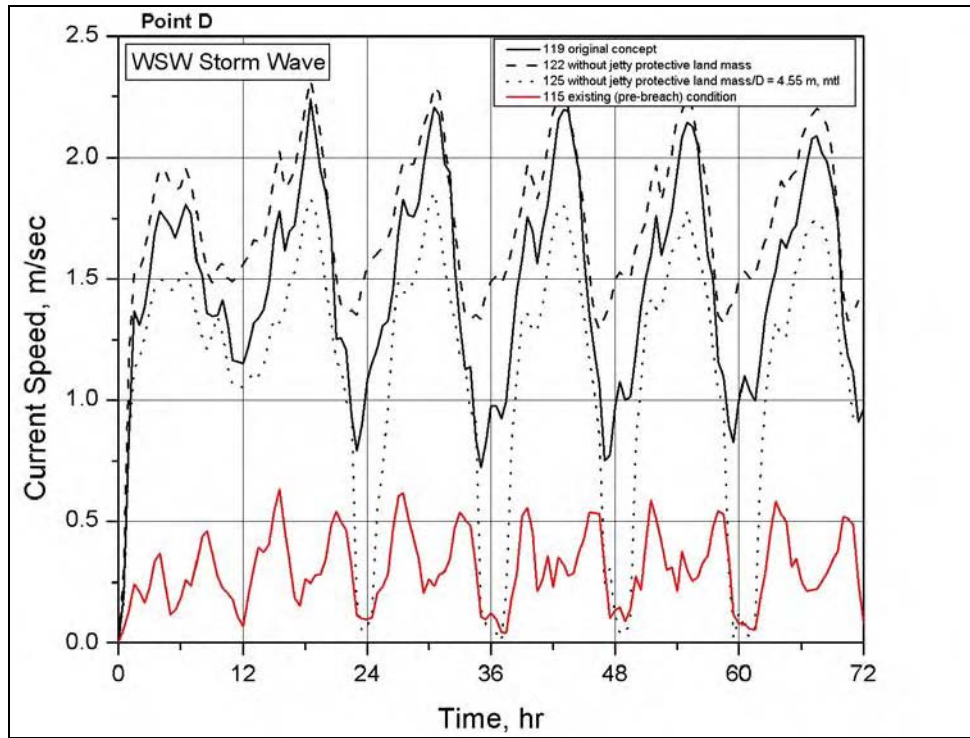


Figure B16. Time series of current speed at Point D for large-breach alternatives, west-southwest storm simulations

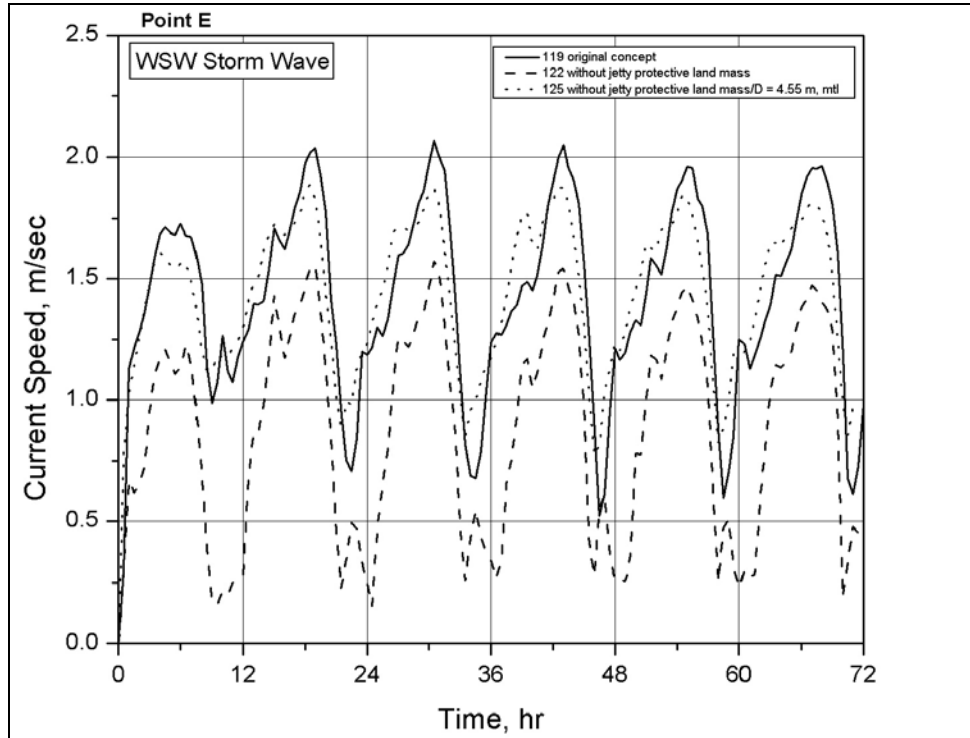


Figure B17. Time series of current speed at Point E for large-breach alternatives, west-southwest storm simulations

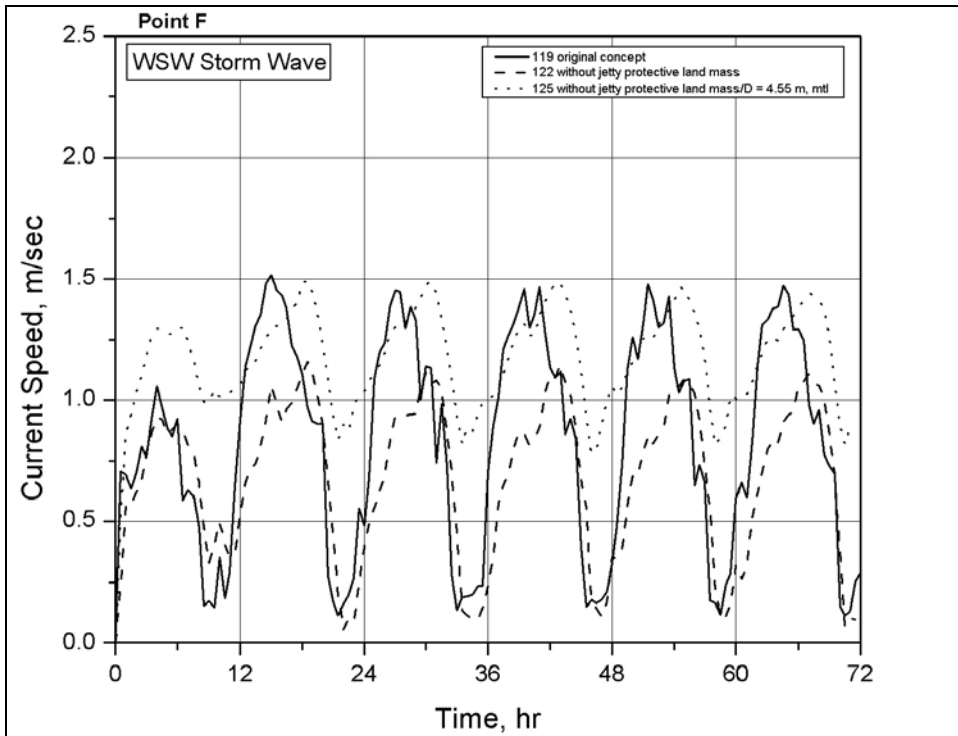


Figure B18. Time series of current speed at Point F for large-breach alternatives, west-southwest storm simulations

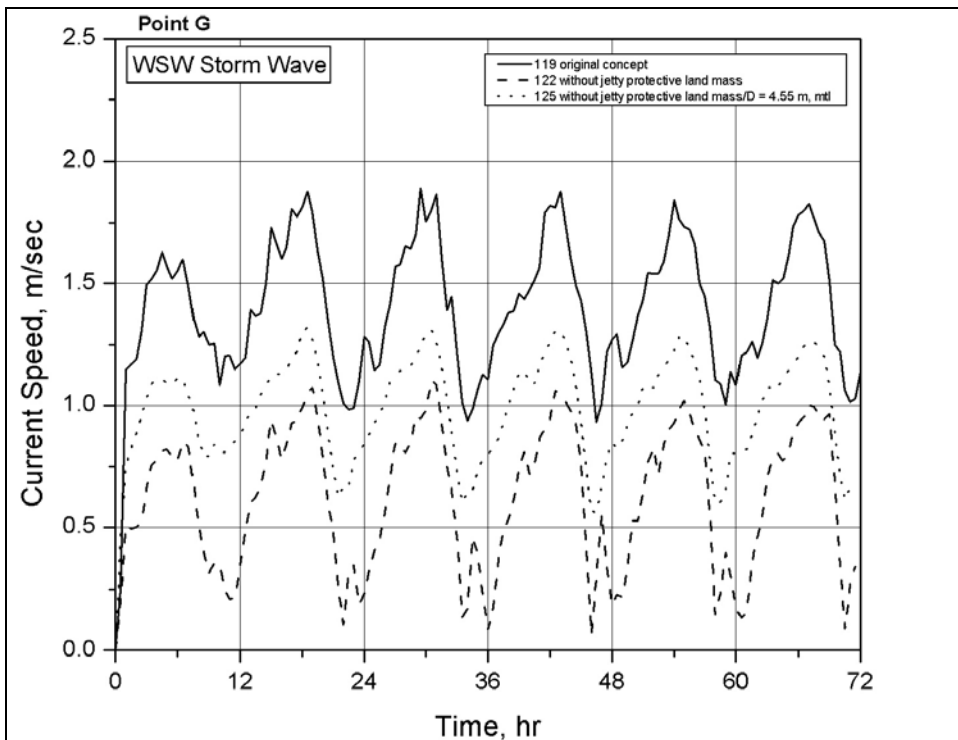


Figure B19. Time series of current speed at Point G for large-breach alternatives, west-southwest storm simulations

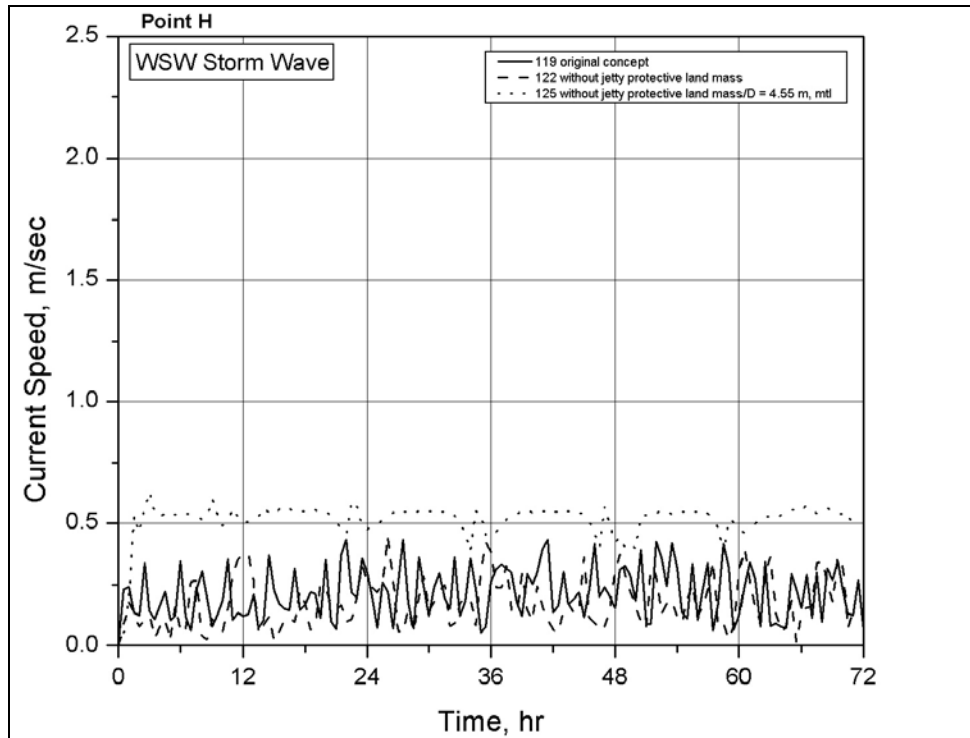


Figure B20. Time series of current speed at Point H for large-breach alternatives, west-southwest storm simulations

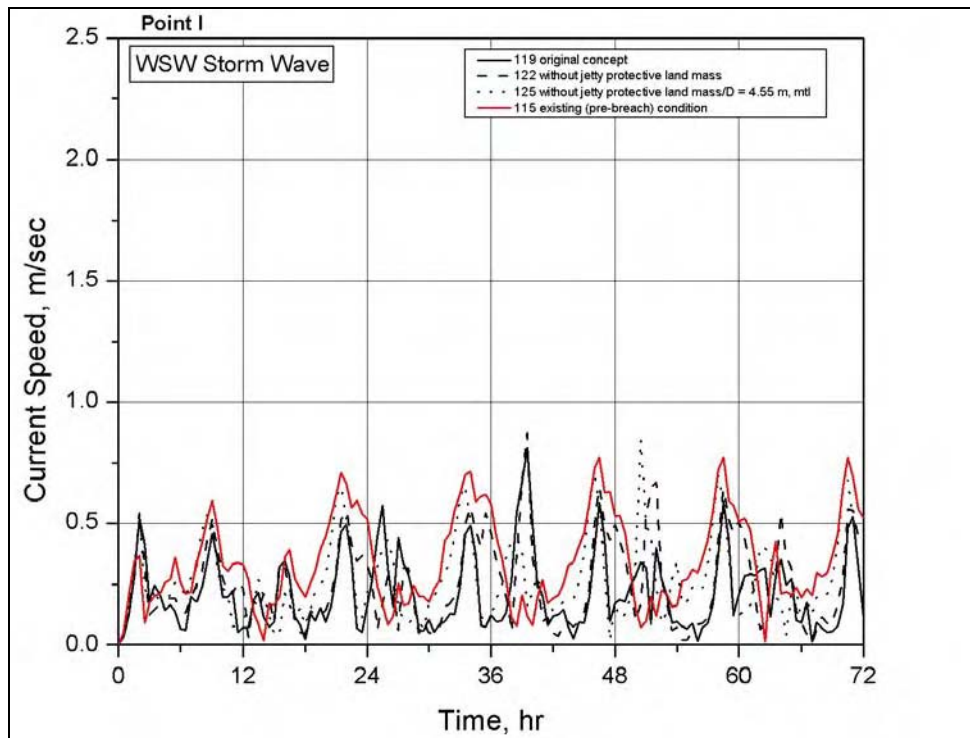


Figure B21. Time series of current speed at Point I for large-breach alternatives, west-southwest storm simulations

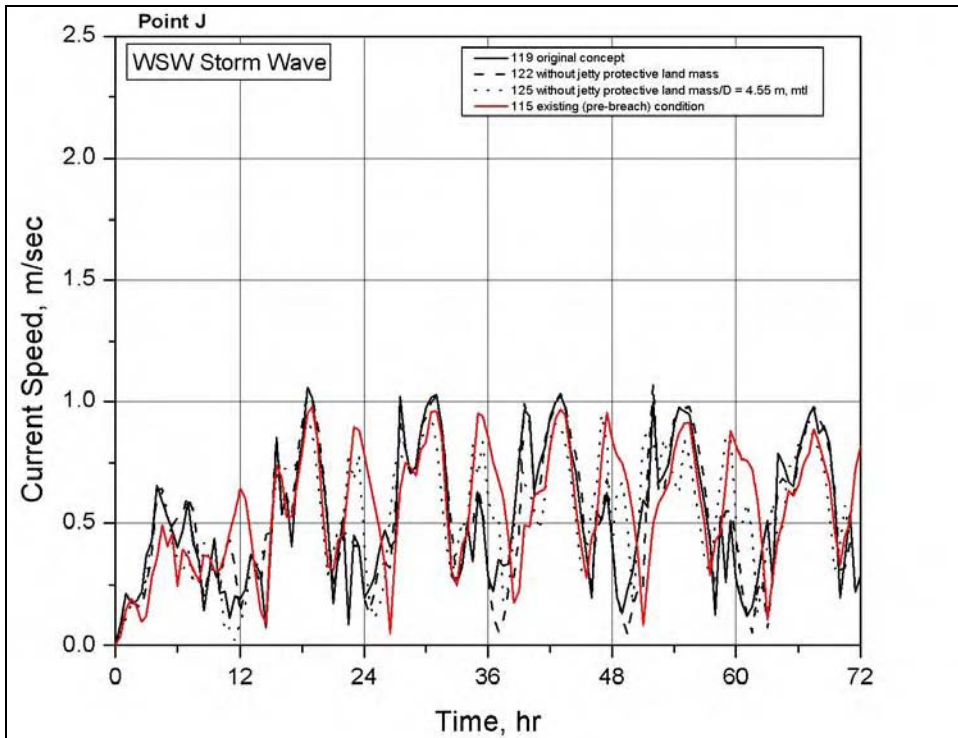


Figure B22. Time series of current speed at Point J for large-breach alternatives, west-southwest storm simulations

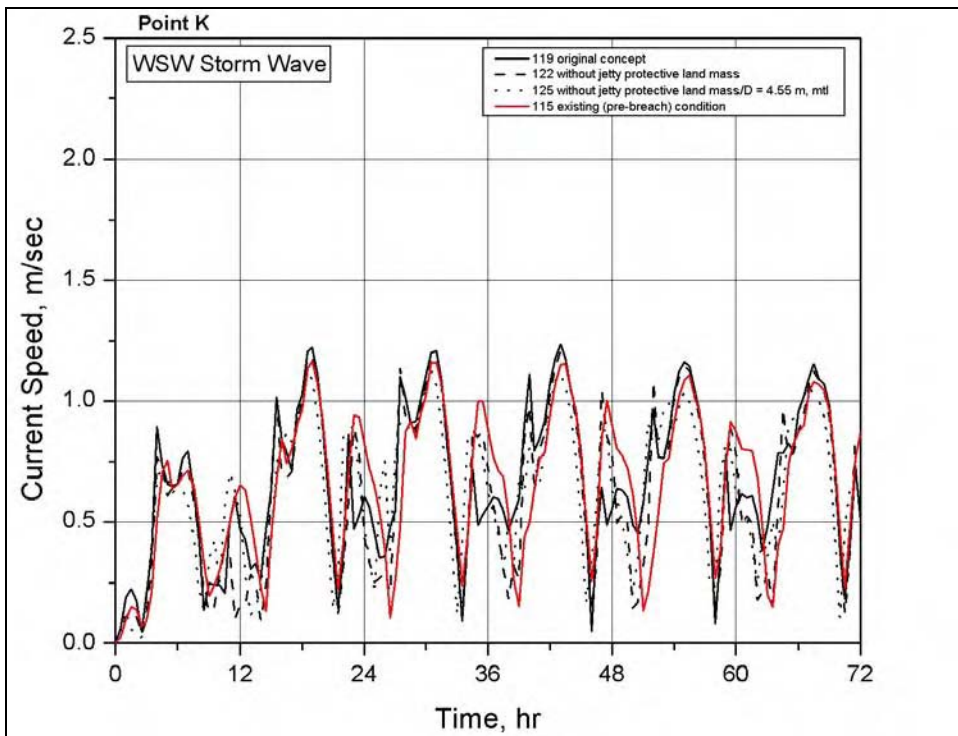


Figure B23. Time series of current speed at Point K for large-breach alternatives, west-southwest storm simulations

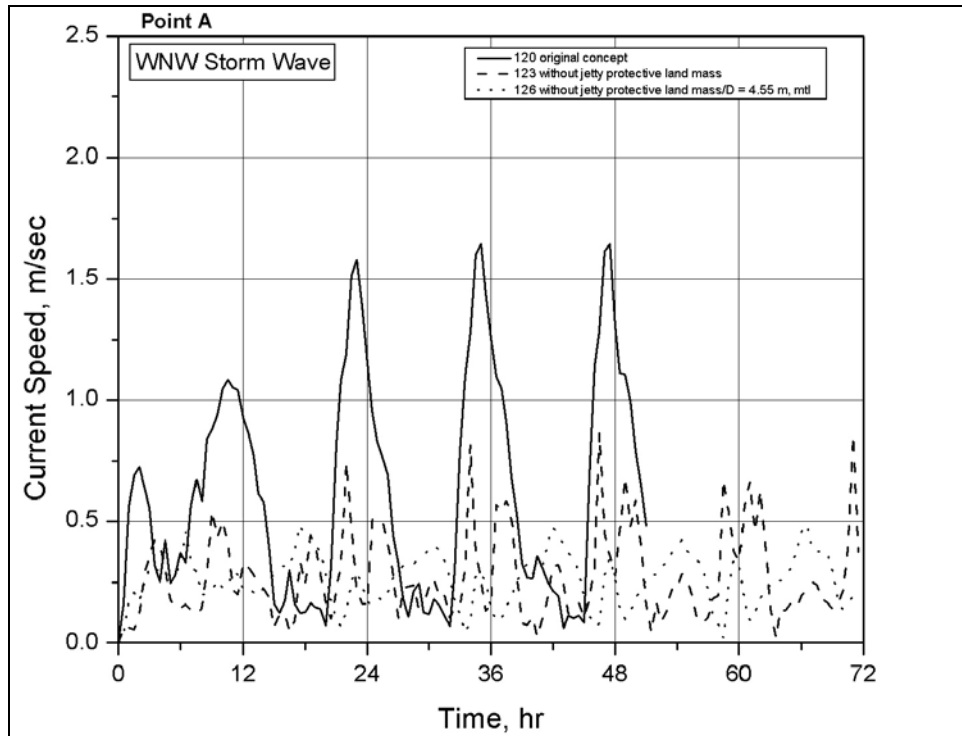


Figure B24. Time series of current speed at Point A for large-breach alternatives, west-northwest storm simulations

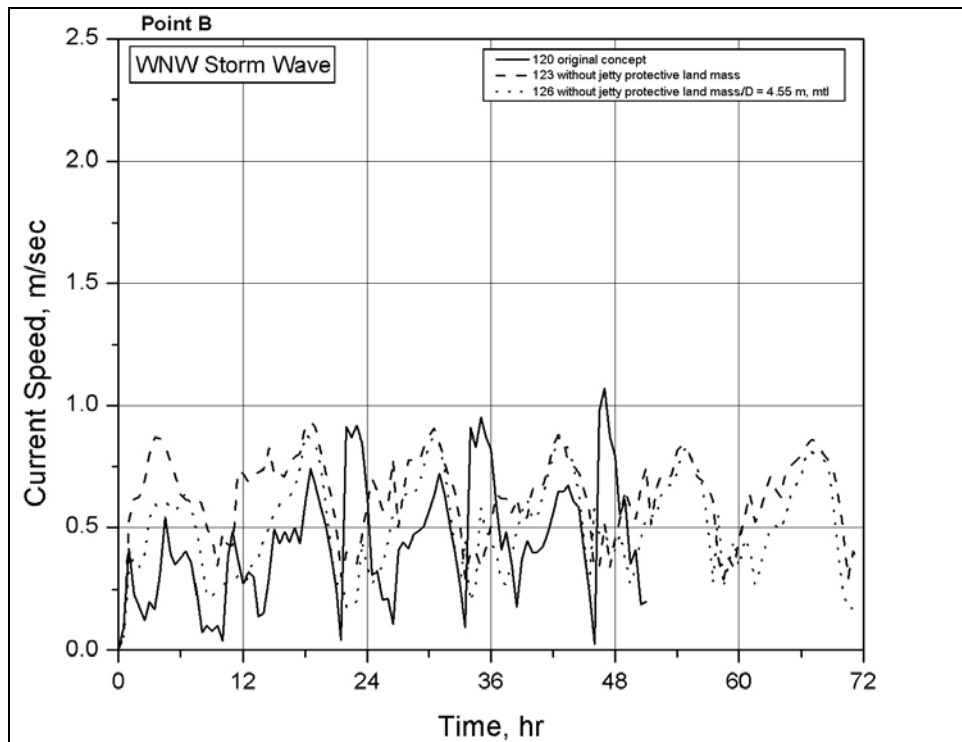


Figure B25. Time series of current speed at Point B for large-breach alternatives, west-northwest storm simulations

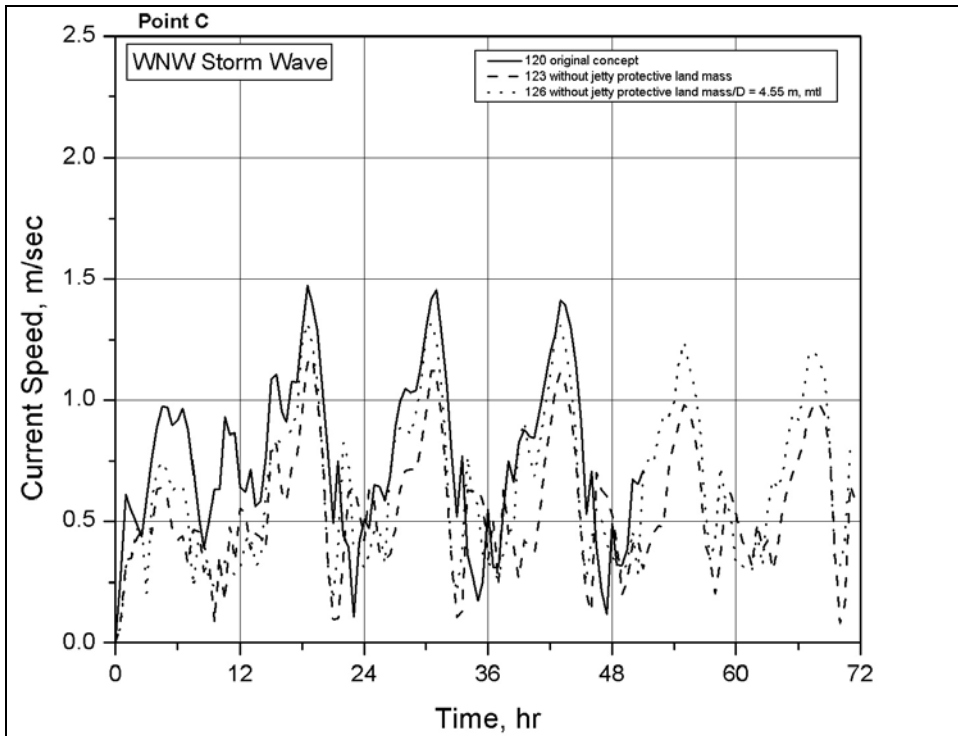


Figure B26. Time series of current speed at Point C for large-breach alternatives, west-northwest storm simulations

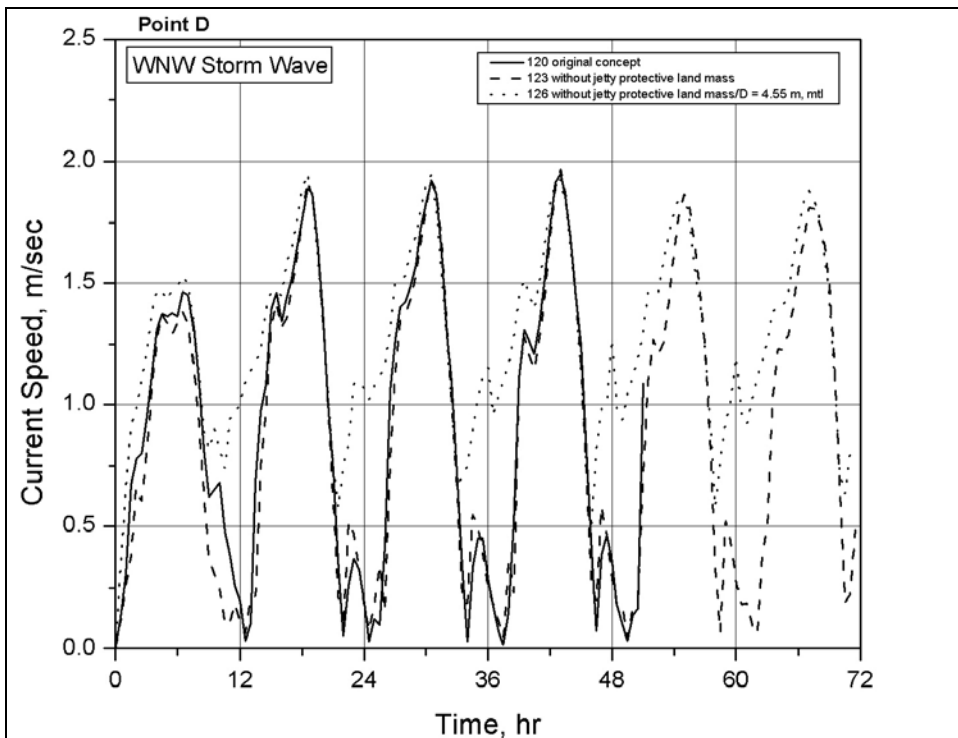


Figure B27. Time series of current speed at Point D for large-breach alternatives, west-northwest storm simulations

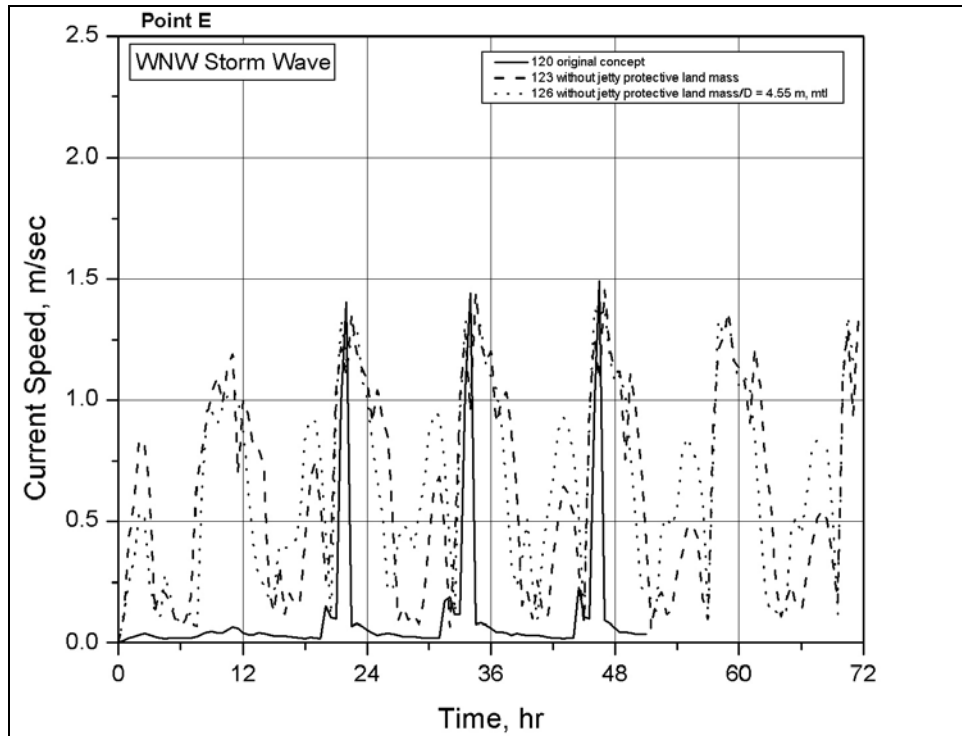


Figure B28. Time series of current speed at Point E for large-breach alternatives, west-northwest storm simulations

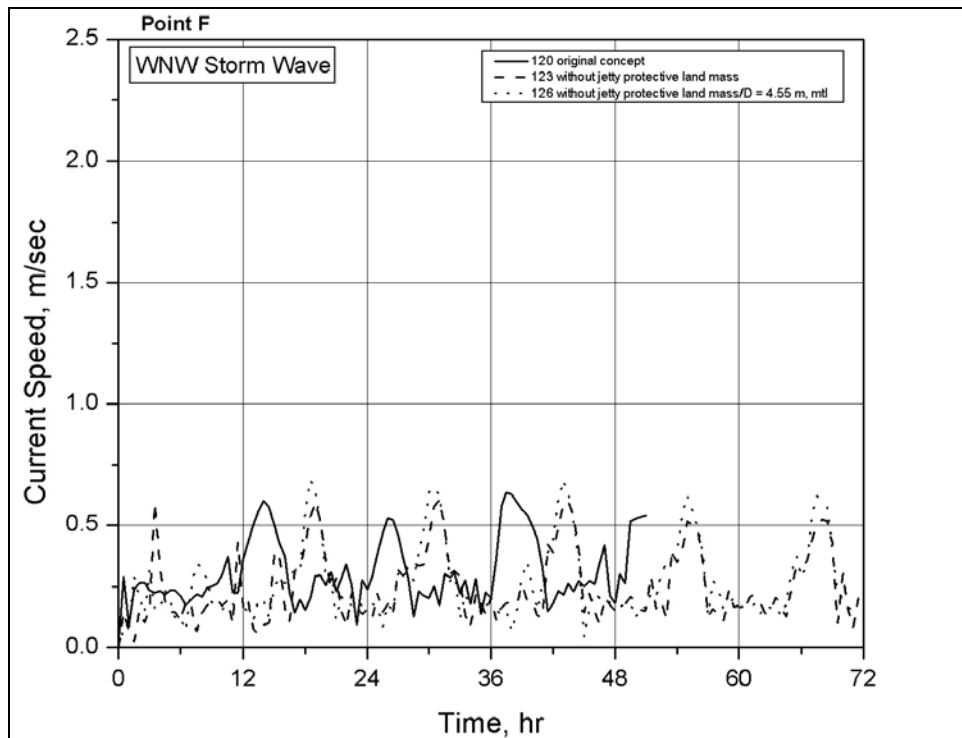


Figure B29. Time series of current speed at Point F for large-breach alternatives, west-northwest storm simulations

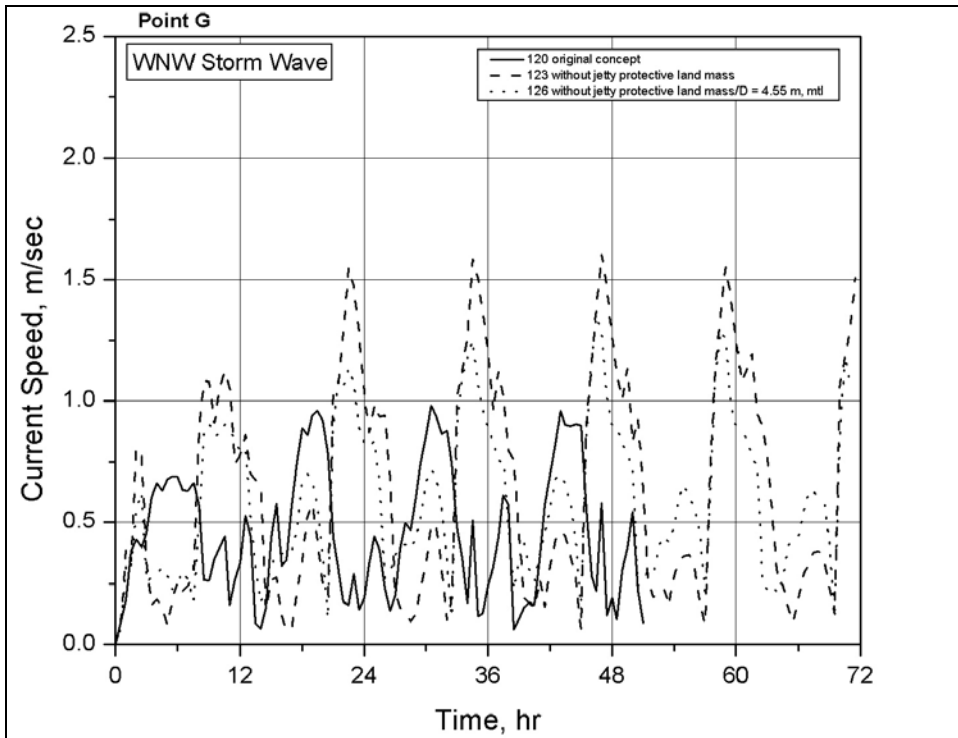


Figure B30. Time series of current speed at Point G for large-breach alternatives, west-northwest storm simulations

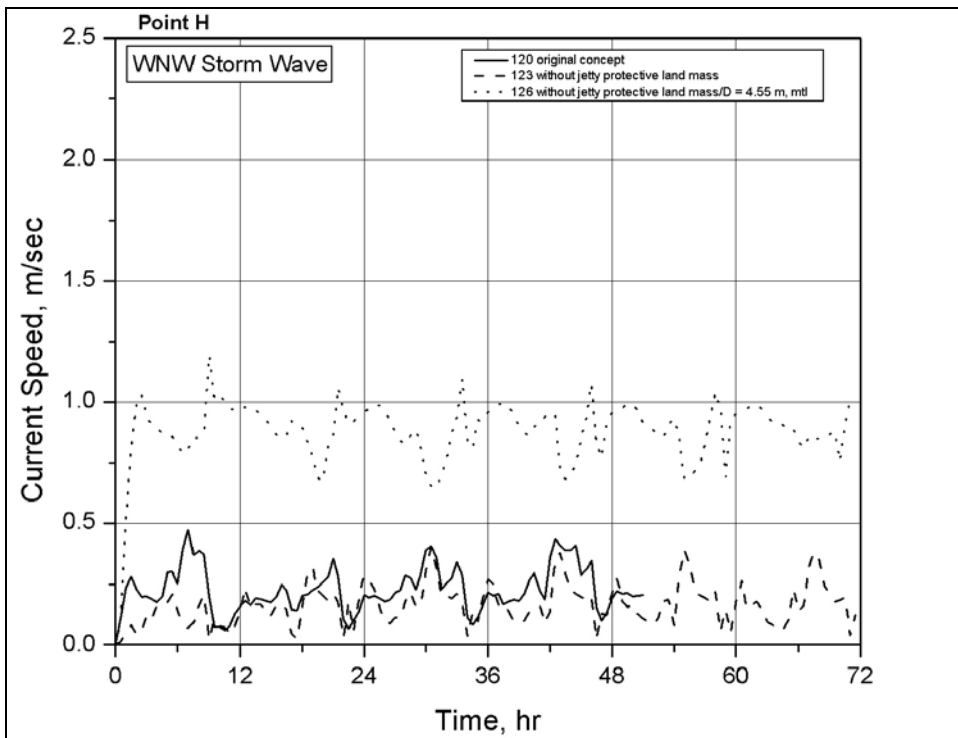


Figure B31. Time series of current speed at Point H for large-breach alternatives, west-northwest storm simulations

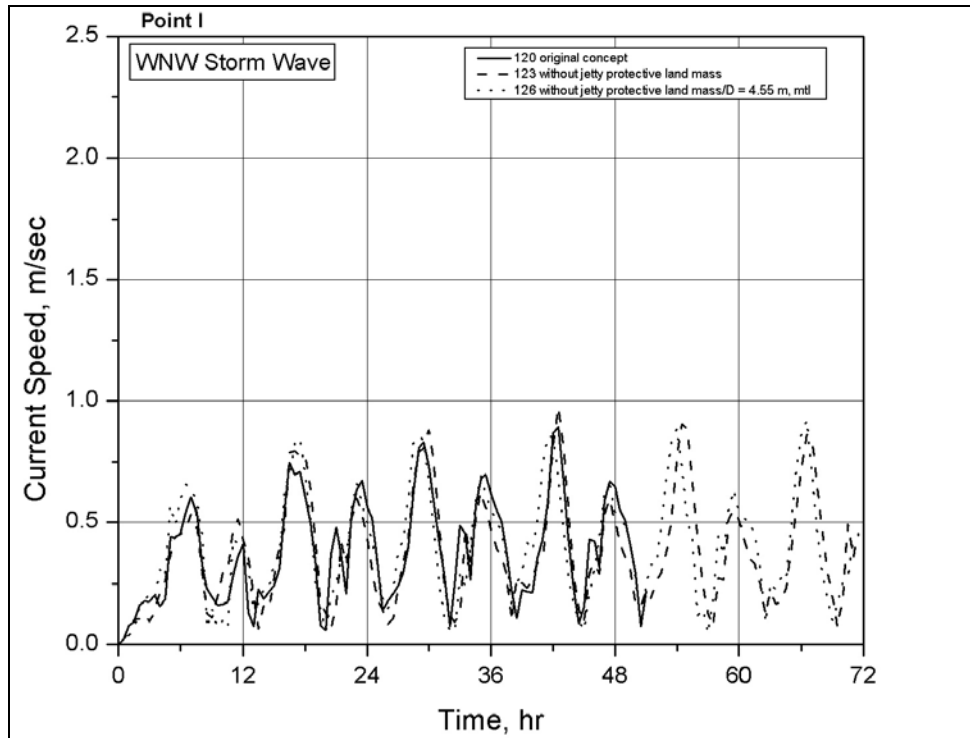


Figure B32. Time series of current speed at Point I for large-breach alternatives, west-northwest storm simulations

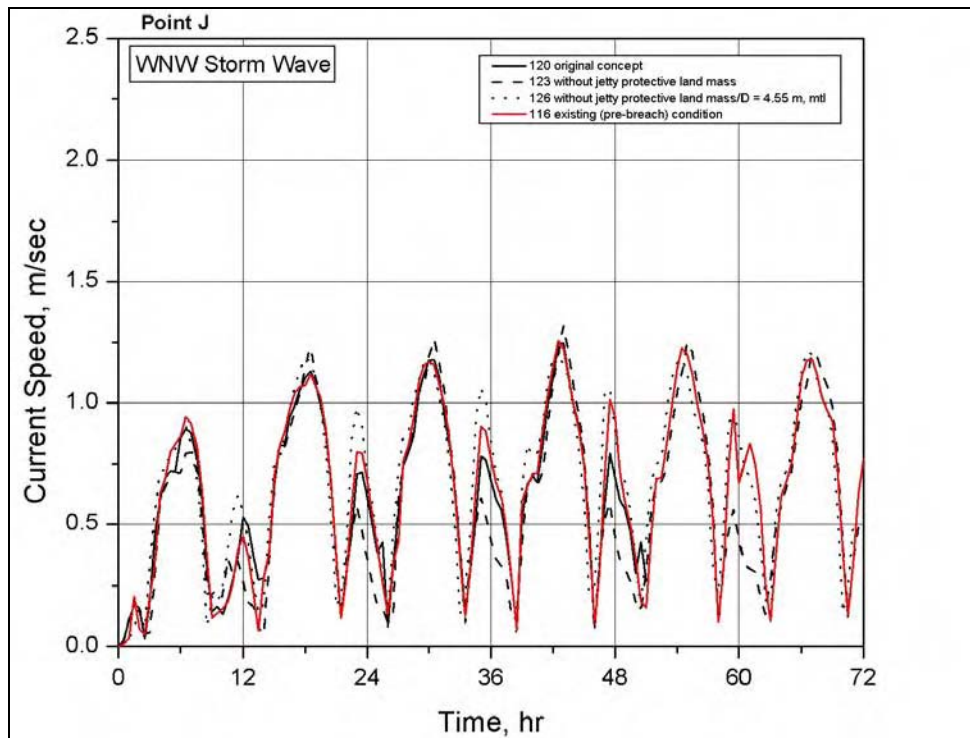


Figure B33. Time series of current speed at Point J for large-breach alternatives, west-northwest storm simulations

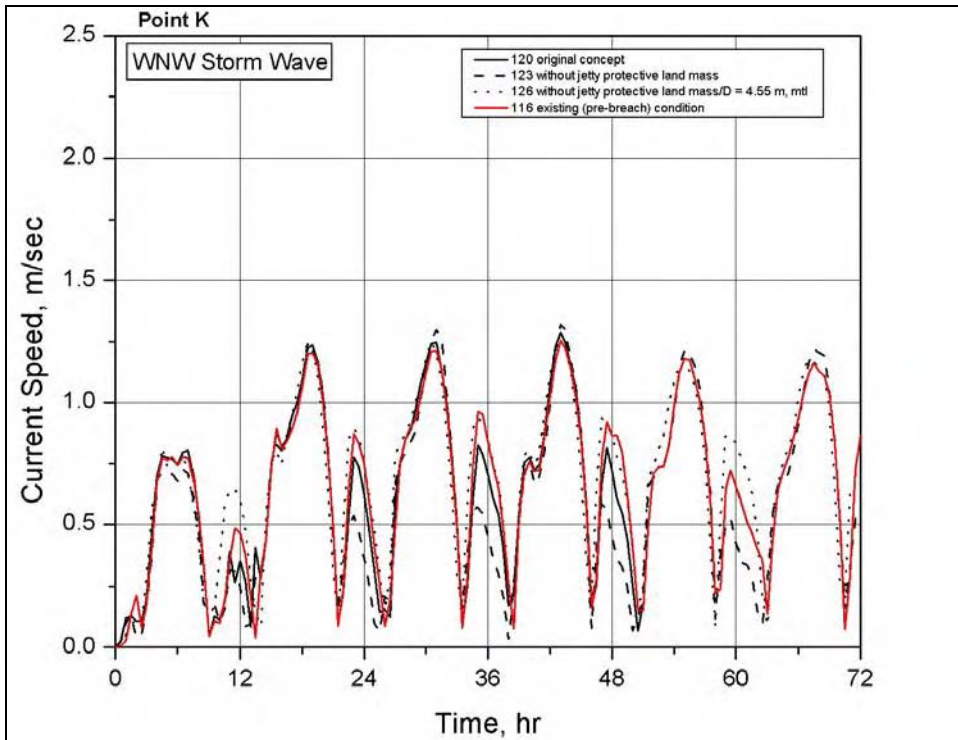


Figure B34. Time series of current speed at Point K for large-breach alternatives, west-northwest storm simulations

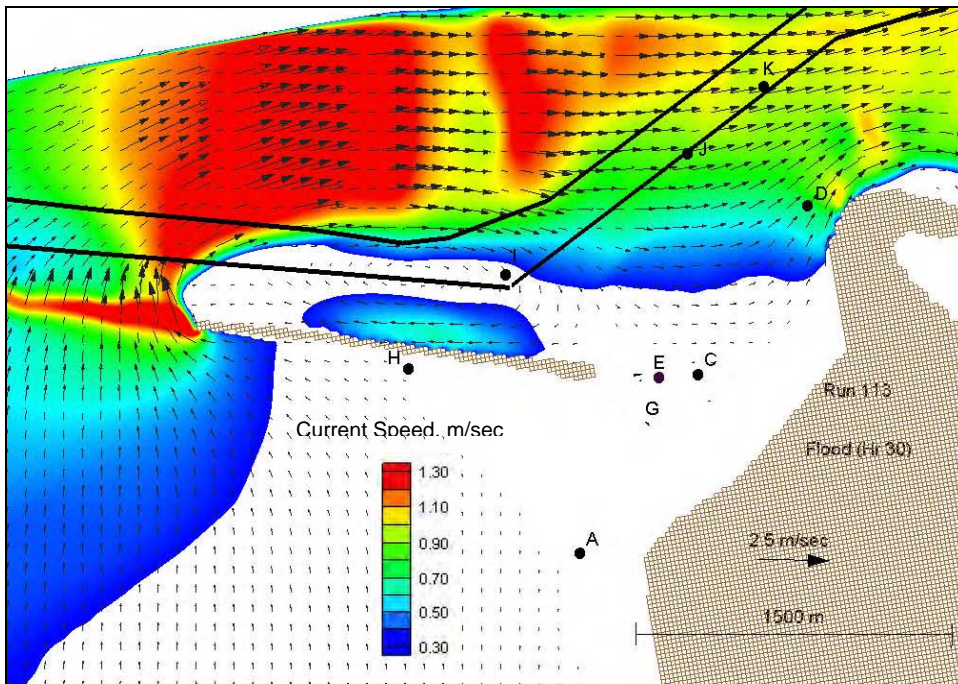


Figure B35. Flood flow for existing (pre-breach), tide only (Run 113)

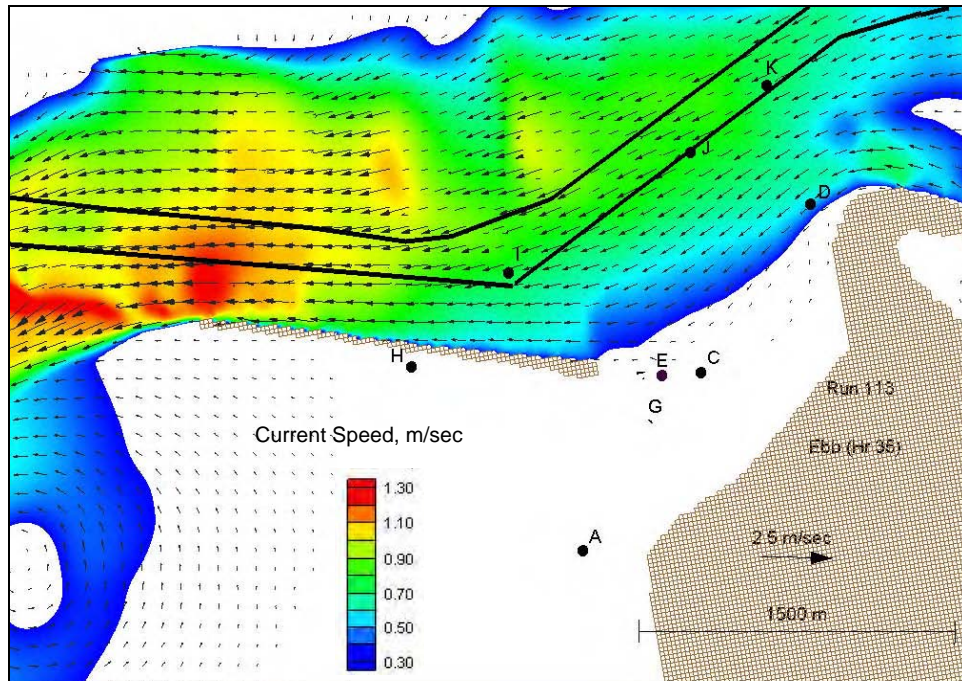


Figure B36. Ebb flow for existing (pre-breach), tide only (Run 113)

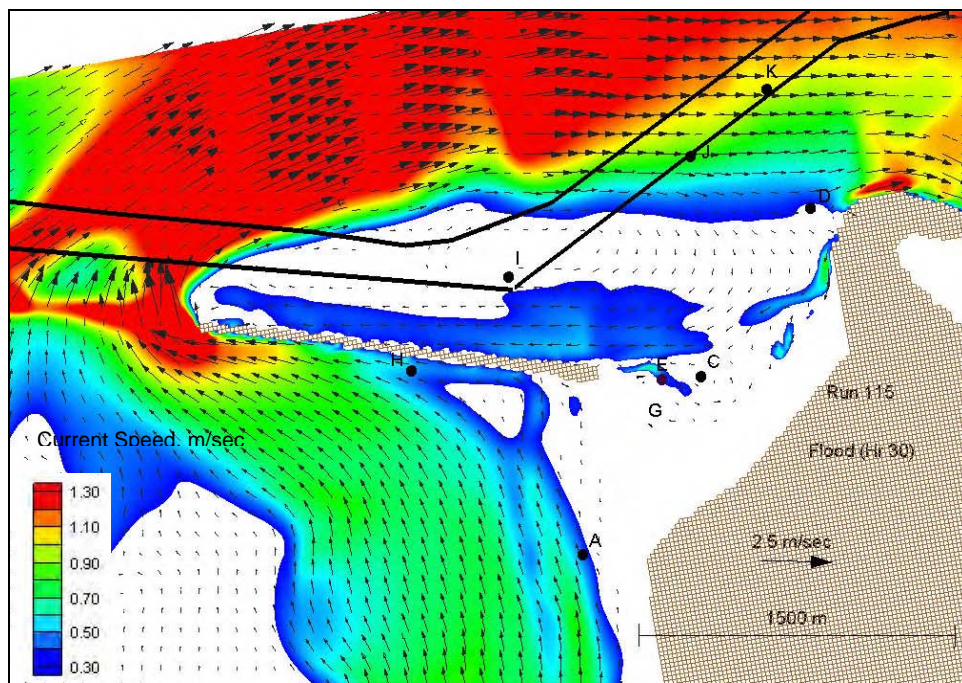


Figure B37. Flood flow for existing (pre-breach), west-southwest storm wave simulation (Run 115)

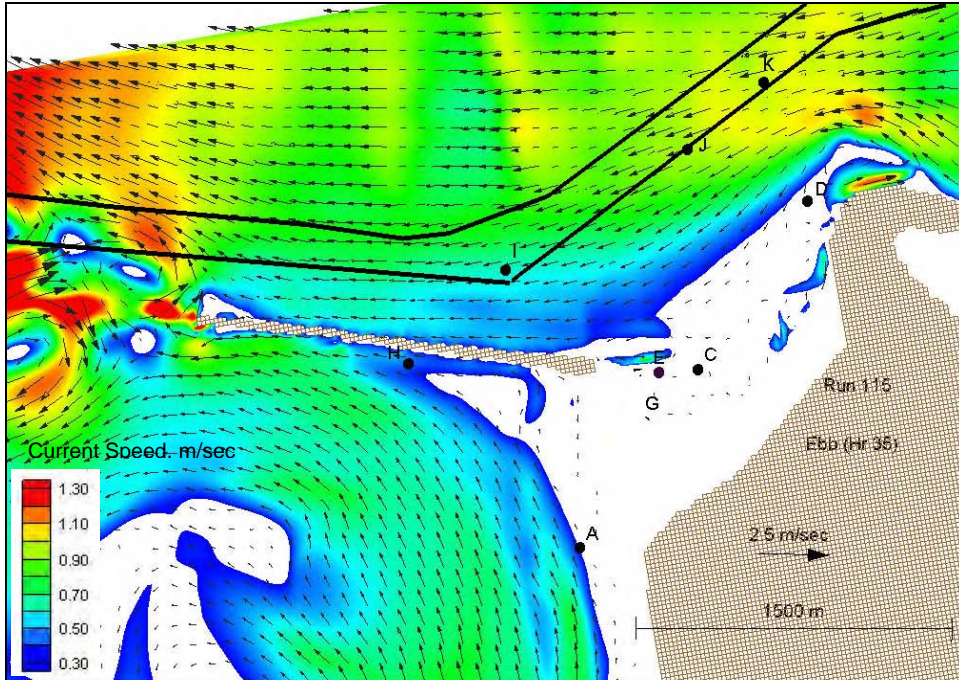


Figure B38. Ebb flow for existing (pre-breach), west-southwest storm wave simulation (Run 115)

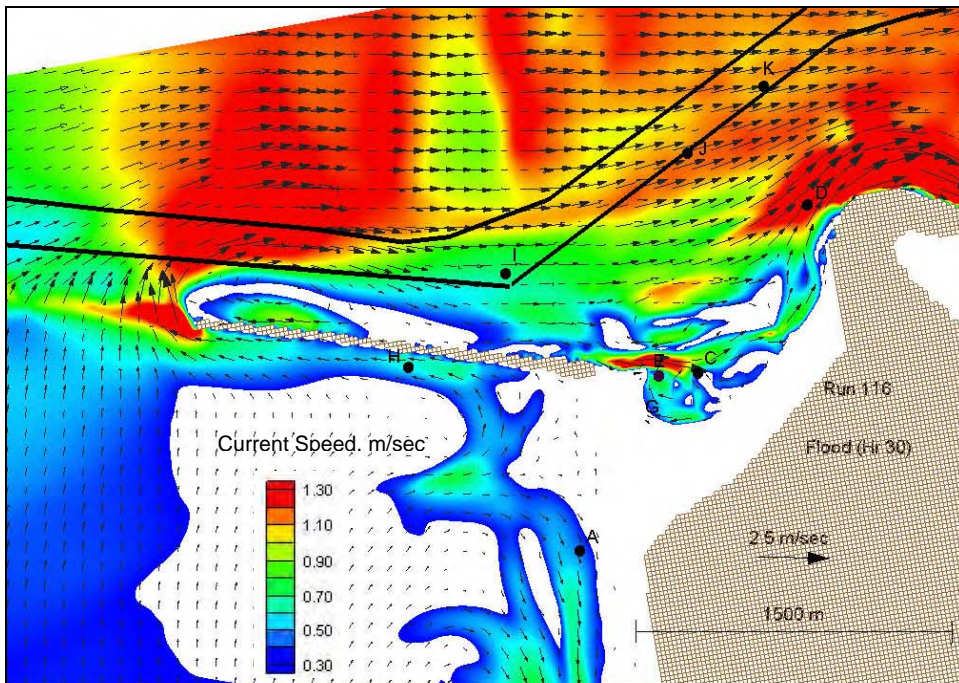


Figure B39. Flood flow for existing (pre-breach), west-northwest storm wave simulation (Run 116)

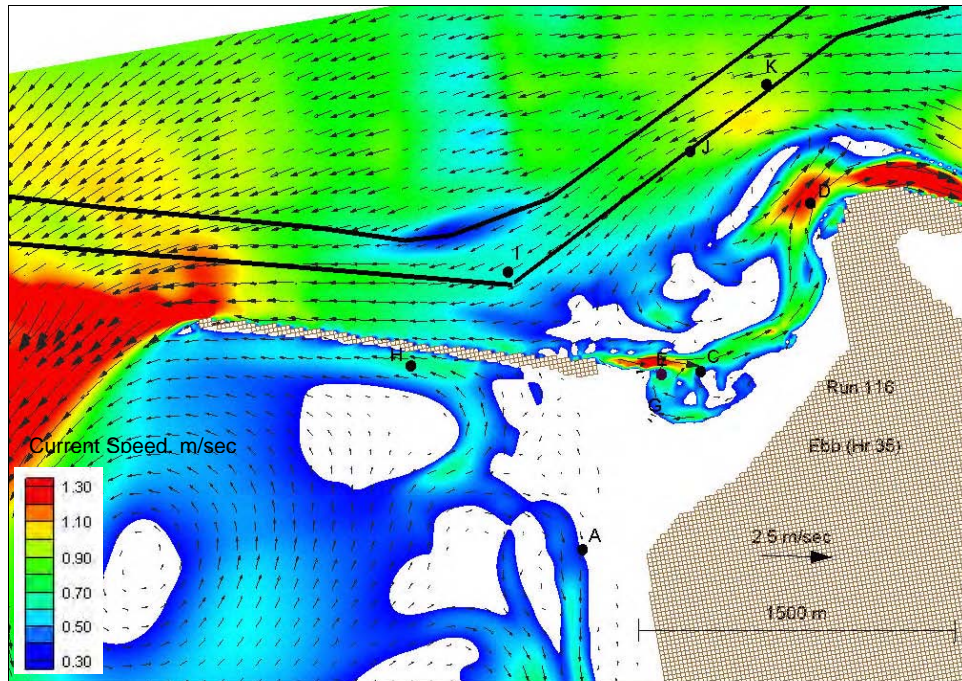


Figure B40. Ebb flow for existing (pre-breach), west-northwest storm wave simulation (Run 116)

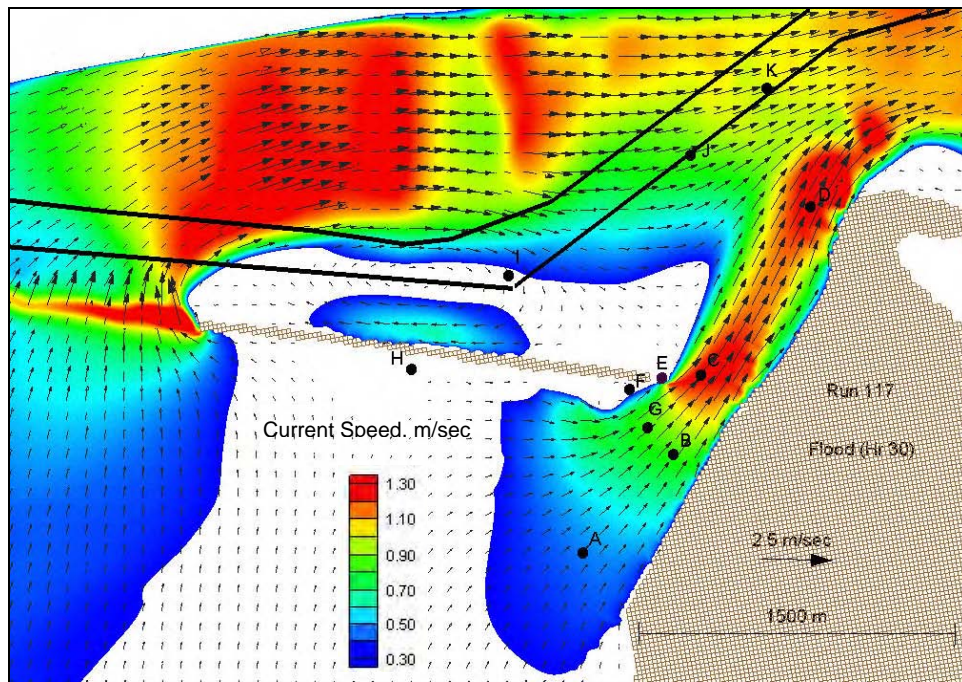


Figure B41. Flood flow for large breach, tide only simulation (Run 117)

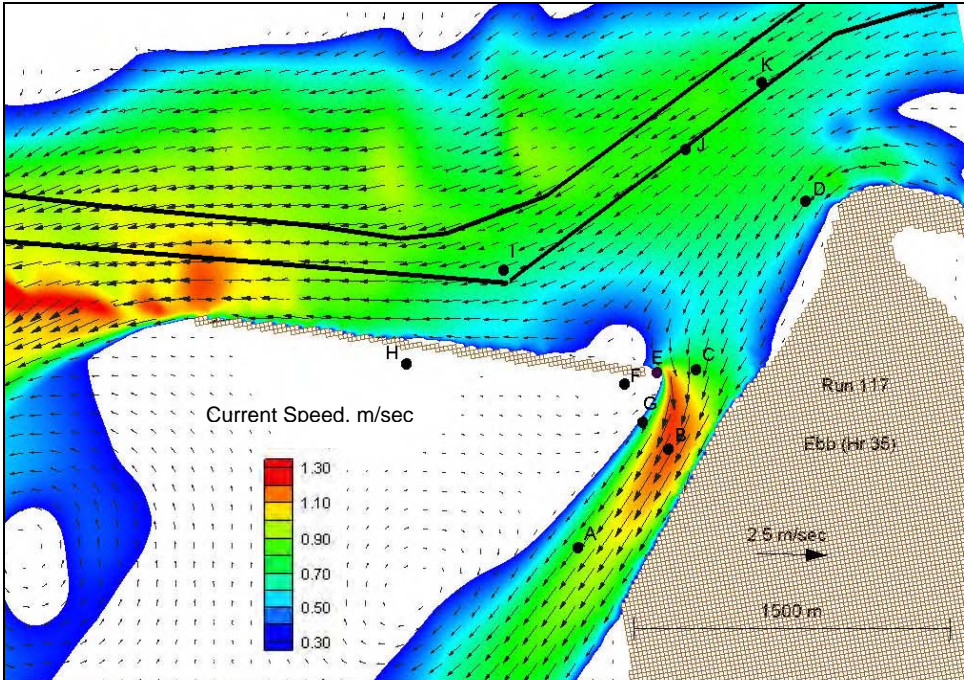


Figure B42. Ebb flow for large breach, tide only simulation (Run 117)

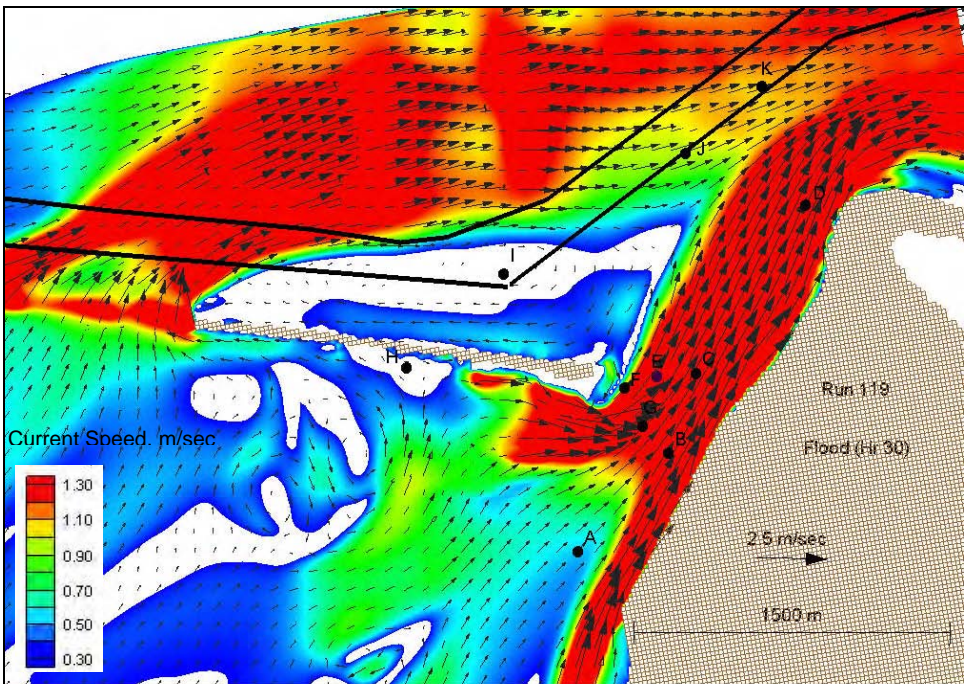


Figure B43. Flood flow for large breach, west-southwest storm wave simulation (Run 119)

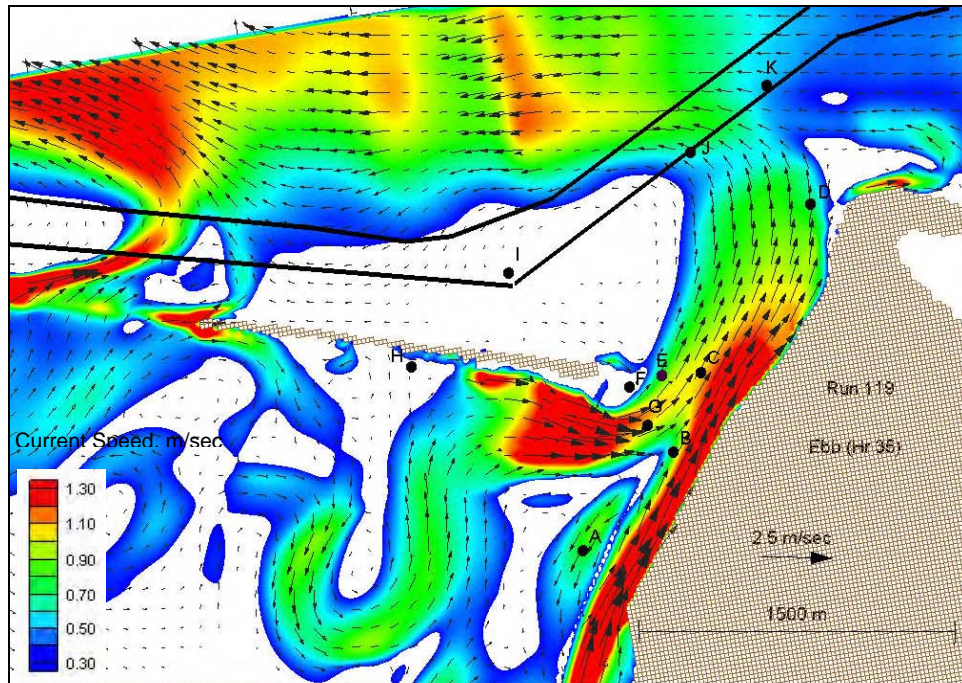


Figure B44. Ebb flow for large breach, west-southwest storm wave simulation (Run 119)

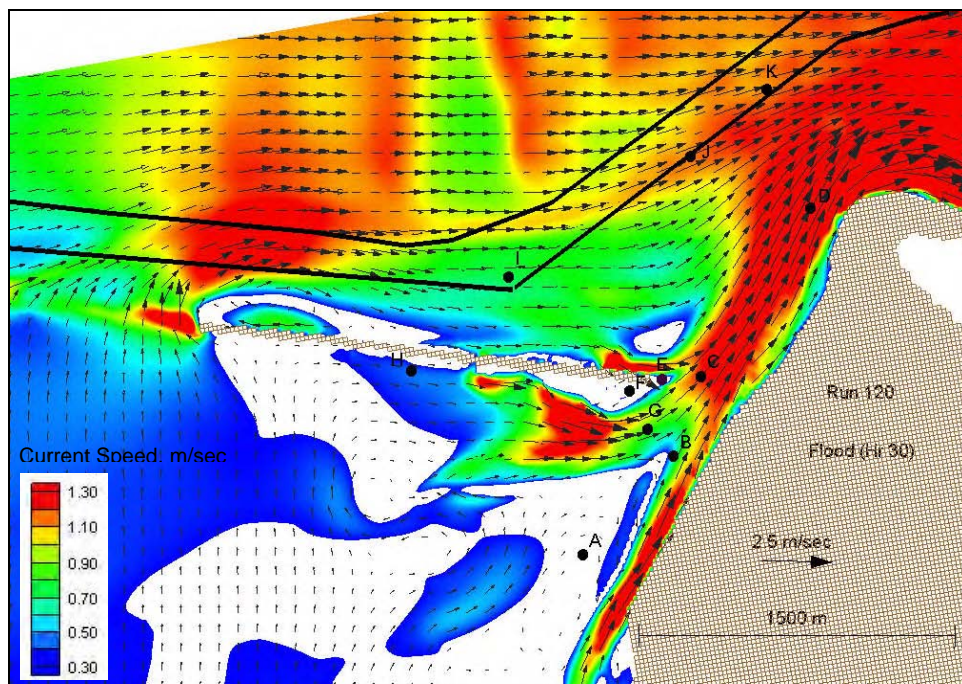


Figure B45. Flood flow for large breach, west-northwest storm wave simulation (Run 120)

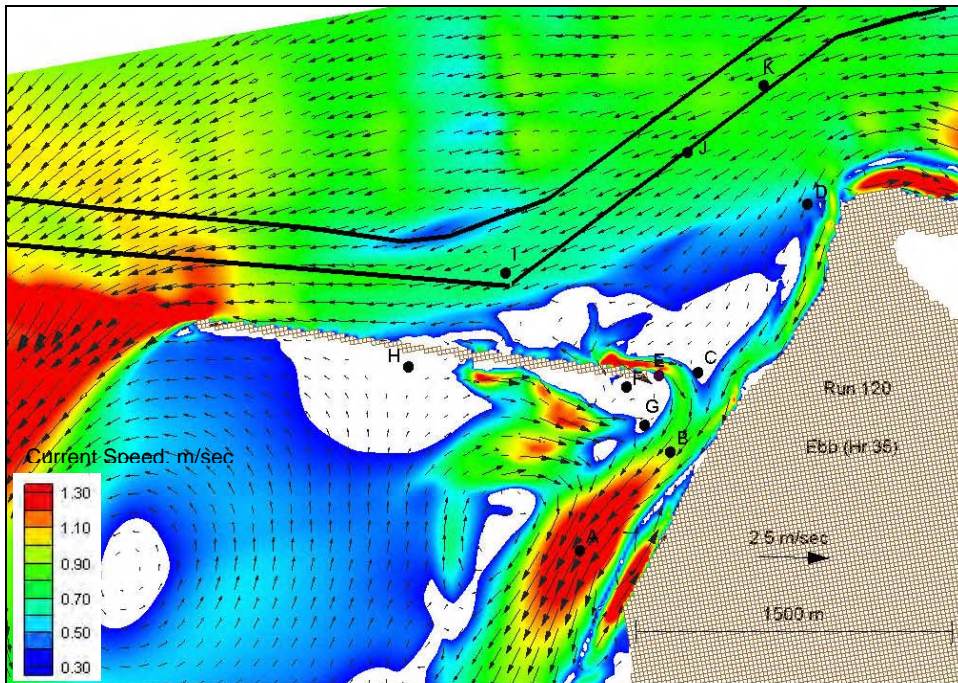


Figure B46. Ebb flow for large breach, west-northwest storm wave simulation (Run 120)

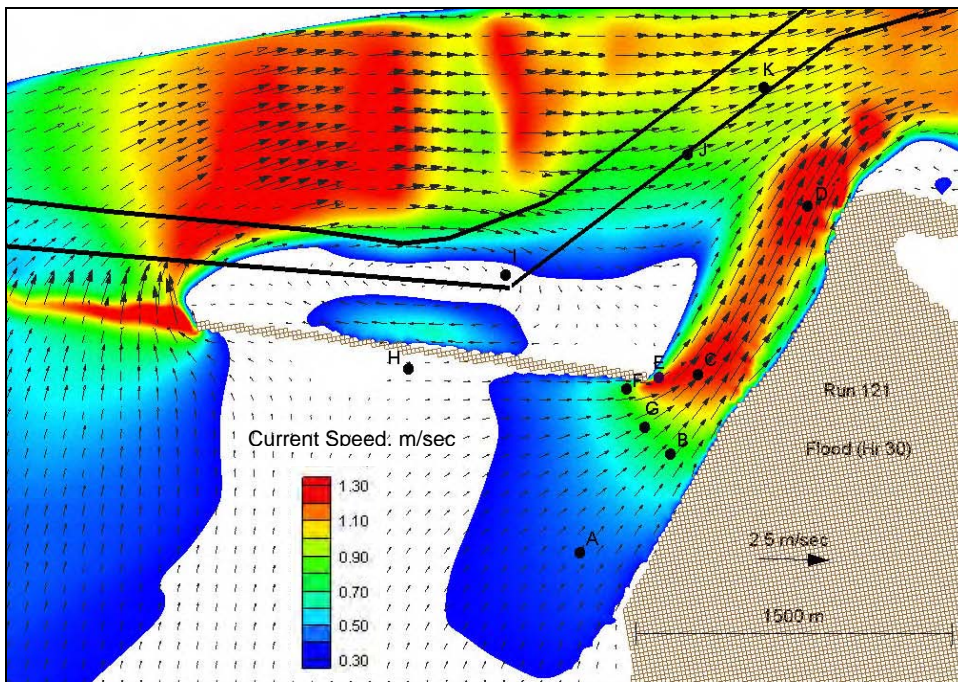


Figure B47. Flood flow for large breach without jetty protective landmass, tide only (Run 121)

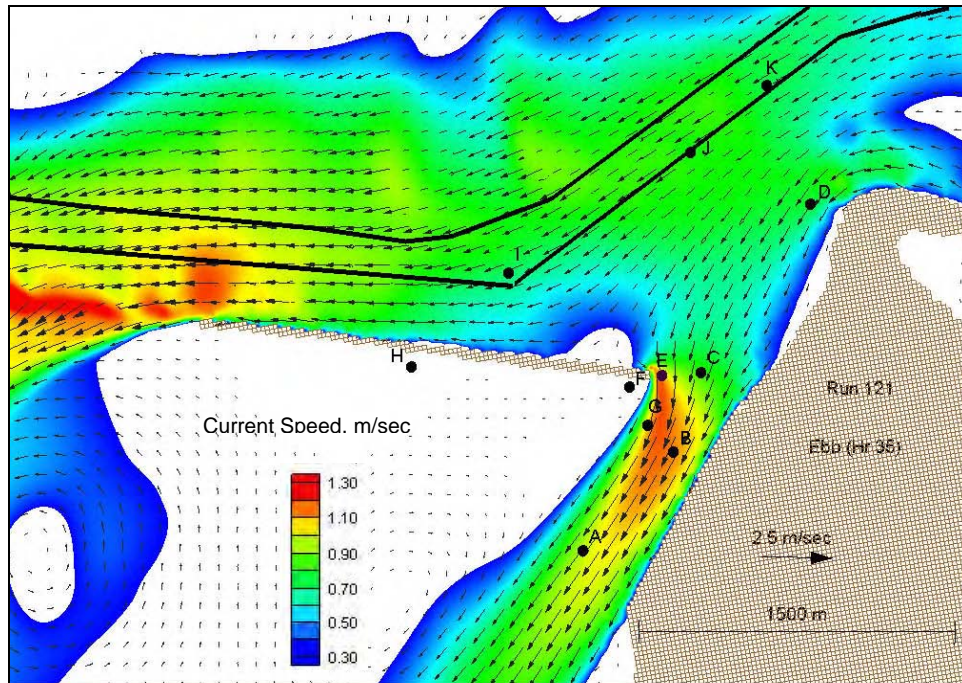


Figure B48. Ebb flow for large breach without jetty protective landmass, tide only (Run 121)

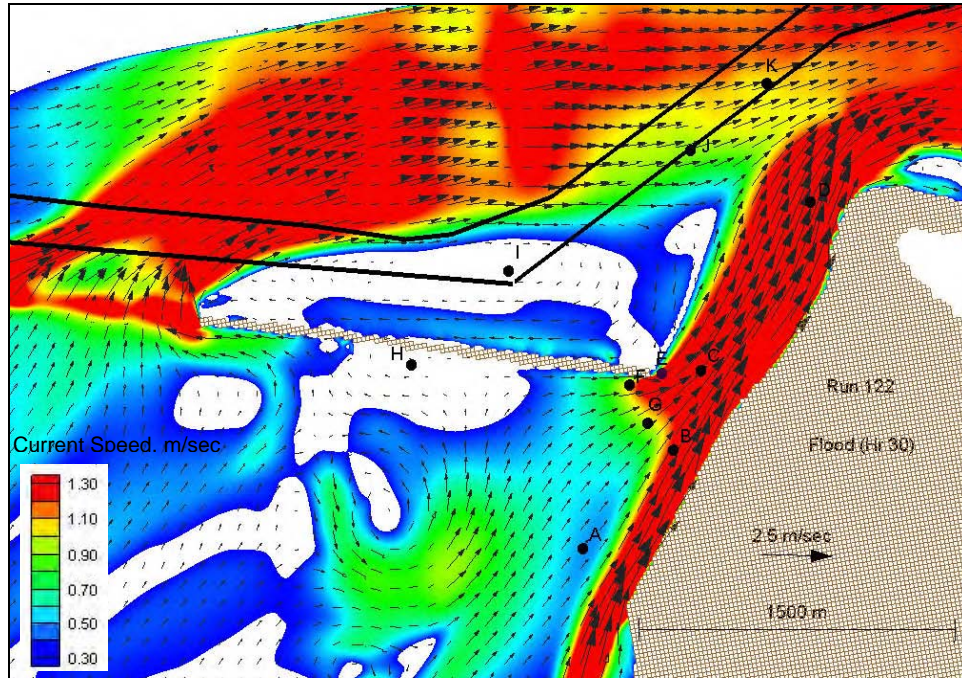


Figure B49. Flood flow for large breach without jetty protective landmass, west-southwest storm wave simulation (Run 122)

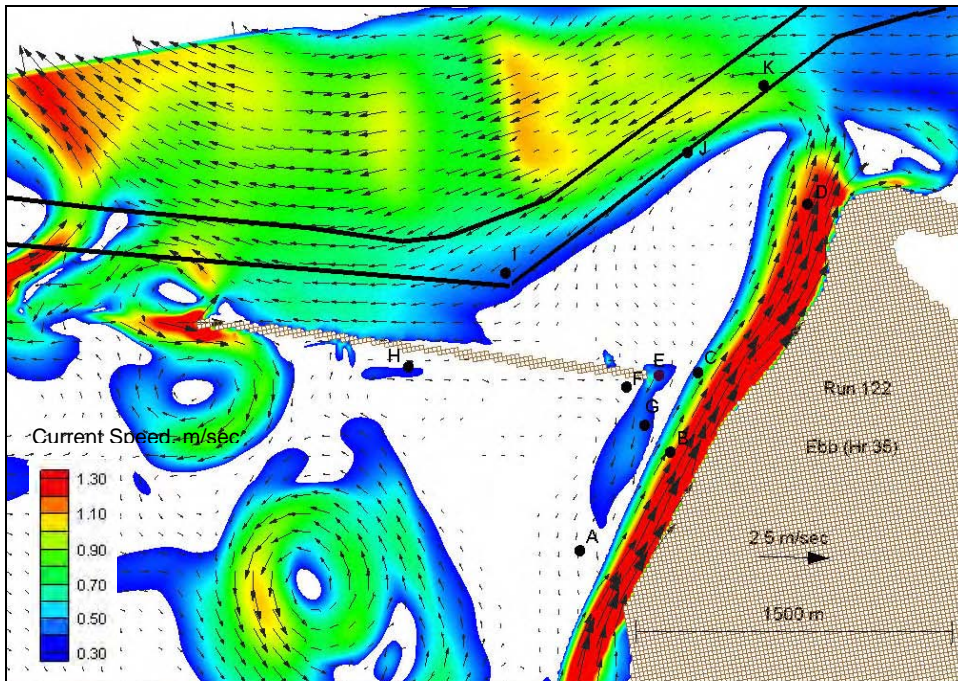


Figure B50. Ebb flow for large breach without jetty protective landmass, west-southwest storm wave simulation (Run 122)

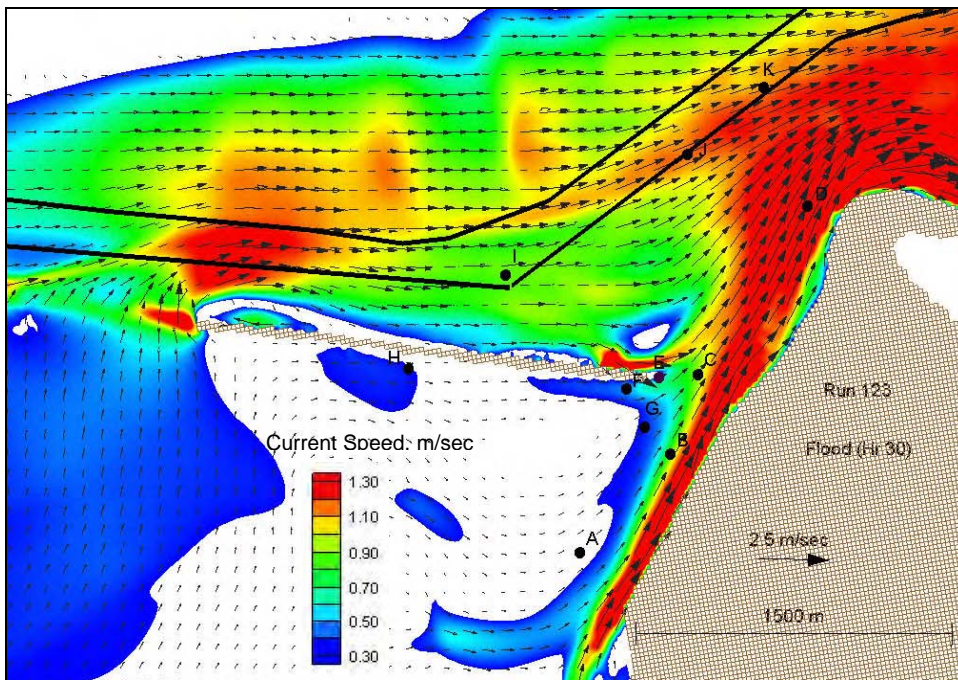


Figure B51. Flood flow for large breach without jetty protective landmass, west-northwest storm wave simulation (Run 123)

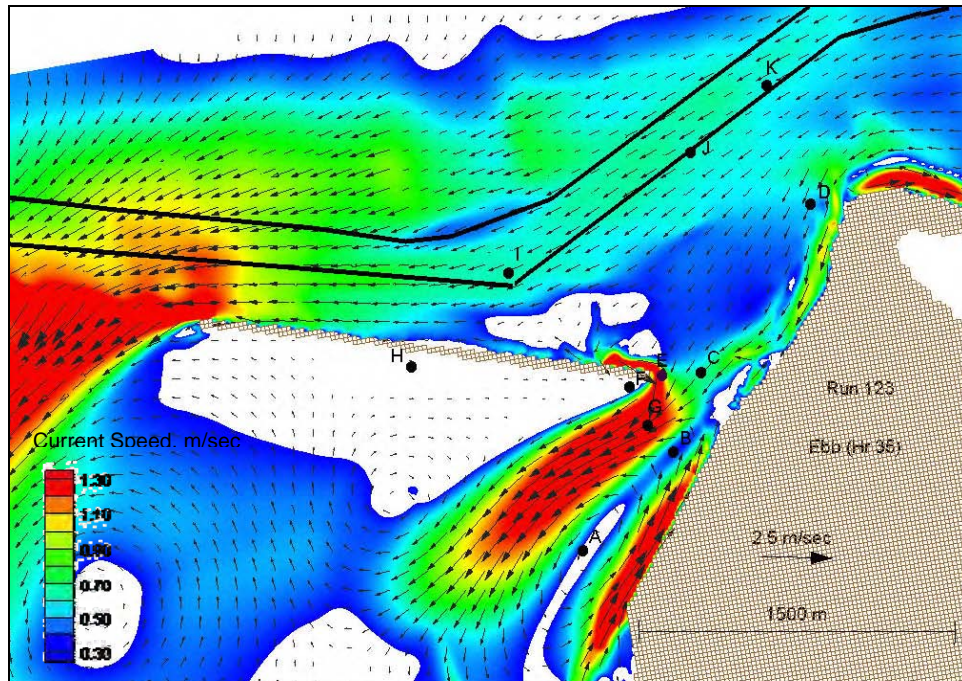


Figure B52. Ebb flow for large breach without jetty protective landmass, west-northwest storm wave simulation (Run 123)

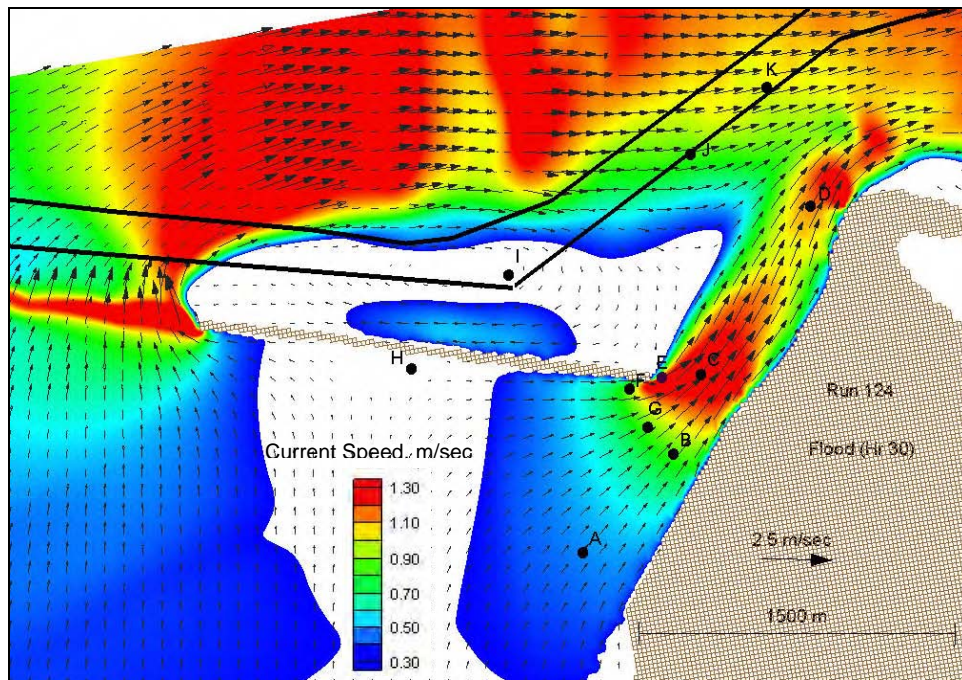


Figure B53. Flood flow for large breach without jetty protective landmass, depth = 4.55 m, mtl, tide only (Run 124)

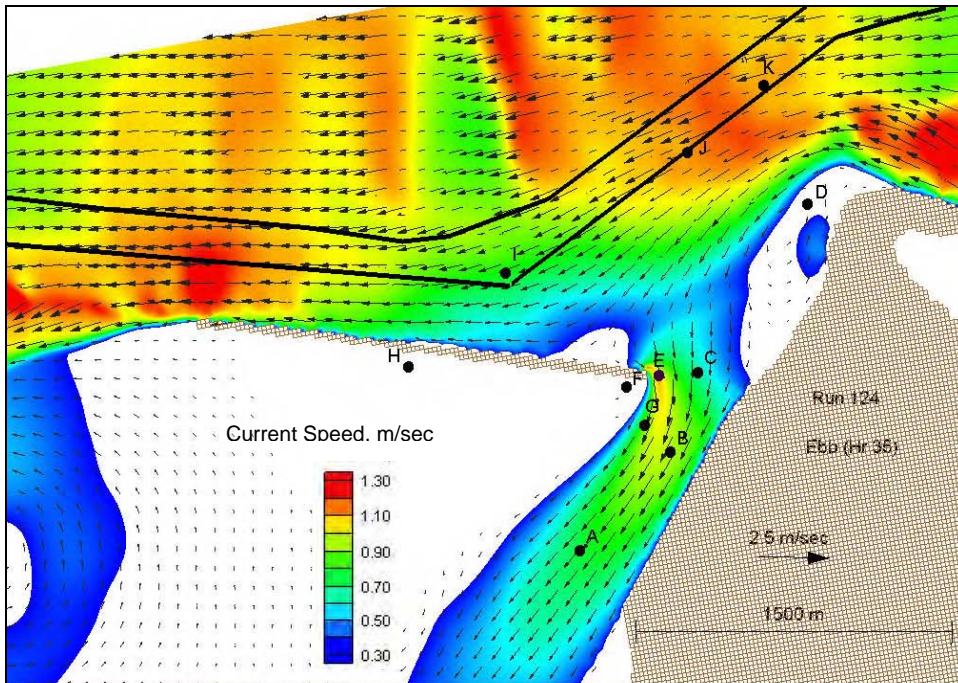


Figure B54. Ebb flow for large breach without jetty protective landmass, depth = 4.55, mtl, tide only (Run 124)

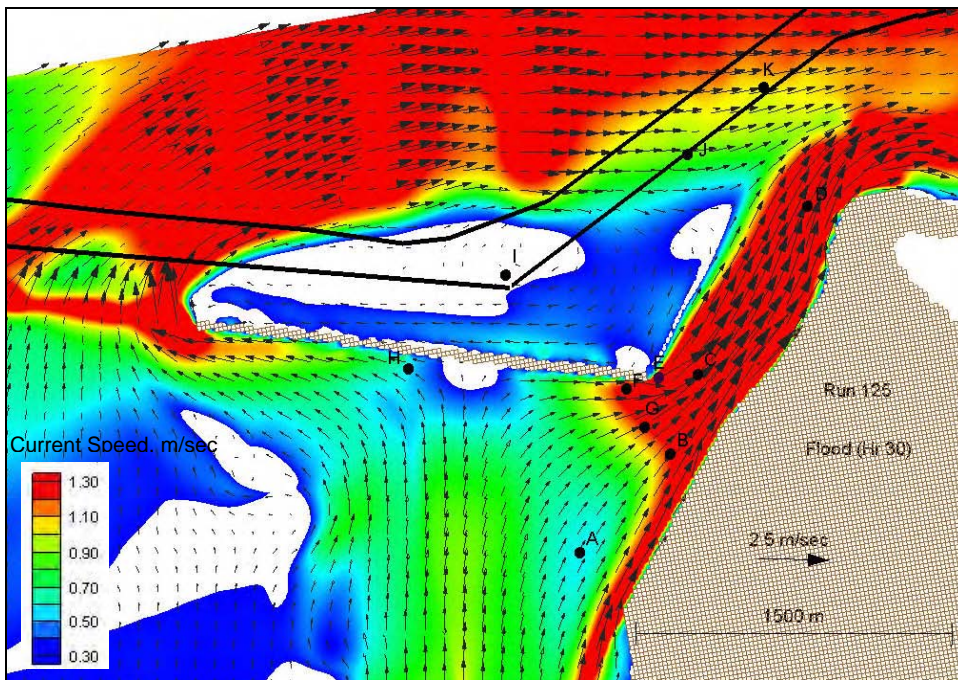


Figure B55. Flood flow for large breach without jetty protective landmass, depth = 4.55, mtl, west-southwest storm wave simulation (Run 125)

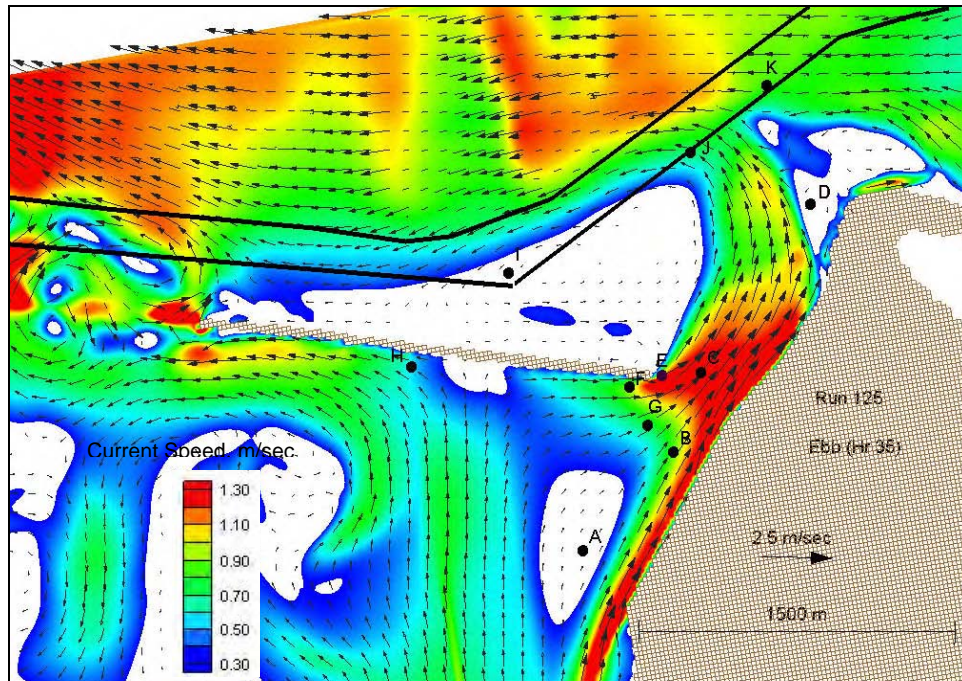


Figure B56. Ebb flow for large breach without jetty protective landmass, depth = 4.55 m, mtl, west-southwest storm wave simulation (Run 125)

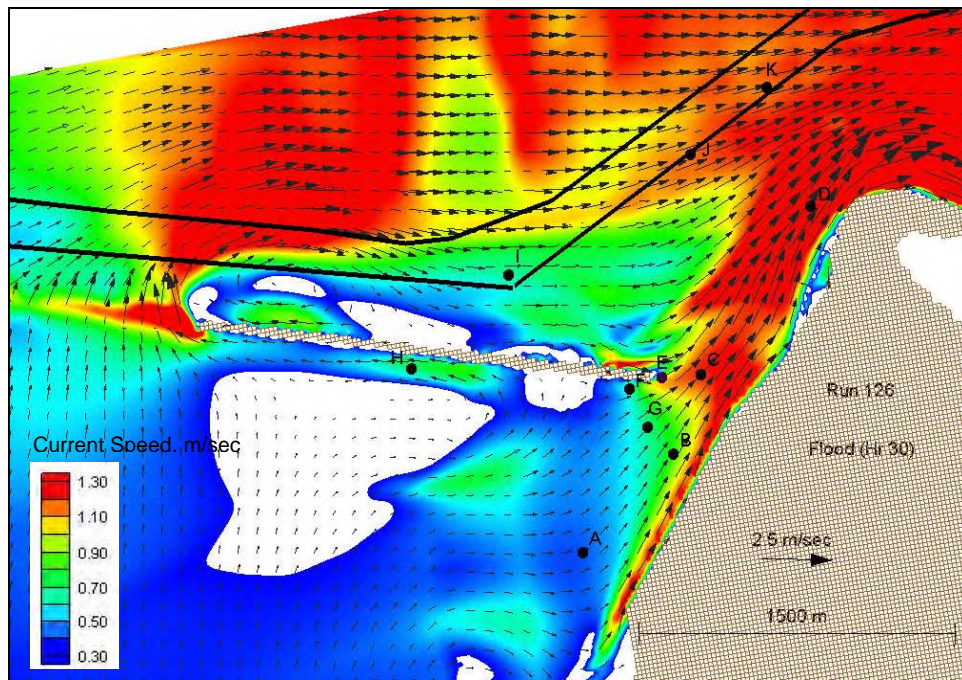


Figure B57. Flood flow for large breach without jetty protective landmass, depth = 4.55 m, mtl, west-northwest storm wave simulation (Run 126)

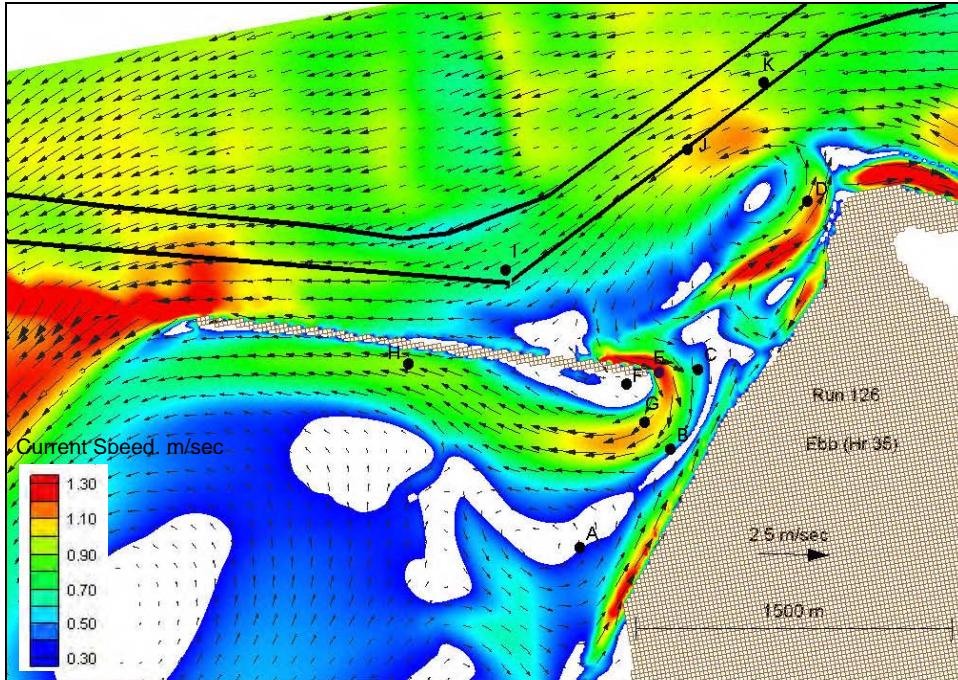


Figure B58. Ebb flow for large breach without jetty protective landmass, depth = 4.55 m, mtl, west-northwest storm wave simulation (Run 126)

Appendix C Independent Technical Review and Response



DEPARTMENT OF THE ARMY
ENGINEER RESEARCH AND DEVELOPMENT CENTER, CORPS OF ENGINEERS
COASTAL AND HYDRAULICS LABORATORY
WATERWAYS EXPERIMENT STATION, 3909 HALLS FERRY ROAD
VICKSBURG, MISSISSIPPI 39180-6199

REPLY TO
ATTENTION OF

CEERD-HV-B

10 May 2006

MEMORANDUM FOR RECORD

Subject: Response to Committee on Tidal Hydraulics, Independent Technical Review Sub-committee, review of Grays Harbor, WA, Numerical and Physical Modeling Draft Reports

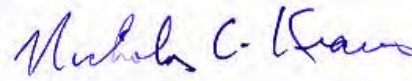
1. This Memorandum for Record is the response to an Independent Technical Review (ITR) of two draft reports submitted to the U.S. Army Engineer District, Seattle (NWS) by the U.S. Army Engineer Research and Development Center (ERDC), Coastal and Hydraulics Laboratory (CHL). The reports addressed NWS concerns about the Federal navigation project and coastal physical processes on the Pacific Ocean beach and bay beach located adjacent to the south jetty at Grays Harbor, WA. The ITR was conducted at the request of NWS by a sub-committee of the Committee on Tidal Hydraulics (CTH).
2. The ITR is entitled "Independent Technical Review of Numerical and Physical Modeling Reports 'Breach History and Susceptibility Study, South Jetty and Navigation Project Grays Harbor,' September 2004, and 'Half Moon Bay, Grays Harbor, WA: Movable-Bed Physical Model Study,' February 2005," and was dated 31 August 2005. It is noted here that the date of the first report listed should have been "January 2005" and not "September 2004," which pertains to an earlier version of that draft report.
3. The draft reports that were provided to NWS by CHL for review by the ITR are:
 - (a) "Breach History and Susceptibility Study, South Jetty and Navigation Project Grays Harbor," dated 21 January 2005, written by Ty V. Wamsley, Mary A. Cialone, and Nicholas C. Kraus; and,
 - (b) "Half Moon Bay, Grays Harbor, WA: Movable-Bed Physical Model Study," dated February 2005, and written by Steven A. Hughes and Julie Cohen.
4. Responses to the ITR report have been placed after the individual items contained in the review to avoid reading two separate documents or summarizing content of the ITR. Phraseology of the ITR report was not

SUBJECT: Response to Committee on Tidal Hydraulics, Independent Technical Review Sub-committee, review of Grays Harbor, WA, Numerical and Physical Modeling Draft Reports

modified, and its format was only slightly changed to facilitate placement of material in the review response. Equations in the original ITR document were corrupt and could not be reproduced in this response.

5. The ITR process contributed to improving the reports, and the comments and questions from the review are appreciated. Work performed in this response and in revision of the draft reports was conducted by Ms. Mary A. Cialone, Mr. Kenneth J. Connell, Dr. Nicholas C. Kraus, and Mr. Ty V. Wamsley for the breach history and susceptibility study, and by Dr. Steven A. Hughes for the movable-bed physical model study. Dr. Kraus compiled and edited this memorandum. Revisions of the draft reports have been made in response to the ITR as described herein.

6. In the following, the word “Reviewers” refers to the ITR Committee and “Authors” to the authors of the original and revised draft reports.



Nicholas C. Kraus, PhD
Senior Scientist Group
ERDC, Coastal and
Hydraulics Laboratory

SUBJECT: Response to Committee on Tidal Hydraulics, Independent Technical Review Sub-committee, review of Grays Harbor, WA, Numerical and Physical Modeling Draft Reports

Independent Technical Review of Numerical and Physical Modeling Reports

“Breach History and Susceptibility Study, South Jetty and Navigation Project Grays Harbor”, September 2004, and

“Half Moon Bay, Grays Harbor, WA: Movable-Bed Physical Model Study”, February 2005.

August 31, 2005

Committee on Tidal Hydraulics

U. S. Army Corps of Engineers

Review by:

Independent Technical Review Sub-committee

Arthur T. Shak, Los Angeles District (Chair) William H. McAnally, Mississippi State University, Joan Oltman Shay, Northwest Research Associates Jim Phipps, Grays Harbor College Bob Dean, University of Florida Independent Technical Review of Numerical and Physical Modeling Reports

“Breach History and Susceptibility Study, South Jetty and Navigation Project Grays Harbor”, September 2004, and

“Half Moon Bay, Grays Harbor, WA: Movable-Bed Physical Model Study”, February 2005.

SUBJECT: Response to Committee on Tidal Hydraulics, Independent Technical Review Sub-committee, review of Grays Harbor, WA, Numerical and Physical Modeling Draft Reports

Review by

Committee on Tidal Hydraulics Independent Technical Review Sub-Committee Introduction

The Independent Review Sub-Committee (ITRC) was formed at the request of the Seattle District of the U. S. Army Corps of Engineers to provide a review of two above listed reports produced by the U. S. Army Engineer Research and Development Center (ERDC) relating to navigation concerns at Grays Harbor, Washington. The ITRC consisted of the following individuals:

Arthur T. Shak, Los Angeles District (Chair of ITRC) William H. McAnally, Mississippi State University Joan Oltman Shay, Northwest Research Associates Jim Phipps, Grays Harbor College Bob Dean, University of Florida

Preparation of the ITRC for this review included some of the Members conducting a Site Visit, briefing by Eric Nelson and Norman Skjelbreia of the Seattle District, the review of the material provided by the District as listed here and additional material.

Prior to presenting our reviews, we wish to commend the Authors of the two reports for their organization and summary of a great deal of information that has facilitated our reviews.

The Independent Technical Review Committee (ITRC) was requested to place emphasis on the following aspects of the subject reports:

- Are the selected models appropriate for the study purpose?
- Have the models been appropriately calibrated and verified?
- Are the study conclusions supported by the model results?
- Do the studies accomplish their goals?

These questions distill down to two basic points: 1) the applicability of the models applied and 2) the validity of the conclusions. The reports in question were not prepared as stand alone products to address the first point and, unfortunately, even reading the background literature may not provide all of the needed information. This therefore places the Reviewers in the position of asking more questions about the application of the models and placing greater emphasis on the second point --do the conclusions "ring true".

SUBJECT: Response to Committee on Tidal Hydraulics, Independent Technical Review Sub-committee, review of Grays Harbor, WA, Numerical and Physical Modeling Draft Reports

In addition to the subject reports, the following were provided to assist in this ITR:

- (1) CEERD-HV-B Memorandum dated 19 January 2005, "Response to 16 November 2004 NWS Civil Soils Section Review Comments on Draft Report 'Breach History and Susceptibility Study, South Jetty and Navigation Project Grays Harbor' Dated 7 September 2004", and
- (2) CEERD-HN-HH Memorandum dated 28 February 2005, "CHL Response to Comments From Civil/Soils Section, U.S. Army Engineer District, Seattle".
- (3) CD Rom containing prior studies of the North and South Jetty, with historic photos and PowerPoint presentations.

Review Summary

The "Breach History and Susceptibility Study, South Jetty and Navigation Project Grays Harbor" was prepared to analyze the December 1993 breach at Grays Harbor, WA, and assess the threat to the federal Navigation Project had the breach not been filled the following fall. The ITRC found the models applied were appropriate. The hydrodynamic codes, ADCIRC and STWAVE are well established; the newer, less-proven model, M2D appears nonetheless appropriate for this study. However, the uncertainty of the geomorphological breach model was found to be large and the validation of the hydrodynamic modeling was alluded to but not presented. The committee believes the assessment of the threat to the federal Navigation Project has not been achieved due to the uncertainty of the breach model and possibly limited validation of the other models. The "worst-case" scenario studied in the hydrodynamic model may not approximate reality and the prediction of an increasing breach depth by the breach model may overstate the risk to the federal Navigation Project. Recognition of the background sediment deficit in the South Beach vicinity portends a long term threat to the federal Navigation Project. However, a quantitative assessment of impacts to the navigation channel and the South Jetty structure is not presented. The ITRC believes that the width of the breach would continue to increase, albeit at a slow enough time-scale that would permit a measured, physical closure response if deemed necessary.

Response: No technical background was presented by the Reviewers for the statement "The ITRC believes that the width of the breach would continue to increase, albeit at a slow enough time-scale that would permit a measured, physical closure response if deemed

SUBJECT: Response to Committee on Tidal Hydraulics, Independent Technical Review Sub-committee, review of Grays Harbor, WA, Numerical and Physical Modeling Draft Reports

necessary.” Therefore, the Authors cannot comment. Also, the subject reports and the Reviewers did not examine breach-response strategies, nor did they estimate the time and effort required to fill breaches of various sizes that might open according to storm severity and frequency. Stockpiling of sand and filling operations of a breach are expected to require a planning and permitting process that would delay breach closure, unless such a plan (with permits) were in place prior to the need for the closure operation.

The purpose of the “Half Moon Bay, Grays Harbor, WA: Movable-Bed Physical Model Study” was to support the Long Term Management Studies (LTMS) of the Seattle District, specifically by assessing the potential long-term response of the Half Moon Bay shoreline to expected storm waves and surge levels. The study Authors clearly recognize the limitations of the physical model to simulate long periods of time where sediment loss to the bay could influence results. As such, a physical model is not the best approach for predicting the long-term shoreline response of Half Moon Bay. However, the study does provide a baseline with which to compare the effects of potential engineering alternatives for long-term stabilization of the bay, and for evaluating alternatives the use of a physical model is most appropriate.

The following sections provide reviews of the two reports in the order listed above.

Review of Report “Breach History and Susceptibility Study, South Jetty and Navigation

Project Grays Harbor”, September 2004

Response: It is noted that the September 2004 version of the subject draft report was superseded by a 21 January 2005 version provided to NWS for the ITR. It is hoped that the 21 January 2005 draft report was available for review by all ITR members, as considerable improvements were made between the September 2004 and January 2005 versions.

SUBJECT: Response to Committee on Tidal Hydraulics, Independent Technical Review Sub-committee, review of Grays Harbor, WA, Numerical and Physical Modeling Draft Reports

Introduction

The following review of this report will first address general comments focused primarily on the four questions provided earlier followed by specific comments.

The purpose of the project documented in this report (Page 1) “*was to analyze the December 1993 breach at Grays Harbor, WA and assess the threat to the Federal Navigation Project had the breach not been filled the following fall.*”

General Comments

(1) This study provides an historical review of the December 1993 breach history to its October to December 1994 closure. Additionally, state of the art numerical models are employed to investigate the hydrodynamic and morphological response characteristics of the actual and hypothesized breaches and to simulate breach evolution.

Are the selected models appropriate for the study purpose?

(2) Although individual investigators would choose different tools to approach the study purpose, the hydrodynamic models selected in the report were appropriate for the study. All models, with the exception of MD2 are well-known and tested. The known models, ADCIRC and STWAVE are appropriate models to use for this study and were appropriately used; ADCIRC provided only the boundary conditions to the area of interest. MD2 is not well-known to the reviewers. However, from the presentation in the report, MD2 also appears to be appropriate for this study.

(3) It is appreciated that hydrodynamic processes (governing equations) are much better understood than processes governing morphological evolution. It is also appreciated that all morphological models have a high degree of uncertainty and that morphological models are necessarily specialized for specific issues, such as inlet breaches. The Authors chose to develop their own breach model for this study and to test and calibrate it against a Dutch physical model and an observational study at Moriches Inlet, NY. To achieve agreement between their model and the Dutch model and Moriches and Grays Harbor observations, two parameters, alpha and beta, required adjustment. Of concern is the more than order of magnitude difference in parameter space for these three case studies.

SUBJECT: Response to Committee on Tidal Hydraulics, Independent Technical Review Sub-committee, review of Grays Harbor, WA, Numerical and Physical Modeling Draft Reports

Response: The Reviewers expresses concern several times about uncertainty and calibration of the newly developed morphologic model (Breach Model). This concern is addressed once in this reply, at Specific Comments Items 16-18, to avoid repetition.

(4) The Authors made a conscientious and thorough effort to evaluate breach evolution. The morphological model developed for this study appears appropriate for the problem considered. However, the uncertainty in any morphological model results is high enough that another model, independently developed, should be implemented before statements about breach growth or recovery can be stated with a modicum of confidence. One model that could serve this purpose will be discussed later.

Response: The Reviewers express concern several times about uncertainty and calibration of the newly developed morphologic model (Breach Model). This concern is addressed once in this reply, at Specific Comments Items 16-18, to avoid repetition.

Have the models been appropriately calibrated and verified?

(5) In studies of this type with application of advanced models, it is desirable that the models be as soundly physics based as possible and to require a minimum of calibration. If calibration is required due to a paucity of related physics, it is encouraging if the calibration coefficients vary little from model to prototype and from one field location to another field location. As noted, the wide range of calibration coefficients required raises concerns regarding the validity of the breach evolution model.

Response: The Reviewers express concern several times about uncertainty and calibration of the newly developed morphologic model (Breach Model). This concern is addressed once in this reply, at Specific Comments Items 16-18, to avoid repetition.

(6) The validation of the ADCIRC model is cited, but not presented. Combined tidal and wave-induced flows in the model(s) are compared anecdotally to field observations, but an organized validation section is not presented. The CHL response to NPS comments that "...calibration of ADCIRC implies calibration of M2D" is incorrect. Given the importance of the flow results to the conclusions, a detailed presentation of the M2D model validation to field data and the modelers' interpretation of that validation are essential.

SUBJECT: Response to Committee on Tidal Hydraulics, Independent Technical Review Sub-committee, review of Grays Harbor, WA, Numerical and Physical Modeling Draft Reports

Response: The ADCIRC model was validated with field data collected in 1999, as documented in Chapter 7 of Technical Report ERDC/CHL TR-03-12 (Kraus and Arden 2003), referenced in the subject report. A sample of ADCIRC validation results is provided in Figures R1 to R5. ADCIRC calculations compared well with the measurements.

The Coastal Inlets Research Program conducted at CHL has linked ADCIRC and M2D for several years and applied this combination at various study sites, with ADCIRC serving as a regional circulation model driving the project-level model M2D. The linkage has been implemented in the Surface-water Modeling System (SMS) since year 2000. Proper development of model grids has shown that a local model will produce comparable results as a regional model, with slight differences possible depending on resolution between the models at the particular comparison point.

The M2D model validation for the present study is given below. M2D results were compared to the 1999 measurements and to ADCIRC results at the stations identified in Figure R1. Figure R2 compares water level at station Tide 1, and Figures R3-R5 compare velocity magnitude at Stations 4, 2, and 5, respectively. Stations 2 and 5 are included in both the M2D outer and M2D inner grids. M2D calculations agree well with the measurements. Water level predictions by M2D and ADCIRC are nearly identical. Current speed calculated with M2D are in phase with the measurements, and the M2D results improve on the peak speed predictions relative to ADCIRC, attributed to finer resolution of the M2D mesh.

SUBJECT: Response to Committee on Tidal Hydraulics, Independent Technical Review Sub-committee, review of Grays Harbor, WA, Numerical and Physical Modeling Draft Reports

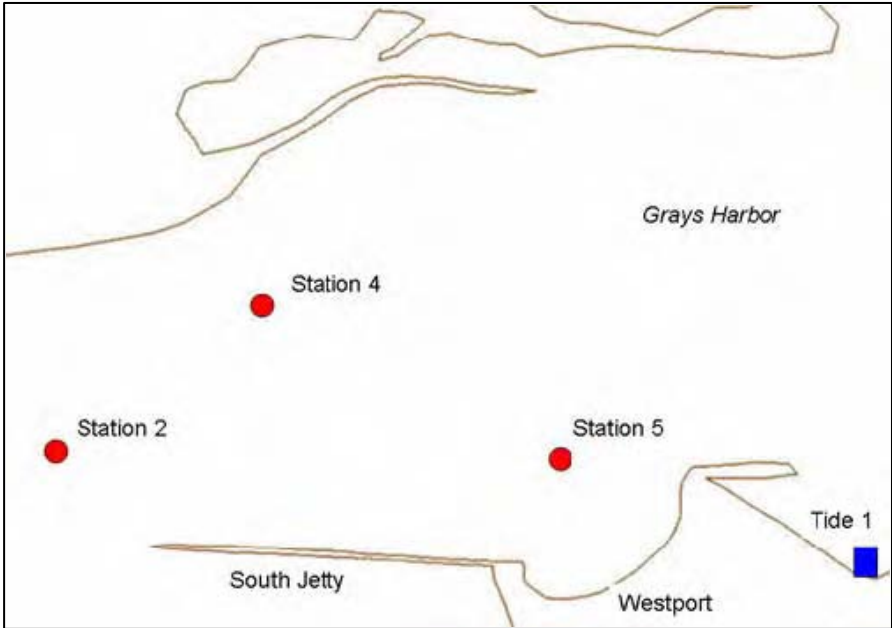


Figure R1. Field data collection station locations, 1999

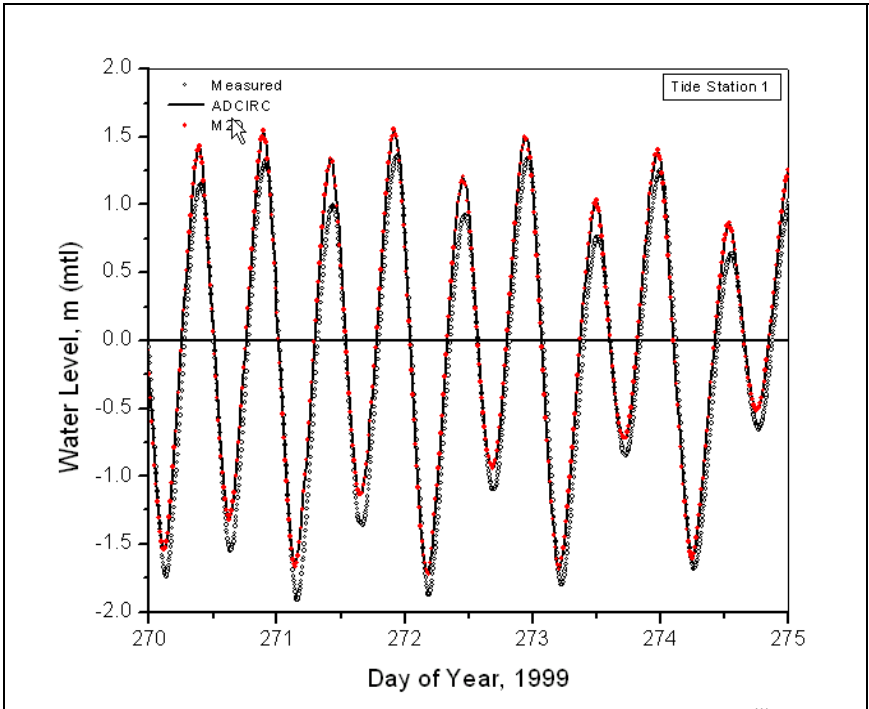


Figure R2. M2D water level results compared to ADCIRC calculations and measurements

SUBJECT: Response to Committee on Tidal Hydraulics, Independent Technical Review Sub-committee, review of Grays Harbor, WA, Numerical and Physical Modeling Draft Reports

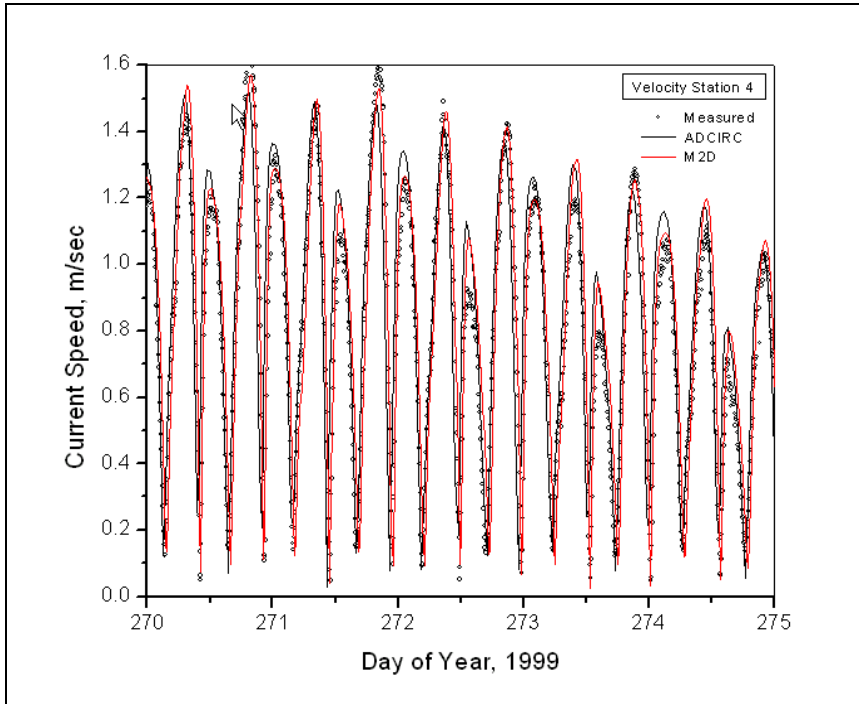


Figure R3. M2D current speed results compared to ADCIRC calculations and measurements at Station 4

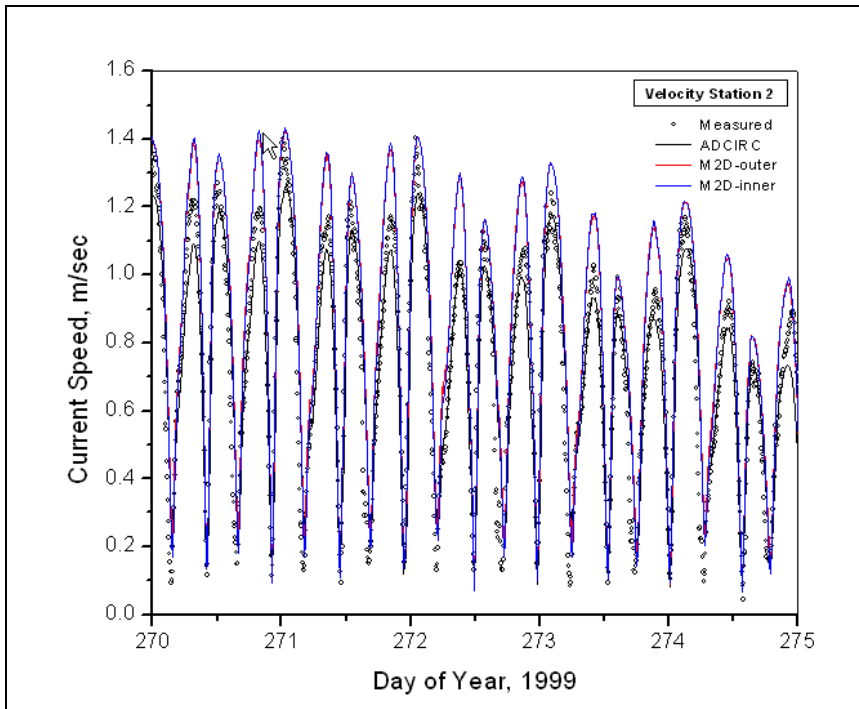


Figure R4. M2D current speed results compared to ADCIRC calculations and measurements at Station 2

SUBJECT: Response to Committee on Tidal Hydraulics, Independent Technical Review Sub-committee, review of Grays Harbor, WA, Numerical and Physical Modeling Draft Reports

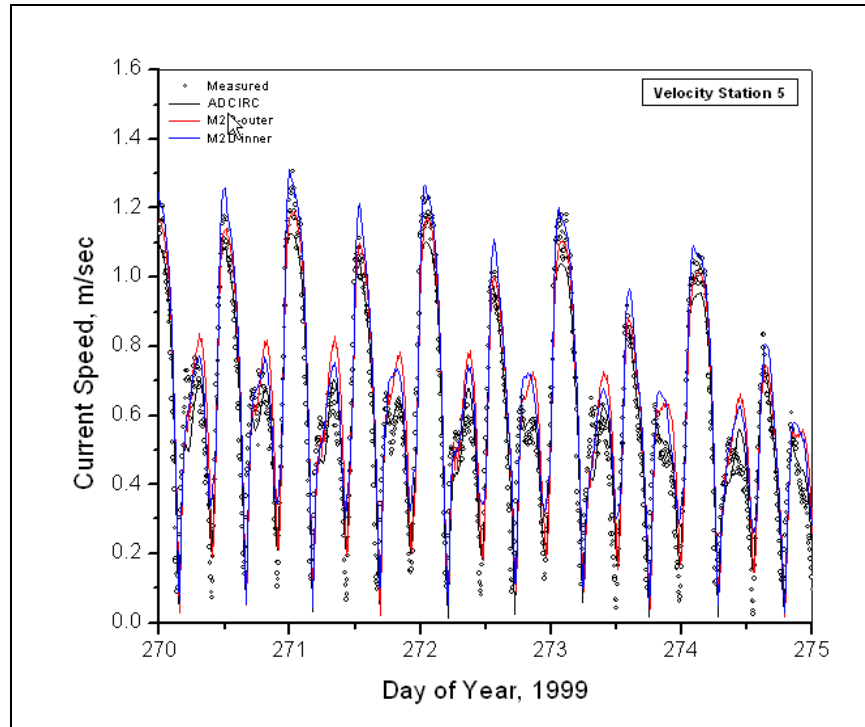


Figure R5. M2D current speed results compared to ADCIRC calculations and measurements at Station 5

Reference

Kraus, N.C., and Arden, H.T., (eds.). (2003). "North jetty performance and entrance Navigation channel maintenance, Grays Harbor, Washington, Volume I: Main Text," Technical Report ERDC/CHL TR-03-12, U.S. Army Engineer Research and Development Center, Vicksburg, MS.

(7) In addition to the explicit treatment of model validation, the effectiveness of the inset 20 m grid should be documented in the report. Driving a finer inset or nested mesh is common in modeling, but has numerous pitfalls that can render the results misleading. A grid refinement test and boundary extension test are needed to demonstrate that consistent breach results are obtained with different boundary specifications.

Response: See response to previous Item. Information on the M2D model can be found in the following two technical reports and the references cited therein:

Buttolph, A.M, Reed, C.W., Kraus, N.C., Ono, N., and Zundel, A.K. (2006). "Two-dimensional depth-averaged circulation model

SUBJECT: Response to Committee on Tidal Hydraulics, Independent Technical Review Sub-committee, review of Grays Harbor, WA, Numerical and Physical Modeling Draft Reports

CMS-M2D: Version 3.0, Report 2, sediment transport and morphology change,” Technical Report ERDC/CHL TR-06-___, U.S. Army Research and Development Center, Vicksburg, MS, in press.

Militello, A., Reed, C.W., Zundel, A.K., and Kraus, N.C. (2004). “Two-dimensional depth-averaged circulation model M2D: Version 2.0, Report 1, technical documentation and user’s guide.” Technical Report ERDC/CHL TR-04-2, U.S. Army Research and Development Center, Vicksburg, MS.

(8) As mentioned above, the Author’s morphology model required large [O(10)] adjustment of two parameters to get the model to agree with the Dutch, Moriches, and Grays Harbor observations, plus initial channel depth and width for Grays Harbor. This, and the fact that all morphological models suffer substantial uncertainty, leads us to recommend using an additional morphological model to study breach evolution. If there is agreement between the two models, then confidence is increased significantly.

Response: The Reviewers expresses concern several times about uncertainty and calibration of the newly developed morphologic model (Breach Model). This concern is addressed once in this reply, at Specific Comments Items 16-18, to avoid repetition.

Are the study conclusions supported by the model results?

(9) Although the model conclusions are supported by model results, we believe there is large uncertainty in the morphological model results and therefore in the concomitant conclusions of this report. Some of our concerns have been mentioned above. Others will be detailed below.

Response: The Reviewers express concern several times about uncertainty and calibration of the newly developed morphologic model (Breach Model). This concern is addressed once in this reply, at Specific Comments Items 16-18, to avoid repetition.

Do the studies accomplish their goals?

(10) We believe that the uncertainty that remains about the evolution of the breach precludes us from having reached the goal of confidently assessing the threat to the Federal Navigation Project (south jetty and navigation channel), or to the integrity of Half Moon Bay and Pt. Chehalis.

SUBJECT: Response to Committee on Tidal Hydraulics, Independent Technical Review Sub-committee, review of Grays Harbor, WA, Numerical and Physical Modeling Draft Reports

Response: The Authors disagree with this conclusion. The exhaustive analysis provided in the draft report, far exceeding any other known analysis of coastal breaching, indicate that there is a clear risk to the entire area should a breach be allowed to occur. Although, as in most coastal sediment process studies, it is not possible to be definitive in predicting breach evolution with complete reliability, findings in the morphologic (observational) record, and in the hydrodynamic and morphologic numerical modeling are consistent with a tendency for breach widening.

(11) From our study of available data, we believe that the 1993 breach may not have evolved to the worst-case, large-breach scenario that was studied. Therefore, the hydrodynamic conditions associated with the deep breach may not approximate reality and the prediction of an increasing breach depth by the morphological model may overstate the risk to the Federal Navigation Project. However, we do believe that the width of the breach would continue to increase, albeit at a slow enough time-scale that would permit a measured, physical closure response if deemed necessary. These points will be discussed further in our Specific Comments to follow.

Response: Calculations from the Reviewers' study of the available data were not provided for the Authors to evaluate, and so we cannot comment. The Reviewers express concern several times about uncertainty and calibration of the newly developed morphologic model (Breach Model). This concern is addressed once in this reply, at Specific Comments Items 16-18, to avoid repetition.

Specific Comments

(1) As recognized by the report Authors, Eq. (16), for longshore sediment transport (Page 91) is not dimensionally consistent. The problem is that if one wishes to apply this equation, it is necessary to know the units of the various dimensional quantities such as water mass density, etc. If one considers these to be in the metric system ($\rho = 1025 \text{ kg/m}^3$), the sediment transport coefficient, K , in the CERC equation is approximately 0.0026 compared to the usual default value of 0.77. It would have been useful to quantify and discuss the small value of this coefficient in the report.

Response: Eq. (16) is an empirical equation for estimating the longshore sediment (sand) transport rate Q in the units of m^3/day , as stated in the draft report, and the equation should not be taken out of that context. These units are convenient because the breaching model calculates in fractions or increments of days. Eq. (16) appears in Komar (1998, page 392), including the empirical factor of 1.1 (which

SUBJECT: Response to Committee on Tidal Hydraulics, Independent Technical Review Sub-committee, review of Grays Harbor, WA, Numerical and Physical Modeling Draft Reports

carries units), obtained for a value of $K = 0.7$. A similar form of the equation, again mindful of the units, is presented in the Shore Protection Manual (1984) on page 4-96; after expressing the energy flux factor in its components, the resultant empirical coefficient becomes 0.625 instead of 1.1, in main part because of use of significant wave height instead of RMS wave height. In summary, Eq. (16) serves its intended purpose and is compatible with a value of $K = 0.7$, close to the usual default value as mentioned by the Reviewers. Eq. (16) does not imply a value of 0.0026 (about three-hundred times smaller than the default value) as stated by the Reviewers. Operationally, if this were the case, longshore sediment transport rates as computed by the breach model in time-dependent manner from the input waves would not have achieved the hundreds of thousands of cubic meters per year as documented in the draft report.

References

- Komar, P.D. (1998). "*Beach processes and sedimentation*," 2nd ed., Prentice Hall, NJ, 544 pp.
- Shore Protection Manual*. 1984, 2 Vols., 2nd ed., U.S. Army Engineer Research and Development Center, Vicksburg, MS, U.S. Government Printing Office, Washington, DC.

(2) The use of "flow depth" relative to MLLW causes semantics issues. Flow depth connotes a water level. Bottom elevation does not and does not run the risk of being misinterpreted. For example, Page 44 states "The breach in December 1993 was 84 m wide with a maximum depth of 1.5 m MLLW (Table 3). Shouldn't this be "controlling elevation of + 1.5 m MLLW"? This use of confusing terminology continues throughout the report.

Response: Information characterizing the Grays Harbor breach of December of 1993 was interpreted from aerial photography. The breach that occurred on 10 December 1993 was photographed on 17 December 1993. A GIS analysis estimated the breach width at 85 m (see draft report Figure 18 and Table 3). The depth in the breach was estimated based on the known tide elevation evident in Figure 13, the locations of the wet-dry line, vegetation line, and other identifiable points. Therefore, reference to a maximum depth in the report is that represented in the grid for the numerical model as determined from the process above (also documented on draft report page 32). In response to the Reviewers, the statement on page 44 referenced above has been changed to "Based on examination of aerial photography, the breach in December 1993 was 85 m wide with a controlling elevation of near +2.0 m, mllw (see Figure 18 and this was applied to generate the grid

SUBJECT: Response to Committee on Tidal Hydraulics, Independent Technical Review Sub-committee, review of Grays Harbor, WA, Numerical and Physical Modeling Draft Reports

for the hydrodynamic simulations).” In addition to page 46 discussed in Item 3 below, depth was originally referenced in survey measurements on pages 24, 27, 32, and 57. These pages were modified to improve clarity of discussion.

- (3) In referring to the March 1994 breach morphology, Page 46 states “The March 1994 breach was measured to be 140 m wide with a maximum elevation of + 1.0 m MLLW (Table 3).” However, Figure 19 (Page 24) shows the controlling depth for March 1994 to be approximately 1.6 m mllw at Transect 1. Clearly, water must pass Transect 1 to flow through the breach and so, for the three transects, this is the controlling transect. Other cross-sections for surveys that are not available could have higher controlling elevations. Greater clarity could be gained by consistent use of a datum and a definition sketch, specifically the relationship of MSL and the other normal tidal planes to MLLW at the entrance, and how Figure 19 MLLW elevations relate to MSL and breach depth in Figures 109 and 111. See Specific Comment (19).

Response: The Reviewers appear to be referring to an older version of the report. The report draft dated 21 January 2005 contained the following: “The March 1994 breach was measured to be 140 m wide with a maximum depth of + 1.0 m mllw (Table 3).” The “maximum depth” was intended to communicate the elevation of the lowest point in the breach. Therefore, the statement on page 46 has been changed to “The March 1994 breach was measured to be 140 m wide, with the lowest point being +1.0 m, mllw (Table 3).” Also, the datum for Figure 111 was changed to mllw for consistency with data presented in Chapter 2. The Water Level section in Chapter 2 discusses the tidal range. The following table was included in the report to identify the relationship between tidal datum planes.

Datum	Adjustment (m)
mhhw	2.79
mhw	2.57
msl	1.50
mlw	0.42
mllw	0

- (4) Did the application of STWAVE include bottom friction or only white-capping as a mechanism of wave energy dissipation? Perhaps this

SUBJECT: Response to Committee on Tidal Hydraulics, Independent Technical Review Sub-committee, review of Grays Harbor, WA, Numerical and Physical Modeling Draft Reports

concern could be answered by providing the South Beach significant breaking wave height for one of the deep water wave heights, say the 5 m deep water wave height. What wave spectrum was used for each of the three wave heights in Table 5?

Response: The version of the STWAVE model applied in this study was validated with field data collected in 1999 and is documented in Chapter 7 of the Technical Report ERDC/CHL TR-03-12 (Kraus and Arden 2003). This version of STWAVE simulates depth-induced wave refraction and shoaling, current-induced refraction and shoaling, depth- and steepness-induced wave breaking, diffraction, wind-wave growth, and wave-wave interactions and white capping that redistribute and dissipate energy in a growing wave field. The modeling and calibration were also reported by Cialone and Kraus (2001), cited in the draft report. The validation of the STWAVE model is demonstrated for selected stations in Figures R6 to R8. The model calculations compare well to the data.

It has been our experience that wave simulations are not sensitive to bottom friction on sandy coasts. To assess the sensitivity of the wave height estimates to bottom friction for Grays Harbor, the model was run with a bottom friction coefficient of 0.01 for a sandy bottom. Figures R6-R8 show calculated wave heights with and without bottom friction for Stations 2, 4, and 5, respectively, together with the measurements. The RMS differences between the with- and without-bottom friction results for each station and are listed in Table ITR-2, and this table has been added to the report. There is no significant difference in calculation results with and without bottom friction, as expected by the Authors, and the simulated results compare well with the measurements. A TMA wave spectrum was applied for each wave condition in Table 5 of the draft report.

Station	RMS Difference (m)
2	0.07
4	0.07
5	0.04

SUBJECT: Response to Committee on Tidal Hydraulics, Independent Technical Review Sub-committee, review of Grays Harbor, WA, Numerical and Physical Modeling Draft Reports

Reference

Cialone, M.A., and Kraus, N.C. (2001). "Engineering study of inlet entrance hydrodynamics: Grays Harbor, Washington, USA," *Proceedings Coastal Dynamics 01*, ASCE, 413-422.

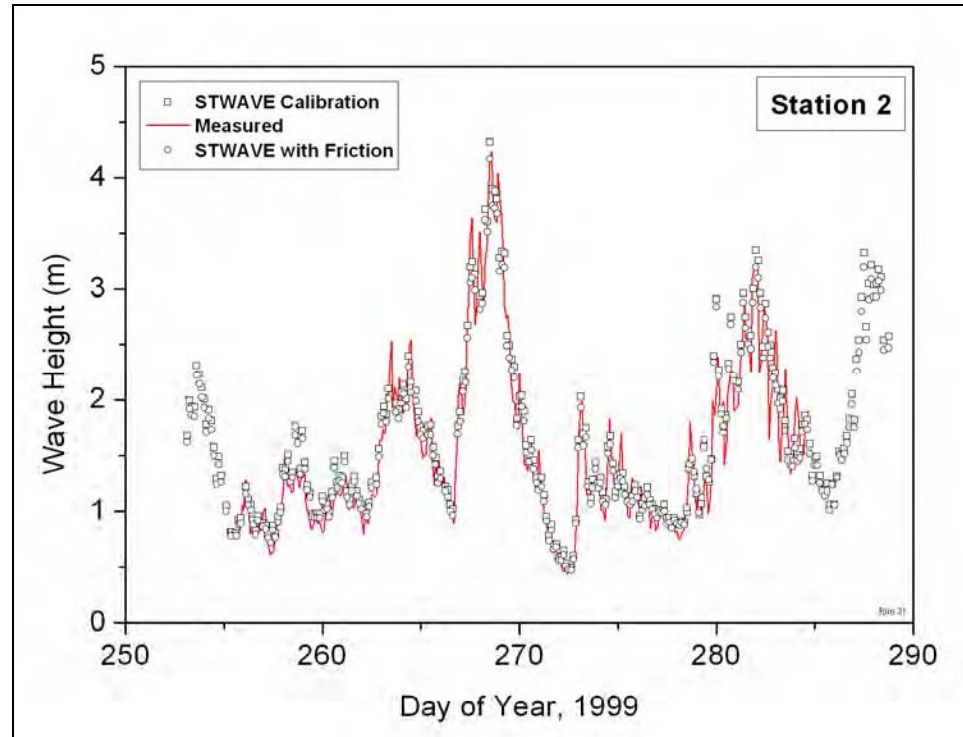


Figure R6. Calculated wave height with and without bottom friction at Station 2 compared to measurements

SUBJECT: Response to Committee on Tidal Hydraulics, Independent Technical Review Sub-committee, review of Grays Harbor, WA, Numerical and Physical Modeling Draft Reports

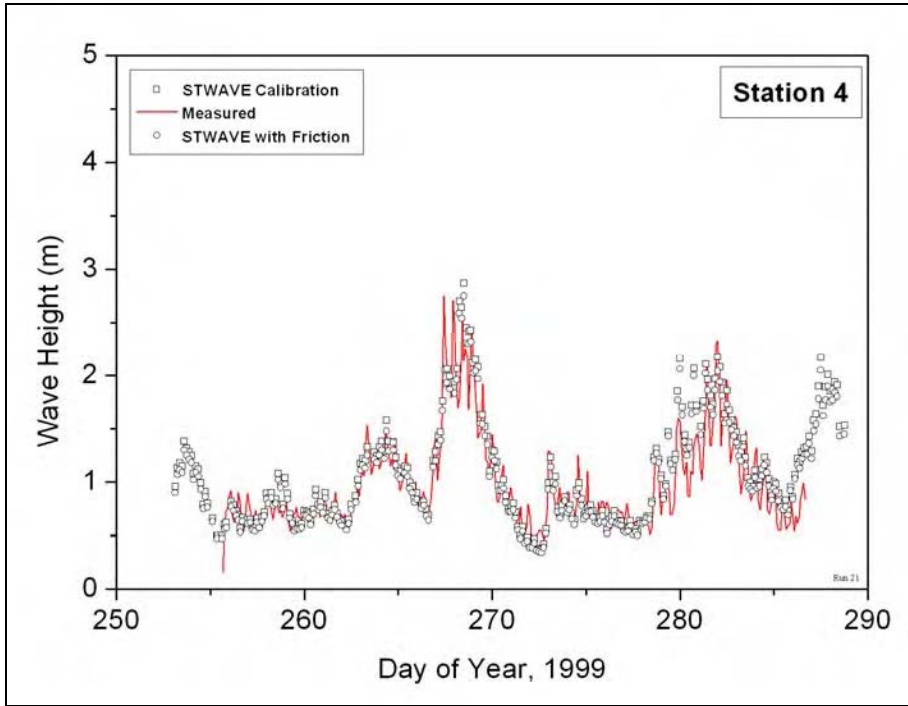


Figure R7. Calculated wave height with and without bottom friction at Station 4 compared to measurements

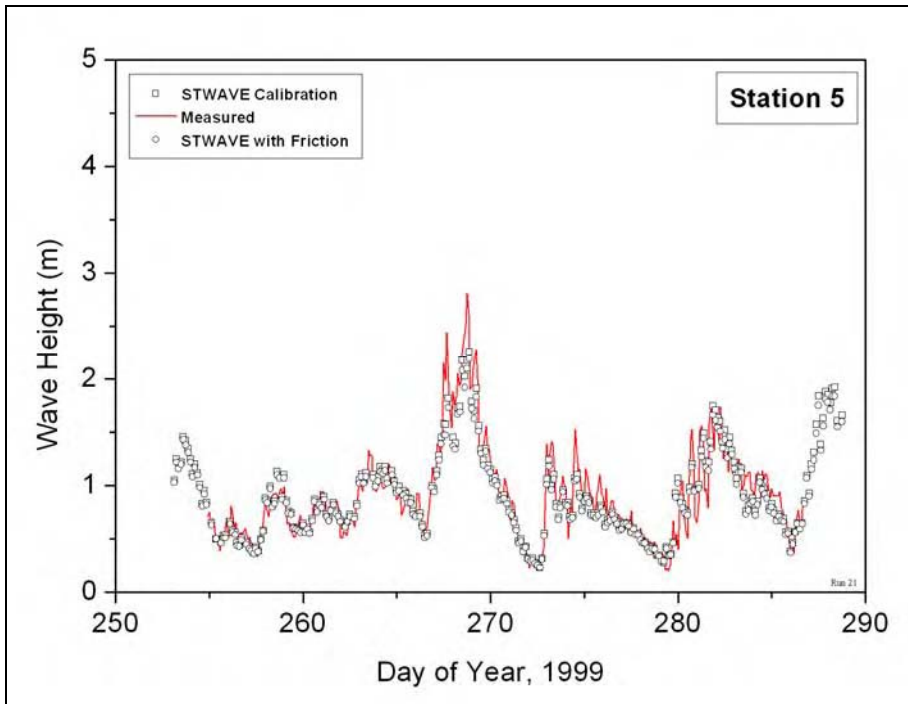


Figure R8. Calculated wave height with and without bottom friction at Station 5 compared to measurements

SUBJECT: Response to Committee on Tidal Hydraulics, Independent Technical Review Sub-committee, review of Grays Harbor, WA, Numerical and Physical Modeling Draft Reports

(5) The Reviewers would have benefited by the presentation of a profile representative of the South Beach. It is stated (Page 15) that 61 million cubic yards were eroded off South Beach. Thus a series of profiles for various times would be extremely useful and relevant. Comment 20 expands on the complexity of the sediment budget and longshore transport estimates; and it is noted that the control volume domain for the 61 million cubic yards appears to be located in a nearshore zone seaward of the wave breaking zone and exclusive of the beach and dunes. The salient point is the beach south of the South Jetty is erosional.

Response: The draft report contains the information that the 61 million cubic yards were lost from the nearshore region off South Beach from 1900 to 1990, an area that is located seaward of the wave breaking zone and is exclusive of the beach and dunes. Beach profiles were not analyzed for this calculation, and the authors are not aware of beach profile data available for this time period. The volume change was calculated from bathymetry survey maps that can be found in Chapter 3 of Technical Report ERDC/CHL TR-03-12 (Kraus and Arden 2003). This information complements the shoreline recession data from the beach south of the jetty. The survey and shoreline data indicate that the South Beach was erosional, which led to dune erosion in the early 1990s and eventually to the breach.

(6) The Reviewers would have benefited by knowledge of the maintenance dredging requirements, the associated locations and the placement locations.

Response: A thorough review of the maintenance dredging and disposal for the Gray Harbor Navigation Project is available in Chapter 2 of Technical Report ERDC/CHL TR-03-12 (Kraus and Arden 2003).

(7) Our understanding is that the output from ADCIRC served as input to the 100-m grid hydrodynamic model M2D, which in turn provided boundary conditions for the 20-m grid M2D model which represented the detailed hydrodynamics over a limited area that included only a limited portion of the area between the jetties (Figure 27). However, ADCIRC did not include wave effects and the longshore currents associated with waves can contribute substantially to the flow magnitudes and directions in the entrance (for example, Figures 34 and 35). Would the contributions from longshore currents affect the boundary conditions for the 100-m grid significantly? To address General Comment (6), it would have been useful to present the ADCIRC domain and validation with the 1999 field data that is presented in the section "Water Level" (p.19); and some

SUBJECT: Response to Committee on Tidal Hydraulics, Independent Technical Review Sub-committee, review of Grays Harbor, WA, Numerical and Physical Modeling Draft Reports

presentation of the ADCIRC boundary conditions used to drive the M2D model.

Response: The regional ADCIRC model grid extends from Vancouver Island, Canada, at its northern limit to Eureka, CA, at its southern limit, reaching to depths of 3,500 m offshore. It is not feasible or necessary to run a surface wave model simultaneously with such a regional ADCIRC model. To provide reliable forcing for the inner M2D model, the outer (100-m cell size) M2D grid extent was established to allow a current to be generated at some distance from the area of interest by wave information calculated with STWAVE, and the inner M2D grid was driven with the resultant water levels and current that includes tide and wave-generated contributions. The ADCIRC domain is documented in ERDC/CHL TR-03-12 (Kraus and Arden 2003), and the calibration was discussed in response to ITR General Comment (6).

(8a) It is unclear from the report which elements of the M2D model output were used as input to the Breach Model. Is M2D/STWAVE only providing the hydrodynamic wave elevations? The wave-driven dynamics seem to be contained only in the Breach model as simple empirical relations (e.g., wave setup). Also the application of wave setup in the Breach Model is unclear.

Response: The Breach Model contains an internal monochromatic wave model that propagates waves, in this study, from the Grays Harbor CDIP gauge to wave breaking. The “epsilon” factor in Eq. 6, pertaining to monochromatic waves in the laboratory (Bowen et al. 1968) was calibrated against setup calculated with the random wave radiation stresses furnished by STWAVE as input the inner M2D circulation model. The comparison point for the setup in M2D is shown in Figure R9. The calculated wave setup was added to the mean water surface elevation input as obtained from water level gauges in the present application. The procedure for calibrating the Breach Model setup equation is described on page 107 of the draft report, and development of input water level measurements is described on pages 19-21.

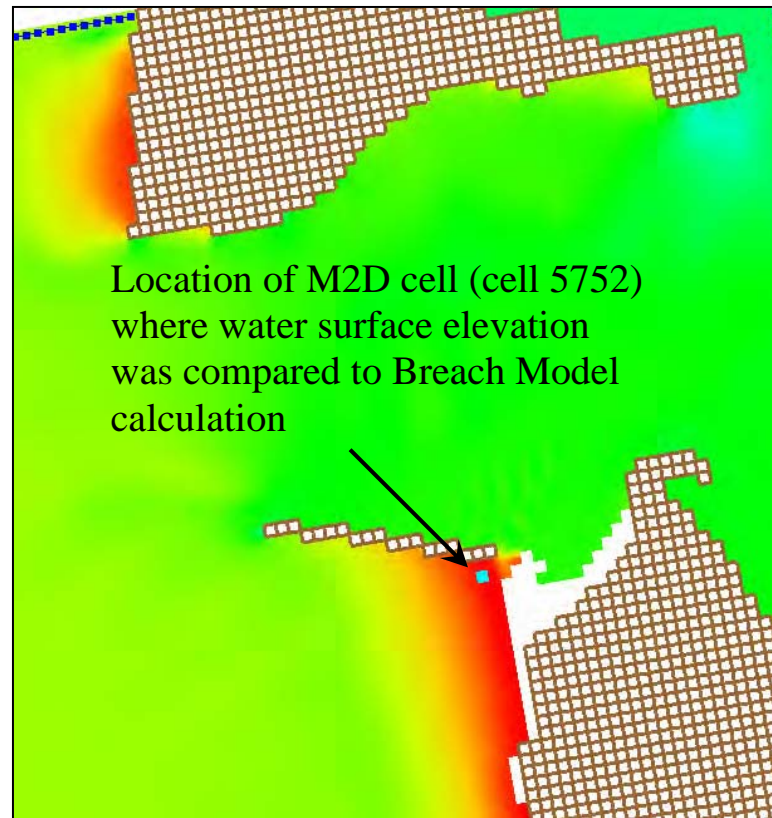


Figure R9. Location of wave setup calibration point in M2D

(8b) The Breach Model wave setup Eq. (6) on page 90 has a laboratory-derived gamma, where H_b is either H_{sig} or H_{rms} (which wave height statistic is used is not clear from the text). In addition, there is a “fix-it” parameter, epsilon, that is obtained in a less than clear way. Northwest beaches have significant wave setup and this process therefore requires care and attention.

Response: H_{sig} was employed in the setup calculation. The value of the adjustment parameter was explained on page 107 and in Figure 109 of the draft report, and reference is made here to discussion at Item (8a).

(8c) The literature is rich with examples of physics-based estimates of wave setup. A common approach is to use the standard wave decay model (Battjes and Janssen 1998) that incorporates the roller concept (Svendsen 1984; Stive and De Vriend 1994) to delay the dissipation of the organized energy. Recently an inner surf zone bore model (Aarninkhof and Roelvink 1999) has been used to extend the computations up to zero water depth.

SUBJECT: Response to Committee on Tidal Hydraulics, Independent Technical Review Sub-committee, review of Grays Harbor, WA, Numerical and Physical Modeling Draft Reports

Response: The Authors question the phraseology “rich,” according to our study of performance of available predictive equations for field use. Eq. 6 of the draft report is physics based, derived from the original work validating the wave radiation stress concept (Bowen et al. 1968). Perhaps the Reviewers meant to say “random wave estimates?” The Breach Model developers have experience with sophisticated wave models including the wave roller (e.g., Smith et al. 1991; Larson and Kraus 1993). However, such computation-intensive models are not compatible with practical engineering calculations at breaches in the field, where little information exists on bottom topography, cross section of the barrier spit or island, and day and time of opening of the breach. It would be a question of calculating with great precision, but little accuracy, while consuming large computer resources as compared to the present Breach Model.

The draft report authors devoted considerable time examining predictive formulas for setup under random waves. Formulas available at the time of the original study did not perform well as judged by operation of the Breach Model. Therefore, the approach of calibrating to the M2D model prediction of wave setup as driven by a random wave model was taken, as described above and in the draft report. Since the time of the original report writing, a new formula for random wave setup has become available (Stockton et al. 2006):

$$\eta_{setup} = 0.35\beta_f\sqrt{H_0L_0}, \text{ where } \beta_f \text{ is the foreshore slope, and } H_0 \text{ and } L_0$$

are the deepwater wave height and wavelength, respectively. This formula produced results similar to those of the original procedure (both in checking against M2D calculations and in performance of the Breach Model for the same inputs) and was, therefore, adopted in the Breach Model. Stockton et al. (2006) document the large scatter in the available field data sets. Associated material in the draft report was revised. We note in passing that beach foreshore slope becomes ambiguous during storms, when the beach profile changes greatly.

SUBJECT: Response to Committee on Tidal Hydraulics, Independent Technical Review Sub-committee, review of Grays Harbor, WA, Numerical and Physical Modeling Draft Reports

References

- Bowen, A.J., Inman, D.L., and Simmons, V.P. (1968). "Wave set-down and wave set-up," *Journal of Geophysical Research*, 73, 2,569-2,577.
- Larson, M., and Kraus, N.C. (1991). "Numerical model of longshore current over bar and trough beaches," *Journal of Waterway, Port, Coastal and Ocean Engineering*, 117(4), 326-347.
- Smith, J.M., Larson, M., and Kraus, N.C. (1993). "Longshore current on a barred beach: Field measurements and calculation," *Journal of Geophysical Research*, 98(C12), 22,717-22,731.
- Stockdon, H.F., Holman, R.A., Howd, P.A., and Sallenger, A.H. (2006). "Empirical parameterization of setup, swash, and runup," *Coastal Engineering*, 53(7), 573-588.

(9) Northwest swash excursions are exceptionally large and therefore significant to any study of beach dynamics. There are empirical formulas that can be used to estimate both wind wave ($f > 0.05\text{Hz}$) and infragravity wave ($f < 0.05\text{Hz}$) swash excursions (Holman and Sallenger 1985; Ruessink et al. 1998). These relations have been recently verified over a large range of reflective and dissipative natural beaches (Stockdon et al. 2002).

Response: The Authors agree and appreciate that swash excursions can be significant on the northwest Pacific coast of the United States. Stockdon et al. (2006) provide empirical predictive formulas for setup, swash, and runup. Uncertainty in predictive capability is large, even for data collected along single transects under reasonably uniform alongshore conditions. The role of extreme swash processes in models of swash sediment transport, barrier island breaching, and beach profile change must be examined in a dedicated research effort that was beyond the scope of the present applied study conducted within a fixed time interval. Problems to be addressed would include appropriateness and representation of 2-percent runup in sediment-transport models.

(10) Page 6 states in referring to crenulate bays in general "If the water level is held constant, an equilibrium shape is reached..." An equilibrium shape requires a downdrift fixed "control point". We recognize that such a downdrift control point exists at Half Moon Bay; however, the statement appears to be meant to be general.

Response: We believe that the Reviewer meant to write "updrift" instead of "downdrift" appearing in two sentences in Item 10. The

SUBJECT: Response to Committee on Tidal Hydraulics, Independent Technical Review Sub-committee, review of Grays Harbor, WA, Numerical and Physical Modeling Draft Reports

subject sentence has been clarified to “If the water level is held constant and a fixed control point such as the south jetty terminus exists, an equilibrium shape is reached similar to an open-coast crenulate bay.”

(11) Was the actual tide used in the simulations or the synthesized tide of Equation 1 (p.20)? It is not specific on what drives ADCIRC to drive M2D, or why the M2D water levels for the ocean and bay are not used to drive the morphological model.

Response: The purpose of the hydrodynamic simulations was to examine the relative change in flow from a no-breach condition to breach in various stages of development. The simulations were done to determine if the breach would hold negative consequences for the Federal navigation project. Because the hydrodynamic simulations were intended for relative comparison, the ADCIRC model was driven with tidal constituents from the calibration period, which included a complete spring-neap tide. The purpose of the morphologic Breach Model was to simulate the historical evolution of the breach. The M2D model was driven by the ADCIRC model. The morphologic model was forced with data corresponding to the time period of the breach to simulate the historical evolution of the breach. The synthesized tide discussed on page 20 of Chapter 2 was applied for this purpose.

(12) Do the data show that waves do not affect water levels in the harbor? See statement on Page 39 “It was found that none of the alternatives examined changed water level significantly.” Does this statement address the bay water levels “far” from the breach? We would expect some differences in the breach area.

Response: The alternatives in the statement on page 39 refer to the alternative breach configurations, not to the various wave conditions. The existence of the breach in the simulations did not change the calculated water level in the vicinity of the breach, because the cross-sectional area of the breach is very small compared to the cross-sectional area of the Grays Harbor entrance. The sentence on page 39 has been changed to “It was found that none of the breach configurations examined changed water level significantly.”

(13) Is it coincidence that the south beach accretion stopped when the south jetty was repaired?

SUBJECT: Response to Committee on Tidal Hydraulics, Independent Technical Review Sub-committee, review of Grays Harbor, WA, Numerical and Physical Modeling Draft Reports

Response: It is unclear as to which jetty repair and beach accretion the Reviewers are referring. The south jetty was constructed from 1898 to 1902. By 1904, the shoreline adjacent to the jetty had advanced 3,000 ft. The jetty deteriorated from 1904 to 1933, and by 1939 the shoreline had receded about 2,700 ft. The first south jetty repair occurred from 1933 to 1939, and by 1946 the shoreline had advanced 1,100 ft from its 1939 position. Jetty deterioration led to shoreline recession after 1959, but stabilized after a second jetty repair in 1966. In the early 1970s, the shoreline again began to recede, and the beach was generally erosional up through the time of the breach. Vegetation line data indicate recession between 1967 and the time of the breach. For additional information on shoreline change near the south jetty, the interested reader can consult Osborne, Wamsley, and Arden (2003), referenced in the draft report.

Reference

Osborne, P.D., Wamsley, T.V., and Arden, H.T. (2003). "South jetty sediment processes study, Grays Harbor Washington: Evaluation of engineering structures and maintenance measures," Technical Report ERDC/CHL TR-03-4, U.S. Army Engineer Research and Development Center, Vicksburg, MS.

(14) There is some confusion regarding the ebb flows for the 1993 breach. For example, Figure 50 (Page 52) presents the time series of current speed for Point 3, the location of which is shown in Figure 49 (Page 51). In referring to Figure 19 (Page 24), Point 3 is at approximately the minimum elevation and thus the ebb flow should persist the longest of the tidal cycle. However, Figure 50 does not show any ebb flows. (We realize that Figure 50 represents "current speed" and thus flow direction is not shown; however, we would expect to see the current speed first drop to zero and then increase as an ebb flow.) Runs 105 and 106 do show ebb flows. These ebb flows in these two runs lasted approximately one-half as long as the flood flows which doesn't seem reasonable, but may be correct. Why not show the velocity (with a sign) rather than the speed to eliminate any ambiguity? To assist in understanding/interpretation, it would have been very useful to present the signed total discharge (positive and negative) through the breach. In this way, the Reviewer could better assess the issues raised in this comment. Perhaps in the same plot, the signed discharge through the jetties could be presented (on a different scale) for comparison purposes. Also, for the large breach, the portions of the flow which are flood and ebb are labeled (example, Figure 77, Page 68). Couldn't this have been done for the other breach geometries?

SUBJECT: Response to Committee on Tidal Hydraulics, Independent Technical Review Sub-committee, review of Grays Harbor, WA, Numerical and Physical Modeling Draft Reports

Response: Draft report Figures 39, 50, and 60-63 were regenerated with the ebb and flood flow indicated on the plot and substituted into the report. Such labeling, which had been inadvertently omitted on the subject figures, is consistent with other figures in the report and allows understanding of direction of the current. It was not feasible to redo all the runs and compute discharges.

(15) Page 112 notes that the 1993 breach resulted in 210,000 m³ (net) being deposited in Half Moon Bay. How does this compare with the results of the breach model?

Response: This was a stimulating question. The volume change estimate of 210,000 m³ is based on a volumetric analysis from measurements as discussed on page 25 of the draft report. For comparison of this estimate to the Breach Model predictions, as suggested by the Reviewers, the model was run with the Stockdon et al. (2006) irregular wave setup prediction for the three potential longshore sediment transport rate regimes (as done in the original report, but with a calibrated monochromatic wave setup prediction). Cumulative volume was tracked for flood and ebb flow from the calculated time of opening of the breach, Table ITR-3 summarizes the calculation results at the beginning and end of August 1994, to the nearest 1,000 m³. The calculated volumes demonstrate a flood bias for sediment transport, and the cumulative volume issuing through the breach on flood best approximates the deposition estimated in the aerial photograph for a smaller longshore transport rate. As the longshore transport rate becomes larger, the breach tends to fill, decreasing depth and current velocity in the breach, hence the sediment transport rate, through it.

Longshore Transport Rate m ³ /year	Flood	Ebb
	1 August; 31 August	1 August; 31 August
200,000	236,000; 282,000	29,000; 46,000
400,000	138,000; 167,000	12,000; 21,000
600,000	48,000; 55,000	1,000; 2,000

(16) The Breach Model is interesting and complex. A substantial and laudable effort was made to calibrate the model to both model and field data with good success. Yet, fairly heavy calibration was required to

SUBJECT: Response to Committee on Tidal Hydraulics, Independent Technical Review Sub-committee, review of Grays Harbor, WA, Numerical and Physical Modeling Draft Reports

achieve agreement in the calibrations. Table 1 lists the calibration coefficients α and β for the Dutch Physical Model, Moriches Inlet, and Grays Harbor. The Grays Harbor calibration also varied the pilot channel size to improve agreement with observations.

Table 1. Calibration Coefficients α and β Used in Breach Model

Calibration With	Calibration Coefficients	
	α	β
Dutch Physical Model	2.5	0.5
Moriches Inlet, NY	0.05	50
Grays Harbor, WA	0.23	15

These calibrations demonstrate requirements for a wide variation in coefficients to provide the best fit for the particular situation, even limiting the comparison to prototype conditions, possibly illustrating a lack of incorporating the correct (and complex) physics. This statement is not intended to not give proper recognition to the efforts made on this difficult problem nor to the advances made, but rather to attempt to put into context the empiricism in the breaching model and the state of art of this complex problem.

Response: The Reviewers' concerns are appreciated, as are the recognition of the difficulty in simulation of coastal inlet breaching and the effort made by the Authors. To the Authors' knowledge, at the time of the subject study, no published process-based model of coastal barrier breaching existed, and at present no other such documented model is yet available. Because of the nature of the pioneering work performed in this study to develop a process-based Breach Model, available pertinent and competent data were examined (Dutch physical model) or developed (Moriches Inlet). As noted in the draft report, the initial condition for the pilot channel in the Dutch physical model and the initial conditions for the barrier spits for both Moriches Inlet and Grays Harbor are not known, which introduce uncertainty into a process-based calculation procedure. Depth measurements were not made in the Dutch physical model (because of the rapid breach opening; verified by the Authors with the Dutch investigators), so the Breach Model comparisons with the Dutch physical model can only be judged as reproducing qualitative trends.

As is well known, coastal sediment transport is difficult to represent quantitatively in small-scale physical models as in the Dutch physical model. Apart from the ambiguity in initial conditions for the available

SUBJECT: Response to Committee on Tidal Hydraulics, Independent Technical Review Sub-committee, review of Grays Harbor, WA, Numerical and Physical Modeling Draft Reports

data, it is considered unproductive and inappropriate to compare Breach Model calibration coefficients determined for a small-scale two-dimensional physical model of catastrophic breaching, as pertains to a dike break in the Dutch physical model, to those determined for natural and gradual breach opening in the three-dimensional situation of one of the largest stabilized coastal inlets in the United States. If the small-scale Dutch physical model with its ambiguous conditions is eliminated from the comparison in the Reviewers' Table 1, the calibration coefficients for the Moriches Inlet and Grays Harbor calculations are within a factor of 4 to 5, a difference that is accounted for in part by ambiguity in initial conditions for both sites.

Subsequent to writing of the subject draft report, in August and September 2005, two moveable-bed physical model experiments of barrier island breaching were conducted at CHL in a 64-m long, 3-m wide wave flume with an idealized, sand-substrate barrier island. A pilot channel was cut in the barrier to initiate flow through breach. The barrier was constructed with a 1:10 foreshore slope, a level plateau, and a 1:7 backshore slope, with total volume of 45.5 m³. The first experiment (BR1) was forced by a near-constant 15-cm head difference sustained on the offshore side of the barrier, with depressed water level on the bay side of the barrier, controlled by pumping water out of the bay and into the offshore. This situation more closely replicates breaching of coastal barriers as compared to catastrophic dike failure under a large head difference (Dutch physical model). The second experiment (BR2) was similar to the first, but with the addition of 0.1-m high monochromatic waves with a 3.1-sec period. Breach depth and width were measured manually. The revised report contains further information on the physical model study, referred to as "USACE" for U.S. Army Corps of Engineers in the present discussion.

Table ITR 4 replicates the Reviewers' Table 1 and includes results of calibration of the Breach Model to the larger scale USACE physical model with and without waves. The value of the main transport rate calibration coefficient α is of the same order as that found for Grays Harbor, whereas the coefficient that tends to govern widening of the breach, β , is smaller than determined for the two field breaches, but larger than for the Dutch physical model. Observations during the USACE physical model experiments showed that slumping of the breach banks greatly controlled breach evolution and was judged to introduce a scaling distortion as compared to processes at a breach in the field. The calibrated Breach Model correctly reproduced the trend in deepening and widening observed in the USACE physical model experiments, shown in Figures R9 and R10.

Table ITR-4 Calibration Coefficients α and β Used in Breach Model		
Calibration With	Calibration Coefficient	
	α	β
Dutch Physical Model	2.5	0.5
Moriches Inlet, NY	0.05	50
Grays Harbor, WA	0.23	15
USACE Physical Model	0.5	1.5 (no waves) 2.3 (with waves)

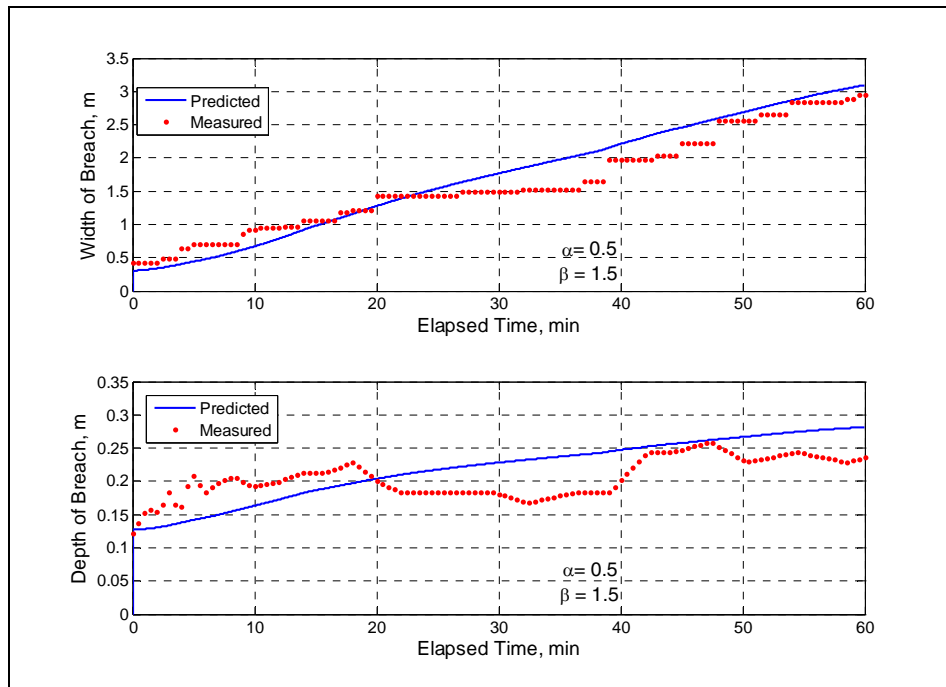


Figure R9. Breach width and depth, BR1

SUBJECT: Response to Committee on Tidal Hydraulics, Independent Technical Review Sub-committee, review of Grays Harbor, WA, Numerical and Physical Modeling Draft Reports

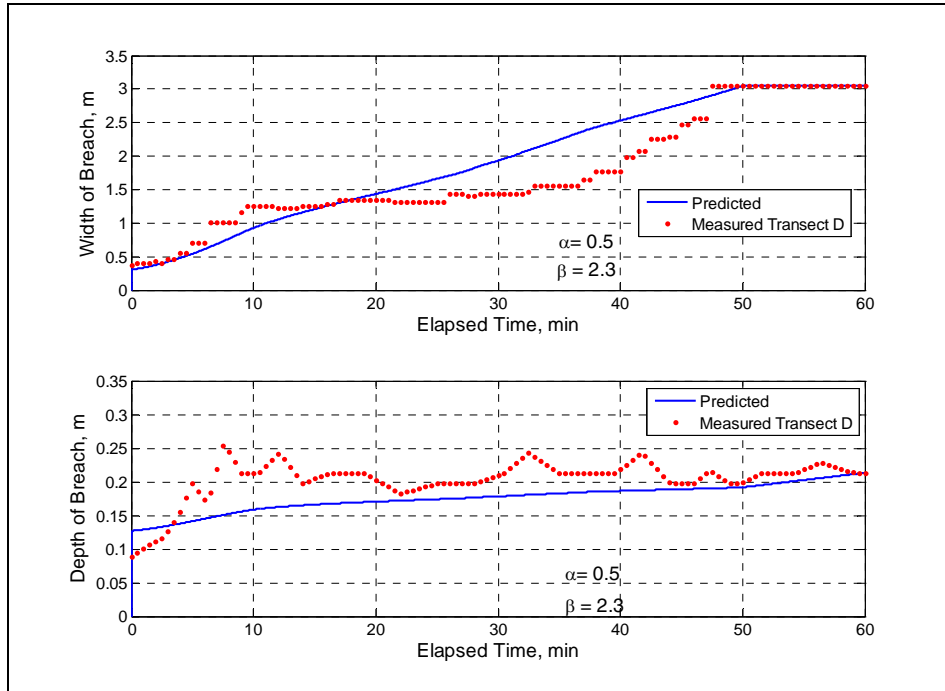


Figure R10. Breach width and depth, BR2

(17) In response to the question regarding the applicability of the models applied to determine the possibility of continuing enlargement of the breach, we again note the complexity of this problem and that some breaches in nature have remained open and dominated adjacent inlets eventually resulting in their closure whereas other breaches have formed during storms and closed shortly thereafter. A factor at Grays Harbor which would favor a breach remaining open and enlarging is the long-term erosion of South Beach.

Due to the complexity of this problem and the low level of understanding of the many factors, it is appropriate to apply as many methods to address this problem as possible. There are other approaches that have been developed to address the stability of multiple openings to a bay system. Although none of the available methods can be considered as valid in a pure predictive mode, the application of more than one method is valuable because comparison of results from different approaches can assist in assessing confidence to be associated with model output.

Two approaches that are available are those of Escoffier (1940) and van de Kreeke (1990). Similar to the breaching method applied, the Escoffier approach provides an approximate method to determine whether a pilot channel is stable or unstable to perturbations and to predict the equilibrium cross-sectional area via the O'Brien relationship between tidal prism and

SUBJECT: Response to Committee on Tidal Hydraulics, Independent Technical Review Sub-committee, review of Grays Harbor, WA, Numerical and Physical Modeling Draft Reports

channel cross-sectional area. Although the Escoffier method evaluates the stability of a single inlet into a bay and thus would not be strictly appropriate for this problem, its application could shed useful information. However, van de Kreeke has further developed the Escoffier concept to represent multiple inlets serving a bay and whether one opening will grow at the expense of the other. Thus, the van de Kreeke method would seem to be an appropriate candidate to apply to Grays Harbor.

In general, experience with the 1993 breach and the current availability of a large stock pile of sand available for closure immediately south of the 1993 breach reduces the possibility of a new breach expanding too rapidly for closure in a timely manner if and when such a decision is made.

Response: We agree with the Reviewers that the long-term erosion at the South Beach, which is well documented, would tend to promote breach enlargement and stability, as well as breach opening, because sediment supply is limited for filling the breach channel and causing closure. Although the beach is eroding, longshore sediment transport still occurs. For this reason, the Breach Model was run with three values of the net longshore transport rate as 200,000, 400,000, and 600,000 m³/year, a range selected to encompass the actual transport condition along the South Beach. The model performed as expected (Figures 110 and 111) in predicting increased depth and width of the breach with decreasing sediment input by longshore sediment transport.

The Escoffier (1940, 1977) analysis for predicting the stability of a single inlet and the van de Kreeke (1985, 1990) extension of the Escoffier analysis to multiple inlets are not applicable to the present situation in which a small inlet (the breach) having a channel cross-sectional area less than 1 percent of the large Grays Harbor Entrance, as shown in Figure 114 (revised; see Item 19), is located next to the larger inlet. Uncertainty in the inlet stability curve relating minimum channel cross section and tidal prism, such as that of Jarrett (1976), entering these analyses is much greater than the uncertainty in combined entrance and breach cross-sectional areas. In addition, such analyses do not explicitly consider variable wave conditions and longshore sediment transport, which includes the sediment deficit along the South Beach emphasized by the Reviewers.

According to observations of inlet entrances and breaches, an inlet with a shorter channel will tend to dominate an inlet with a longer channel because of less frictional impedance. Therefore, a breach through a narrow barrier island adjacent to a long inlet such as at

SUBJECT: Response to Committee on Tidal Hydraulics, Independent Technical Review Sub-committee, review of Grays Harbor, WA, Numerical and Physical Modeling Draft Reports

Grays Harbor would tend to be stable and capture the flow, based on that consideration alone. Such a consideration is consistent with the van de Kreeke analysis, which employs the one-dimensional Keulegan (1951 1967) hydrodynamic model that incorporates inlet length and friction. The Breach Model employs a more complete version of the Keulegan model and is in that sense consistent with the Escoffier and van de Kreeke methods, but includes many other physical processes such as time-dependent longshore sediment transport and representation of fair-weather waves, storms waves and water level, wave set up, and channel sediment bypassing.

The Authors are unsure of the regulatory requirements and protocols necessary for stockpiling and accessing material to close a breach that might occur on the South Beach at Grays Harbor. Experience with coastal breaches (as well as predictions of the Breach Model) indicates that if a breach continued to enlarge, the growth is exponential toward equilibrium. Therefore, with passage of time after breach opening, the volume of sediment required to fill the breach, difficulty in operation, and cost increase greatly. It is noted that approximately 2 months were required to close the 1993 breach at Grays Harbor (October to 7 December 1994). The strategy of stockpiling, accessing, and having permits in force as appropriate to close a breach in a timely manner may be acceptable, but it might also be viewed as a reactive gamble as compared to proactive maintenance of a strong barrier island to prevent breaching. From a regional sediment management perspective, protection of the Federal navigation project at Grays Harbor is one of many considerations in approaching the issue of preventing or managing a breach.

References

- Escoffier, F. F. (1940). "The stability of tidal inlets," *Shore & Beach* 8(4), 114-115.
- Escoffier, F. F. (1977). "Hydrodynamics and stability of tidal inlets," GITI Report 13, U.S. Army Corps of Engineers, Coastal Engineering Research Center, Vicksburg, MS.
- Jarrett, J.T. (1976). "Tidal prism-inlet area relationships," GITI Report 3, U.S. Army Corps of Engineers, Waterways Experiment Station, Vicksburg, MS.
- Van de Kreeke, J. (1985). "Stability of tidal inlets; Pass Cavallo, Texas," *Estuarine, Coastal and Shelf Science*, 21, 33-43.
- Van de Kreeke, J. (1990). "Can multiple inlets be stable?," *Estuarine, Coastal and Shelf Science* 30, 261-273.

SUBJECT: Response to Committee on Tidal Hydraulics, Independent Technical Review Sub-committee, review of Grays Harbor, WA, Numerical and Physical Modeling Draft Reports

(18) In our view, the breaching model does not recognize adequately the sediment deficit in the breach area (erosion of the ocean beaches). It is stated (for example, Pages 61 and 79) “If the current velocity were to fall below a critical velocity threshold for sediment transport, then material would deposit in the breach, and eventually it would close ...”. This statement does not recognize the background sediment deficit in the South Beach vicinity.

Response: The quoted sentences pertain to the time-dependent calculations of sediment transport in the Breach Model, for which the South Beach shore and associated sediment supply are assumed to exist. In a long-term perspective, if there is greatly diminished sediment supply by longshore transport, then indeed enlargement and stability of a breach would be promoted. The full quotation from the above is “If the current velocity were to fall below a critical velocity threshold for sediment transport, then material would deposit in the breach, and eventually it would close at a minimal elevation (mllw; or, e.g. mllw).” The subject sentence and material following convey the concept that such a closure might be weak, and that the breach area could be re-opened by a subsequent storm.

(19) Figure 114 is interesting and indicates that the cross-sectional growth rate of the breach would accelerate. Would the flows through the breach eventually dominate those through the jetties or is this extrapolating too far? This question is central to the issue of whether the breach will affect the Federal Navigation Project. Specific Comment (3) refers to Figure 19 and the ambiguity in MSL relative to MLLW and the control sections. NOAA’s published values for MSL at nearby stations range from about 1.3 to 1.7 m above MLLW. If a MSL value of 1.5 MLLW is assumed on Figure 19, the MSL area of the controlling section (transect 1) of the Aug 94 cross-sections is about $0.5 \times 0.5 \times 50 = 12.5$ sq.m. The ratio of 12.5 to 26,000 (the cross sectional area of the main inlet) is 0.05%, whereas Figure 114 is indicating a Aug 94 ratio of about 2.8%. The ratio is very small by either number, but the authors should check these figures and remove the ambiguity.

Response: The Authors appreciate the Reviewers’ attention to detail by independently calculating cross-sectional area based on the breach topographic profile data. This concern revealed inconsistent results in the calculated ratio of inlet and breach cross-sectional area. The Authors examined the discrepancy and determined that the cross-sectional area of the breach was calculated with breach depth measured with respect to the top of the barrier island (msl +3 m), a convenient origin for the Breach Model. A vertical adjustment was

SUBJECT: Response to Committee on Tidal Hydraulics, Independent Technical Review Sub-committee, review of Grays Harbor, WA, Numerical and Physical Modeling Draft Reports

applied to bring the breach depth to msl, and the ratio of cross-sectional areas was recalculated. Instead of an August 1994 estimated ratio (by modeling) of about 2.8 percent, a ratio of approximately 0.6% was obtained. We observed that this was still larger than the 0.05% estimate from the measured profiles, so the cross-sectional area ratio was calculated for net longshore transport rate of 200,000, and 600,000 m³/year as well as the 400,000 m³/year that was previously calculated. The measured cross-sectional area likely falls somewhere between the cross-sectional areas predicted with 600,000 m³/year and 400,000 m³/year as input. The updated results are displayed in Figure R11.

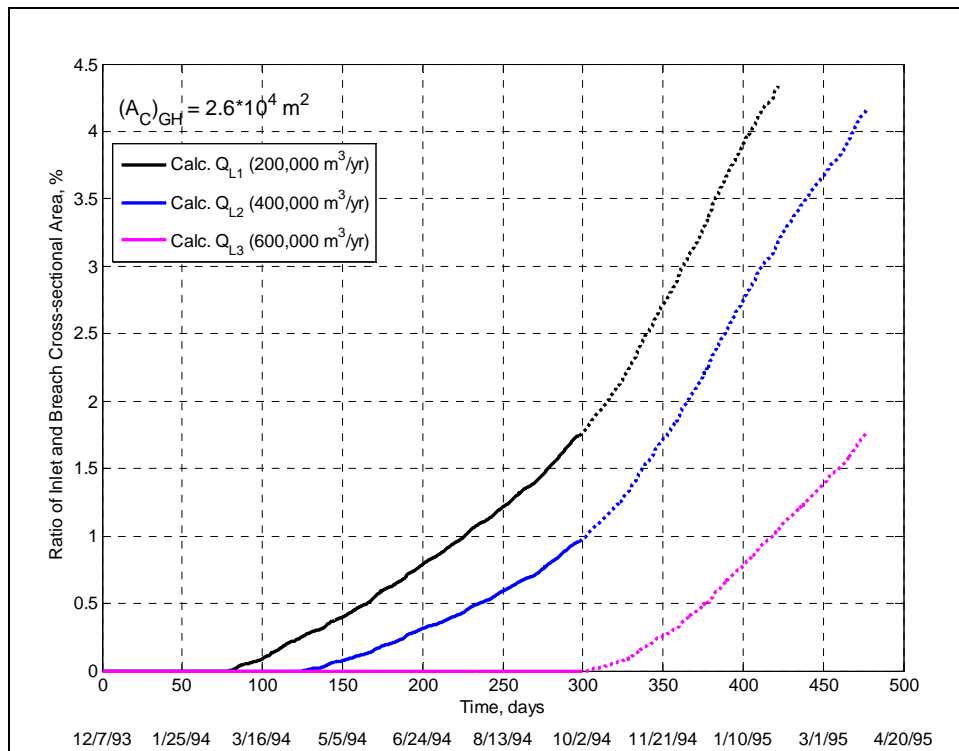


Figure R11. Calculated breach channel cross-sectional area

(20) The effect of longshore sediment transport was evaluated in the breach model. However, with the south jetty interpreted as deflecting the longshore sediment transport seaward and around the south jetty, is this the same as, say for Moriches Inlet where there was an accumulation against the updrift jetty? Also note the later discussion of uncertainties in the net longshore sediment transport and magnitude.

Response: According to the available data, the barrier island east of Moriches Inlet breached on 13 January 1980 at its narrowest point

SUBJECT: Response to Committee on Tidal Hydraulics, Independent Technical Review Sub-committee, review of Grays Harbor, WA, Numerical and Physical Modeling Draft Reports

located about 300 m east of the east jetty. The photographic record indicates that the remaining barrier island segment between the breach and the east jetty eroded steadily and had disappeared by 01 April 1980 (see Figure 103 in the draft report). This situation was also described to the Authors by Mr. Gilbert Nersesian, former Senior Coastal Engineer at the U.S. Army Engineer District, New York. Therefore, there was no accumulation against the updrift (east) jetty at Moriches Inlet after the breach opened, as described in Item 20. The material adjacent to the east jetty was in place as part of the barrier island when the breach occurred. The 1992-1993 breach at the Grays Harbor south jetty evidently followed the same pattern, breaching at the narrowest section, some distance south of the jetty (Figure 13b).

(21) Page 114 interprets the Osborne et al (2003) sediment budget as the outer Half Moon Bay “had a net sediment gain of sediment from 1996 to February 2002 of about 1.1 million cu m.” Our examination of the Osborne sediment budget in Figure 115 is that outer Half Moon Bay experienced a net loss of 1.04 million cu m.

Response: The area referred to as “Outer Half Moon Bay” in Osborne et al. 2003 (ERDC/CHL TR-03-4) had a positive net sediment budget between 1996 and 2002 (+1.46 M cu yd). We do not understand how the conclusion was made by the Reviewers that the area had a net loss of 1.04 M cu yd.

(22) The ITRC considers the issue of net longshore magnitude and direction to be unresolved but relevant to the issues of breach evolution. The report under review implies that the net transport direction and rate are well-known (Page 107) “Northward-directed sediment transport was calculated and calibrated by comparing with the long-term annual sediment transport rate, 400,000 m³/year...”. Buijsman, et al (2003) also report that the net sediment transport is northerly over the entire Washington side of the Columbia River Littoral Cell. They use 800,000 cubic meters per year, twice the value used by the Authors. The direction and values are based on bathymetric-and topographic-change analysis over the entire Columbia River Littoral Cell for the last 160 years, and there is strong geomorphic and petrologic evidence for their conclusion. However, there are other estimates of the net longshore sediment transport rates and directions based primarily on the nearshore wave climate as reviewed below. A discussion of the prevailing coastal processes would appropriately be presented much earlier in the report under the section on “Regional Processes” starting on Page 8.

SUBJECT: Response to Committee on Tidal Hydraulics, Independent Technical Review Sub-committee, review of Grays Harbor, WA, Numerical and Physical Modeling Draft Reports

The 1967 Committee on Tidal Hydraulics (CTH) states (Page 12) “The predominant direction of littoral drift is southward.” The 1995 CTH also concludes that the net direction is southerly south of the south jetty but northerly on the beaches north of the north jetty. These results were based on calculations employing hindcast data from WIS Station 48 with the calculated results presented in Table 2.

Table 2

Longshore Sediment Transport Characteristics Found in CTH
1995 Study (Based on WIS Hindcast Waves at Station 48)

Beach	Annual Transport Rates (Millions m ³ /year)			
	Northerly	Southerly	Net	Gross
North	12.0	11.0	1.0 (Northerly)	23.0
South	10.5	14.7	4.2 (Southerly)	25.2

The April 2003 ERDC report (Osborne, et al.) references a 2000 study conducted by ERDC for the Seattle District which used the Grays Harbor buoy wave data and transport models developed by ERDC. This study concluded that there was north-directed net transport along North Beach and South-directed transport along South Beach.

A similar sediment transport exercise to that contained in the 1995 CTH report was carried out here with the exception that the Scripps summary of wave data was used as input rather than the WIS data. The equation for longshore sediment transport based on deep water wave conditions is

[Equations were found to be corrupted and were deleted in this Response]

in which K is the sediment transport coefficient, H is the deep water wave height, g is gravity, T is wave period, β is the azimuth of the outward normal to the local shoreline, α is the azimuth of the direction from which the deep water wave arrives, S is the relative density of the sediment with relative to the water in which it is immersed (usually taken as 2.65), p is the in-place porosity of the sediment (usually taken as 0.35 to 0.4) and κ is the ratio of breaking wave height to breaking water depth (usually taken as 0.78 for a single wave or approximately 0.4 for the significant wave height). Applying usual values, Eq. (1) can be reduced to

[Equations found to be corrupted and were deleted in this Response]

SUBJECT: Response to Committee on Tidal Hydraulics, Independent Technical Review Sub-committee, review of Grays Harbor, WA, Numerical and Physical Modeling Draft Reports

and it will be assumed that $\cos^{0.2}(\beta\alpha) \approx 1.0$. The above equations represent the longshore sediment transport by waves. Applying the above equation to the wave data from the Grays Harbor Buoy # 036 in deep water results in a net northerly transport on the beaches north of the entrance and a net southerly transport on the beaches south of the entrance. The annual values calculated are summarized in Table 3; however, wave dissipation as the waves propagate from deep water to the surf zone where most of the transport occurs was not taken into account, so it is recognized that these values are excessively large. As an example, a wave height reduction of 50% from deep water to breaking would reduce the values in Table 3 by approximately 81%. However, wave dissipation should not change the direction of net transport, but rather reduce all transport components approximately proportionally.

Table 3

Longshore Sediment Transport Characteristics Found in Present Study
(Based on Grays Harbor Buoy Wave Data August 1993 to July 2005)

Beach	Azimuth of Outward Normal to Beach (o)	Annual Transport Rates (Millions of m ³ /year)			
		Northerly	Southerly	Net	Gross
North	268.3	4.15	1.66	2.48 (Northerly)	4.14
South	257.7	3.26	7.92	4.66 (Southerly)	11.18

It is somewhat interesting that the net longshore sediment transports as determined in the 1995 CTH report (Table 2) based on WIS hindcasts and those determined here based on the Grays Harbor wave data (Table 3) are reasonably similar; however, the gross transport rates differ substantially.

The above discussion applies to wave driven transport. We appreciate that the sediments in the area were derived from the Columbia River and that there may be current driven sediment transport in deeper water. There is the possibility that there have been long-term (perhaps cyclical) changes in the predominant wave direction. Also, it is noted that a so-called “sand wave” appears to be migrating northward and may cause an accretionary cycle south of the south jetty in coming decades.

Response: The discussion of the Reviewers on regional longshore sediment transport is interesting and could be continued substantially. “Regional” connotes “long term,” for which the morphologic record of bathymetry is considered by the Authors to provide the most reliable estimate of net sediment transport rates. As the Reviewers note, longshore sediment transport calculated from wave data is sensitive to shoreline orientation, which can change through time in the vicinity of inlets. The calculated rate is also sensitive to wave direction, the trend

SUBJECT: Response to Committee on Tidal Hydraulics, Independent Technical Review Sub-committee, review of Grays Harbor, WA, Numerical and Physical Modeling Draft Reports

of which can change on several temporal scales from decades, through seasons, to hours. Wave direction as measured at buoys has a large uncertainty. Monochromatic wave analysis has limitations. The irregular morphology at the entrance to Grays Harbor has evolved greatly since construction of the jetties, modifying the waves and longshore sediment transport rate.

Calculation of longshore sediment transport through wave transformation and application of predictive formulas in the vicinity of an inlet cannot neglect the inlet morphology (ebb shoal and bypassing bars, channel) and diffraction at the jetties, as done by the Reviewers. In addition, blockage of waves, longshore current, and longshore sediment transport at the south jetty, as well as the rip current along the south jetty will greatly control the local longshore sediment transport rate. The local pattern of longshore sediment transport near the south jetty is likely not consistent with the regional trend because of these and other factors.

Fortunately, recession of the shoreline along the South Beach in the area of the south jetty has been measured (draft report Page 26 and Table 4, where work by other investigators is summarized) and can serve for engineering studies at the site, such as for maintenance of a minimum barrier width and volume. As a barrier beach loses volume and width, it becomes more vulnerable to breaching by storms. Figure R12 plots the number of occurrences of storms at Grays Harbor with significant wave height exceeding 6 m, as compiled from National Data Center Buoy 46029 and Coastal Data Information Program array 036. The December 1993 breach was opened by a moderate storm, and a minor storm in March 1994 again eroded the beach. Had a major storm occurred prior to mechanical closure of the breach over October to 7 December 1994, the breach would have been susceptible to even greater enlargement than observed. The number of storms per year has remained high relative to the number in 1993-1994, raising the potential for breaching. We note that a shallow breach occurred on Damon Point, located on the north side of the Grays Harbor entrance, in late January to early February, 2006, during a large storm.

SUBJECT: Response to Committee on Tidal Hydraulics, Independent Technical Review Sub-committee, review of Grays Harbor, WA, Numerical and Physical Modeling Draft Reports

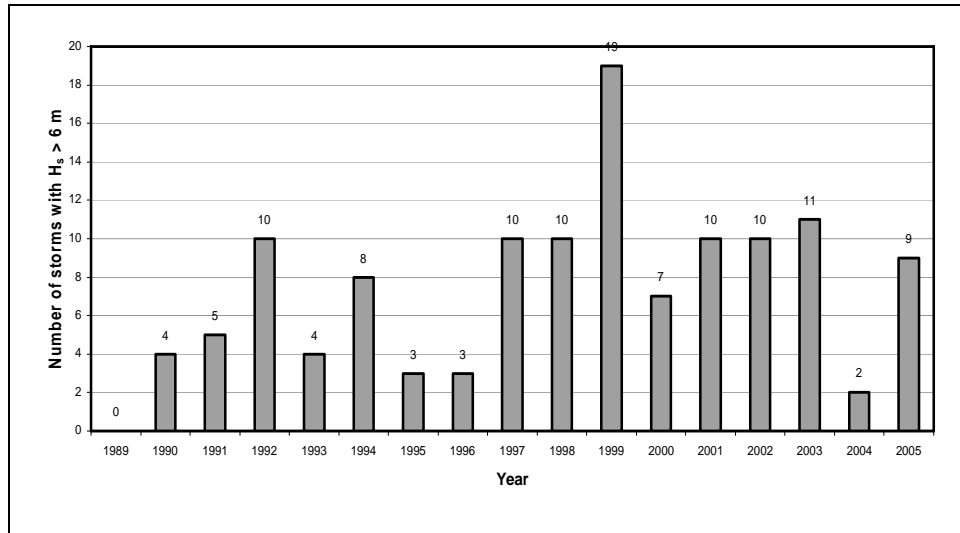


Figure R12. Grays Harbor, number of storms/year with significant wave height exceeding 6 m

References

Aarninkhof, S.G.J., Roelvink, J.A. (1999) "Argus-based Monitoring of Intertidal Beach Morphodynamics" Proc. of Coastal Sediments Conf, Long Island NY, USA, pp. 2429-2444.

Battjes, J.A., Jannssen, J.P.F.M. (1998). "Energy Loss and Set-up Due to Breaking in Random Waves" Proc of 16th Int. Conf. on Coastal Eng., ASCE, pp. 569-587.

Buijsman, M.C.; C.R. Sherwood; A.E. Gibbs; G. Gelfenbaum; G. Kaminsky; P. Ruggiero; J. Franklin. 2003. Regional Sediment Budget of the Columbia River Littoral Cell, USA. United States Geological Survey Open File Report 02-281, 150p. Escoffier, F. F. (1940) "The Stability of Tidal Inlets", Shore and Beach, Vol. 8, No. 4, pp. 114 – 115.

Holman, R.A., Sallenger Jr., A.H. (1985). "Setup and Swash on a Natural Beach," Journal of Geophysical Research, 90, 945-953.

Osborne, P. D., Wamsley, T. V. and H. T. Arden. (2003). "South Jetty Sediment Processes Study, Grays Harbor Washington: Evaluation of Engineering Structures and Maintenance Measures", ERDC/CHL TR-03-4, U. S. Army Engineer Research and Development Center, Coastal and Hydraulics Laboratory, Vicksburg, MS.

SUBJECT: Response to Committee on Tidal Hydraulics, Independent Technical Review Sub-committee, review of Grays Harbor, WA, Numerical and Physical Modeling Draft Reports

Ruessink, B.G., Kleinmans, M.G., Van Beukel, P.G.L. (1998). "Observations of Swash Under Highly Dissipative Conditions," *Journal of Geophysical Research* 103,3111-3118.

Stive, J.J.F., De Vriend, H.J. (1994). "Shear Stresses and Mean Flow in Shoaling and Breaking Waves," *Proc Int Conf Coastal Eng ASCE*, pp. 594-608.

Stockdon, H.F., Holman, R.A., Sallenger Jr., A.H. (2002). "Parameterization of Incident and Infragravity Swash Variance," *Eos Trans. AGU*, vol 83 (47), p. F746. Fall Meeting Suppl.

Svendson, I.A. (1984). "Wave Heights and Set-up in a Surf Zone," *Coastal Engineering* 8, 303-329.

Van de Kreeke, J. C. (1990) "Can Multiple Tidal Inlets be Stable", *Estuarine, Coastal and Shelf Science*, Vol. 30, pp 261 – 273.

SUBJECT: Response to Committee on Tidal Hydraulics, Independent Technical Review Sub-committee, review of Grays Harbor, WA, Numerical and Physical Modeling Draft Reports

Half Moon Bay, Grays Harbor, WA: Movable-Bed Physical Model Study, February 2005.

Introduction

As for the previous report, the following review of this report will first address general comments focused primarily on the four questions provided earlier followed by specific comments.

The purpose of the project documented in this report (Page 87) *“was to support the LTMS studies being conducted by the Seattle District. Specifically, the model results will be used to assess the potential long-term response of the Half Moon Bay shoreline to expected storm waves and surge levels, provided the breach fill between South Beach and the bay remains intact.”*

General Comments

(1) The modeling skill of the lead Author, Dr. Steve Hughes, is evident throughout the study in overcoming the difficult complexities of the problem at hand.

Is the selected model appropriate for the study purpose?

(2) Based on the documentation provided for this study, it is evident that the objective of this study evolved over time from two purposes to the one presented above. Originally, the lead Author was requested to: 1) evaluate the expected long-term shoreline planform if the narrow barrier between South Beach and Half Moon Bay remains intact and no further engineering modifications of project features occur; and 2) provide a baseline with which to compare the effects of potential engineering alternatives for long-term stabilization of the bay. The latter objective supports the use of a physical model. However, the study was later limited to objective 1 and as such may not be the best approach for this question alone. We will address this point in greater detail in our Specific Comments.

Response: Agreed.

Has the model been appropriately calibrated and verified?

(3) In evaluating the model, it is essential to recognize the general complexity of the system to be modeled. This complexity is due to a number of factors including sand and cobble/gravel material, waves

SUBJECT: Response to Committee on Tidal Hydraulics, Independent Technical Review Sub-committee, review of Grays Harbor, WA, Numerical and Physical Modeling Draft Reports

arriving with variable heights, periods and directions, and variable water levels. The final model tests have been conducted with one incident wave direction (295 degrees) and one water level (+12 ft MLLW).

(4) The model required substantial modifications to achieve the degree of agreement possible. These included reorienting the wavemaker, adjusting the wave conditions applied and artificial means of reducing the longshore current in the vicinity of Point Chehalis.

(5) The model limitations are clearly identified.

(6) Considering the complexities noted above, the model has been appropriately calibrated and verified to the degree possible with existing field data -- calibration metrics of model agreement were successfully applied. The model resulted in reasonably good qualitative agreement with observations. However, as noted in Specific Comment 4 below, comparison of model and prototype wave characteristics would have been useful in this regard.

Response: Agreed.

Are the study conclusions supported by the model results?

(7) Yes. The Authors clearly recognize the limitations of the physical study and only state conclusions that can be drawn from the model results. One significant model limitation is explicitly stated -- an inability to model long periods of time where sediment loss to the bay could influence results (page 89). Another important limitation is not stated -- the validation of the model, dependent on several non-scaling expedients (including those listed above), cannot be extended to large changes in initial or boundary changes.

Response: Agreed. The following paragraph has been added to the Interpretation of *Physical Model Results* section of Chapter 7.

“The model validation, to the extent validation was achieved, only applies to perturbations in the modeled region shoreline being driven by similar hydrodynamic forcing that was used to calibrate the model. Large system perturbations such as large changes to the initial Half Moon Bay shoreline configuration, substantial changes to the bay bathymetry (e.g., significant infilling of the bay using dredge material placement), or vastly different characteristic hydrodynamic conditions could not be simulated using this physical model without additional validation.”

SUBJECT: Response to Committee on Tidal Hydraulics, Independent Technical Review Sub-committee, review of Grays Harbor, WA, Numerical and Physical Modeling Draft Reports

Does the study accomplish the goal?

(8) The study results more effectively move towards accomplishing the original two goals than the final revised single goal of establishing the long-term planform. The Authors clearly states this in the summary comments. Finally, simulation of the existing condition in the movable-bed physical model provided a baseline case for physical model comparison with engineering alternatives that might be developed in the LTMS for strengthening the breach fill between South Beach and Half Moon Bay or for mitigating or preventing recession of the bay shoreline.

(9) We believe that for a movable bed model, the model constructed for this purpose was appropriate.

(10) We believe that the study conclusions are supported by the model results as qualified above.

(11) Taking the system complexities into consideration, we believe that the studies did accomplish their goals.

(12) The report states (Page 89) that The movable-bed model was originally constructed to evaluate potential alternatives for long-term stabilization of the Half Moon Bay shoreline. The model would be more appropriate for this original purpose than the modified purpose of evaluating absolute shoreline change.

Response: Agreed.

Specific Comments

(1) Sections 3 and 4 document appropriate care in the design and construction of the model.

(2) At several places in the report, it is stated (for example Page 87 and earlier), that sediment incipient motion will require a relatively larger flow speed than in nature. This statement is correct for sediment transport due to currents alone; however, within the surf zone, mobilization by breaking wave turbulence may reduce this difference.

Response: Agreed. The above statement is correct, and scale effects for the two distinct modes of sediment transport were discussed in more detail in the draft report Chapter 3 section titled *Potential Scale and Laboratory Effects*. Items (c) and (d) in the list of potential scale

SUBJECT: Response to Committee on Tidal Hydraulics, Independent Technical Review Sub-committee, review of Grays Harbor, WA, Numerical and Physical Modeling Draft Reports

effects in the Chapter 8 *Summary of Study Tasks* section have been expanded slightly. The revised version is given below.

c. Bedload sediment transport of sand in the physical model was not in similitude because the model sediment could not be reduced to the correct size without introducing cohesive forces. Consequently, erosion in the model will not be as severe as in nature, sediment incipient motion under bedload conditions will require a relatively larger flow speed than in nature, and sediment in motion will settle at relatively greater flow speeds than in the prototype. Despite this scale effect, the model was expected to indicate the correct locations of erosion and deposition of sand, but the absolute magnitudes will be less than expected in nature.

d. Sand thrown into suspension by turbulent fluid motion within the surf zone and transported in suspended mode was nearly in similitude, so that erosion produced by energetic wave action with strong breaking and turbulence generation was nearly correct. Eventually, suspended sand grains will settle out of the water column in less turbulent regions.

(3) Page 18, states This does not mean that sediment transport has ceased, it means that the net longshore sediment transport is not sufficient to change the general shoreline planform shape. Considering that the profiles advance or retreat without change of form, the change in planform shape depends only on the gradient of longshore sediment transport, not on the net transport.

Response: The third paragraph in the Chapter 3 section titled, *Dominant Physical Processes in Half Moon Bay* has been modified to that given below.

“The theory of crenulate-shaped bays (Silvester 1991) postulates that planform shape equilibrium occurs if the diffracted wave front breaks normal to the shoreline at all locations, and there is no alongshore current generated. However, crenulate-shaped bays will retain their planform shape provided there is no gradient in alongshore sediment transport. This does not mean that sediment transport has ceased; rather, it means that the gradient of alongshore sediment transport is not sufficient to change the general shoreline planform shape. Distribution of sand on shore-normal profiles seaward of the shoreline will vary with wave conditions and water level. More severe storm conditions could cause the shoreline to recede while still retaining the approximate crenulate-bay planform shape.”

SUBJECT: Response to Committee on Tidal Hydraulics, Independent Technical Review Sub-committee, review of Grays Harbor, WA, Numerical and Physical Modeling Draft Reports

(4) The field measurements of waves in Half Moon Bay are valuable. The dependency of waves at Gages 3 and 4 on tide are quite apparent with the wave height at Gage 3 dropping to near zero at low tides. Is this due to wave breaking seaward of the gages or other effects. What were the water depths in which these gages were located? Although the model (Froude) should replicate the wave processes, were the model measurements compared with the prototype data? This could assist in identifying the most appropriate wave directions at the wavemaker. Thus, it would have been useful if comparisons between the model and prototype (field) gauge data had been presented.

Response: The prototype wave measurements are presented in the report to give the reader a sense of wave reduction as waves propagate into Half Moon Bay, and to indicate the main directions of incident wave energy. The wave data were acquired independent of the physical model task. Water depth elevations of the inshore gages relative to mllw are approximately as follows: Gage 1: -20 ft; Gage 2: -10 ft; Gage 3: -5 ft; and Gage 4: -5 ft. Because of its relatively shallow water Gage 3 recorded only small waves at lower tide levels.

The model wave measurements were not compared directly to the prototype measurements, but the same relative trends between the gauges were noted. In the physical model, the constant water elevation of +12 ft mllw rendered direct comparison to prototype measurements at lower elevations less meaningful. The wave direction roses constructed from the prototype data were used for initial setting of the wave approach angle. The second paragraph in Chapter 5 section titled *Model Wave Conditions* has been modified by addition of the approximate bottom elevation relative to mllw at the four inshore wave gage locations.

(5) Page 34 discusses the effects of the gravel/cobble transition on the downdrift (east) shorelines. Unless the area hardened by the gravel/cobble is in equilibrium, the gravel/cobble hard point would be associated with a discontinuity and the downdrift shoreline would be expected to erode at a more rapid rate than if the hardening were not present. We have not determined whether the equilibrium downdrift shoreline position would be affected by the hardening.

Response: The above comment refers to a discussion of measured profiles beginning on page 54 under the section titled *Historic Erosion Event Selected for Calibration*. Hughes agrees with the concept that

SUBJECT: Response to Committee on Tidal Hydraulics, Independent Technical Review Sub-committee, review of Grays Harbor, WA, Numerical and Physical Modeling Draft Reports

the termination point of the gravel/cobble protection is a discontinuity that could cause more rapid erosion downdrift. This assumes the protected shoreline is seaward of where the equilibrium shoreline would be if this stretch of shore were not protected. The following sentences have been added to the second paragraph in the section titled *Historic Erosion Event Selected for Calibration*.

“Under the assumption that the reach of shore protected by the gravel/cobble is not in equilibrium, the unprotected shore immediately downdrift of the gravel termination point would be expected to see increased erosion and greater recession. This study did not investigate whether or not the gravel-protected shore is at equilibrium. Such a determination should be based on field observation over an extended time period.”

(6) Page 54, Second Paragraph. One would expect that with the higher water levels resulting in a smaller surf zone width (and thus higher average shear stresses within the surf zone), the longshore transport would be accentuated by the higher water levels.

Response: The above comment pertains to the second paragraph under the section heading *Calibration Philosophy* in Chapter 6 starting on page 53. The Reviewers are correct in stating that longshore sediment transport would be accentuated at higher water level due to increased average shear stresses in the surf zone. As noted in the report at the end of the second paragraph, running the model at a higher water level was considered, but rejected because of the extensive wave overtopping that would have occurred at the beach near Point Chehalis. Even with model water levels higher than what might have occurred in nature, the increased longshore transport in the model was still not enough to overcome the sediment scale effect as discussed in Chapters 7 and 8.

(7) Page 64, Figure 40. Are the + marks the model results? Also, the first paragraph uses the words shoreline and dune in a confusing manner. It is also stated that The seaward solid line is the 2003 shoreline&; however, the figure shows the seaward solid line (at least in the westward portion of Half Moon Bay) as Shore 2002.

Response: The “plus” marks on Figure 40 represent the model results for edge of the dune scarp. The text in this paragraph has been modified to indicate this fact more clearly. The terminology of dune recession and shoreline recession is to distinguish between the location of the edge of the dune and the location of the intersection of the water

SUBJECT: Response to Committee on Tidal Hydraulics, Independent Technical Review Sub-committee, review of Grays Harbor, WA, Numerical and Physical Modeling Draft Reports

and normal high tide level. The seaward solid line is in fact the 2002 shoreline as indicated on Figure 40. This was a typographical error, and it has been corrected in the text.

(8) Many different metrics could be identified to quantify model performance. One approach is to compare volume density changes (volume change per unit beach length) which provides an overall measure of the total profile change. The following table compares contour changes at the + 12 ft MLLW elevation for the prototype, the model after the Second Calibration and the model after the Final Run.

Profile	+12 ft MLLW Contour Change (ft)		
	Prototype (Figures 31-33)	Model After Second Calibration Effort Figures 41-43	Model After Final Run Figures 55-57
P1	0	+40	0
P2	-2	0	-5
P3	-75	0	-25
P4	-90	+0	-70
P5	-5	+70	-15
P6	-10	+30	-15
P7	-5	+65	-50
P8	-5	-105	-130
P9	-15	-160	-100

It is seen that there is considerable improvement in the western and central portions of Half Moon Bay from the Second Calibration to the Final Run. As an overall measure of the improvement, the root mean square difference (Model to Prototype) for all profiles decreased from 80.6 feet to 55.7 feet from Second Calibration to the Final Run.

Response: Agreed. The Reviewers have illustrated just one of the possible metrics that could be used to compare and evaluate the Half Moon Bay physical model tests. The table above is a good idea for implementation if the study continues with the original intention of evaluating project alternatives. While not said explicitly, it is understood that the Reviewers intend that such a metric is an additional point for comparative evaluation, and it is not meant to replace the profile and planform comparisons shown in the report.

(9) (Page 58. It is stated that the irregular waves were characterized by a TMA spectrum with a $\gamma = 10$. What were typical values of γ from the larger wave events obtained at the CDIP buoy? Is the γ -value for the TMA spectrum similar to that for a Jonswap spectrum?

SUBJECT: Response to Committee on Tidal Hydraulics, Independent Technical Review Sub-committee, review of Grays Harbor, WA, Numerical and Physical Modeling Draft Reports

Response: Wave data available from the CDIP buoy do not include the spectral width parameter γ . Typical values of γ for storm waves are in the range of $\gamma = 3 - 4$ corresponding to a fairly broad spectral shape. This value of gamma was used initially for irregular waves during the first calibration run, but when it was recognized that dune recession was minimal, the value of γ was increased to $\gamma = 10$. This had the effect of narrowing the wave spectra to resemble more closely a swell-wave condition featuring more wave groupiness. The goal was to promote more dune recession, and it should be considered a necessary “tweak” in an attempt to calibrate the model. The TMA spectrum is the Jonswap spectrum with an additional term representing shallow water. Therefore, γ is the same in both spectral representations.

(10) Were any long waves observed in the basin as a result of the irregular wave forcing?

Response: Unintended long waves are always a concern in coastal physical models, particularly in basins where active wave absorption is problematic. Spurious long waves resulting from generating irregular wave signals using a first-order algorithm were observed in the test basin. The effect of these long waves on experiment results is unknown and difficult to assess. Experiment protocol included time intervals with no wave action to allow the basin to still before commencing the next wave sequence (see Table 6). During the basin stilling time, water elevations were monitored at each wave gauge location to confirm the long waves were being quelled. The duration of the basin stilling was based on observation of long wave reduction and experience.

